University of Strathclyde

Department of Electronic and Electrical Engineering

Enhanced Control and Protection for Inverter Dominated Microgrids

Xinyao Li

A thesis presented in fulfilment of the requirements for the degree of

Doctor of Philosophy

2014

This thesis is the result of the author's original research. It has been composed by the author and has not been previously submitted for examination which has led to the award of a degree.

Signed: Date: 30-05-2014

Abstract

Implementation of distributed energy resources (DER) has the potential to lower the carbon oxygen emissions, reduce the power distribution losses and improve the overall system operation. Despite the numerous advantages brought by these small-scale DERs, effective protection and control of such systems are still unsolved challenges. The distribution system is increasingly being confronted with congestion and voltage problems, which limits further penetration of DERs. Numerous studies have been conducted to analyse these challenges and provide recommendations or guidance for protection and control in the past few years. There is also a lot of effort to develop an advanced regime for integration of large amounts of DERs, such as the "microgrid". Microgrids are designed to provide control and protection of a cluster of DERs, storage units and loads in a way that can coordinate with the conventional utility grid operation with little conflict. As flexible as it is, a microgrid is connected to the utility grid behaving as a controllable entity in normal operation, and can be disconnected from the grid to present itself as a power island in emergency, e.g. system black-out. Since most of the DERs are interfaced with inverters, this thesis is dedicated to provide in-depth investigation of protection and control within inverter dominated microgrids.

The thesis provides two main valuable contributions. Firstly, an enhanced control scheme for a microgrid consisting of multi inverter interfaced generators (IIG) is developed and compared to the conventional droop based decentralized control. The proposed control scheme is particularly designed for systems with IIGs interconnected via relatively long cable lengths (several kilo metres). It also allows switchless mode transition between islanded operation and grid-connected operation, which reduces the transient voltage and current oscillations, and enhances the transient behaviour of the IIGs. Compared to the conventional droop based decentralized control, the proposed control scheme has better operational stability and is immune to different lengths and R/X ratios of connecting cables. The proposed control also brings better voltage regulation and has a larger power output capacity. Secondly, a new travelling wave based protection scheme is developed

which involves modification of an application friendly signal processing technique – Mathematical Morphology. The impact of distance to fault, fault inception angle and fault impedance is analysed and quantified. The thesis proposes a systematic protection solution which is proved to be immune to the changes of system topology, modes of operation and load conditions.

Acknowledgement

I feel very grateful for the incredible support and encouragement from Professor Graeme Burt, and Dr Adam Dyśko by providing very significant academic guidance and resources for my work. I thank my husband and my parents who all supported me during my study. I would also like to send many thanks to all my colleagues for their friendship and providing a good cooperative work environment.

Table of Contents

Abstract V

Acknowledgement VII

Table of Contents VIII

List of Figures XVII

List of Tables XXII

List of Abbreviations, Symbols & Nomenclatures XXIII

1. Introduction 1

1.1 Thesis Background 1

1.1.1 Electric Power System Operations 1

1.1.2 Microgrid Definition and Structure 2

1.1.3 Existing and Ongoing Microgrid Projects Worldwide 3

1.1.3.1 USA 3

1.1.3.2 EU 5

1.1.3.3 Other countries 5

1.2 Main Unresolved Issues and Research Objectives 7

1.3 Main Contributions 9

1.4 Presumptions of the Work 9

1.5 Layout of the Thesis 10

1.6 List of Publications 12

1.7 Chapter References 13

2. Challenges, Issues and Overview of Microgrid Control with IIG Integration..... 16

2.1 Introduction 16

2.2 Microgrid Operational Features, Control Structure and Challenges..... 17

2.2.1 Microgrid Operational Features and Requirements 17

2.2.2 Microgrid Control Structure..... 18

2.2.3 Microgrid Control Challenges..... 20

2.3 Basic Principle of Single IIG Control 22

2.3.1 Control Reference Frame 22

2.3.2 Components of the IIG controller 24

2.3.2.1 Phase-locked Loop 24

2.3.2.2 Modulation Scheme 26

2.3.2.3 Voltage and Current Control Loop 27

2.3.3 IIG Control under Grid-Connected Mode..... 30

2.3.4 IIG Control under Islanded Mode 31

2.4 Review of Existing Control Methods for Multi-IIG Based Microgrid System 32

2.4.1 Centralized Control Principles of Islanded Multi IIGs 34

2.4.1.1 Circular Chain Current Programming..... 34

2.4.1.2 Master-slave 35

2.4.1.3 Current Distribution Programming 36

2.4.2 Decentralized Control Principles of Islanded Multi IIGs 38

2.4.2.1 Harmonic Sharing with Nonlinear Loads 39

2.4.2.2 Line Impedance Effect and Active/Reactive Power Decoupling..... 40

2.4.2.3 Transient response quality..... 41

2.4.2.4 Stability assessment 42

2.4.2.5 Hierarchical control structure..... 43

2.4.3 A Summary and the Issues of the Multi-IIG Control Methods..... 44

2.4.4 Control Strategy of Mode Transfer between Islanded and Grid-Connected Operation..... 46

2.4.4.1 Mode Switch Based Transfer..... 46

2.4.4.2 Non-mode Switch Transfer..... 46

2.4.4.3 Resynchronization Process 47

2.5 Chapter Summary..... 47

2.6 Chapter References 48

3. Review of Microgrid Protection..... 59

3.1 Introduction..... 59

3.2 Conventional Distribution Network Protection 60

3.3 DER Impact on Distribution Network Protection Performance 62

3.3.1 Dynamic Responses and Fault Behaviour of DERs..... 62

3.3.1.1 Synchronous Machine..... 63

3.3.1.2 Induction Machine 64

3.3.1.3 IIG 64

3.3.1.4 DFIG 66

3.3.2 Under or Over Reach of the Overcurrent Protection 66

3.3.3 False Tripping of the Overcurrent Protection 67

3.3.4 Loss of Mains/Islanding Detection 67

3.3.5 Coordination with Reclosers 68

3.4 Protection Issues with Microgrids 68

3.4.1 Concerns over Microgrid Features 69

3.4.2 Special Concerns of IIG Based Microgrids 69

3.5 Overview of Microgrid Protection Schemes 70

3.5.1 Adaptive Protection of Microgrid 70

3.5.2 Transmission Level Protection 71

3.5.3 Symmetrical Current Components Based Methods 72

3.5.4 Voltage Based Methods 72

3.5.5 External Devices for Manipulating the Fault Current Level 73

3.5.5.1 Fault Current Limiter 73

3.5.5.2 Fault Current Source 74

3.5.6 Harmonic Content Based Scheme 74

3.5.7 Travelling Wave Based Protection 75

3.5.8 Protection Schemes Feasible for IIG Based Microgrid 75

3.6 Moving Towards the Travelling Wave Based Protection Schemes 76

3.6.1 The Definition of the Travelling Wave 77

3.6.2 Boundary Features of the Travelling Wave Reflection..... 79

3.6.3 Main Issues in Applying the Travelling Wave Theory to Microgrid Protection 82

3.6.3.1 Sampling and Instrument 82

3.6.3.2 Line Type 83

3.6.3.3 Topology 84

3.6.4 Existing Protection Methods Based on the Travelling Wave Theory..... 85

3.6.4.1 Cross-correlation Function..... 85

3.6.4.2 Multi-channel Bandpass Filters 86

3.6.4.3 Wavelet Decomposition Filters..... 87

3.6.4.4 Mathematical Morphological Filters..... 92

3.7 Chapter Summary..... 95

3.8 References..... 96

4. An Enhanced Decentralized Control Scheme for the Multi-IIG Based Microgrid 105

4.1 Introduction..... 105

4.2 Conventional Droop Based Control..... 107

4.2.1 Droop Characteristics..... 108

4.2.2 Virtual Impedance and Its Limitations..... 113

4.3 Direct P/Q Controller to Achieve Good Operational Stability and Flexibility 115

4.3.1 Principle of Operation..... 115

4.3.2 Transition between Islanded and Grid-Connected Operation 117

4.4 Simulation Based Validation of the Controller's Performance in a Simple Network 120

4.4.1 Comparison of IIG's Transient Performance during Load Changes 122

4.4.2 Comparison of IIG's Operational Stability with Unbalanced Output Impedances 124

4.5 Systematic Validation of the New Control Scheme 128

4.5.1.1 Transient Performance during Load Step Change 129

4.5.1.2 Operational Stability under System Topology Change 131

4.5.1.3 Transient Performance during Operational Mode Transfer 133

4.5.1.4 Wide-area Angle Synchronization 136

4.6 Chapter Summary 137

4.7 Chapter References 138

5. Travelling Wave Based Protection Using Mathematical Morphology 141

5.1 Introduction 141

5.2 Underlying Principles of the New Protection Scheme 142

5.2.1 Single-end Method 143

5.2.2 Double and Multi-end Method 144

5.2.2.1 Wide-Area Comparison of the Time Information 145

5.2.2.2 Comparison of Waveform Polarities at the Same Busbar 146

5.2.2.3 Overall Strategy of the New Primary Protection Scheme 147

5.3 Comparison of the Signal Processing Techniques for the Travelling Wave Based Protection 149

5.3.1 Critical Discussion on the Applicability of the DWT Technique to the Proposed Protection Scheme 150

5.3.1.1 Choice of Mother Wavelet 151

5.3.1.2 The Choice of the Level of DWT Decomposition 153

5.3.1.3 Polarity Detection Using DWT 156

5.3.1.4 Signal Denoising Using DWT 158

5.3.2 Development and Analysis of a New MM Based Technique 162

5.3.2.1 Choice of Feature-Extraction MMFs and Corresponding SE 162

5.3.2.2 Polarity Detection Using MMF 165

5.3.2.3 Signal Denoising Using MM Technology 167

5.3.2.4 Analysis of the Application of Multi-Resolution MMFs 170

5.3.2.5 Multi-resolution Feature-extraction MMF 171

5.3.2.6 Multi-resolution Signal-denoising MMF 173

5.4 Chapter Summary 175

5.5 Chapter References 177

6. Modelling, Simulation and Analysis – Fault Behaviour and Systematic Verification of the New Protection Scheme 179

6.1 Introduction 179

6.2 System Configuration for the New Protection Scheme 180

6.3 Verification of the Low Fault Current Contribution from an IIG 182

6.4 Validation of the Performance of the Proposed Protection Scheme 184

6.4.1 CASE 1 – External Fault outside the Microgrid 185

6.4.2 CASE 2 – Internal Fault in the Ring Network 186

6.4.3 CASE 3 – Internal Fault at a Line Equipped with Single-end Measurement 187

6.5 Validation of the Sensitivity and Stability 190

6.5.1 Impact of Fault Inception Angle and Fault Resistance 190

6.5.2 Impact of Sampling Frequency 193

6.5.3 Impact of Earthing Arrangement 194

6.5.4 Impact of Signal Noise 196

6.5.5 Stability under Non-fault Transient Disturbances 197

6.5.6 Performance under Connection with Synchronous Machine 199

6.6 Potential Hardware Implementation 200

6.7 Chapter Summary 200

6.8 Chapter References 201

7. Conclusions 203

7.1 Conclusions and Contributions 203

7.1.1 Development of an Enhanced Control Scheme for Multi-IIG Based System 204

7.1.2 A Systematic Protection Scheme Based on Traveling Wave Theory Using Mathematical Morphology 206

7.2 Future work 209

Appendix A: The parameters of the underground cable 211

List of Figures

Figure 2-1: Multi-level microgrid control schematic 19

Figure 2-2: Single phase circuit diagram of one IIG 24

Figure 2-3: Block diagram of a simple PLL circuit 26

Figure 2-4: Sinusoidal pulse-width modulation 27

Figure 2-5: The equivalent block diagram of (2-12) and (2-13) and their corresponding controllers 29

Figure 2-6: Control block diagram of the current based controller for a single grid-connected inverter [5] 31

Figure 2-7: Control block diagram of the nested controller for a single standalone inverter [5] 32

Figure 2-8: 3C Control Strategy of multi-inverter based system [29] 35

Figure 2-9: Master-slave Control Strategy of multi-inverter based system [31] 35

Figure 2-10: Current Distribution Programming Control Strategy of multi-inverter based system [24] 37

Figure 3-1: Coordination of overcurrent protection in a radial distribution network 61

Figure 3-2: Basic connections of IIG [10] 65

Figure 3-3: Classification of protection schemes for IIG based microgrids 76

Figure 3-4: A mini PI section of the lump model under single phase view 77

Figure 3-5: Wave reflection at the boundary in a system 79

Figure 3-6: The spectrum of reflection factor of the line boundary with varied busbar capacitance 81

Figure 3-7: The DWT decomposition tree 89

Figure 4-1: A brief diagram of the multi-IIG based system 105

Figure 4-2: A brief diagram of a single IIG 108

Figure 4-3: The P-ω/Q-V droop characteristics of the decoupled power 111

Figure 4-4: The implementation of the virtual impedance for conventional droop control [7-8] 113

Figure 4-5: The block diagram of the conventional droop controller with virtual impedance 114

Figure 4-6: The block diagram of the proposed direct P/Q control 116

Figure 4-7: The implementation of the virtual impedance for direct P/Q control ... 117

Figure 4-8: Control diagram of the voltage and phase angle synchronization 119

Figure 4-9: Overall block diagram of the proposed mode flexible control..... 119

Figure 4-10: a simple two-IIG network for control study..... 120

Figure 4-11: Comparison of IIG behaviour with fixed impedance load..... 123

Figure 4-12: Comparison of IIG behaviour with fixed power load 123

Figure 4-13: Comparison of IIG behaviour with motor starting..... 124

Figure 4-14: Transient performance under load step change using the conventional controller with different virtual inductance..... 126

Figure 4-15: The response of the conventional controller to the change of length of output feeder..... 127

Figure 4-16: The response of the direct P/Q controller to the change of length of output feeder..... 127

Figure 4-17: Benchmark mirogrid system model simulated to test the overall component controller 128

Figure 4-18: The active and reactive power sharing performance of four IIGs through the microgrid system under load step changes..... 131

Figure 4-19: Active and reactive power sharing performance of the new controller during system topology change with (1~6s) and without (6s~10s) virtual impedance 132

Figure 4-20: Comparison results of the active and reactive power sharing performance during system topology change from meshed network to radial network. 133

Figure 4-21: Active and reactive power sharing performance of four IIGs in a meshed 20KV microgrid system during mode transfer 135

Figure 4-22: Angle synchronization of IIG1 and IIG4 at 1s and 1.1s respectively . 136

Figure 4-23: Output power response of IIG4 with different time deviation of the starting angle synchronization from other IIGs. 137

Figure 5-1: Lattice diagram for a fault at F..... 142

Figure 5-2: Meshed network with identical parallel 146

Figure 5-3: The overall protection logic diagram of the new protection scheme 148

Figure 5-4: A simple two-end network with a fault in the middle..... 150

Figure 5-5: The modulus maxima with different mother wavelets..... 153

Figure 5-6: The error of the reconstruction with different mother wavelets..... 153

Figure 5-7: The modulus maxima of the detailed coefficients with different levels of DWT decompostion 155

Figure 5-8: The polarity detection under different level of DWT decomposition... 157

Figure 5-9: The signs with different fault locations from both ends using DWT.... 157

Figure 5-10: Signal denoising using five levels of DWT decomposition..... 160

Figure 5-11: The corresponding transient feature extraction of denoised signals using DWT decomposition..... 161

Figure 5-12: The comparison of MMFs (OCDF and DEDF) for extraction of fault transients..... 163

Figure 5-13: The transient features extracted by different length of SE at sampling rate of 1MHz (a) and 200kHz(b)..... 164

Figure 5-14: DEDF response comparison..... 166

Figure 5-15: Signal polarity at different fault locations using DEDF..... 167

Figure 5-16: Signal denoising using three different MMFs (DEDF, OCMF, OCCOMF)..... 168

Figure 5-17: The corresponding transient feature extraction of denoised signals using different MMFs..... 169

Figure 5-18: The denoised signal by different lengths of SE (3,30,60)..... 170

Figure 5-19: The pyramid of multi-resolution morphological analysis..... 172

Figure 5-20: SDEDF analysis under two level of decomposition..... 173

Figure 5-21: The basic theory of SOCCOMF..... 173

Figure 5-22: Signal denoising using SOCCOMF..... 174

Figure 5-23: The corresponding transient feature extraction of denoised signals using SOCCOMF..... 175

Figure 6-1: Single phase diagram of CIGRE 20kV benchmark microgrid system with three fault locations..... 180

Figure 6-2: Fixed current limiter of the IIG 182

Figure 6-3: The fault behaviour of IIG under three different types of faults: (a) ABC fault; (b) AB fault; (c) AG fault. 183

Figure 6-4: The detection of initial travelling wavefronts throughout the microgrid under CASE 1. 185

Figure 6-5: The detection of initial travelling wavefronts throughout the microgrid under CASE 2 186

Figure 6-6: The detection of initial travelling wavefronts throughout the microgrid under CASE 3 187

Figure 6-7: Peak value of the traveling wavefront according to different fault impedances and fault inception angles (islanded operation)..... 191

Figure 6-8: Peak value of the traveling wavefront according to different fault impedances and fault inception angles (grid connected operation). 192

Figure 6-9: Time and polarity information of the extracted initial wavefronts from IT54 and IT35 with different sampling frequencies 194

Figure 6-10: The PCC implemented with a Y-G-Y-G interface transformer. 195

Figure 6-11: Detection of wavefronts after OCCOMF based noise-reduction (POW = 90˚) 196

Figure 6-12: Detection of wavefronts after OCCOMF based noise-reduction (POW = 5˚) 197

Figure 6-13: The responses of MM based protection scheme to non-fault system disturbances..... 198

Figure 6-14: The responses of MM based protection scheme under Connection with Synchronous Machine 199

List of Tables

Table 2-1: Control strategies for IIG control in a microgrid..... 22

Table 2-2: A summary of different centralized control methods for multi IIGs..... 45

Table 4-1: Power droop with different output impedance 112

Table 4-2: Parameters of the two-IIG based network model 121

Table 4-3: Load parameters of the 20kV MV microgrid model 130

Table 4-4: The load condition settings for transient performance assessment during mode transfer..... 134

Table 5-1: The number sequence of the corresponding mother wavelet 152

Table 6-1: Results Using MM Based Protection Scheme Under Different Fault Scenarios. 188

Table 6-2: Results of a main-grid fault with POW = 90° and a Yg-Yg interface transformer between microgrid and main grid. 195

List of Abbreviations, Symbols & Nomenclatures

The following are the abbreviations, symbols and nomenclatures used throughout this thesis.

Abbreviations

3C	Circular Chain Control
AC	Alternate Current
AG	Phase A to Ground Fault
AB	Phase A to Phase B Fault
ABC	Three Phase Symmetrical Fault
CB	Circuit Breaker
CCF	Cross-Correlation Function
CERTS	Consortium for Electric Reliability Technology Solutions
CHP	Combined Heat and Power
CT	Current Transformer
CVT	Capacitive Voltage Transformer
DC	Direct Current
DEDF	Dilation-Erosion Difference Filter
DEMF	Dilation and Erosion Median Filter
DER	Distributed Energy Resources
DFIG	Doubly-Fed Induction Generator
DWT	Discrete Wavelet Transform

FCL	Fault Current Limiter
FCS	Fault Current Source
GPS	Global Positioning Signal
HF	High-pass Filter
HIF	High Impedance Fault
HV	High Voltage
IED	Intelligent Electronic Device
IIG	Inverter Interfaced Generator
IT	Instrument Transformer
LC	Load Condition
LF	Low-pass Filter
LOM	Loss-of-Mains
LV	Low Voltage
MGCC	Micogrid Control Centre
MM	Mathematical Morphology
MMF	Mathematical Morphological Filter
MV	Medium Voltage
NRF	Natural Reference Frame
OCCOMF	Open-Close and Close-Open Median Filter
OCDF	Opening-Closing Difference Filter
OCMF	Open and Close Median Filter
PCC	the Point of Common Coupling
PI	Proportional-Integral
PLL	Phase-Locked Loop
POW	Point-on-Wave
PR	Proportional-Resonant

R/X	Resistance/Reactance
RMS	Root Mean Square
RRF	Rotating Reference Frame
SDEDF	Series of Dilation-Erosion Difference Filter
SOCCOMF	Series of Open-Close and Close-Open Median Filter
SE	Structural Element
SNR	Signal-to-Noise Ratio
SPWM	Sinusoidal Pulse-Width Modulation
SRF	Stationary Reference Frame
VT	Voltage Transformer
WFT	Windowed Fourier Transform
WT	Wavelet Transform

Symbols

*	Reference Value
ˆ	A Stored Window of Data
$\oplus$	Dilation Function in MM Technology
$\ominus$	Erosion Function in MM Technology
$\circ$	Open Function in MM Technology
$\bullet$	Close Function in MM Technology
$\downarrow 2$	Down Sampling Operator by 2

Parameters

V_i, I_i	RMS Value of Inverter Inner Voltage and Current [V]

V_o, I_o	RMS Value of Inverter Output Voltage and Current [V]
V_{DC}	DC-link Voltage [V]
V_g	RMS Value of Grid Voltage [V]
v_{oa}, v_{ob}, v_{oc}	Three Phase Inverter Output Voltage [V]
v_{ia}, v_{ib}, v_{ic}	Three Phase Inverter Inner Voltage [V]
i_{oa}, i_{ob}, i_{oc}	Three Phase Inverter Output Current [A]
i_{ia}, i_{ib}, i_{ic}	Three Phase Inverter Inner Current [A]
$v_{o\alpha}, v_{o\beta}$	Clark Transformed Inverter Output Voltage Components [V]
$i_{o\alpha}, i_{o\beta}$	Clark Transformed Inverter Output Current Components [A]
v_{od}, v_{oq}	Park Transformed Inverter Output Voltage Components [V]
v_{id}, v_{iq}	Park Transformed Inverter Inner Voltage Components [V]
i_{od}, i_{oq}	Park Transformed Inverter Output Current Components [A]
i_{id}, i_{iq}	Park Transformed Inverter Inner Current Components [A]
L_f, C_f	Inverter Output Filter Inductance [H] and Capacitance [F]
ω_g	Grid Radial Frequency [rad/s]
ω	Inverter Radial Frequency [rad/s]
ω_0	Nominal Radial Frequency [rad/s]
V_0	Nominal Voltage [V]
e	Difference Between the Grid and Inverter Radial Frequency [rad/s]
φ	Inverter Reference Phase Angle [rad]

θ	Inverter Output Impedance Phase Angle [rad]
Z_{out}	Magnitude of Inverter Output Impedance [ohm]
Z_d	Magnitude of Virtual Impedance [p.u.]
R_d	Magnitude of Virtual Resistance [ohm]
L_d	Magnitude of Virtual Inductance [H]
$K_{p,PLL}, K_{i,PLL}$	Proportional and Integral Coefficient for Phase-Locked Loop Circuit
K_p	Droop Factor of P-ω Droop Controller [Hz/W]
K_q	Droop Factor of Q-V Droop Controller [V/VAr]
A_m	Amplitude of the Modulation Signal in SPWM [V]
A_c	Amplitude of the Carrier Signal in SPWM [V]
m_{index}	Modulation Index of SPWM
P_{out}, Q_{out}	IIG Output Active [MW] and Reactive [MVAr] Power
P_{local}, Q_{local}	IIG Local Active [MW] and Reactive [MVAr] Power Reference
f_1	Forward Component of the Travelling Wave
f_2	Backward Component of the Travelling Wave
μ	Travelling Velocity of the Travelling Wave [m/s]
Z_0	Characteristic Impedance [ohm]
k_V	Reflection Factor of the Voltage Travelling Wave
k_c	Reflection Factor of the Current Travelling Wave
C_s	Busbar Capacitance [F]
k_{safe}	The Safety Factor for Calculating the Least Sampling Frequency
ca	Approximated Component After DWT Decomposition
cd	Detailed Component After DWT Decomposition
w	The Mother Wavelet Signal

Z_1, Z_2	IIG Connecting Cable Impedance [ohm]
dP, dQ	Active Power [MW] and Reactive Power [MVAr] Difference between the Expected Average Power Output and the Actual Individual IIG Power Output
P_1, P_2	Active Microgrid System Loads [MW]
Q_1, Q_2	Reactive Microgrid System Loads [MVAr]
$Tpeak$	Time Stamps of the Travelling Wavefront [ms]
$Ppeak$	Polarity Information of the Travelling Wavefront
f_{dil}, f_{ero}	Dilation and Erosion Component after MM Processing
f_{cl}, f_{op}	Close and Open Component after MM Processing
$\rho^{\uparrow}, \sigma^{\uparrow}$	Approximate and Detailed Operator of SDEDF
n	Integer
T_s, f_s	Sampling Rate [s] and Sampling Frequency [Hz]
T_c	Travelling Time through a Cable [s]
ε	Threshold of Detecting the Lag or Lead Feature in MM Technology
M	Window Length of Structural Element

1. Introduction

1.1 Thesis Background

1.1.1 Electric Power System Operations

Distributed Energy Resources (DERs) are normally defined as any generation which is connected directly to the distribution network rather than to the transmission network. DERs including generators and energy storage cover many technologies ranging from traditional thermal generating units to the modern renewable energy resources. They are expected to be installed on a massive scale in the near future [1-2]. Conventional distribution network is usually designed to operate in a radial configuration, in which the power flow is uni-directional and the generation of power is determined by one or several large power utilities. The use of DERs will change the way energy is dispatched through the utility power grid, initiating a new level of freedom on the energy usage and delivery, and enabling more effective use of small renewable energy resources. The ability to exploit renewable energy with little pollution and potentially low costs is also attractive and gains increasing interests in many countries. Initially starting with the development of DER technologies, ranging from traditional power sources such as diesel generators to new technologies like microturbines, fuel cells, photovoltaics and wind turbines, there is a slight difference in goals between US and Europe. There are more concerns about the security of supply and operational reliability in US, where DERs are implemented in cases of emergency or in order to relieve the burden of transmission system and big thermal power plant. On the other hand, Europe is pushing for more renewable energy in order to meet the requirements of reduction in carbon emissions (CO_2).

While the application of DERs provides many potential advantages, the increasing penetration of different types of DERs brings new challenges for operating and controlling the network. Thereby in order to understand and resolve these challenges, studies have been conducted to either evaluate and reduce the influences without making large modification to the conventional protection and control of the

distribution system, or propose some new concepts for integrating the DERs into the grid with some controllable storage units and loads.

The DER impacts on the power system operation, control and protection have been reported in many technical publications. Al-Hinai et al [3], Sedghisgarchi et al [4] and Jurado et al [5] studied the effects of the fuel cells and microturbines on the power system stability. The large-scale integration of wind generation and its effect on the system stability have been studied in [6-9]. Studies on the grid integration of solar photovoltaic arrays can be seen in [10-12].

The microgrid is a new concept initially proposed in the USA [1] which is able to effectively control a cluster of DERs, storage units and loads. The microgrid concept introduces a way to connect the DERs to the distribution network in plug-and-play style, which partially addresses the operating and controlling challenge of high penetration of DERs. Microgrid can be formed at either LV or MV (1~33kV) levels; the structure of the microgrid is diverse according different requirements on the operation or topology arrangements.

1.1.2 Microgrid Definition and Structure

A microgrid is an aggregated network containing various types of small generators, loads and storage units used to support local loads in the electrical network of MV (1~33kV) or LV (<=1kV) level. The majority of the DERs and storage units are power converter interfaced and the whole microgrid system is controlled with flexibility to operate in either islanded or grid-connected mode. In normal operation, microgrid is connected to the utility side at a point of common coupling (PCC). It will not be disconnected unless utility outage happens or due to other serious concerns, e.g. deterioration of power quality. The structure of the microgrid is diverse according to different requirements on the operational or topology arrangements. To control and protect this kind of network, a tertiary central controller should be applied to PCC, which is also named as the microgrid control centre (MGCC). If microgrid contains multiple distributed resources,

communication channels are normally required to link them to each other, so that reliable and accurate control and protection schemes can be applied. Moreover, as the microgrid has two types of operational modes (islanded and grid-connected), and is characterised by high penetration of distributed resources, its fault current and voltage level is likely to vary significantly. Since traditional overcurrent protective schemes or even voltage restraint protective schemes are highly dependent on the current grading at one predetermined fault level, the protective system for microgrid need to be dramatically redesigned and the network should be treated as a quasi-transmission network.

1.1.3 Existing and Ongoing Microgrid Projects Worldwide

With regard to the microgrid experiences around the world, there are various microgrid implementations in the real power system or as test beds. Some of the experiments are run for purely R&D purposes, whereas others are deployed on islands for geographical and economic reasons.

1.1.3.1 USA

The most well-known and the earliest microgrid was proposed under the Consortium for Electric Reliability Technology Solutions (CERTS) in US, which was established in 1999 and dedicated to explore the influences upon the system operational reliability and efficiency of electricity markets under the new emerging generation and storage technologies, control and communication methods, system analysis tools and grid regulations. The benefits and issues of implementing DERs are recognized and revealed later on in 2002 in a white paper [13].

CERTS microgrid is physically achieved by building up the Dolan Technology Centre in Columbus Ohio. This test bed includes three 60kW synchronous machines, static switch and various switchgears and monitoring equipment. The up-to-date progress and information of this test bed can be referred online at http://certs.lbl.gov/.

Other projects based on the CERTS concept microgrid are conducted to develop necessary tools and equipment for running the microgrid. Two examples are the μGrid Analysis Tool from Georgia Institute of Technology, and the Distribution Energy Resources Customer Adoption Model (DER-CAM) developed at Berkeley Lab and other institutes worldwide. Targeted to analyse the microgrid with a broad scale of possible arrangements, μGrid Analysis Tool is designed to present the accurate physical features under various topology configurations, earthing arrangements, dynamic interaction with different components and particularly their control systems, and so on. It is worth noting that the design and control of power electronic interfaces have drawn great interest and effort in this project. DER-CAM, on the other hand is an optimized model with a number of adopted DERs, targeted to minimize the cost of operating on-site generators and CHP systems. The test bed for DER-CAM is built in a huge building in the southern part of California. However, it is to be noted that this project is still mainly based on a thermally energized system, only with a small penetration of PV DERs.

In the meantime in US, General Electric (GE) co-funds a project with US Department of Energy (DOE) aimed to develop a microgrid energy management (MEM) framework in order to provide a unified control, protection and energy management platform. This project is conducted through two phases. Phase I is focused on the investigation of the fundamental controls and energy management techniques. Phase II is dedicated to validate all these methods and technologies by both simulation and field test execution. In this project, the microgrid platform considers the renewable resources, where the operating costs and integration management of solar and wind energy are particularly studied and optimized.

Another example based on the idea of CERTs microgrid is at Northern Power and the National Renewable Energy Laboratory (NREL). NREL provides microgrid testing services for the Sacramento Municipal Utility District and Portland General Electric, US. In an early project, NREL provides a new switch technology from Cyberex and two 100kW CHP modules with inverter and droop control. Both projects investigate the influences from IIGs and interconnection transformers under faulty and normal conditions.

1.1.3.2 EU

In EU, National Technical University of Athens (NTUA) leads an initial program to study in-depth with the LV microgrids with a large scale integration of DERs. This project is supported by utilities and manufacturers all around Europe, which covers control, protection, grid regulations, communications, and laboratory demonstrations of microgrid systems. The achievement includes the new islanded and interconnecting operating philosophies, agent based hierarchical control strategies, earthing and protection schemes, and DER models plus steady-state and dynamic analysis tools. The test beds were built up in the labs of Germany, UK, France and Greece.

"More microgrids" is a follow-up European Commission project, with the full name of Advanced Architecture and Control Concepts for More Microgrids (http://www.microgrids.eu). This project aims at providing solutions to support the widespread deployment of microgrids, and covers a broad set of applications including protection, control, communication, economic and commercial evaluation, and standardization. EU demonstration sites are located widely in the Europe. These sites include the Kythnos island microgrid in Greece, Continuon's MV/LV facility in Netherland, MVV Residential microgrid in Germany, and others. The main generation technology in these microgrids is PV.

1.1.3.3 Other countries

The main reason for Japan to develop microgrids is that it can contribute to efficient operation of DERs and stabilize the power supply for customers. New Energy and Industrial Technology Development Organization (NEDO) started a series of research projects, in order to deal with the integration of renewable energy resources in the local microgrids [14]. Multiple field tests of microgrids are held in Aomori, Aichi, Kyoto, Sendai, and other places. These tests demonstrate the feasibility of the microgrids with incorporation of renewable energy in grid connected mode. Intentional islanding is only conducted during emergency. Later on, Japan's first demonstration project for isolated microgrid system for small islands was commenced in 2009. The on-going project, entrusted from Japan Ministry of

Economy, Trade and Industry, aims to promote the high penetration of renewable energy resources such as PV and wind turbines to achieve a low-carbon society and low-cost of electricity power supply.

About 60% of Russia's regions have no centralized electricity supply because of geographical reasons [15]. On behalf of APEC, Russia leads several microgrid projects mainly for remote and isolated areas. Two projects have been conducted: One is Prospects for Marine Current Energy Generation in APEC Region; the other is Piloting smart/micro grid projects for insular and remote localities in APEC economics.

Regarded a step to smart grid adoption, microgrids in Canada are more focused on the implementation at MV level. Projects related with the smart microgrids, as quoted, are managed by the CANMET Energy Technology Centre, funded by Technology and Innovation program of Natural Resources Canada (NRCan) and supported by over 10 research institutions, 8 utilities and 24 technology providers/end customers. Similar with other countries, the objective of these projects is also to develop the optimized operation, control, protection schemes based on the up-to-date communication and information technologies. The test bed is situated in BCIT campus with CHP microturbines and batteries based distributed storages. Field tests are further achieved in remote microgrids, grid-connected microgrids, microgrids which can be transferred between two modes.

Apart from the abovementioned projects, there are many more projects dealing with integration of high penetration of DERs. These projects might not be literally related to microgrid study, are nonetheless developing standards, methods, and technologies supporting microgrid deployment. IEEE Standards Coordinating Committee presents a draft guide for design, operation and integration of distributed resource islanded systems [16]. This document covers microgrids and intentional islands containing DERs connected to the electrical power systems.

1.2 Main Unresolved Issues and Research Objectives

With a great number of existing and ongoing projects and experiments, challenges and issues exist in the areas of microgrid control, protection and optimization [17].

Most of the DERs need to be connected to the network through power electronic interfaces, in particular through inverters. This type of DER is named as Inverter-Interfaced Generators (IIG). IIG control is therefore of significant importance in microgrid operation. The design of such control system requires a detailed analysis of IIG operation and response to different events in the microgrid. However, while there is a well-established body of work done for conventional network consisting of rotating machines (i.e. synchronous generators and induction generators), there is quite limited knowledge from widely accepted standards or guidelines for control and operation of the inverter based microgrid. Actually, the behaviour of the IIG under system faults or disturbances probably may vary significantly from one manufacturer to another. As a result, the first goal of the thesis is to investigate as well as realize the best potential control methods for multi IIG considering the fundamental requirements and features of a microgrid operation.

Moreover, existing control schemes for a network containing many IIG still suffer from one or multiple issues which have been demonstrated in some publications. For example, the line impedances among the IIGs impose a significant negative impact on the operational stability and power sharing performance; the mode transfer performance may suffer large transient voltage and current spikes due to the mode switch inside the hardware control circuit, therefore better mode transfer control is needed; power sharing performance of the IIGs needs to be improved without compromising good voltage and frequency regulation. Generally, to be noticed that high bandwidth communications are not desirable for reliability concern, there are few promising control schemes which can fully support “plug-and-play” requirement for DER performance: DER can be disconnected from the grid and reconnected to the grid with full flexibility and freedom. Hence in this thesis, another goal in this thesis is to identify a proper control scheme, which is feasible for a flexible IIG-

based microgrid system, suitable for varied modes of operation, system topologies, load conditions and operating points of inverter-based microgrid while also based on moderate communication assistance.

The introduction of DER and the formation of microgrids have a profound impact on the protection system at distribution level. Conventional time graded overcurrent principles can hardly satisfy the microgrid, because the microgrid has various operational modes, ever-changing power flow paths and fault current level caused by plug-and-play DER units and loads. The design of the protection scheme for an islanded IIG-based microgrid, in particular, requires extensive investigation on the IIG's special fault behaviour such as fault current contribution. Based on the new proposed controller in this thesis, it is also one of the important goals to evaluate the fault behaviour of IIG before introducing a systematic protection strategy. The ultimate goal of this thesis is to realize a systematic protection strategy suitable for an IIG-based microgrid. The validation process is based on simulation, incorporating with the developed IIG control technique.

Referring to the system optimization, it is always assumed to be the responsibility of the Energy Manager, where the tertiary control is installed. A hierarchical control concept is a widely favoured idea [2,18], where the secondary controller level is used to control the voltage/power target for optimized operation. There are also efforts in distributed optimizer by taking advantage of the local measurements, communications and controllers [19]. It needs to be noted that apart from technical issues, regulatory barriers that microgrid encounter to operate as legal entity still exist [20]. However these issues are out of the scope of this thesis. With the development of electricity market and microgrid technologies, these issues will be probably solved.

The overall objective of this thesis is to provide optimal solutions for both protection and control of an IIG based microgrid, where the control design is particularly important as it is actually the basis for further protection scheme design, test and validation. The main objectives of the thesis are therefore three folds:

1. The first goal is to investigate the features and requirements for multi IIG protection and control in a microgrid regime.
2. The second goal is to develop a control scheme catering for a flexible microgrid concept.
3. The third and final goal is to design a promising protection strategy for the IIG-based microgrids with both good stability and sensitivity.

1.3 Main Contributions

Two major contributions have been established by this thesis.

Firstly, an enhanced decentralized inverter control scheme predominantly dependent on local measurements only was developed for a MV microgrid system incorporating multi IIGs considering significant interconnection impedances. A hierarchical control strategy is established with focus on the primary control for IIGs.

Secondly a new communication assisted travelling wave based protection scheme was presented with the development of an enhanced signal processing tool – modified Mathematical Morphology (MM) technology. A new technique of signal polarity detection using MM is achieved using the apparent features from dilation and erosion waveforms. Several different Mathematical Morphological Filters (MMFs) were employed and modified for both accurate extractions of the high frequency travelling waves and proper noise-reduction of power system measurements.

1.4 Presumptions of the Work

The study carried out in this thesis is all based on software simulation using PSCAD/EMTDC and Matlab/Simulink. There are some presumptions listed as below:

1. The network model used for control and protection design is relatively ideal, with presumptions of identical cable materials and simplified cable parameters.
2. The IIG model is a detailed switching model with ideal constant source at the DC side, which represents a DER with good storage system.
3. All IIGs simulated in the network are identical with the same power ratings.
4. It is assumed that the microgrid has sound communication system in place, and the study of the communication technology is out of the scope of this thesis.
5. In consideration of system noise for validating the protection scheme, only white noise is considered.

1.5 Layout of the Thesis

Chapter 2 gives an introduction to the fundamentals of microgrid control system for IIG integration. Starting from the controller of a single IIG, this chapter investigates the basic principles of voltage and current control loops, phase-lock-loop (PLL) and pulse-width modulation (PWM) technique. Then this chapter moves on to the detailed studies in multi-IIG controller. A review of the existing control schemes for multi IIGs, not limited to microgrid application, helps outline the overall development and unsolved issues in the control system for a multi-IIG based network.

Chapter 3 investigates the impact of high penetration of different types of distributed generators on the fault current level. It was found that there are big restrictions on the utilization of the conventional overcurrent relays, especially for islanded IIG based system. Besides, a review of existing protection schemes for microgrid systems indicates the requirement of developing new protection algorithms or devices. Moving towards the design of the new protection scheme, critical discussions are made to clarify the advantages of the using travelling wave based protection, originally applied to the transmission level of system. Discussions are extended to the distribution level and microgrid systems, considering the special system features at distribution level including high resistive lines, topology and the earthing

arrangements. Based on this, minimum requirements on the choice of proper signal processing tools are defined for utilization of the travelling wave based protection scheme in microgrid system.

Chapter 4 develops a new control scheme for multi-bus IIG based micorgird system. This scheme is a decentralized method, developed from the idea of grid-connected controller, in which the active power is independently controlled by the active current in d-axis and the reactive power is controlled by the active current in q-axis. Compared to the conventional droop-based controller, this new scheme provides better voltage regulation and flexibility towards the varied lengths of connecting cables. Based on the wide-area synchronization technique, the control scheme is realized to be mode-adaptive without need of a mode switch. A systematic study using the benchmark MV microgrid system validates the feasibility of the new control scheme and demonstrates its advantages over the conventional control method.

In the first part of Chapter 5, an analysis of the present popular signal processing tools of Wavelets and Mathematical Morphology (MM) is presented. In the study of comparison between the two processing tools, it is shown that Wavelet Transform (WT) has poor directionality for polarity detection, inherent shift variance resulting in inconsistent time location through different levels of decomposition and obvious signal fluctuations after processing. Traditional MM, on the other hand, does not have the function of polarity detection. Based on this analysis, a new MM technique which can achieve good polarity detection is proposed, using apparent features of waveform erosion and dilation (fundamental algorithms of MM technique). In the second part of Chapter 5, a new MM based multi-end protection scheme using initial travelling wavefronts is developed. This method uses both time and polarity information of the travelling waves with moderate communication requirements, delivering dependable and secure performance under different system topologies and modes of operation. Moreover, based on a systematic design, two new protection schemes are proposed and implemented, in order to meet the requirements of more sophisticated system configurations and arrangements including, meshed network with parallel lines and remote feeders with only single-end instruments.

In order to combine the contributions on control and protection of the two previous chapters, Chapter 6 is dedicated to present a systematic validation for the overall protection performance. A modified MV IIG based microgrid model is developed in PSCAD/EMTDC based on the original CIGRE benchmark microgrid model. The model of IIG and underground cable are paid extensive attention since they are of significant importance for fault behaviour and corresponding fault transients' performance through the network. Applying the new control strategy to the system, the fault current level from IIGs is verified to be low and insufficient to activate the traditional overcurrent relays. Then based on this, the new protection scheme is verified in a systematic way, considering different types of faults, fault positions, and the impact of fault impedance, non-fault events and system noises.

The conclusions and future work are presented in Chapter 7.

1.6 List of Publications

The following publications are achieved in the conduct of the work contained in the thesis and during the whole period of Ph.D study.

- X. Li, A. Dysko, G. Burt, *Travelling wave based protection for inverter dominated microgrid using mathematical morphology*, IEEE Transaction on Smart Grid, 2014 (Accepted).
- X. Li, A. Dysko, *Hardware prototype and real-time validation of the satellite communication based loss-of-mains protection*, IET DPSP, Copenhagen, Denmark, 2014.
- X. Li, A. Dysko, G. Burt, *Enhanced mode adaptive decentralized controller for inverters supplying a multi-bus microgrid*, ISGT, Copenhagen, 2013.
- X. Li, A. Dysko, G. Burt, *Enhanced protection for inverter dominated microgrid using transient fault information*, IET DPSP, Birmingham, UK, 2012.
- I. Abdulhadi, X. Li, F. Coffele, P. Crolla. *International white book on DER protection: review and testing procedures*, DERlab, 2012.

- S. Loddick, U. Mupambireyi, S. Blair, C. Booth, X. Li, A. Roscoe, K. Daffey, and J. Watson, *The use of real time digital simulation and hardware in the loop to de-risk novel control algorithms*, in 2011 IEEE Electric Ship Technologies Symposium (ESTS), 2011, pp. 213–218.
- X. Li, A. Dysko, G. Burt, *Application of communication based distribution protection schemes in islanded systems* in UPEC 2010.

1.7 Chapter References

[1] R. Lasseter, A. Akhil, C. Marnay, J. Stephens, J. Dagle, R. Guttromson, A. S. Meliopoulous, R. Yinger, and J. Eto, "White Paper for Integration of Distributed Energy Resources - the CERTS Microgrid Concept", Consortium for Electric Reliability Technology Solutions, Apr 2002.

[2] F. Katiraei and M. R. Iravani, "Power Management Strategies for a Microgrid With Multiple Distributed Generation Units", IEEE Trans. Power Syst., vol 21, no 4, pp 1821–1831, 2006.

[3] A. Al-Hinai, K. Sedhisigarchi, and A. Feliachi, "Stability enhancement of a distribution network comprising a fuel cell and a microturbine", in IEEE Power Engineering Society General Meeting, 2004, 2004, pp 2156–2161 Vol.2.

[4] K. Sedghisigarchi and A. Feliachi, "Dynamic and Transient Analysis of Power Distribution Systems with Fuel Cells-Part II: Control and Stability Enhancement", IEEE Trans. Energy Convers., vol 19, no 2, pp 429–434, 2004.

[5] F. Jurado, A. Cano, and J. Carpio, "Enhancing the distribution system stability using micro-turbines and fuel cells", in Transmission and Distribution Conference and Exposition, 2003 IEEE PES, 2003, vol 2, pp 717–722 vol.2.

[6] B. H. Chowdhury, H. T. Ma, and N. Ardeshna, "The challenge of operating wind power plants within a microgrid framework", in Power and Energy Conference at Illinois (PECI), 2010, 2010, pp 93–98.

[7] S. Bae and A. Kwasinski, "Dynamic Modeling and Operation Strategy for a Microgrid With Wind and Photovoltaic Resources", IEEE Trans. Smart Grid, vol 3, no 4, pp 1867–1876, 2012.

[8] J. W. Smith and D. L. Brooks, "Voltage impacts of distributed wind generation on rural distribution feeders", in Transmission and Distribution Conference and Exposition, 2001 IEEE/PES, 2001, vol 1, pp 492–497 vol.1.

[9] L. Meegahapola and D. Flynn, “Impact on transient and frequency stability for a power system at very high wind penetration”, in 2010 IEEE Power and Energy Society General Meeting, 2010, pp 1–8.

[10] D. Yan, S. Jianhui, and S. Yong, “A unified power controller for photovoltaic generators in microgrid”, in 2011 4th International Conference on Electric Utility Deregulation and Restructuring and Power Technologies (DRPT), 2011, pp 1121–1125.

[11] H. Kanchev, D. Lu, F. Colas, V. Lazarov, and B. Francois, “Energy Management and Operational Planning of a Microgrid With a PV-Based Active Generator for Smart Grid Applications”, IEEE Trans. Ind. Electron., vol 58, no 10, pp 4583–4592, 2011.

[12] M. Sechilariu, B. Wang, and F. Locment, “Building Integrated Photovoltaic System With Energy Storage and Smart Grid Communication”, IEEE Trans. Ind. Electron., vol 60, no 4, pp 1607–1618, 2013.

[13] N. Hatziargyriou, H. Asano, R. Iravani, and C. Marnay, “Microgrids: An Overview of Ongoing Research, Development, and Demonstration Projects”, http://cleanenergysolutions.org, pp 78–94, 2007.

[14] T. Funabashi and R. Yokoyama, “Microgrid field test experiences in Japan”, in IEEE Power Engineering Society General Meeting, 2006, 2006, p 2 pp.–.

[15] K. V. Suslov, “A microgrid concept for isolated territories of Russia”, in 2012 3rd IEEE PES International Conference and Exhibition on Innovative Smart Grid Technologies (ISGT Europe), 2012, pp 1–5.

[16] “IEEE Draft Guide for Design, Operation, and Integration of Distributed Resource Island Systems with Electric Power Systems”, IEEE P15474D11 March 2011, pp 1–55, 2011.

[17] R. H. Lasseter, “MicroGrids”, in IEEE Power Engineering Society Winter Meeting, 2002, 2002, vol 1, pp 305–308 vol.1.

[18] Y. Zoka, H. Sasaki, N. Yorino, K. Kawahara, and C. C. Liu, “An interaction problem of distributed generators installed in a MicroGrid”, in Proceedings of the 2004 IEEE International Conference on Electric Utility Deregulation, Restructuring and Power Technologies, 2004. (DRPT 2004), 2004, vol 2, pp 795–799 Vol.2.

[19] A. Costabeber, T. Erseghe, P. Tenti, S. Tomasin, and P. Mattavelli, “Optimization of micro-grid operation by dynamic grid mapping and token ring control”, in Proceedings of the 2011-14th European Conference on Power Electronics and Applications (EPE 2011), 2011, pp 1–10.

[20] T. E. Del Carpio Huayllas, D. S. Ramos, and R. L. Vasquez-Arnez, “Microgrid Systems: Current Status and Challenges”, in Transmission and Distribution

Conference and Exposition: Latin America (T D-LA), 2010 IEEE/PES, 2010, pp 7–12.

2. Challenges, Issues and Overview of Microgrid Control with IIG Integration

2.1 Introduction

As introduced in Chapter 1, control is one of the most critical elements in determining the introduction of the microgrid concept to the utility grid and its wide acceptance. The main objective of microgrid control is to continuously supply power to the loads regardless of the changes in the utility system. Starting from the summary of requirements for microgrid operation and control, the first part of this chapter is dedicated to investigate the general structure of the microgrid control system and the main challenges of the microgrid control. In general, microgrids are established based on distributed control and can operate in either grid-connected mode or islanded mode. Typically, microgrids are formed by interconnection of small modular generation, storage devices and controllable loads. This structure imposes a number of issues related to the microgrid regime, including individual DER stability and operational challenges, coordination difficulty between the multi-technologies based DER controllers, power sharing management and smooth mode transfer challenges between islanded and grid-connected conditions.

Since most of the small scale DERs are power electronics interfaced generators, this chapter introduces the basic principles and development of IIG control methods. It has been briefly mentioned in Chapter 1 that IIG has a significant impact on microgrids in terms of power sharing accuracy, voltage and frequency regulation, and harmonic distortion. In order to have a better understanding of this, the basic components for controlling an individual IIG are presented in this chapter, including PLL circuit, modulation circuit, inner control loops and mode-switch circuit for operational mode transfer.

Discussion is then extended to the control of parallel IIGs or multi IIG connected to different busbars. Multi-IIG control is a much more complicated topic which has withdrawn numerous interests from the researchers. Based on a literature review of

the relevant field, the thesis outlines the major technologies used in an inverter dominated system and the unsolved issues and challenges, providing the knowledge basis for the development of the proper control scheme in Chapter 4.

2.2 Microgrid Operational Features, Control Structure and Challenges

2.2.1 Microgrid Operational Features and Requirements

In general, during normal operation a microgrid should be connected to the utility at a point of common coupling (PCC), in which way it performs as a controllable aggregated load or a virtual plant for the utility grid. The microgrid will only be running in an autonomous mode in case of emergency, when the utility grid suffers a blackout or the microgrid itself is in some geometrically isolated places. For a grid-connected microgrid, autonomous operation is realized by opening the static switch at PCC. Once the microgrid is isolated from the utility grid, the generation, storage units and management asset in the microgrid are responsible for maintaining the voltage and frequency as well as proper load sharing among the generation and storage units, i.e. proportional power output according to their power capacity. Therefore appropriate load sharing or load management is one of the main operational features of the microgrid. Another feature of the microgrid is to ensure stable operation during system faults and various network disturbances. The microgrid is able to maintain the stability during the external fault and isolate the internal faulty area in a relative short period. Other operational features of the microgrid are integration of wide variety of generation, storage units and loads with flexible operation supporting plug-and-play function as discussed in [1-9].

Particularly, the control of most of the DERs and loads in the microgrid is required to present a certain degree of intelligence – it shall not only satisfy the power demand of the microgrid but also possess the following special characteristics:

1) The microgrid should be mainly based on local measurement, or with requirements of only moderate communications, which enables plug-and-play capability of the generation, storage and load units, catering for the concept of a flexible microgrid [10].
2) It is preferable to have the same control circuit and hardware for all different modes of operation, in order to avoid significant voltage and current distortions during the transition periods.
3) The microgrid should have the stable and fast operation irrespective of types of loads, load amount variations and network topology changes. It requires a certain degree of toleration of harmonics generated by nonlinear loads and new technology based DERs.
4) It is necessary to provide black start capability.
5) Good voltage and frequency control needs to be guaranteed for all time of microgrid operation.

2.2.2 Microgrid Control Structure

The level of decentralization of the microgrid control can be varied, ranging from centralized control, partially centralized control to fully decentralized control. However, the fully decentralized control, or distributed control, is preferred since it provides effective solutions for a number of specific operational problems. For example, centralized control introduce additional cost and safety issues, and it is not regarded as reliable for primary control system to be dependent on communications; moreover, some generation, storage and load units are far from the control centre and private holders may not be happy to listen to the central command. On the other hand, fully distributed control can hardly maintain the voltage and frequency to the nominal value in an islanded network. Hence, the control system for a microgrid is normally designed as a multi-level structure, which is based on partially centralized control. The generalized structure and potential control schematic of a microgrid are shown in Figure 2-1. In this figure, it can be seen that at least two levels of control are required in a reliable microgrid: fully distributed primary DER, storage and load control, and energy manager or optimization operator as a tertiary control [1-2].

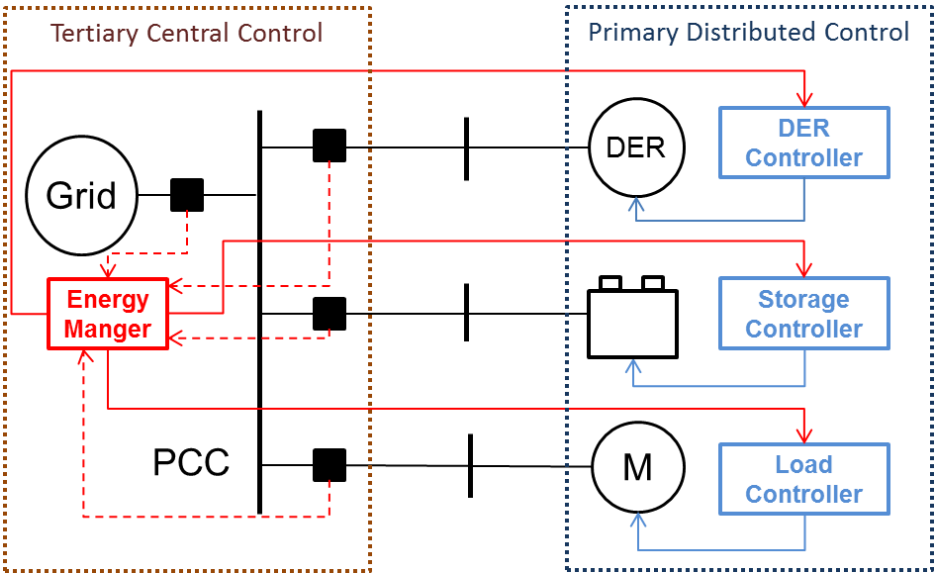

Figure 2-1: Multi-level microgrid control schematic

Primary DER controller is one of the basic components of the microgrid control infrastructure. It regulates the power output from each DER and sometimes voltage and frequency at each interface (i.e. during islanded operation or under significant system disturbances). This controller is required to respond in milliseconds to disturbances and load changes without relying on high bandwidth communications. In addition to these control functions, smooth and reliable transfer between the islanded mode and grid-connected mode is another important function for this control level, which is normally achieved through low bandwidth communications. Voltage and angle resynchronization philosophies and techniques must be studied by the designers of microgrids to determine appropriate approaches.

Tertiary central controller, in other words, central energy manager, provides operational control of the microgrid through dispatch of power, voltage and/or frequency set points to each DER, storage and controllable load unit. The set points can be calculated using power flow algorithms or by personal operators. The main objective is to ensure the voltage and frequency around nominal value, power balance of demand and supply, and optimization of the microgrid operation [3]. The

centralized tertiary control only requires low bandwidth communication, and is designed to communicate with the loads, generators and storage units [2, 4]. This controller is required to respond in minutes and maximize the operational efficiency of the DER and insure that the microgrid satisfies the utility side regulation.

2.2.3 Microgrid Control Challenges

The main challenges of microgrid control are actually imposed by integration of variety of the DER technology. Most of the DERs require DC to AC or AC to DC to AC converters as interface between an AC network and the DER. Storage devices, as an indispensable part of microgrid for effective usage of energy and voltage regulation are also generally interfaced by power electronic converters [11-12]. All research on power electronic converters such as inverter control can, therefore, be linked to the microgrid research field.

In a power system, the converters can provide reactive power, voltage support, and even power quality management that traditional synchronous machines cannot achieve. However, the introduction of converters requires much more complicated control system and the converter behaviour has not yet been standardized or fully investigated. With no available clear standards or widely accepted practice for controlling the IIG based network, IIG controllers are versatile with absolutely different behaviour and transient responses in the power system compared to the control of traditional rotating machines. The main challenges are listed as follows:

1) Unlike traditional rotating machines, IIGs do not necessary contribute system inertia. But inertia is essential for maintaining the system frequency regulation and stability under system disturbances such as load changes and transient fault situations.
2) The IIG control’s objective in grid-connected mode is different from that in islanded mode, as shown in

3)

4) Table 2-1. In the grid-connected mode, the IIG can run in either the current/power following way (output current or power are directly feed forwarded to the control loops as references), or the definite current/power exporting or importing way (additional current or power references are assigned to the control loops from the energy manager). While in the islanded mode, the IIG must be able to actively regulate the voltage and the frequency of the local system. In order to achieve a smooth and reliable transfer between the islanded and the grid-connected mode, most of the existing IIG controllers are often equipped with a hardware control switch, or named as mode-switch. This is, however, not friendly for practical implementation because switching on the control circuits and devices might cause significant transient voltage and current spikes [13]. In addition, it might also shorten the using age of the IIG control circuit.
5) Power or load sharing management is another big challenge for multi-IIG control. Control schemes based on high bandwidth communication channels carrying the real-time voltage, current and power information to each IIG or a central controller is a widely accepted solution but not cost-effective or reliable [14]. It is of course beneficial to implement a decentralized wireless controller with no or moderate low bandwidth communications. The most popular decentralized control scheme for load sharing is the droop control. However, the infamous droop regulation has its inherent issues which will be discussed in the next few sections.
6) Unequal inverter circuit and control parameters, output line impedances seen by the inverters and conflicting control schemes will cause circulating power/current among the IIGs. This circulating power/current is also a serious issue which undermines the overall stability of the system [15].

All these issues and challenges will be discussed in the following sections, with an overview of existing inverter control schemes.

Table 2-1: Control strategies for IIG control in a microgrid

	Grid-connected mode	**Islanded mode**
Primary DER control	Current/Power following	Voltage and frequency control
Tertiary control	Power sharing accuracy	Power sharing accuracy

There are two major types of microgrids: one is to serve as a backup system normally imports energy from the utility side, or just generates enough energy for local loads; the other one is an exporting system which generates more energy than that locally consumed. The former type of microgrid is normally regarded as having fewer challenges than the latter one in that, the exporting microgrid is more sensitive to the separation (nuisance separation especially) from the utility side, as this causes over-frequency and overvoltage damaging the local devices within the microgrid.

2.3 Basic Principle of Single IIG Control

2.3.1 Control Reference Frame

In case of a three-phase AC power system, three phase voltage and/or current signals are normally transformed to a reference frame for easier control. Three reference frames can be used to achieve the IIG control: the Natural Reference Frame (NRF) abc using the original three phase components, the Stationary Reference Frame (SRF) $\alpha - \beta$ using the equation presented in (2-1), or the Rotating Reference Frame (RRF) $d - q$ as described in (2-2).

$$\begin{bmatrix} x_\alpha \\ x_\beta \end{bmatrix} = \sqrt{\frac{2}{3}} \cdot \begin{bmatrix} 1 & -\frac{1}{2} & \frac{1}{2} \\ 0 & \frac{\sqrt{3}}{2} & -\frac{\sqrt{3}}{2} \end{bmatrix} \cdot \begin{bmatrix} x_a \\ x_b \\ x_c \end{bmatrix} \quad (2\text{-}1)$$

$$\begin{bmatrix} x_d \\ x_q \end{bmatrix} = \begin{bmatrix} sin\,\omega t & cos\,\omega t \\ -cos\,\omega t & sin\,\omega t \end{bmatrix} \cdot \begin{bmatrix} x_\alpha \\ x_\beta \end{bmatrix} \quad (2\text{-}2)$$

The idea of control in NRF is to have an individual controller for each phase; however, it needs to consider different configurations under different IIG interface transformer connections, i.e. delta, star with or without isolated neutral, etc. Under delta or isolated neutral connections, the IIG's three phases interact to each other; while in the third condition, the IIG's three phases have to be treated separately. From this point of view, control in either SRF or RRF has less complexity than the control in NRF, which is only based on two axis. The two transforms of SRF control and RRF control are named as Clark Transform and Park Transform respectively.

In an AC power system, control in RRF is generally preferred to that in SRF. The main reason of this is due to the fact that dq components in RRF are dc signals, which can be easily controlled with zero steady state error under widely used Proportional-Integral (PI) control. Control in SRF, on the other hand, requires more complicated Proportional-Resonant (PR) controllers, which is not very cost-effective. Hence, in this thesis, all the designed controllers are in RRF. However, it needs to be noted that different from the control in RRF, control in SRF is advantaged in selective harmonic compensation without requiring excessive computational resources. There are existing publications [16-19] studying the controllers in SRF, which have declared themselves to be more advantageous in unbalanced or harmonic operations.

2.3.2 Components of the IIG controller

In order to explain the basic principles of controlling a single three-phase IIG, a single phase diagram of an IIG connected to the grid is used as shown in Figure 2-2. The diagram contains three parts of a typical IIG: An inverter powered from a DC source, output power filter and interface transformer. From this figure, four measurements can be obtained from the point of filter inductance and filter capacitance: I_o, V_o, I_i, V_i, and will be used for presenting the principle equations.

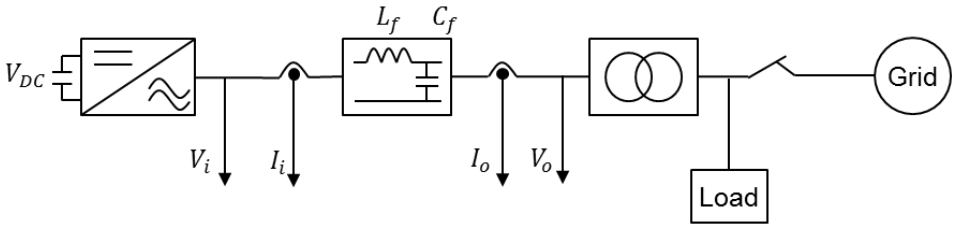

Figure 2-2: Single phase circuit diagram of one IIG

2.3.2.1 Phase-locked Loop

A phase-locked loop (PLL) is a control system that generates an output signal whose phase is synchronized with the phase of the input signal. In the microgrid control, IIG's phase angle is synchronized with the network using PLL applied to the voltage measurements from the connecting bus.

If ω_g is the radial frequency of the grid and ω is the radial frequency of the IIG, the PLL controller is to minimize the difference between the two frequencies by taking the indicator as presented in (2-3).

$$e = (\omega_g - \omega)t \tag{2-3}$$

If the indicator e is sufficiently small the above equation can be approximated by (2-4).

$$e \approx sin(\omega_g - \omega)t = sin\,\omega_g t\,cos\,\omega t - cos\,\omega_g t\,sin\,\omega t \tag{2-4}$$

Since the three-phase output voltage of one IIG can be defined as:

$$\begin{aligned} v_{oa} &= V_o\,cos(\omega_g t) \\ v_{ob} &= V_o\,cos(\omega_g t - 120°) \\ v_{oc} &= V_o\,cos(\omega_g t - 240°) \end{aligned} \tag{2-5}$$

The corresponding real and imaginary parts of the output voltage vector in SRF can be written as:

$$\begin{aligned} v_{o\alpha} &= V_o\,cos\,\omega_g t \\ v_{o\beta} &= V_o\,sin\,\omega_g t \end{aligned} \tag{2-6}$$

Substituting (2-6) into (2-3), the indicator can be rewritten as show in

$$e \approx \frac{v_{o\beta}}{V_o} cos\,\omega t - \frac{v_{o\alpha}}{V_o} sin\,\omega t \tag{2-7}$$

In order to get a sufficiently small e, a PI controller can be used. The basic algorithm of this PI controller can be written as below, where $K_{p,PLL}$ and $K_{i,PLL}$ stand for the parameters of proportional and integrator units respectively.

$$\omega = (K_{p,PLL} + \frac{K_{i,PLL}}{s}) \cdot e \tag{2-8}$$

Based on the above equations, a block diagram displaying the functional components of a generic PLL can be established as shown in Figure 2-3. It is basically a closed loop frequency control system. In this figure, the feedforward frequency ω_0 is the nominal frequency: $\omega_0 = 100\pi$.

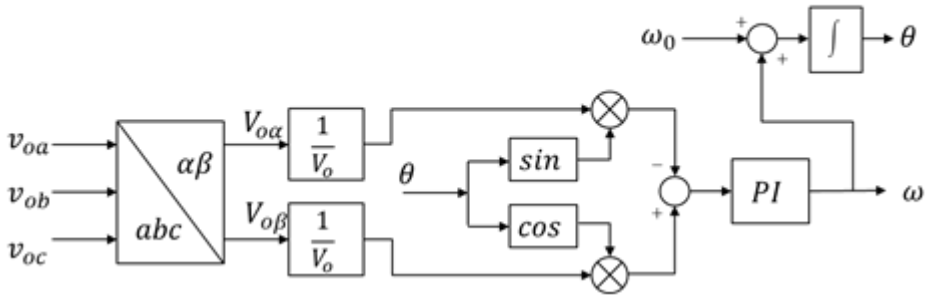

Figure 2-3: Block diagram of a simple PLL circuit

2.3.2.2 Modulation Scheme

Sinusoidal Pulse-Width Modulation (SPWM) is one of the most popular modulation techniques that provide the gate signal for switching of the power electronic valves. In the most straightforward implementation, generation of the desired output voltage is achieved by comparing the desired reference waveform (modulating wave) with a high-frequency triangular carrier wave as depicted schematically in Figure 2-4. The modulating signal is a sinusoid wave with the amplitude of A_m. The carrier signal is a triangular wave with the amplitude of A_c. The ratio $m = A_m/A_c$ is known as the modulation index. The carrier signal frequency is closely related to the switching frequency of an IIG, therefore, should be high enough to prevent noise contamination. In a three-phase system, it is advisable that the ratio of carrier frequency to modulating wave frequency is dividable by three.

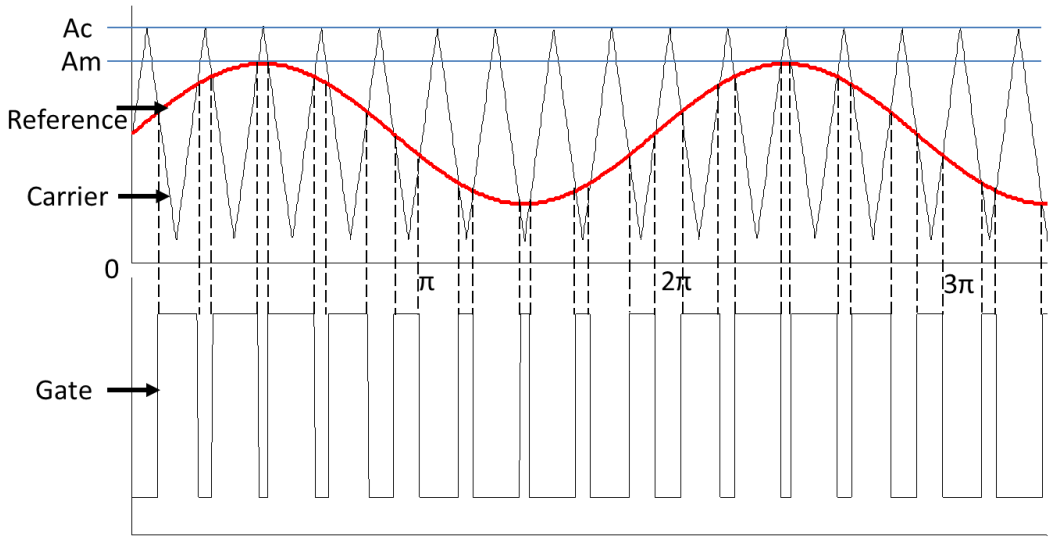

Figure 2-4: Sinusoidal pulse-width modulation

2.3.2.3 Voltage and Current Control Loop

Current and voltage are two basic control loops for IIG control, which are dedicated to produce the voltages fed into SPWM to generate the high frequency gating signals for driving the three-phase inverter. The principles of the two control loops are based on the electrical circuit equations. Based on the single phase diagram of the IIG with the output power filter as shown in Figure 2-2, the following equations can be obtained:

$$V_i = L_f \frac{dI_i}{dt} + V_o$$
$$I_i = C_f \frac{dV_o}{dt} + I_o \tag{2-9}$$

Considering three-phase measurements in an AC system, the following two equations can be easily obtained:

$$\begin{bmatrix} v_{ia} \\ v_{ib} \\ v_{ic} \end{bmatrix} = \begin{bmatrix} L_f & 0 & 0 \\ 0 & L_f & 0 \\ 0 & 0 & L_f \end{bmatrix} \begin{bmatrix} \dot{\imath}_{ia} \\ \dot{\imath}_{ib} \\ \dot{\imath}_{ic} \end{bmatrix} + \begin{bmatrix} v_{oa} \\ v_{ob} \\ v_{oc} \end{bmatrix} \tag{2-10}$$

$$\begin{bmatrix} i_{ia} \\ i_{ib} \\ i_{ic} \end{bmatrix} = \begin{bmatrix} C_f & 0 & 0 \\ 0 & C_f & 0 \\ 0 & 0 & C_f \end{bmatrix} \begin{bmatrix} \dot{v_{oa}} \\ \dot{v_{ob}} \\ \dot{v_{oc}} \end{bmatrix} + \begin{bmatrix} i_{oa} \\ i_{ob} \\ i_{oc} \end{bmatrix} \tag{2-11}$$

Applying the Clark and Park transform to (2-10) and (2-11), the variables used for controllers in RRF can be obtained, as shown in (2-12) and (2-13).

$$\begin{bmatrix} i_{id}^* \\ i_{iq}^* \end{bmatrix} = \begin{bmatrix} \frac{1}{L_f} & 0 \\ 0 & \frac{1}{L_f} \end{bmatrix} \begin{bmatrix} v_{id} - v_{od} \\ v_{iq} - v_{oq} \end{bmatrix} + \begin{bmatrix} 0 & \omega_0 \\ -\omega_0 & 0 \end{bmatrix} \begin{bmatrix} i_{id} \\ i_{iq} \end{bmatrix} \tag{2-12}$$

$$\begin{bmatrix} v_{od}^* \\ v_{oq}^* \end{bmatrix} = \begin{bmatrix} \frac{1}{C_f} & 0 \\ 0 & \frac{1}{C_f} \end{bmatrix} \begin{bmatrix} i_{id} - i_{od} \\ i_{iq} - i_{oq} \end{bmatrix} + \begin{bmatrix} 0 & \omega_0 \\ -\omega_0 & 0 \end{bmatrix} \begin{bmatrix} v_{od} \\ v_{oq} \end{bmatrix} \tag{2-13}$$

In these equations, v_{id} and v_{iq} are the inner voltages; i_{id} and i_{iq} are the inner currents; v_{od} and v_{oq} are the output voltages measured at the filter capacitance; i_{od} and i_{oq} are the output load currents; v_{od}^* and v_{oq}^* are the reference output voltages; i_{id}^* and i_{iq}^* are the reference active current and reactive current respectively, set up by following the actual power demand; v_{id}^* and v_{iq}^* are the reference voltages for the SPWM switching; C_f and L_f are the filter capacitance and inductance; ω_0 is the nominal frequency. The corresponding block diagrams of (2-12) and (2-13) are shown in the Figure 2-5 (a) and (b) respectively. Based on these blocks, the current controller and voltage controller can be easily established.

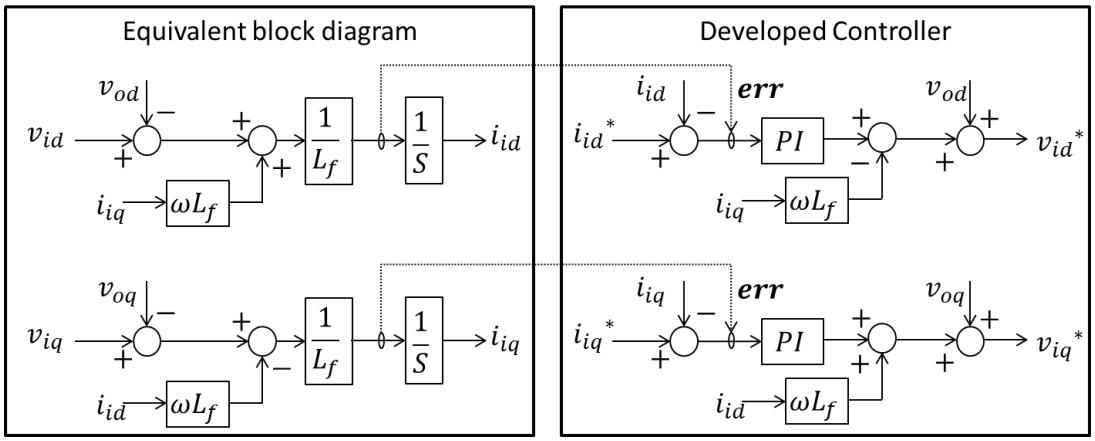

(a) Current controller development

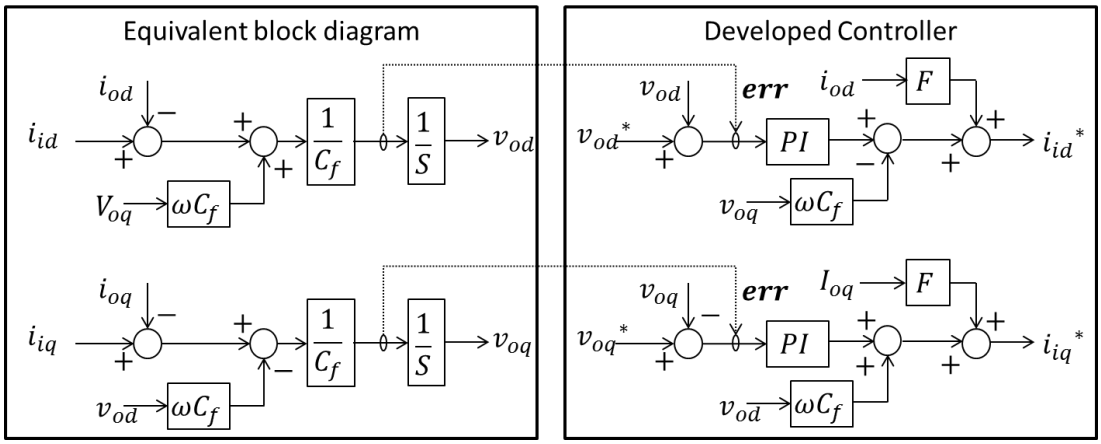

(b) Voltage controller development

Figure 2-5: The equivalent block diagram of (2-12) and (2-13) and their corresponding controllers

During the grid-connected operation, the main target of the IIG controller is to achieve the given power target or passively follow the grid power demand. For the latter type of operation, the power demand is calculated from the output voltage and output current. The output power as a function of output voltage and current is presented in (2-14) [20].

$$\begin{aligned} P_{out} &= v_{od} \cdot i_{od} + v_{oq} \cdot i_{oq} \\ Q_{out} &= v_{od} \cdot i_{oq} - v_{oq} \cdot i_{od} \end{aligned} \tag{2-14}$$

In actual system, the referencing angle for the Park transform of the voltage and current is in phase with V_{od}, hence V_{oq} is always kept close to zero. A simplified equation is established in (2-15).

$$\begin{aligned} P_{out} &= v_{od} \cdot i_{od} \\ Q_{out} &= v_{od} \cdot i_{oq} \end{aligned} \tag{2-15}$$

Since during normal operation, the d-axis voltage V_{od} is fixed to be near the nominal value, and the dq output currents I_{od} and I_{oq} actually dominate the IIG control. In this direct current controller, the reactive current I_{oq} is controlled to meet the reactive power demand and the active current I_{od} is controlled to meet the active power demand.

2.3.3 IIG Control under Grid-Connected Mode

The main objective of the grid-connected IIG control is to export a controlled amount of power into the grid. Considering that voltage is maintained by the grid, the grid-connected controller can be reduced to a simple current based controller [21]. In a passive current/power following mode, the reference currents are calculated directly from the output power and the connecting bus voltage magnitude. But the reference currents can also be generated based on the expected power demand and the connecting bus voltage magnitude. This expected power demand is normally obtained from the energy manager, which ensures corporation among the controllable units. As shown in Figure 2-6, a control block diagram of the basic current based controller is presented. The close-loop current controller allows good power demand tracking. It is to be noted that some standard components of the power electronics control are added to the simple current control loop: SPWM, PLL, decoupling control of the dq-axis components and feed-forward load current compensation for enhanced transient performance [8].

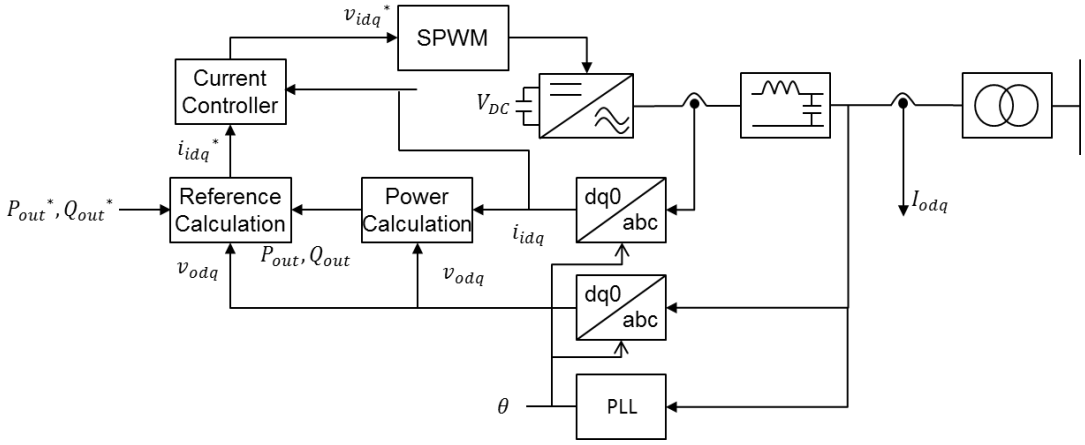

Figure 2-6: Control block diagram of the current based controller for a single grid-connected inverter [5]

However, the current based controller is disadvantaged in its lack of voltage control if the grid voltage is harmonically distorted. The low-pass filter for current references may lead to a distorted power output at frequencies related to the voltage harmonics. Hence in order to improve the voltage quality, in addition to the current based controller, a voltage controller is often applied to the outer of the current control loop to formulate a repetitive controller. Repetitive controller offers proper voltage harmonic damping performance and supports the nonlinear loads better. The harmonic components of the voltage at the filter capacitor are sensed and fed back to generate the current reference [22-23]. If it is allowed to provide DER voltage control, a control loop for full spectrum voltage can be used.

2.3.4 IIG Control under Islanded Mode

Different from the grid-connected IIG control, the objective for the islanded IIG control is mainly to support the network voltage and frequency. The simplest control for standalone IIG is the voltage based controller with a sine wave voltage reference generator, which provides the reference voltage magnitude and reference phase angle. However, there are short-comings to this approach, i.e. it lacks the limiter of the transient high currents.

The most popular alternative is the multi-loop or nested loop control. An inner current loop is included to quickly control the current and limit the transient current magnitude, and the outer voltage loop is added to give the current reference as well as regulate the output voltage to be the reference value. The control block diagram is presented in Figure 2-7. From the diagram, it can be seen that the nested controller is also based on a sine wave voltage reference generator which sets the system frequency. Furthermore, load currents are feed-forwarded to the current loop in order to improve the IIG's transient response to the load changes.

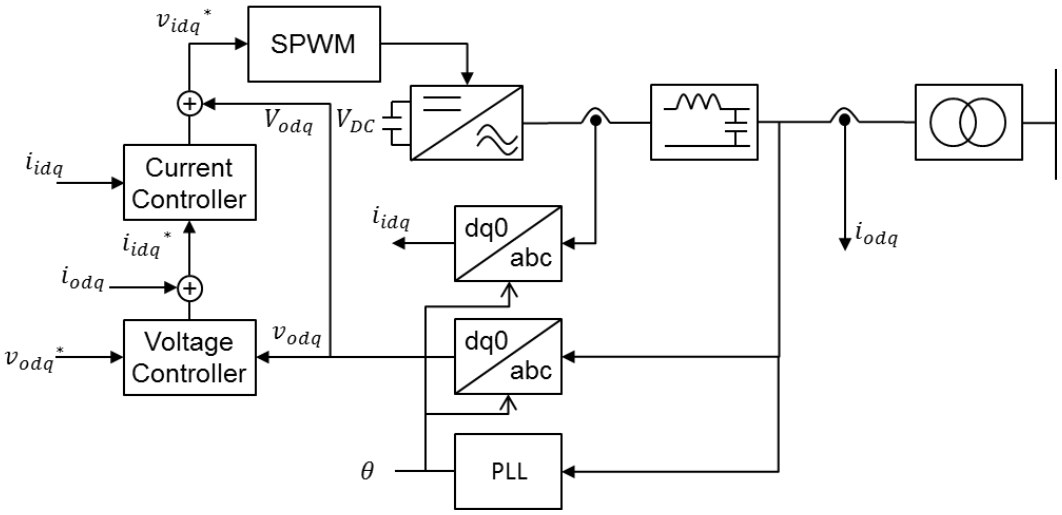

Figure 2-7: Control block diagram of the nested controller for a single standalone inverter [5]

2.4 Review of Existing Control Methods for Multi-IIG Based Microgrid System

The simplest method to connect two or more IIGs in parallel is to physically add an inductor at the output of the IIGs and control their output voltage magnitude to a fixed reference value. With the inductors, additional output impedances are physically introduced to the IIGs, which might consequently balance the output line impedances, output voltages and power. However, the inductors increase the size and cost of the whole system, and more importantly, they increase the power loss.

There are several challenges associated with the design of the multi-IIG controllers: they are expected to meet the islanded and grid-connected modes of operation; they should have sound power sharing performance under both linear and non-linear load condition; low communication request is highly demanded in rural networks with certain electrical distance between power sources; operational stability should be secured under the scenario of unbalanced output impedance in rural networks. The control schemes described in literature are generally designed to meet one or most of these expectations. During grid-connected operation, the voltage and frequency of each inverter are always maintained. Therefore, compared to that of islanded mode, the control of grid-connected multi-inverters is fairly simple, and the main challenges always lie in the islanded mode [24]:

1) Islanded inverters are quite sensitive to voltage and frequency disturbances. Harmonics caused by non-linear loads and switching activity of the inverters, or DC ripples from non-transformer interfaced inverters impose significant stability issues.
2) Output power balancing or load sharing control becomes more difficult since an inverter has relatively low overload capacity – only 150%~200% of the rating, otherwise it will result in damage of the power electronic components. However, with unequal connecting feeder impedances, accurate load sharing is difficult to achieve without communication assistance.
3) Varied configurations of inverter control and circuits available on the market add complexity to coordination and cause compatibility issues. One way of addressing this issue would be to standardize the inverter controller design in terms of expected performance.

Generally, the control schemes suggested in the literature for islanded operation can be categorized into two simple groups: centralized method and decentralized method. But to be noticed, this categorization is not strict at all, as some of the solutions have combined the two with either a hierarchical regime or a mixed regime. The hierarchical control schemes deploy decentralized architecture to the primary level of control, and centralized monitoring and control to the secondary/territory level of control [25]. The mixed control schemes deploy centralized principle to control

inverters in close proximity, and decentralized principle to control remotely connected inverters [26-27]. In the reminder of this chapter, a literature review of different centralized and decentralized control principles will be presented.

2.4.1 Centralized Control Principles of Islanded Multi IIGs

In the centralized control methods, the interfaces of all the IIGs are monitored and controlled in real-time to obtain a stable operation, proper power sharing and voltage/frequency regulation. The requirement for intercommunication links is mandatory for centralized control methods. They are also named as active load-sharing methods, since they offer active functionality on both current sharing and voltage regulation [28].

2.4.1.1 Circular Chain Current Programming

Wu et al propose a circular chain control (3C) strategy for inverters in parallel operation [29]. In this regime, inverters are arranged in a successive order, forming a circular chain, as shown in Figure 2-8. Each inverter module tracks the current of the previous inverter in order to achieve equal current distribution and the first inverter module tracks the one at the end of the chain; each inverter is responsible for its own voltage and frequency regulation by applying an inner current loop and an outer voltage loop. An alternative 3C control strategy uses a master module to control the voltage and others track the currents of the preceding modules, which can be included in the group of Master-slave control schemes as introduced in the next section [30]. This method is advantageous in its efficient use of control interconnections. However, problems occur if any of the inverters is damaged: the successive inverters will lose tracking reference and thus the control chain is broken.

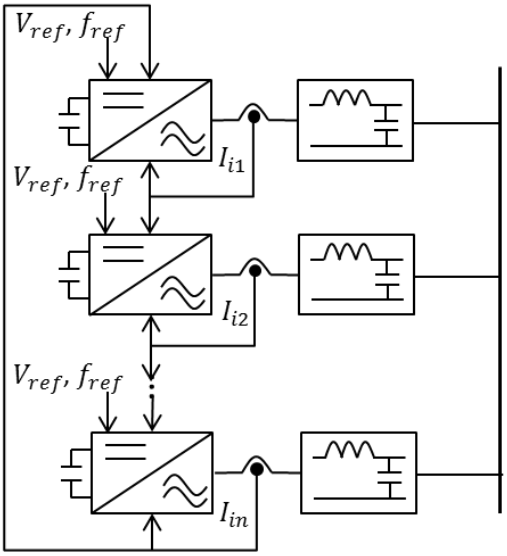

Figure 2-8: 3C Control Strategy of multi-inverter based system [29]

2.4.1.2 Master-slave

The basic idea of master/slave control methods is to pick-up one IIG (master) to control the voltage and frequency while other IIGs in the system (slaves) follow by operating as current sources [31-35]. Figure 2-9 presents a typical configuration of this control strategy.

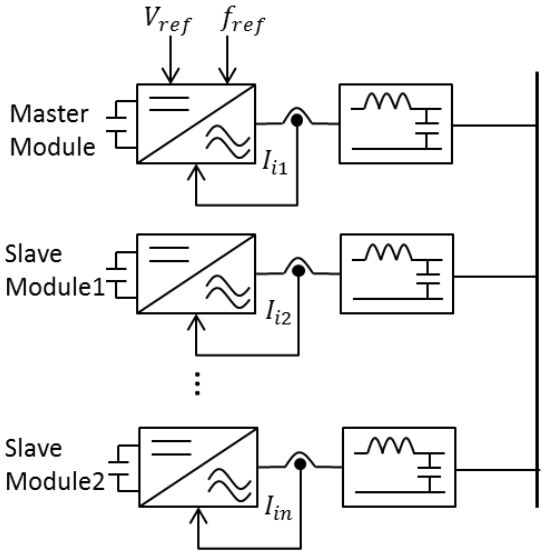

Figure 2-9: Master-slave Control Strategy of multi-inverter based system [31]

There are some variants to this group of methods. The master module is normally selected arbitrarily. The fixed master unit is responsible for both voltage and frequency regulation. The slave units can automatically follow the master unit without any current, frequency or phase angle references. The synchronisation between the slaves and the network can be realized through PLL. As an alternative, the master module can be also selected based on the real-time performance of the IIG. For example, the module that produces maximum power output is chosen to be the master module in [35], and a central power sharing controller is used to control and compensate the power deviation in the slave modules. In this way the master module is automatically chosen by the controller. Hence this type of control is also named as Auto-master/slave control. Unlike the previous type of master/slave method, this alternative strategy requires instantaneous communication of both voltage and current values.

In either type of the master/slave methods, the master unit takes the whole responsibility of the voltage and frequency regulation. In the grid connected mode of operation, the utility grid can be regarded as the master unit; while in the islanded mode, the DER with the largest power rating is normally chosen to be the master unit. Thus the master/slave methods intrinsically work for both grid-connected and islanded operation. However in practice, they may lead to large master current transients during system disturbances or mode transitions, especially in a large system where the master unit has to provide the transient demand from the whole system. Not only that, the high bandwidth of the communication link also introduces extra expenses and a time or phase delay between the output current of each slave unit might exist.

2.4.1.3 Current Distribution Programming

Among centralized methods, the current programming methods are the most popular ones [20, 24, 36-43]. The idea of controlling the inverters in parallel using current distribution control are initially proposed by [24, 36-37], as shown in Figure 2-10. Different from master/slave control scheme, there is no master unit in this method. The method requires a current sharing bus and reference synchronization for the voltage and frequency. The general assumption in this method is that stable and

relatively high communication bandwidth is available to communicate the relevant voltage/current/frequency signals. At the early development, limited by the switching frequency of the power electronics, the average root-mean-square (RMS) value of the output current or power is used to average the current from all inverter modules, and used as the reference for each module. This scheme can be simply implemented by using a single wire which carries the average current information. The average current information can be obtained either centrally or locally through analogue type computation using a resistor connected to the current sensor of each module, in which the resistor can be configured according to the power rating of individual inverter [38]. Kawabata et al averages output current by controlling the power deviation [24], whereas Lee et al [39] and Chen et al [40] use the current deviation.

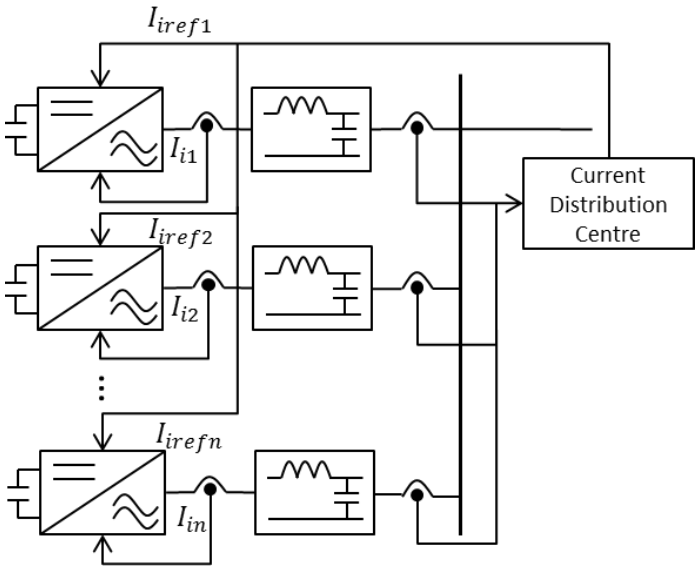

Figure 2-10: Current Distribution Programming Control Strategy of multi-inverter based system [24]

With development of the high speed switching technologies, instantaneous current sharing can be achieved. Xing et al [42] and Sun et al [20] provide good examples of the instantaneous current sharing method, followed by a detailed optimization process proposed in [43]. Moreover, in order to improve the performance of supplying nonlinear loads, frequency partitioned current sharing approach is proposed in [8]. In this way, each inverter module can take part in the voltage and

frequency regulation, as well as the current regulation. This ‘democratic’ feature allows the system to run in a reliable way regardless of the number of IIGs connected to the common bus – the failure of one IIG does not cause the whole microgrid to collapse. Moreover, it allows good performance of all the IIGs both in terms of load sharing and voltage regulation. The main disadvantage of this group of methods is the high request of the reliable communications.

The centralized control methods suffer from many issues in practice, for example:

1) Large expenses for the communication lines and supervisory control centre are required. Hence, it is difficult to apply in a highly distributed and large system.
2) The flexibility of connecting IIGs with a plug-and-play function is restricted, and the system’s redundancy is degraded.
3) The operational stability and performance are still affected by the unequal output impedances of the IIGs.

Recently effort has been made to improve the current distribution methods by considering the line impedance effect [44]. The effect of the line impedance is explored and an adaptive gain-scheduling approach is included to compensate for the line impedance mismatch.

2.4.2 Decentralized Control Principles of Islanded Multi IIGs

In order to avoid high capital expenditure and prevent low reliability in the microgrid operation, decentralized control methods are preferable in the primary control [45]. Regarding the decentralized control methods for islanded multi IIGs, the main principles utilized are based on the droop characteristics, which are able to avoid the need for communication channels. They are particularly attractive when the IIGs are located far away from each other. This allows cost-effective implementation of IIGs and provides flexibility of physical location of the modules. It also makes it easy to achieve control redundancy and avoids the complexity of system expansion and the

requirement of high reliability of a supervisory system. The droop characteristic is based on a well-known concept of a rotating machine performance, which presents drooping effect of frequency vs. active power and voltage vs. reactive power. By mimicking this effect, the islanded IIGs are able to support the grid with good operational stability and reliability.

Early papers have proposed the method based on P-ω/Q-V droop characteristics [24, 46-50], which are deducted from the power flow equations. The droop characteristics will be presented in details in Chapter 4. However, the standard conventional droop controllers have the following issues:

1) The methods ignore the effect of unequal line impedances and nonlinear loads. In the LV or MV distribution system, the lines are highly resistive and the resistance will challenge the power sharing controller's efficacy.
2) Operational stability is one of the issues when considering the line impedance effect and different ratings of inverters. In order to improve the power sharing accuracy, high droop gains are needed, which unfortunately bring a negative impact on overall stability of the system.
3) Besides, resistive part of the line also causes a coupling effect between the active and reactive power, which results in a coupled voltage and frequency droop characteristic. The traditional P-ω/Q-V droop characteristic is no longer feasible for this case.
4) Furthermore, the conventional droop controller exhibits relatively slow response since it requires low-pass filters to calculate the average power.
5) Last but not least, there is an inherent trade-off between the power sharing and the voltage/frequency regulation. The infamous droop regulation is obtained by associating a permissible error on the voltage and frequency values with real and reactive power values. Therefore a secondary control becomes inevitable, but presents a relatively slow response.

2.4.2.1 Harmonic Sharing with Nonlinear Loads

In order to feed the nonlinear loads, Tuladhar et al [51] decompose the measurements and associate control loops into different frequency components. As an alternative,

some publications [52-54] establish a dedicated harmonic droop control loop. It should be noted that abovementioned controller in NRF-frame can easily achieve this function. Besides, opposite voltage and frequency droop (P-V /Q-ω) associated with resistance decoupling is also an alternative to share power among nonlinear loads, since the resistive droop allows the inverter voltage to be actively adjusted by the inverter current which results in precise harmonic sharing [55-58].

2.4.2.2 Line Impedance Effect and Active/Reactive Power Decoupling

As mentioned above, resistive part of the line impedance imposes significant coupling effect between active power and reactive power, which affects the feasibility of conventional P-ω/Q-V droop characteristic.

It has been recommended in some literature that in LV high resistive network, the opposite P-V/Q-ω droop characteristics shall be utilized [55-60]. However, comparison results presented in [61] show that the conventional P-ω/Q-V has better compatibility with the existing rotating machines and also supports more accurate active power dispatch. Moreover, the opposite P-V/Q-ω droop does not eliminate the coupling effect between the active and reactive power, and negative impact on the operational stability and power sharing accuracy remains. Therefore, in this thesis, conventional P-ω/Q-V droop assisted with compensation is taken as the preferred control scheme.

Two alternative ways of compensating the active and reactive power coupling and unequal line impedance effects are based either on: (a) modification of the droop gains or (b) based on additional decoupling control loop. For the former method, Li et al [62] improve the power sharing accuracy by modifying the droop gains considering both the line impedance and the power ratings of the IIGs. Adaptive voltage droop scheme considering the line impedance is proposed by [63]. It configures the voltage reference of each inverter to be adaptively drooped to its active and reactive power outputs. This approach allows the reactive power sharing to be less affected by the real power control and output impedances. The later method (b), based on the active and reactive power decoupling algorithms, attracts more academic and industrial interest. In order to decouple the P and Q, solutions

found in literature are categorized into the following groups: active signal injection methods, virtual impedance methods, virtual frame methods.

Active signal injecting method **–** Tuladhar et al. [64] propose a method for decoupling active and reactive power by injecting a control signal into the network, and by drooping frequency of the control signals based on the measured reactive power. Similarly, He et al [65-66] improves the reactive power sharing accuracy through injecting small real power disturbances. In this way, the sharing performance is improved at the expense of reduced stability of the system.

Virtual impedance method **–** Chandorkar et al [67] use interface inductors to eliminate the active and reactive power coupling. Decoupling task can also be achieved by manipulating the output impedances using emulated 'lossless' resistor [55], inductance [68] or complex impedance [69]. This idea is then widely applied to the later innovative control schemes [28, 54, 60, 71-74]. Li et al [73] provide detailed investigation on the design of the virtual impedance. It proves that the standard virtual impedance based method needs careful design in terms of the virtual impedance based on the knowledge of the output impedance and inverter rating, or else, the operational stability of the whole network is at risk. Recently, as an enhanced solution, additional low-bandwidth communication signals of real and reactive power are used to mitigate the power sharing performance [53, 75-76].

Virtual frame method **–** Brabandere et al in [70] and [77] propose two other alternative solutions based on the virtual active/reacitve power or the virtual active/reactive currents, which only require the value of the R/X ratio of the line impedance. Later on Li et al in [78] and [79] propose a method based on virtual voltage/frequency frame, which avoids the complexity of design of the virtual impedance. Unfortunately, all these methods are restricted by the IIG rating and system allowed range of frequency and voltage regulation.

2.4.2.3 Transient response quality

The conventional droop based method exhibits very slow dynamic response. A great improvement in transient response is achieved by introducing power derivative-

integral terms into a conventional droop scheme [80-83]. The power derivative integral term has an adaptive gain which provides means of active damping of the low frequency power sharing oscillatory modes. In this way, the dynamic performance of the inverter can be adjusted without affecting the steady-state regulation requirements.

2.4.2.4 Stability assessment

Stability analysis is one of the major tasks of controller design. Normally, dynamic stability is validated through time-domain simulation [84-88]; the steady state stability, on the other hand, is usually validated through small signal analysis [48, 89-92].

The dynamic events in power system usually include operational mode transfers, faults, system topology changes, and abrupt load changes. Thus, a proper control scheme for microgrid system needs to be reliable for both grid-connected and islanded modes, and must not compromise the steady-state operational stability.

Small-signal stability is one of the important concerns when assessing the performance of a control system. Unlike well-established conventional power systems with standard synchronous machine models, small-signal model of a microgrid containing inverters and nonlinear loads need careful investigation. Once the small-signal model is formed, typically two stability analysis tools can be used, which are called root-loci analysis and bode plot analysis. Eigenvalues are identified which indicate the frequency and damping of the system's small-signal transient response. Ceolho et al [48] initially conducted small-signal analysis for parallel inverters, based on the assumption of ideal inverter models ignoring the inner PI control units. Pogaku et al [89] and [90] developed a systematic analysis tool for a larger network model consisted of both cables and loads, considering the detailed inverter control loops. Iyer et al [91] proposed a computational method to determine stability of a multi-inverter based microgrid. Katiraei et al [92] conducted the small signal analysis on a microgrid system consisted of both conventional rotating machines and inverter interfaced generators. Through small-signal analysis, the

factors affecting the steady state stability can be summarized as follows (similar study was also conducted in [88]):

Droop gain – It is found that droop gains play a significant role in the microgrid's steady state stability, in addition to the loading conditions and network parameters [89-95]. Although high gain of frequency/angle droop ensures accurate load sharing, it has a negative impact on the overall system stability. Moreover, frequency regulation constraint also puts a limit on the permissible range of the gain.

Inverter controller parameters – The stability is affected by the inverter controller and power filter parameters [8, 91-92, 96-97]. Essentially, frequency bandwidth of each layer of control needs careful arrangement in order to coordinate with the inverter switching frequency and the resonance frequency of the output power filter [8].

Network parameters – Network parameters such as the resistance/reactance (R/X) ratio of the connecting lines impose significant impact on stability due to real/reactive power coupling effect [28, 78, 84]. As mentioned in Section 2.4.2.2, power coupling effect brings negative impact on the system stability [79]. In order to realize decoupled power control and improve the system stability, a number of different enhanced droop control methods have been proposed [13, 54, 60, 70-79, 98].

2.4.2.5 Hierarchical control structure

The major advantage of a microgrid for the utility network is that it can be regarded as a controlled entity within the power system that can be operated as an aggregated load incorporating a cluster of distributed resources. However, based on the decentralized droop control scheme, it is difficult to maintain the voltage and frequency of each unit exactly at the nominal value. In practice, when inverters are controlled by droop characteristics, secondary control is required for restoring the voltage and frequency back to the nominal value. Although in some literature, as an alternative to frequency regulation, angle shift control is proposed instead [53, 55, 59, 70, 75, 77, 93, 99]. This solution provides a frequency control loop which does not require secondary restoration. Similarly Rowe et al [98] propose a new frequency

droop control based on the "Arctan power". These methods do not impose any deviation from nominal frequency in steady state condition. Lee et al [100] and [101] proposed P-ω/Q-V' droop control to also eliminate the voltage deviation. The method utilizes the rate of the change of voltage noted as V' as the drooped component.

However, for the majority of the droop based methods, frequency and voltage restoration is still needed. In order to meet this requirement, a hierarchical control regime is developed and becomes widely accepted in many publications. The hierarchical control in most of the publications [19, 80, 102-106] consists of three levels, including primary control (based on the droop method), secondary restoration control, and the tertiary control (for managing power flow at the top level). The primary control usually operates in real-time without any communication requirements; the secondary control is responsible for restoring the voltage and frequency back to the nominal value and operates in minutes; the tertiary control provides the modification of the droop gains or power reference settings, operates very infrequently (e.g. during large system transients) in the time scale of 15-20 minutes [105].

It is also of interest to report that in publication [25] three-level hierarchy is established through special physical arrangement: the DERs are connected to DC buses through DC/AC/DC or AC/DC converters; these DC buses are integrated into an AC bus through inverters; this AC bus is then connected to the utility grid. This physically arranged hierarchy provides good flexibility and reliability for IIG integration and control.

2.4.3 A Summary and the Issues of the Multi-IIG Control Methods

As a summarization the characteristics of all the discussed centralized control methods, Table 2-2 is presented.

Table 2-2: A summary of different centralized control methods for multi IIGs

Methods	Category	Disadvantages	Advantages
Circular chain current (3C)	Centralized	Hazard of breaking up the chain by one IIG's malfunction.	Efficient use of interconnections between the IIGs.
Current distribution	Centralized	Requirement of high communication bandwidth of current signals.	Fairly easy software programming; good voltage and frequency regulation and balanced power sharing performance.
Master-slave[1]	Centralized	Requirement of high communication bandwidth of voltage and current signals; potential imbalanced power sharing during transients.	Good voltage and frequency regulation and accurate steady-state power sharing performance.
Master-slave[2]	Decentralized	Hazard of losing the master unit.	Cost-effective arrangement and no need of communications.
Droop control	Decentralized	Trade-off between power sharing performance and voltage and frequency regulation; Large line impedance effect and power coupling.	Good flexibility of connecting IIGs in plug-and-play function and system expansion; easy to achieve control redundancy under hierarchical control design.

2.4.4 Control Strategy of Mode Transfer between Islanded and Grid-Connected Operation

During grid connected mode the control objective is determined according to load requirements and the availability of IIG capacity. However, in the case of islanding, the main control strategy is to maintain the voltage and frequency by adjusting power targets. Smooth transfer between islanded and grid-connected modes is challenging but crucial. There are major two types of control strategies for mode transfer: mode switch type and non-switch type. Traditionally, control schemes are designed in two distinct phases for two distinct operation modes [11]. However, in the light of growing interest in developing the flexible microgrid, non-switch based transfer regime is preferred since it prevents the switching process on the controller circuit which may cause current or voltage spikes and stability hazards [56].

2.4.4.1 Mode Switch Based Transfer

Mode switch based transition schemes are developed in [12, 47, 107-109]. Majumder et al [107] propose a seamless mode transfer by changing state feedback control to voltage control and vice versa. If islanded, the repetitive controller is switched to voltage control mode after detecting islanded operation; if reconnected to the utility grid, angle and voltage resynchronization is required, and voltage references are updated in the central controller to achieve proper voltage control. Serban et al [109] propose a control strategy based on a hybrid converter with integrated mode transfer switches and with different controllers in corresponding operational modes.

2.4.4.2 Non-mode Switch Transfer

Mode flexible controller is proposed by [13, 72, 85, 110]. Guerrero et al [13] and [72] developed a PI controller combined with conventional droop control for all modes of operation, in order to formulate a flexible microgrid. In this method, inverters always act as voltage sources. However, the power references require updates during mode transfer through low bandwidth communications, especially when the microgrid exports the power in to the utility. Kim et al [85] proposed a mode-adaptive control method which only needs reactive power information transmitted among inverters to

enhance reactive power sharing accuracy. The same controller circuits are used for full mode of operation. All these methods require certain level of low bandwidth communications for enhanced power sharing and regulation. Yao et al [110] presented a novel seamless transfer method for single-phase inverters based on the voltage and current nested controller. In this method, the reference voltage for each inverter is refreshed during mode transfer.

2.4.4.3 Resynchronization Process

In practice, before reconnection of the microgrid system to the utility grid, the voltage phasor and frequency at PCC shall be resynchronized to the connecting bus at the utility side. The synchronization block can be implemented as compensators on the original control loop of each IIG [25, 49, 66, 86, 101-111] or only of the nearest IIG to PCC [85, 112]. In the first case, the voltage magnitude error and phase angle error are sent to each IIG controller and fed to the real and reactive power droop control. In the second case, the nearest IIG needs to have the largest power capacity as a dominant power source [85], otherwise this IIG can become overloaded during the synchronization process. As a conclusion, in practice with many IIGs installed in the microgrid, the use of communications for wide-area synchronization is unavoidable [106]. Choi et al [111] propose an active synchronizing method based on the wide-area control of all DERs to adjust their frequency and voltage. The command of synchronization operation is sent from the control centre of the microgrid.

2.5 Chapter Summary

The content of this Chapter has served four purposes:

1) to give an overview of the operation features and many issues regarding the operation and control of microgrid;
2) to describe the basic principles of inverter control, including PLL, SPWM, voltage and current based control techniques, mode transition technique;

3) to investigate the existing control schemes for islanded multi-IIG based network with respect to the concerns of harmonic sharing, power sharing accuracy, stability, dynamic response, mode transfer performance and control schematic;
4) to highlight the need for more research into the study of multi-IIG control for flexible microgrid regime.

The literature review has revealed a research gap in the control of multi-inverter based microgrids with requirements of operational flexibility and stability. Although decentralized control schemes are preferable for cost saving concern and better reliability, there are always issues like the trade-off between voltage regulation and power sharing performance, the difficulty of achieving non-switch mode transfer control and good stability with relatively large distances inbetween the inverters.

In Chapter 4, a full investigation of the conventional droop based controller will be carried out and based on what a new control strategy will be proposed to improve the operational stability as well as achieve non-switch mode transfer control. The new control scheme will be designed to fit for different modes of microgrid operation, system topologies and load conditions.

2.6 Chapter References

[1] R. Lasseter, A. Akhil, C. Marnay, J. Stephens, J. Dagle, R. Guttromson, A. S. Meliopoulous, R. Yinger, and J. Eto, "White Paper for Integration of Distributed Energy Resources - the CERTS Microgrid Concept", Consortium for Electric Reliability Technology Solutions, Apr 2002.

[2] M. Agrawal and A. Mittal, "Micro Grid Technological Activities Across the Globe: a Review", International Journal of Research and Reviews in Applied Sciences, vol 7, pp 147–152, 2011.

[3] Y. Zoka, H. Sasaki, N. Yorino, K. Kawahara, and C. C. Liu, "An interaction problem of distributed generators installed in a MicroGrid", in Proceedings of the 2004 IEEE International Conference on Electric Utility Deregulation, Restructuring and Power Technologies, 2004. (DRPT 2004), 2004, vol 2, pp 795–799 Vol.2.

[4] J. A. Peas Lopes, C. L. Moreira, and A. G. Madureira, “Defining control strategies for MicroGrids islanded operation”, IEEE Transactions on Power Systems, vol 21, no 2, pp 916–924, 2006.

[5] T. C. Green and M. Prodanović, “Control of Inverter-based Micro-grids”, Electric Power Systems Research, vol 77, no 9, pp 1204–1213, 2007.

[6] Y. Li, D. M. Vilathgamuwa, and P. C. Loh, “Design, analysis, and real-time testing of a controller for multibus microgrid system”, IEEE Transactions on Power Electronics, vol 19, no 5, pp 1195–1204, 2004.

[7] R. H. Lasseter, “MicroGrids”, in IEEE Power Engineering Society Winter Meeting, 2002, 2002, vol 1, pp 305–308 vol.1.

[8] A. L. Dimeas and N. D. Hatziargyriou, “Operation of a Multiagent System for Microgrid Control”, IEEE Transactions on Power Systems, vol 20, no 3, pp 1447–1455, 2005.

[9] Y. Uno, G. Fujita, M. Matubara, T. Tsukui, R. Yokoyama, and T. Toyoshima, “Evaluation of Micro-grid Supply and Demand Stability for Different Interconnections”, in Power and Energy Conference, 2006. PECon ’06. IEEE International, 2006, pp 612–617.

[10] A. A. Zaidi and F. Kupzog, “Microgrid Automation - a Self-configuring Approach”, in Multitopic Conference, 2008. INMIC 2008. IEEE International, 2008, pp 565–570.

[11] T. S. Ustun, C. Ozansoy, and A. Zayegh, “Recent developments in microgrids and example cases around the world—A review”, Renewable and Sustainable Energy Reviews, vol 15, no 8, pp 4030–4041, 2011.

[12] C.-W. Chang and Y.-R. Chang, “Energy Storage Systems for Seamless Mode Transfer in Microgrid”, in 2011 IEEE Ninth International Conference on Power Electronics and Drive Systems (PEDS), 2011, pp 799–802.

[13] J. M. Guerrero, J. C. Vasquez, J. Matas, M. Castilla, and L. G. de Vicuna, “Control Strategy for Flexible Microgrid Based on Parallel Line-Interactive UPS Systems”, IEEE Transactions on Industrial Electronics, vol 56, no 3, pp 726–736, 2009.

[14] T. C. Green and M. Prodanović, “Control of Inverter-based Micro-grids”, Electric Power Systems Research, vol 77, no 9, pp 1204–1213, Jul 2007.

[15] M. Prodanovic and T. C. Green, “High-Quality Power Generation Through Distributed Control of a Power Park Microgrid”, IEEE Transactions on Industrial Electronics, vol 53, no 5, pp 1471–1482, 2006.

[16] R. Teodorescu, F. Blaabjerg, M. Liserre, and P. C. Loh, “Proportional-resonant Controllers and Filters for Grid-connected Voltage-source Converters”,

Electric Power Applications, IEE Proceedings -, vol 153, no 5, pp 750–762, 2006.

[17] K. T. Tan, P. L. So, and Y. C. Chu, “Control of parallel inverter-interfaced distributed generation systems in microgrid for islanded operation”, in 2010 IEEE 11th International Conference on Probabilistic Methods Applied to Power Systems (PMAPS), 2010, pp 1–5.

[18] M. Hamzeh, H. Karimi, and H. Mokhtari, “A New Control Strategy for a Multi-Bus MV Microgrid Under Unbalanced Conditions”, IEEE Transactions on Power Systems, vol 27, no 4, pp 2225–2232, 2012.

[19] M. Savaghebi, A. Jalilian, J. C. Vasquez, and J. M. Guerrero, “Secondary Control for Voltage Quality Enhancement in Microgrids”, IEEE Transactions on Smart Grid, vol 3, no 4, pp 1893–1902, 2012.

[20] X. Sun, Y.-S. Lee, and D. Xu, “Modeling, Analysis, and Implementation of Parallel Multi-inverter Systems with Instantaneous Average-current-sharing Scheme”, IEEE Transactions on Power Electronics, vol 18, no 3, pp 844–856, 2003.

[21] I. J. Balaguer, Qin Lei, Shuitao Yang, U. Supatti, and Fang Zheng Peng, “Control for Grid-Connected and Intentional Islanding Operations of Distributed Power Generation”, IEEE Transactions on Industrial Electronics, vol 58, no 1, pp 147–157, Jan 2011.

[22] J. Liang, T. C. Green, G. Weiss, and Q.-C. Zhong, “Evaluation of Repetitive Control for Power Quality Improvement of Distributed Generation”, in Power Electronics Specialists Conference, 2002. pesc 02. 2002 IEEE 33rd Annual, 2002, vol 4, pp 1803–1808.

[23] M. J. Ryan and R. D. Lorenz, “A High Performance Sine Wave Inverter Controller with Capacitor Current Feedback and ‘Back-EMF’ Decoupling”, in , 26th Annual IEEE Power Electronics Specialists Conference, 1995. PESC ’95 Record, 1995, vol 1, pp 507–513 vol.1.

[24] T. Kawabata and S. Higashino, “Parallel operation of voltage source inverters”, IEEE Transactions on Industry Applications, vol 24, no 2, pp 281–287, 1988.

[25] Z. Jiang and R. A. Dougal, “Hierarchical Microgrid Paradigm for Integration of Distributed Energy Resources”, in 2008 IEEE Power and Energy Society General Meeting - Conversion and Delivery of Electrical Energy in the 21st Century, 2008, pp 1–8.

[26] J. Liang, T. C. Green, G. Weiss, and Q.-C. Zhong, “Hybrid control of multiple inverters in an island-mode distribution system”, in Power Electronics Specialist Conference, 2003. PESC ’03. 2003 IEEE 34th Annual, 2003, vol 1, pp 61–66 vol.1.

[27] Y. Xu, H. Li, and L. M. Tolbert, “Inverter-based Microgrid Control and Stable Islanding Transition”, in 2012 IEEE Energy Conversion Congress and Exposition (ECCE), 2012, pp 2374–2380.

[28] J. M. Guerrero, L. Hang, and J. Uceda, “Control of Distributed Uninterruptible Power Supply Systems”, IEEE Transactions on Industrial Electronics, vol 55, no 8, pp 2845–2859, 2008.

[29] T.-F. Wu, Y.-K. Chen, and Y.-H. Huang, “3C Strategy for Inverters in Parallel Operation Achieving an Equal Current Distribution”, IEEE Transactions on Industrial Electronics, vol 47, no 2, pp 273–281, 2000.

[30] S. J. Chiang, C.-H. Lin, and C. Y. Yen, “Current Limitation Control Technique for Parallel Operation of UPS Inverters”, in Power Electronics Specialists Conference, 2004. PESC 04. 2004 IEEE 35th Annual, 2004, vol 3, pp 1922–1926 Vol.3.

[31] J.-F. Chen and C.-L. Chu, “Combination Voltage-controlled and Current-controlled PWM Inverters for UPS Parallel Operation”, IEEE Transactions on Power Electronics, vol 10, no 5, pp 547–558, 1995.

[32] J.-F. Chen, C.-L. Chu, and Y.-C. Lieu, “Modular Parallel Three-phase Inverter System”, in , Proceedings of the IEEE International Symposium on Industrial Electronics, 1995. ISIE ’95, 1995, vol 1, pp 237–242 vol.1.

[33] H. Van der Broeck and U. Boeke, “A Simple method for Parallel Operation of Inverters”, in Telecommunications Energy Conference, 1998. IN TEL EC. Twentieth International, 1998, pp 143–150.

[34] W.-C. Lee, T.-K. Lee, S.-H. Lee, K.-H. Kim, D.-S. Hyun, and I.-Y. Suh, “A Master and Slave Control Strategy for Parallel Operation of Three-phase UPS Systems with Different Ratings”, in Nineteenth Annual IEEE Applied Power Electronics Conference and Exposition, 2004. APEC ’04, 2004, vol 1, pp 456–462 Vol.1.

[35] Y. Pei, G. Jiang, X. Yang, and Z. Wang, “Auto-master-slave Control Technique of Parallel Inverters in Distributed AC Power Systems and UPS”, in Power Electronics Specialists Conference, 2004. PESC 04. 2004 IEEE 35th Annual, 2004, vol 3, pp 2050–2053 Vol.3.

[36] S. Ogasawara, J. Takagaki, H. Akagi, and A. Nabae, “A Novel Control Scheme of a Parallel Current-controlled PWM Inverter”, IEEE Transactions on Industry Applications, vol 28, no 5, pp 1023–1030, 1992.

[37] K. Siri, C. Q. Lee, and T.-F. Wu, “Current Distribution Control for Parallel Connected Converters. II”, IEEE Transactions on Aerospace and Electronic Systems, vol 28, no 3, pp 841–851, 1992.

[38] H.-M. Hsieh, T.-F. Wu, Y.-E. Wu, H.-S. Nien, and Y.-E. Wu, "A Compensation Strategy for Parallel Inverters to Achieve Precise Weighting Current Distribution", in Industry Applications Conference, 2005. Fourtieth IAS Annual Meeting. Conference Record of the 2005, 2005, vol 2, pp 954–960 Vol. 2.

[39] C. S. Lee, S. Kim, C. B. Kim, S. C. Hong, J. S. Yoo, S.-W. Kim, C. H. Kim, S. H. Woo, and S. Y. Sun, "Parallel UPS With a Instantaneous Current Sharing Control", in Proceedings of the 24th Annual Conference of the IEEE Industrial Electronics Society, 1998. IECON '98, 1998, vol 1, pp 568–573 vol.1.

[40] Y.-K. Chen, T.-F. Wu, Y.-E. Wu, and C.-P. Ku, "A Current-sharing Control Strategy for Paralleled Multi-inverter Systems Using Microprocessor-based Robust Control", in TENCON 2001. Proceedings of IEEE Region 10 International Conference on Electrical and Electronic Technology, 2001, vol 2, pp 647–653 vol.2.

[41] Z. He, Y. Xing, and Y. Hu, "Low Cost Compound Current Sharing Control for Inverters in Parallel Operation", in Power Electronics Specialists Conference, 2004. PESC 04. 2004 IEEE 35th Annual, 2004, vol 1, pp 222–227 Vol.1.

[42] Y. Xing, L. Huang, S. Sun, and Y. Yan, "Novel Control for Redundant Parallel UPSs with Instantaneous Current Sharing", in Power Conversion Conference, 2002. PCC-Osaka 2002. Proceedings of the, 2002, vol 3, pp 959–963 vol.3.

[43] X. Sun, L.-K. Wong, Y.-S. Lee, and D. Xu, "Design and Analysis of an Optimal Controller for Parallel Multi-inverter Systems", IEEE Transactions on Circuits and Systems II: Express Briefs, vol 53, no 1, pp 56–61, 2006.

[44] A. M. Roslan, K. H. Ahmed, S. J. Finney, and B. W. Williams, "Improved Instantaneous Average Current-Sharing Control Scheme for Parallel-Connected Inverter Considering Line Impedance Impact in Microgrid Networks", IEEE Transactions on Power Electronics, vol 26, no 3, pp 702–716, 2011.

[45] R. H. Lasseter, "Smart Distribution: Coupled Microgrids", Proceedings of the IEEE, vol 99, no 6, pp 1074–1082, 2011.

[46] M. C. Chandorkar, D. M. Divan, and R. Adapa, "Control of parallel connected inverters in standalone AC supply systems", IEEE Transactions on Industry Applications, vol 29, no 1, pp 136–143, Feb 1993.

[47] M. C. Chandorkar, D. M. Divan, and R. Adapa, "Control of Parallel Connected Inverters in Standalone AC Supply Systems", IEEE Transactions on Industry Applications, vol 29, no 1, pp 136–143, 1993.

[48] E. A. A. Coelho, P. C. Cortizo, and P. F. D. Garcia, "Small-signal Stability for Parallel-connected Inverters in Stand-alone AC Supply Systems", IEEE Transactions on Industry Applications, vol 38, no 2, pp 533–542, 2002.

[49] Y. Li, D. M. Vilathgamuwa, and P. C. Loh, “Design, Analysis, and Real-time Testing of a Controller for Multibus Microgrid System”, IEEE Transactions on Power Electronics, vol 19, no 5, pp 1195–1204, 2004.

[50] J. A. Peas Lopes, C. L. Moreira, and A. G. Madureira, “Defining Control Strategies for MicroGrids Islanded Operation”, IEEE Transactions on Power Systems, vol 21, no 2, pp 916–924, 2006.

[51] A. Tuladhar, K. Jin, T. Unger, and K. Mauch, “Parallel Operation of Single Phase Inverter Modules with No Control Interconnections”, in Applied Power Electronics Conference and Exposition, 1997. APEC ’97 Conference Proceedings 1997., Twelfth Annual, 1997, vol 1, pp 94–100 vol.1.

[52] U. Borup, F. Blaabjerg, and P. N. Enjeti, “Sharing of Nonlinear Load in Parallel-Connected Three-phase Converters”, IEEE Transactions on Industry Applications, vol 37, no 6, pp 1817–1823, 2001.

[53] M. N. Marwali, J.-W. Jung, and A. Keyhani, “Control of distributed generation systems - Part II: Load sharing control”, IEEE Transactions on Power Electronics, vol 19, no 6, pp 1551–1561, 2004.

[54] J. M. Guerrero, J. Matas, L. G. de Vicuña, M. Castilla, and J. Miret, “Wireless-Control Strategy for Parallel Operation of Distributed-Generation Inverters”, IEEE Transactions on Industrial Electronics, vol 53, no 5, pp 1461–1470, 2006.

[55] S. J. Chiang, C. Y. Yen, and K. T. Chang, “A Multimodule Parallelable Series-connected PWM Voltage Regulator”, IEEE Transactions on Industrial Electronics, vol 48, no 3, pp 506–516, 2001.

[56] C. K. Sao and P. W. Lehn, “Control and Power Management of Converter Fed Microgrids”, IEEE Transactions on Power Systems, vol 23, no 3, pp 1088–1098, 2008.

[57] H. Laaksonen, P. Saari, and R. Komulainen, “Voltage and Frequency Control of Inverter Based Weak LV Network Microgrid”, in 2005 International Conference on Future Power Systems, 2005, p 6 pp.–6.

[58] T. L. Vandoorn, B. Renders, B. Meersman, L. Degroote, and L. Vandevelde, “Reactive Power Sharing in an islanded microgrid”, in Universities Power Engineering Conference (UPEC), 2010 45th International, 2010, pp 1–6.

[59] R. Majumder, A. Ghosh, G. Ledwich, and F. Zare, “Load Sharing and Power Quality Enhanced Operation of a Distributed Microgrid”, IET Renewable Power Generation, vol 3, no 2, pp 109–119, 2009.

[60] J. M. Guerrero, J. Matas, L. G. de Vicuna, M. Castilla, and J. Miret, “Decentralized Control for Parallel Operation of Distributed Generation Inverters Using Resistive Output Impedance”, IEEE Transactions on Industrial Electronics, vol 54, no 2, pp 994–1004, 2007.

[61] A. Engler, “Applicability of Droops in Low Voltage Grids”, International Journal of Distributed Energy Resources, vol 1, no 1, 2005.

[62] Y. W. Li and C.-N. Kao, “An Accurate Power Control Strategy for Power-Electronics-Interfaced Distributed Generation Units Operating in a Low-Voltage Multibus Microgrid”, IEEE Transactions on Power Electronics, vol 24, no 12, pp 2977–2988, 2009.

[63] E. Rokrok and M. E. H. Golshan, “Adaptive voltage droop scheme for voltage source converters in an islanded multibus microgrid”, IET Generation, Transmission Distribution, vol 4, no 5, pp 562–578, 2010.

[64] A. Tuladhar, H. Jin, T. Unger, and K. Mauch, “Control of Parallel Inverters in Distributed AC Power Systems with Consideration of Line Impedance Effect”, IEEE Transactions on Industry Applications, vol 36, no 1, pp 131–138, 2000.

[65] J. He and Y. W. Li, “An Accurate Reactive Power Sharing Control Strategy for DG Units in a Microgrid”, in 2011 IEEE 8th International Conference on Power Electronics and ECCE Asia (ICPE ECCE), 2011, pp 551–556.

[66] J. He and Y. W. Li, “An Enhanced Microgrid Load Demand Sharing Strategy”, IEEE Transactions on Power Electronics, vol 27, no 9, pp 3984–3995, 2012.

[67] M. C. Chandorkar, D. M. Divan, Y. Hu, and B. Banerjee, “Novel Architectures and Control for Distributed UPS Systems”, in Applied Power Electronics Conference and Exposition, 1994. APEC ’94. Conference Proceedings 1994., Ninth Annual, 1994, pp 683–689 vol.2.

[68] A. Engler, “Control of Parallel Operating Battery Inverters”, presented at the PV Hybrid Power Systems, Germany, 2000.

[69] W. Yao, M. Chen, J. Matas, J. M. Guerrero, and Z. Qian, “Design and Analysis of the Droop Control Method for Parallel Inverters Considering the Impact of the Complex Impedance on the Power Sharing”, IEEE Transactions on Industrial Electronics, vol 58, no 2, pp 576–588, 2011.

[70] K. De Brabandere, B. Bolsens, J. Van den Keybus, A. Woyte, J. Driesen, and R. Belmans, “A Voltage and Frequency Droop Control Method for Parallel Inverters”, IEEE Transactions on Power Electronics, vol 22, no 4, pp 1107–1115, Jul 2007.

[71] K. . De Brabandere, B. Bolsens, J. . Van den Keybus, A. Woyte, J. Driesen, and R. Belmans, “A Voltage and Frequency Droop Control Method for Parallel Inverters”, IEEE Transactions on Power Electronics, vol 22, no 4, pp 1107–1115, 2007.

[72] J. C. Vasquez, J. M. Guerrero, A. Luna, P. Rodriguez, and R. Teodorescu, “Adaptive Droop Control Applied to Voltage-Source Inverters Operating in Grid-Connected and Islanded Modes”, IEEE Transactions on Industrial Electronics, vol 56, no 10, pp 4088–4096, 2009.

[73] J. He and Y. W. Li, “Analysis, Design, and Implementation of Virtual Impedance for Power Electronics Interfaced Distributed Generation”, IEEE Transactions on Industry Applications, vol 47, no 6, pp 2525–2538, 2011.

[74] J. He, Y. W. Li, J. M. Guerrero, J. C. Vasquez, and F. Blaabjerg, “An Islanding Microgrid Reactive Power Sharing Scheme Enhanced by Programmed Virtual Impedances”, in 2012 3rd IEEE International Symposium on Power Electronics for Distributed Generation Systems (PEDG), 2012, pp 229–235.

[75] R. Majumder, G. Ledwich, A. Ghosh, S. Chakrabarti, and F. Zare, “Droop Control of Converter-Interfaced Microsources in Rural Distributed Generation”, IEEE Transactions on Power Delivery, vol 25, no 4, pp 2768–2778, 2010.

[76] H. Liang, B. J. Choi, W. Zhuang, and X. Shen, “Stability Enhancement of Decentralized Inverter Control Through Wireless Communications in Microgrids”, IEEE Transactions on Smart Grid, vol 4, no 1, pp 321–331, 2013.

[77] K. De Brabandere, B. Bolsens, J. Van Den Keybus, A. Woyte, J. Driesen, R. Belmans, and K. U. Leuven, “A Voltage and Frequency Droop Control Method for Parallel Inverters”, in Power Electronics Specialists Conference, 2004. PESC 04. 2004 IEEE 35th Annual, 2004, vol 4, pp 2501–2507 Vol.4.

[78] Y. Li and Y. Li, “Decoupled Power Control for an Inverter Based Low Voltage Microgrid in Autonomous Operation”, in Power Electronics and Motion Control Conference, 2009. IPEMC ’09. IEEE 6th International, 2009, pp 2490–2496.

[79] Y. Li and Y. W. Li, “Power Management of Inverter Interfaced Autonomous Microgrid Based on Virtual Frequency-Voltage Frame”, IEEE Transactions on Smart Grid, vol 2, no 1, pp 30–40, 2011.

[80] Y. A.-R. I. Mohamed and A. A. Radwan, “Hierarchical Control System for Robust Microgrid Operation and Seamless Mode Transfer in Active Distribution Systems”, IEEE Transactions on Smart Grid, vol 2, no 2, pp 352–362, 2011.

[81] J. M. Guerrero, L. G. de Vicuna, J. Matas, J. Miret, and M. Castilla, “A Wireless Load Sharing Controller to Improve Dynamic Performance of Parallel-connected UPS Inverters”, in Power Electronics Specialist Conference, 2003. PESC ’03. 2003 IEEE 34th Annual, 2003, vol 3, pp 1408–1413 vol.3.

[82] J. M. Guerrero, L. G. de Vicuna, J. Matas, M. Castilla, and J. Miret, “A Wireless Controller to Enhance Dynamic Performance of Parallel Inverters in Distributed Generation Systems”, IEEE Transactions on Power Electronics, vol 19, no 5, pp 1205– 1213, Sep 2004.

[83] Y. A.-R. I. Mohamed and E. F. El-Saadany, “Adaptive Decentralized Droop Controller to Preserve Power Sharing Stability of Paralleled Inverters in

Distributed Generation Microgrids", IEEE Transactions on Power Electronics, vol 23, no 6, pp 2806–2816, 2008.

[84] M. B. Delghavi and A. Yazdani, "An Adaptive Feedforward Compensation for Stability Enhancement in Droop-Controlled Inverter-Based Microgrids", IEEE Transactions on Power Delivery, vol 26, no 3, pp 1764–1773, 2011.

[85] J. Kim, J. M. Guerrero, P. Rodriguez, R. Teodorescu, and K. Nam, "Mode Adaptive Droop Control With Virtual Output Impedances for an Inverter-Based Flexible AC Microgrid", IEEE Transactions on Power Electronics, vol 26, no 3, pp 689–701, 2011.

[86] M. A. Zamani, A. Yazdani, and T. S. Sidhu, "A Control Strategy for Enhanced Operation of Inverter-Based Microgrids Under Transient Disturbances and Network Faults", IEEE Transactions on Power Delivery, vol 27, no 4, pp 1737–1747, 2012.

[87] F. Katiraei, M. R. Iravani, and P. W. Lehn, "Micro-grid autonomous operation during and subsequent to islanding process", IEEE Transactions on Power Delivery, vol 20, no 1, pp 248–257, 2005.

[88] Z. Miao, A. Domijan, and L. Fan, "Investigation of Microgrids With Both Inverter Interfaced and Direct AC-Connected Distributed Energy Resources", IEEE Transactions on Power Delivery, vol 26, no 3, pp 1634–1642, 2011.

[89] E. Barklund, N. Pogaku, M. Prodanovic, C. Hernandez-Aramburo, and T. C. Green, "Energy Management in Autonomous Microgrid Using Stability-Constrained Droop Control of Inverters", IEEE Transactions on Power Electronics, vol 23, no 5, pp 2346–2352, 2008.

[90] N. Pogaku, M. Prodanovic, and T. C. Green, "Modeling, Analysis and Testing of Autonomous Operation of an Inverter-Based Microgrid", Power Electronics, IEEE Transactions on, vol 22, no 2, pp 613 –625, Mar 2007.

[91] S. V. Iyer, M. N. Belur, and M. C. Chandorkar, "A Generalized Computational Method to Determine Stability of a Multi-inverter Microgrid", IEEE Transactions on Power Electronics, vol 25, no 9, pp 2420–2432, 2010.

[92] F. Katiraei, M. R. Iravani, and P. W. Lehn, "Small-signal Dynamic Model of a Micro-grid Including Conventional and Electronically Interfaced Distributed Resources", IET Generation, Transmission Distribution, vol 1, no 3, pp 369–378, 2007.

[93] R. Majumder, B. Chaudhuri, A. Ghosh, R. Majumder, G. Ledwich, and F. Zare, "Improvement of Stability and Load Sharing in an Autonomous Microgrid Using Supplementary Droop Control Loop", IEEE Transactions on Power Systems, vol 25, no 2, pp 796–808, 2010.

[94] G. Diaz, C. Gonzalez-Moran, J. Gomez-Aleixandre, and A. Diez, "Scheduling of Droop Coefficients for Frequency and Voltage Regulation in Isolated

Microgrids", IEEE Transactions on Power Systems, vol 25, no 1, pp 489–496, 2010.

[95] X. Yu, H. H. Wang, A. M. Khambadkone, and S. T. Sing, "A Hybrid Control Architecture for Low Voltage Microgrid", in 2010 IEEE Energy Conversion Congress and Exposition (ECCE), 2010, pp 3161–3168.

[96] I.-Y. Chung, W. Liu, D. A. Cartes, J. Collins, E.G., and S.-I. Moon, "Control Methods of Inverter-Interfaced Distributed Generators in a Microgrid System", IEEE Transactions on Industry Applications, vol 46, no 3, pp 1078–1088, 2010.

[97] Q. Lei, F. Z. Peng, and S. Yang, "Multiloop Control Method for High-Performance Microgrid Inverter Through Load Voltage and Current Decoupling With Only Output Voltage Feedback", IEEE Transactions on Power Electronics, vol 26, no 3, pp 953–960, 2011.

[98] C. N. Rowe, T. J. Summers, R. E. Betz, D. J. Cornforth, and T. G. Moore, "Arctan Power-Frequency Droop for Improved Microgrid Stability", IEEE Transactions on Power Electronics, vol 28, no 8, pp 3747–3759, 2013.

[99] R. Majumder, A. Ghosh, G. Ledwich, and F. Zare, "Angle Droop Versus Frequency Droop in a Voltage Source Converter Based Autonomous Microgrid", in IEEE Power Energy Society General Meeting, 2009. PES '09, 2009, pp 1–8.

[100] C.-T. Lee, C.-C. Chu, and P.-T. Cheng, "A New Droop Control Method for the Autonomous Operation of Distributed Energy Resource Interface Converters", in 2010 IEEE Energy Conversion Congress and Exposition (ECCE), 2010, pp 702–709.

[101] C.-T. Lee, R.-P. Jiang, and P.-T. Cheng, "A Grid Synchronization Method for Droop-Controlled Distributed Energy Resource Converters", IEEE Transactions on Industry Applications, vol 49, no 2, pp 954–962, 2013.

[102] J. C. Vasquez, J. M. Guerrero, J. Miret, M. Castilla, and L. G. de Vicuña, "Hierarchical Control of Intelligent Microgrids", IEEE Industrial Electronics Magazine, vol 4, no 4, pp 23–29, 2010.

[103] J. M. Guerrero, J. C. Vasquez, and R. Teodorescu, "Hierarchical Control of Droop-Controlled AC and DC Microgrids - a General Approach Toward Standardization", in 35th Annual Conference of IEEE Industrial Electronics, 2009. IECON '09, 2009, pp 4305–4310.

[104] A. Mehrizi-Sani and R. Iravani, "Potential-Function Based Control of a Microgrid in Islanded and Grid-Connected Modes", IEEE Transactions on Power Systems, vol 25, no 4, pp 1883–1891, 2010.

[105] A. Colet-Subirachs, A. Ruiz-Alvarez, O. Gomis-Bellmunt, F. Alvarez-Cuevas-Figuerola, and A. Sudria-Andreu, "Centralized and Distributed Active and

Reactive Power Control of a Utility Connected Microgrid Using IEC61850", IEEE Systems Journal, vol 6, no 1, pp 58–67, 2012.

[106] J. M. Guerrero, J. C. Vasquez, J. Matas, L. G. de Vicuña, and M. Castilla, "Hierarchical Control of Droop-Controlled AC and DC Microgrids - A General Approach Toward Standardization", IEEE Transactions on Industrial Electronics, vol 58, no 1, pp 158–172, 2011.

[107] R. Majumder, A. Ghosh, G. Ledwich, and F. Zare, "Control of Parallel Converters for Load Sharing with Seamless Transfer Between Grid Connected and Islanded Modes", in 2008 IEEE Power and Energy Society General Meeting - Conversion and Delivery of Electrical Energy in the 21st Century, 2008, pp 1–7.

[108] S.-J. Ahn, J. Park, I.-Y. Chung, S.-I. Moon, S.-H. Kang, and S.-R. Nam, "Power-Sharing Method of Multiple Distributed Generators Considering Control Modes and Configurations of a Microgrid", IEEE Transactions on Power Delivery, vol 25, no 3, pp 2007–2016, 2010.

[109] E. Serban and H. Serban, "A Control Strategy for a Distributed Power Generation Microgrid Application With Voltage- and Current-Controlled Source Converter", IEEE Transactions on Power Electronics, vol 25, no 12, pp 2981–2992, 2010.

[110] Z. Yao, L. Xiao, and Y. Yan, "Seamless Transfer of Single-Phase Grid-Interactive Inverters Between Grid-Connected and Stand-Alone Modes", IEEE Transactions on Power Electronics, vol 25, no 6, pp 1597–1603, 2010.

[111] C. Cho, J.-H. Jeon, J.-Y. Kim, S. Kwon, K. Park, and S. Kim, "Active Synchronizing Control of a Microgrid", IEEE Transactions on Power Electronics, vol 26, no 12, pp 3707–3719, 2011.

[112] M. Dewadasa, A. Ghosh, and G. Ledwich, "Dynamic response of distributed generators in a hybrid microgrid", in 2011 IEEE Power and Energy Society General Meeting, 2011, pp 1–8.

3. Review of Microgrid Protection

3.1 Introduction

Microgrid protection is one of the most crucial elements for successful implementation of microgrids. It has a close relationship with operation and control (discussed in Chapter 2), and therefore, needs to be consistent with the operation and control requirements, i.e. flexible operation under different operational modes, system topology change and connection or disconnection of units.

In a conventional radial distribution network, the power flow is always unidirectional and always from the HV transmission system to the MV/LV distribution feeders. Thus if a fault occurs in this radial network, the fault current is merely provided by the upstream centrally located large rotating machines, and only flows in one direction. In this way, a regular design of the conventional distribution system protection can be based on the overcurrent protection using the time/magnitude-grading principle.

With integration of DERs, the power can also be supplied from the end of the feeders, and both the fault current level and direction can be significantly changed. As the microgrid has two types of operational modes (islanded and grid-connected), and has high penetration of "plug-and-play" DERs, storage units and controllable loads, the fault current level and direction are likely to possess even more frequent changes. However, traditional overcurrent protective schemes or even voltage restraint protective schemes are highly dependent on the predetermined and relatively constant fault current level. Thus the protective system for microgrid should be dramatically redesigned to take into account both the variability of fault level and power flow direction. This chapter aims mainly to investigate issues and challenges of microgrid protection, based on the review of existing protection schemes.

3.2 Conventional Distribution Network Protection

Before elaborating on distribution network protection, it is useful to recall the fundamental attributes any protection system should possess. These desired attributes are [1-3]:

1) **Sensitivity**: a protection system must be able to detect the fault at the presence of the smallest indicators: i.e. smallest fault current for overcurrent relays.
2) **Selectivity and stability**: a protection system should operate correctly. By correct operation the protection has the ability to discriminate between faults and non-fault events: it can isolate the fault by disconnecting the minimum section of the network and stay inoperative during non-fault events.
3) **Speed**: a protection system should trip on the fault with the minimum time delay to avoid damages and dangerous situations to healthy sections of the network or people. However, there is normally a conflict between speed and stability: the faster the relay trips, the more difficult for it to guarantee the stability.
4) **Reliability and Dependability**: the probability of failure of a protection system exists due to the failure of any one or more elements, such as wiring, PT, CT, circuit breaker, battery and relay. A protection system should be redundant at some level, at least providing "back-up" plans under failure of any of these elements, and keep it simple and robust. For example, protection zones in transmission line protection always overlap with the zones of neighbouring protection devices, and the discrimination between main and backup protection is achieved by time grading.

There are a number of protection functions that have been used in power system. Different network topologies require different protection schemes. The topology of a conventional distribution network is radial and the power always flows from the upstream HV system to the downstream MV/LV system. Based on this scenario,

time/magnitude graded overcurrent protection is normally sufficient to protect the distribution network.

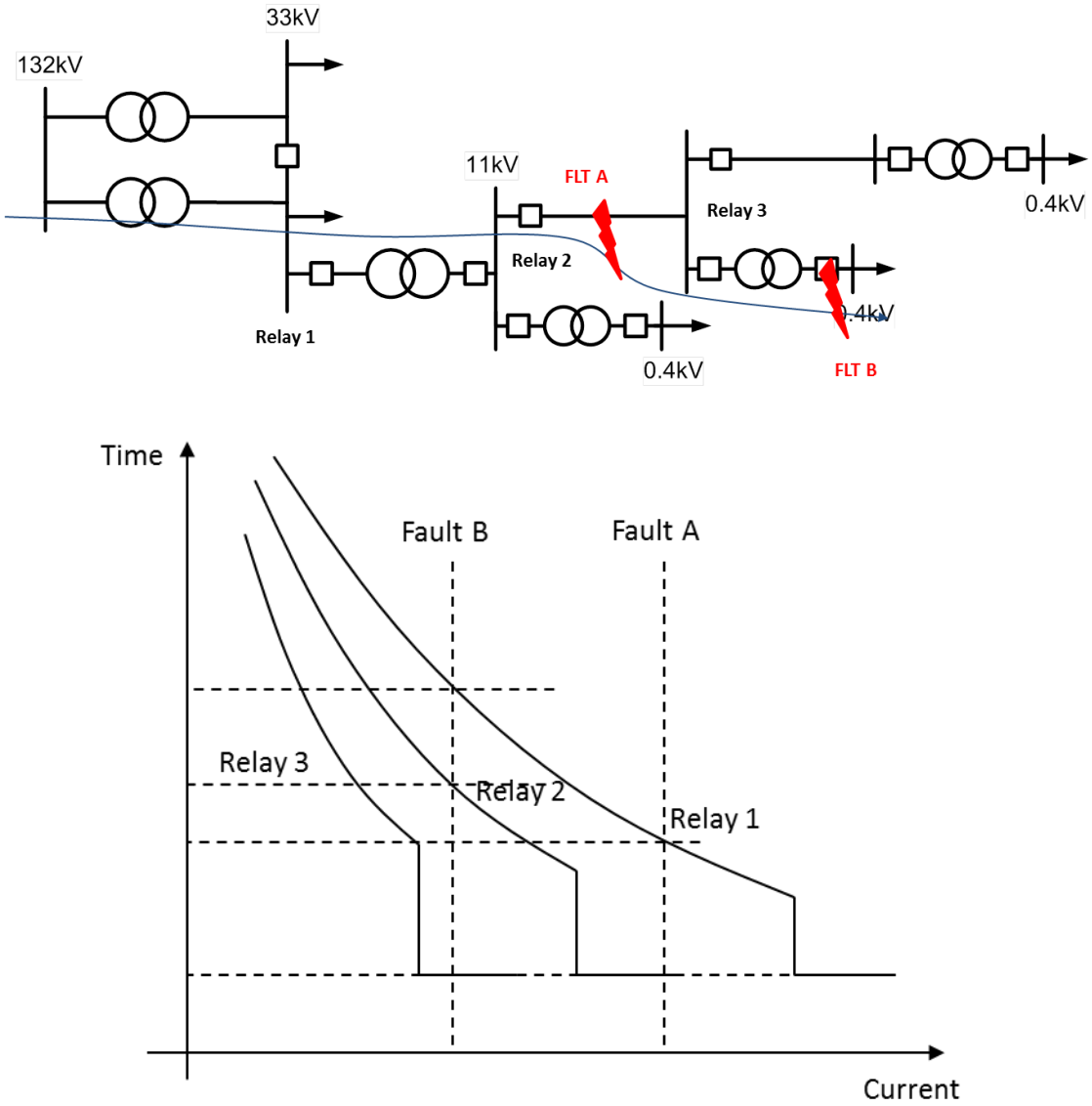

Figure 3-1: Coordination of overcurrent protection in a radial distribution network

Overcurrent protection is typically implemented using fuses or relays with circuit breakers. Overcurrent relays are classified based on their time/current operating characteristic as: definite-current, definite-time and inverse-time. Definite-current protection operates instantaneously when the current reaches the current setting threshold. Definite-time overcurrent protection operates with a fixed time delay when

the current reaches the threshold, and the inverse-time overcurrent protection operates on a fault with a time delay inversely proportional to the fault current magnitude, according to a standardized inverse current characteristic. Figure 3-1 shows an example of coordinated operating characteristics of overcurrent relays in a radial feeder. Each relay is supplied with a definite-current element and an inverse-time element. In this way, the protection can isolate the fault with minimum number of operations on the circuit breakers.

Another popular configuration in the conventional distribution system protection is to implement the reclosing function into each circuit breaker by considering the fact that majority of faults only occur during a transient short time (especially in overhead lines). The relay normally sends the reclosing signal after a predetermined time following the trip command. This guarantees the reliable fault clearance as well as maintenance of the most part of the recovered and healthy network.

3.3 DER Impact on Distribution Network Protection Performance

3.3.1 Dynamic Responses and Fault Behaviour of DERs

In the earlier discussions, it has already been clear that the presence of DERs in the downstream feeders affects the system load flow and fault level. Usually, installing a DER in the distribution increases the value of fault current at the fault point thus requiring some upgrading of the equipment of the network. Indeed, when a fault is applied to the distribution network with DERs at the end of the feeder, the fault current is provided from all connected power sources, and the equivalent Thevenin impedance of the network is reduced. From the protection point of view, it is difficult (often impossible) to configure the current threshold for conventional overcurrent protection to achieve proper discrimination on the fault location. However the impact on the fault current contribution actually varies with installation of different types of DERs. Besides, the DER impact on the fault current level also

depends on its generator size and location. The following subsections are dedicated to describe the impact on the fault behaviour by different types of generators: synchronous machine, induction machine, IIGs and etc.

3.3.1.1 Synchronous Machine

Most conventional thermal generators as well as CHP micro-generation driven by reciprocating engines are in the format of the three-phase synchronous machines. A synchronous generator uses an external DC source for its excitation. It always runs at a synchronous speed with a rotor angle corresponding to its electrical output power [4].

During a transient fault situation, although the electric power output is reduced, the field current supported by the excitation system persists, which maintains the voltage in the stator winding and in turn supplies a continuous fault current. This results in a sustained short-circuit current with a decaying DC offset. As the short circuit current continues to flow in the system, the machine's winding equivalent impedance increases. This results in a faster fault current decay. Three reactance variables (subtransient, transient and synchronous) have been introduced by IEEE Std. 141-1993 to characterise this phenomenon [5]. According to [6], the decaying fault current characteristic depends on the fault position and rated power of the machine: close-up faults will have longer decay times than remote faults. Even small synchronous machines with limited fault current capability can produce up to three times full load output after a relatively short decay due to their excitation systems.

Should the grid fail to absorb sufficient amount of generator kinetic energy, gained from acceleration during the fault, the synchronous machine becomes unstable (i.e. loses synchronism with the rest of the system) after the disturbance is cleared. In this case, suitable protection should be provided to detect this instability and disconnect the DER from the utility network (e.g. pole slip protection). Alternatively, other methods of improving the transient stability of synchronous DER are used and can be found in [7].

3.3.1.2 Induction Machine

Though induction machines are more commonly used as motors in the power system, some DERs utilise this type of generator due to their simplicity of construction and ability of producing active power at varying rotor speeds. They are often used in wind turbines and some micro-hydro generators. The prime mover drives the induction machine rotor above the synchronous speed, thus producing the active power into the utility network.

Since induction machines do not use external DC sources for excitation, the field flux decays rapidly when the loss of external source of voltage occurs as a result of a fault. Consequently, there is no steady state fault current and the current output rapidly decays to zero. Therefore, only a subtransient component exists for induction machines [8].

3.3.1.3 IIG

Power electronics can be used as an interface for a wide variety of energy sources. They convert the DC energy for connection to the AC system or decouple small rotating machines from the network and thus provide more flexibility in terms of machine rotational speed and efficiency of energy capture (e.g. wind). Other benefits of power electronic interfaces are their fast control of active and reactive power as well as voltage regulation, which can potentially enhance the operation of a weak remote network or support intentional islanding [9]. The typical arrangements of using a power electronics interface for DER installations are presented in Figure 3-2. When interfacing with the DC power sources (fuel cells, batteries, etc.), a DC-AC inverter is used to regulate the AC output of DER into the grid. When used with a rotating machine, an AC-DC rectifier is added to rectify the uncontrolled AC power source. Sole DC-AC inverters are almost always found in photovoltaic battery charging systems to regulate and optimise the power input [10].

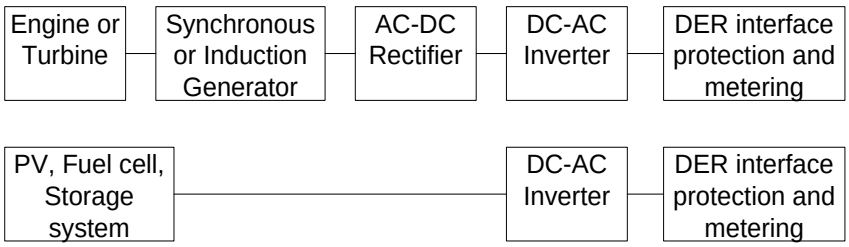

Figure 3-2: Basic connections of IIG [10]

The fault behaviour and capability of the IIG is a closely related to the control design and the size of the power electronic components. This area is currently not completely understood or standardised and there are only limited guidelines presenting the minimum or recommended fault contribution of an IIG [10]. A number of publications demonstrate that the fault current from IIG can be up to two or three times the IIG's full load current for 20ms or less. For example, [8] includes test results and discussion of fault characteristics of an IIG which shows that grid connected inverters can produce up to 2-4 times the rated current, but only for a very short period of 0.06-0.25 cycles. This is within the subtransient period for synchronous generators and such currents would have little impact on the operation of traditional overcurrent relays. Therefore, during grid-connected mode, the small contribution to the fault current is positive from the point of view of existing coordination of the protection system. During intentional islanding mode, however, the fault current is too small to activate the traditional overcurrent relays. In this case, alternative schemes which are not based on the fault to load current ratio are required [11]. Furthermore, there may be a problem with IIG's internal protection reacting too quickly and too sensitively to faults on the network; in some cases, a network fault could lead to unnecessary tripping of many IIGs and, in an islanded system, this could have severe consequences.

3.3.1.4 DFIG

Crow-bar protection is used in a doubly-fed induction generator (DFIG). Its fault characteristic is a mixture of the response of an induction machine and an IIG. Crowbar protection is often used to protect this generator against over currents caused by large system disturbances or faults. When a fault is detected, the rotor windings are short circuited using power electronic 'crowbar' switches, and added with external rotor impedance until the fault is cleared to limit the rotor current.

To sum up, for the microgrid consisting of great number of IIGs, the fault current level during grid-connected operation is similar to the original system without IIGs, and becomes insufficient to activate the overcurrent protection during islanded operation; whereas for microgrid consisting of rotating machines, the fault current is likely to exceed the rating of existing switchgear in grid-connected mode, in which case the fault current limiters may be the only feasible solution.

3.3.2 Under or Over Reach of the Overcurrent Protection

The current threshold in the overcurrent protection is usually determined by the maximum load current. Fault current needs to be sufficiently larger than the maximum load current in order to be "seen" as a fault by the overcurrent relays or fuses [12-13]. However, if a fault occurs in the middle of a feeder connecting the DERs to the grid, fault current flows from both the upstream and downstream network, which indicates that the fault current seen by the overcurrent protection is reduced. On the other hand, if a fault occurs at the downstream line from DER connecting point, fault current seen by the downstream line includes both the current from DER and the supply grid, causing an over-reach of overcurrent protection [14]. Moreover, due to irregular nature of the DER power output (especially for intermittent energy resources), fault current becomes quite difficult to predict and conventional distribution network protection based on the fixed protection settings is not feasible.

3.3.3 False Tripping of the Overcurrent Protection

The change of power flow path in the network may also cause mal-coordination between the protection devices. In other words, protection selectivity is degraded [15]. For example, the adjacent line fault might activate the overcurrent protection when the feed-in current from the local healthy line exceeds the current threshold. This issue causes particular concern if the DER is a synchronous generator, which can provide sustained large short-circuit current. In order to solve this problem, the directional units can be added into the overcurrent relays. However, the busbar protection and arcing fault protection need further reconfiguration [13]. Moreover, conventional fuses will have to be abandoned in protection of such systems [12].

3.3.4 Loss of Mains/Islanding Detection

With installation of DERs at downstream of the distribution network, in case of a fault in the utility network, a part of the network containing some DERs and a cluster of loads might be isolated through the operation of the utility protection devices or manual operation. In this case, a power island is formed. The term used to describe this condition in which a part of the network is energized by a cluster of DERs or one DER while being disconnected from the utility grid is “loss of main” or “islanding”. Unplanned loss-of-main (LOM) can be dangerous for both people and devices. Since in some distribution systems (i.e. HV distribution systems operating at voltages below 132kV), only one earthing point is provided by the upstream network, LOM can result in loss of earthing causing large voltage potential during asynchronous faults. The voltage and current level may not be maintained in a standard permissible level. The engineering work safety is threatened by unawareness of DERs powering up. The reclosing may result in out of phase reclosing of DERs, which might result in DER damages and significant system transients. Therefore the present engineering standards and recommendation document do not permit islanding operation in LOM and require disconnection all the DERs within an islanded network, i.e. Engineering Recommendation G59/2 and IEEE P547. Even for a microgrid specially designed to have the islanding capability, it is still important to detect the LOM event which

allows the corresponding control and protection schemes adjusting themselves to different modes of operation [16-17].

The network protection needs to coordinate with the DER islanding detection. The network protection should trip faster than the islanding detection to prevent false tripping of the islanding protection. After clearing the fault, if there is still islanding event detected, the control centre sends the signals to each DER interface specifying the status of the operational mode [18].

3.3.5 Coordination with Reclosers

Autoreclosing is used in the power system in order to minimise the power loss to customers and restore the connection of healthy (or recovered) utility network and loads when the fault has a transient nature (e.g. fault is cause by lightning). However, automatic reclosing onto the network with life DER has a few major issues. needs to be disconnected before the recloser operates, in order to allow sufficient dead time for arc extinction [13]. Moreover, it is necessary to trip the DER before reclosing; otherwise, the transient islanding may lead to large voltage strikes imposed by connecting voltages with different phases between the DER and the network. Indeed, once the DER is islanded unintentionally, the DER accelerates and decelerates and soon is out of phase with the utility source of supply. In order to avoid the issues of out-of-phase reconnection of the generator, a reclosure interval of more than 1.0s (or even no reclosing) is sometimes recommended [19].

3.4 Protection Issues with Microgrids

Regarding the protection of a microgrid containing a cluster of DERs, it needs to be designed not only to consider the impact from the DER's dynamic response and fault behaviour, but also to satisfy intrinsic requirements of microgrids for running in both grid-connected mode and islanded mode. In this case, the protection design becomes more complicated since the network topology and power flows can change

dramatically during operational mode transitions. It is expected to offer good sensitivity and selectivity for faults in both modes of operation. The operation also needs to be sufficiently fast to protect sensitive loads and DER units.

3.4.1 Concerns over Microgrid Features

Microgrid mode transfer imposes a significant change of fault current level. With high penetration of DERs in the microgrid, even in grid-connected mode, the conventional overcurrent protection performance can be affected due to their significant contribution of fault current irregularly alternating the power flow paths [20]; needless to say, in islanded mode, fault current level drops significantly.

The protection system must be able to correctly respond to both the microgrid and the distribution system faults. For a fault within the microgrid, the protection system is required to isolate the smallest possible section of the network; if a fault occurs on the main grid, the protection system should be able to isolate the microgrid from the fault.

Microgrids normally operate as connected to the major grid [21]. This interconnection generally guarantees stable power flow and robust regulation of voltage and frequency both for microgrid and utility grid. Low voltage ride through/ fault ride through capability under external transient faults is thus proposed for reliability enhancement of the microgrid [22]. This arrangement needs the protective system installed at the PCC to embrace a characteristic of fault-ride-through, to maintain this interconnection during transient voltage sags.

3.4.2 Special Concerns of IIG Based Microgrids

As introduced in Section 3.3.1.3, the fault behaviour of an IIG and its capability of generating currents above the rating have not been standardized and are significantly dependent on the configuration by the individual manufacturer. In islanded mode of operation, the fault contribution from IIGs is limited to about twice of the rated current, resulting in ineffective operation of overcurrent protection. Moreover,

different control principles or even different control reference frames also have a great impact on the fault response of the inverters [23]. Haron et al [20] emphasized the protection of inverter-dominated microgrids as the major issue calling for research on new protection principles.

Based on the above evaluation, the following issues were listed for consideration:

1) Coordination of DER side protection with system side protection.
2) Operating conditions and loading condition of a microgrid are constantly changing because of the intermittent microsources and periodic load variation.
3) The network topology can be regularly changed aimed at loss minimization or achievement of other economic or operational targets.
4) Insufficient level of short-circuit current in the islanded operational mode, especially with many power-electronics interfaced DERs.
5) Reduction in the permissible tripping times for faults in the distribution network, in order to maintain the stability of the microgrid.

3.5 Overview of Microgrid Protection Schemes

3.5.1 Adaptive Protection of Microgrid

One interesting solution is adaptive protection. Adaptive protection refers to the protection that can change settings and features according to the real-time conditions of network topology, connected DERs, operational mode and fault status [24-25]. The procedure of changing settings and features is normally conducted through automatic numerical calculation.

Adaptive protection concept was initially proposed for applications in the transmission network [24]. Application in the distribution network was then studied in [26-29]. Brahma et al [26] introduced a Global Positioning System (GPS) based adaptive protection scheme for a distribution network with high penetration of DER. The distribution network was divided into zones by the circuit breakers according to a reasonable balance of the DER and local loads. A main relay is responsible for the

data analysis and communications with the zone breakers. Schaefer et al [28] specified an adaptive protection scheme based on two types of processing blocks: real-time block which is responsible for analysing the real-time state of the network and non-real-time block which uses the prediction data based on the existing experiences. Mahat et al [29] proposed an adaptive protection strategy for an islanded system only based on local measurements. However, it only considers three phase faults.

Gradually, the concept of adaptive protection is also introduced into microgrid protection [11, 25, 30-35]. A possibility of using adaptive overcurrent settings is firstly considered in [30]. Qudalov et al [11] utilize directional relay with directional interlock capability for incorporating a centralized architecture. Han et al [31] proposed an adaptive method based on the estimated impedance of the system using voltage and current fault component. Dang et al [32] proposed an adaptive methodology based on zero-sequence current to solve the earth fault protection problems. Ustun et al [33] used the characteristic of limited fault current from IIG to discriminate a fault.

3.5.2 Transmission Level Protection

There is a group of methods which are based on modified transmission system protection schemes. Among all the transmission level protection schemes, current differential protection was regarded as the most effective solution [36-37].

Zeineldn et al [17] and Dewadasa et al [38] addressed the protection issue by introducing the current differential protection into the microgrid. Equipping each line with current transformers (CTs) at both ends, the proposed protection scheme is designed to operate in 50ms to coordinate with the islanding detection. Conti et al [39] also applied the differential protection scheme to a test microgrid containing both rotating machines and IIGs. Sortomme et al [40] provided an application schematic using instantaneous differential protection, based on synchronized phasor measurements and numerical relays. Similar to current differential protection, Halabi

et al [41] presented a current phase comparison scheme. These methods are all based on the assumption that the high bandwidth communication channels are available.

Dewadasa et al [42] investigated the application of distance protection scheme for inverter based microgrid. In this method, two zones of protection with Mho characteristic were designed to cover 80% of the protected line and 50% of the adjacent line respectively. However, the effectiveness of this method was not proven. A few years later, the author proposed an admittance relay for protection of microgrids in both modes of operation [43]. Still, the reliability of admittance measurement under different fault scenarios is an issue, especially when the line impedance is relatively small. Moreover, the coordination of the proposed protection has not been fully studied.

3.5.3 Symmetrical Current Components Based Methods

Nikkhajoei et al [44] assumed a protection scheme based on modified current signals such as symmetrical or differential current components through a network zoning approach. Similar to overcurrent principles, the coordination of this scheme is still based on the grading of the current components. Time delay can be more than ten cycles and the performance might be problematic in a meshed microgrid. Moreover, it can only detect unbalanced faults.

3.5.4 Voltage Based Methods

The voltage based method was initially proposed by the research group at the University of Bath for accelerating the fault detection in a inverter based microgrid, which is valid for all types of faults [45-47]. The voltage measurements are converted to DC components by ABC-dq Park transform. In order to differentiate between in-zone and out-of-zone faults, some thresholds are applied to the voltage drop. The type of fault is established by taking the wave shape as an indicator inside

the algorithm. In order to avoid the difficulty of fault type discrimination based on the wave shape, Loix et al [48] proposed an enhanced method based on symmetrical components derived from the measuremed voltage.

However, the voltage based method makes use of the voltage level gradient throughout the network during faults, which implies its application is limited to relatively large scale networks. Furthermore, it cannot deal with high impedance faults (HIF). The author of this thesis found out that there is a noticeable Non Detection Zone for this scheme [37]. Therefore, the voltage gradient based method is normally recommended to be a back-up scheme [49].

3.5.5 External Devices for Manipulating the Fault Current Level

With regard to the fault current level in a microgrid, its drastically ever-changing characteristic poses significant challenge to protection system design. As an alternative to the methods based on novel detection algorithms, a number of researchers also work on developing external devices for manipulating the fault level, essentially, equalizing the fault level in different modes of operation, load conditions or network topologies. These devices can be classified either as fault current limiters (FCL) or fault current sources (FCS), according to their basic principles of limiting or increasing the fault current respectively.

3.5.5.1 Fault Current Limiter

When the microgrid contains synchronous DER, the fault current level may exceed the rating of individual devices in the microgrid, e.g. current breaking capacity for circuit breakers (CBs). Therefore, in order to overcome the increased impact of fault currents from DERs the fault current limiters (FCL) are used. In distribution system FCLs are connected in series with network impedance and the coordination of overcurrent protection is retained. Different types of FCL embodiments exist in the literature including solid state FCL topologies, superconducting fault current limiters and modified inverter control loops with FCL component [50]. Oudalov et al [11]

provided two promising current limiting techniques and highlighted the requirement for the FCL in microgrids. Khan et al [51] analysed the performance of superconducting fault current limiters in microgrids. Detailed review and discussion of FCL technologies, also including performance analysis, have been presented in [52]. Vilathgamuwa et al [53] proposed a fault current limiter based on a voltage source inverter between the microgrid and the utility grid. The current limiting algorithms are installed in this inverter which works as a virtual impedance in series with the distribution feeder. Khederzadeh et al [54] also put the fault current limiter at the PCC using a static series compensator.

3.5.5.2 Fault Current Source

Early at this stage, Jayawarna et al [55] mentioned the application of flywheel energy storage system to increase the fault level during islanded operation. Based on this idea, more publications were written to clarify the implementation and control of the storage system [56-58]. With the development of storage technologies and control, most of the running microgrids are equipped with energy storage devices (e.g. batteries, flywheel, etc.) which can provide sufficient fault current into the network [59]. As an alternative, Overbeeke et al [60] developed an oversized power electronic device with special control, named Fault Current Source (FCS) which could offer sufficient fault current into the islanded inverter based microgrid to guarantee reliable fault detection. Nevertheless, it can be viewed as unreliable from the protection reliability point of view, as the whole protection system relies on a single electrical device.

3.5.6 Harmonic Content Based Scheme

Harmonic content based method was another solution for inverter based microgrid proposed by Al-Nasseri et al [61]. Since the protection scheme is based on the harmonic content produced by the power electronic devices, the type of the DER in the microgrid is limited to IIG and all of them need to be connected to a common bus. The proposed harmonic content based method is intended to protect the generator

rather than the network as its operation only contains switching off the DER. Moreover, the threshold of the harmonic content based method is difficult to define.

3.5.7 Travelling Wave Based Protection

Very few papers have discussed the idea of introducing fault generated traveling wave as a guiding principle for the microgrid protection. David et al [62] applied this idea to a zonal DC marine system. However, with no dedicated signal analysis, fault transients are not properly extracted, and their arrival time and polarity information are vague. Furthermore, the method requires very high communication bandwidth to transport high frequency sampled real time current measurements. Shi [63] introduced a hybrid protection idea using fault generated current traveling wave and superimposed power frequency voltage using multi-resolution wavelet analysis. However, the method is not validated through either simulation or experiments.

3.5.8 Protection Schemes Feasible for IIG Based Microgrid

For an IIG based microgrid, the fault current level during islanded operation is very much limited for silicon switching. The protection schemes based on overcurrent principle are no longer feasible, including the adaptive overcurrent protection which is still based on the fault current and load current ratio. The potential solutions include methods based on different current components, additional fault current manipulating devices, transmission level protection and various other types of indicators.

Figure 3-3 gives the outline of the major protection principles dedicated to serve the inverter based microgrid. These protection solutions can be seen as largely independent of the fault to load current ratio.

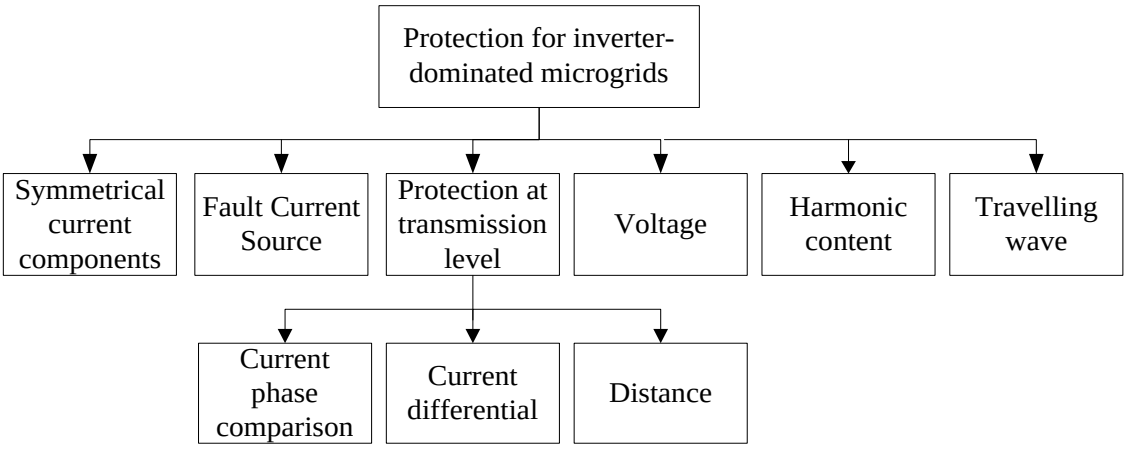

Figure 3-3: Classification of protection schemes for IIG based microgrids

3.6 Moving Towards the Travelling Wave Based Protection Schemes

Most of the conventional power system protection methods are based on the power frequency components and in only a few cases low harmonic components are introduced as relaying signals (e.g. third harmonics for earthing protection of generator units or second harmonic for blocking the transformer differential protection during magnetising inrush). Travelling waves or high frequency transients were originally regarded as noise to be filtered out from relaying signals.

The idea of introducing travelling wave theory into protection was initially proposed in the 80s of the last century [64], after pointing out that performance of traditional distance protection (as well as accuracy of fault location) was limited under high impedance fault (HIF) conditions. The travelling wave theory was then utilized in practice, mainly in fault location area.

The travelling waves, also depicted as part of the high frequency fault transients, can be analysed and explained by the superposition theory. They are generated by the virtual faulty source according to the abrupt voltage collapse at the point of fault. The publications [65-66] are the two early papers that provide theoretical clarification of the relation between the fault and travelling wave: the dominant part of the fault

transients are referred to as travelling waves propagating along the transmission lines from the fault point.

3.6.1 The Definition of the Travelling Wave

In the power system, a sudden voltage change by fault at any point will generate a series of high frequency transients, propagating along the lines in all directions. When hitting on the singularities of the system (i.e. system loads, busbars, connecting points between different power system devices and lines), these high frequency transients will experience refractions and reflections, showing a series of step ups and downs. These high frequency transients are also known as the travelling waves.

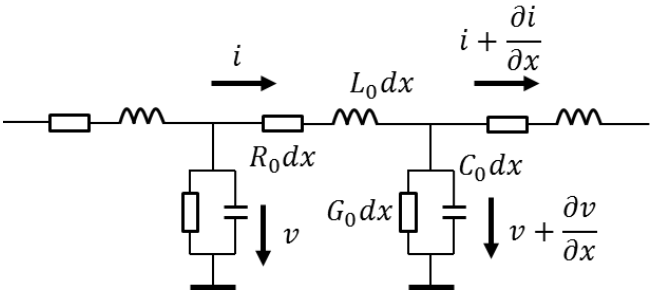

Figure 3-4: A mini PI section of the lump model under single phase view

In order to introduce the basic principles of the travelling waves, a mini section of a lumped transmission line model (including underground cables) is established as shown in Figure 3-4. It is an equivalent PI circuit representing a very small section of a line (with a length of dx). In theory, the entire line is composed of an infinite number of these small sections. The resistance R_0, capacitance C_0 and inductance L_0 are all the same for each mini section, representing the parameters evenly distributed along the line. From Figure 3-4 it can be seen that this mini PI circuit can be regarded as a two-terminal network. The relationship between the terminals can be obtained by solving the Telegrapher's equations. The Telegrapher's equations are presented in (3-1).

$$\begin{cases} -\dfrac{\partial v(x,t)}{\partial x} = R_0 i(x,t) + L_0 \dfrac{\partial i(x,t)}{\partial t} \\ -\dfrac{\partial i(x,t)}{\partial x} = G_0 v(x,t) + C_0 \dfrac{\partial v(x,t)}{\partial t} \end{cases} \tag{3-1}$$

Based on the Telegrapher's equations, the wave propagation along a lossless transmission line can be expressed as a mixture of forward section f_1 and backward section f_2 travelling waves [67,68]:

$$\begin{cases} v(x,t) = f_1(x-\mu t) + f_2(x+\mu t) \\ i(x,t) = \dfrac{f_1(x-\mu t) - f_2(x+\mu t)}{Z_0} \end{cases} \tag{3-2}$$

where $v(x,t)$ and $i(x,t)$ are the measured voltage and current, μ is the travelling velocity of the travelling waves and Z_0 is the characteristic impedance of the line. To be more explicit, $f_1(x-\mu t)$ is the voltage forward travelling wave, $f_2(x+\mu t)$ is the voltage backward travelling wave, $f_1(x-\mu t)/Z_0$ is the current forward travelling wave and $f_2(x+\mu t)/Z_0$ is the current backward travelling wave. By solving the set of equations (3-1) the forward and backward voltage components are extracted as follows:

$$\begin{cases} f_1(x-\mu t) = \dfrac{v(x,t) + i(x,t)\cdot Z_0}{2} \\ f_2(x+\mu t) = \dfrac{v(x,t) - i(x,t)\cdot Z_0}{2} \end{cases} \tag{3-3}$$

When the travelling waves are propagating smoothly in a uniform material, the backward component is equal to zero. Only after reaching a singularity, where the input impedance is inconsistent with the characteristic impedance, a backward component is generated, and the measured current/voltage signals will increase/decrease in the magnitude. This phenomenon is also known as signal reflection and refraction. The characteristics of the reflection/refraction of the travelling waves, also named as the boundary characteristics, are therefore the key

features of the travelling wave based protection, and will be discussed in the next section.

3.6.2 Boundary Features of the Travelling Wave Reflection

As stated above, the basic principle of the travelling wave based protection is to utilize a series of wavefronts within the fault generated voltage or current transients, based on the behaviour of reflections of the voltage or/and current travelling waves at the "singularities" of the system. These "singularities", as well known as the transmission boundaries for the travelling waves' reflections and refractions, include busbars, transformers, and all the connection points between different electrical components in the power system. Based on (3-1), (3-2) and (3-3), the boundary features can be explained by introducing the reflection factor. A simple diagram is presented to illustrate the basic principle of the travelling wave reflection as shown in Figure 3-5.

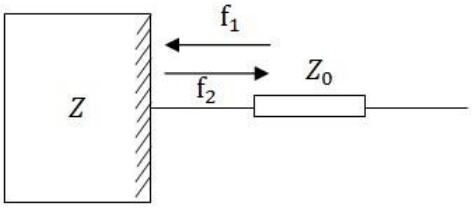

Figure 3-5: Wave reflection at the boundary in a system

The reflection factor of the voltage travelling wave, which is used to measure the amount of energy reflected back to the local system is derived by (3-4), where Z is the equivalent impedance of the system, and Z_0 is the characteristic impedance of the line.

$$k_V = \frac{f_2}{f_1} = \frac{Z - Z_0}{Z + Z_0} \tag{3-4}$$

For current signal, its reflection factor is negative to that of the voltage signal, as presented in (3-5):

$$k_c = -\frac{Z - Z_0}{Z + Z_0} \tag{3-5}$$

It is to be noted that, the reflection factor is calculated by dividing the forward component by the backward component, which cannot be directly measured from the actual power system. Hence if accurate extraction of the voltage or current travelling waves is needed, it appears to be mandatory to sample both voltage and current signals. However, in most cases, the fault location can be distinguished utilizing the time intervals of the travelling waves hit at one singularity rather than the full details of the voltage/current travelling waves. As current and voltage travelling waves share the same time intervals of reflections/refractions, in actual developed protection schemes, quite a few of them are realized based on either mere voltage signals or mere current signals.

It is clear that the detectable transient features are dependent on the characteristics of Z_0 and Z. Known the characteristic impedance of the travelling line $Z_0 = 200$ohms, a brief study on the voltage and current reflection coefficient by the impact of the type of Z can be conducted based on simple analysis using (3-4) and (3-5). The most popular singularities in the transmission and distribution systems are the busbars. The impact from the busbar capacitance is presented in Figure 3-6. It is clear from the figure that with the increase of the frequency, the voltage reflection coefficient gets closer to $-1(1\angle 180°)$. Similarly, we can also dictate the current reflection coefficient by just adding a negative sign before the voltage reflection coefficient. When the voltage reflection factor reaches -1, the energy of the voltage signal totally passes through the singularity, leading to a smoothed measurement and no travelling wavefronts can be detected; while the corresponding current reflection factor reaches 1, with full reflection of the current signal, leading to a clear wavefront measured from the current instrument. This phenomenon meets the well-known theory that the capacitance cannot suffer abrupt change of the voltage change.

Therefore when the busbar capacitance is relatively high, the better components for travelling wave based protection with larger frequency bandwidth are current signals.

The travelling wave theory does not normally apply to the generator protection. The characteristics impedance of this type of components is mainly depicted as a combination of resistance and inductance. Inductance greatly affects the effective reflections of the current signals. This kind of boundaries brings even more complexity as they are nonlinear inherently. It is necessary to add a portion of cable/line or isolation device (line trap) to establish the feasible boundary feature for observable travelling wave reflections.

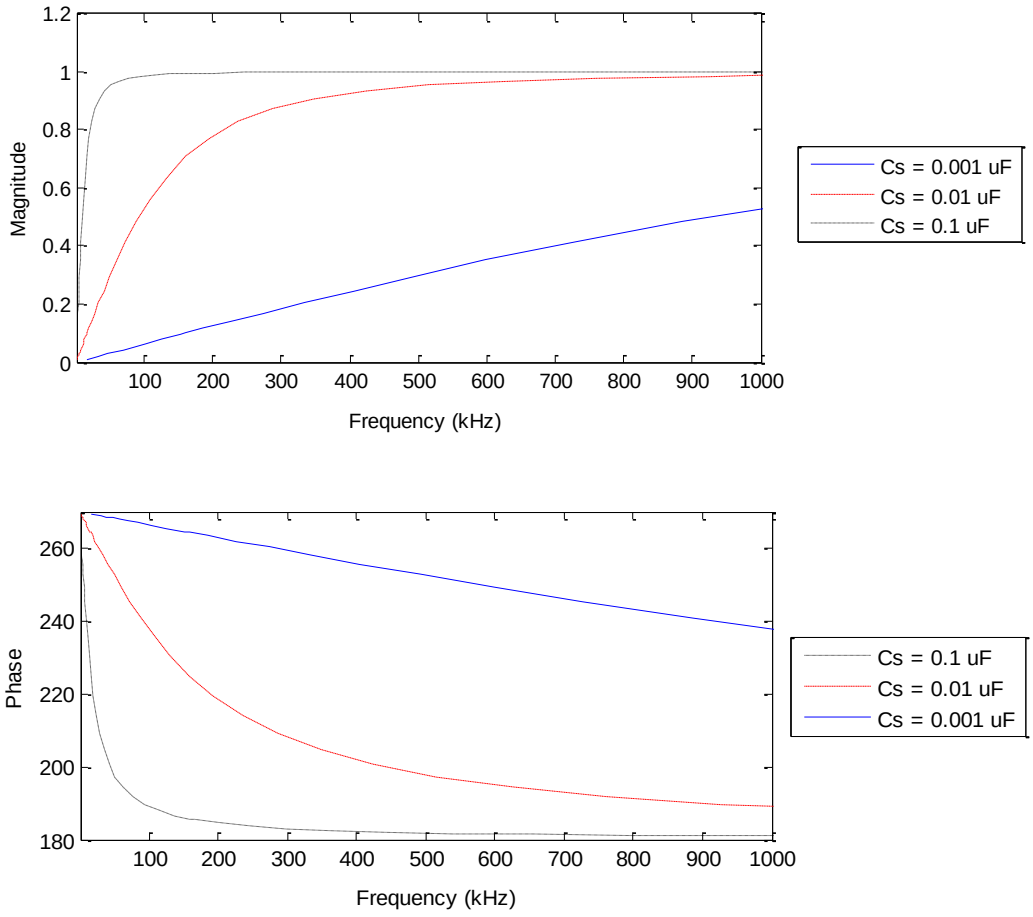

Figure 3-6: The spectrum of reflection factor of the line boundary with varied busbar capacitance

3.6.3 Main Issues in Applying the Travelling Wave Theory to Microgrid Protection

The travelling wave based methods described in the literature are mostly applied to transmission systems. Very few papers extend the idea to the distribution system. It is regarded to be overcomplicated, and economically prohibitive due to high cost of large bandwidth CTs, voltage transformers (VT), or capacitive voltage transformers (CVTs). In a distribution system, short travelling times due to short lines require fast sampling and large bandwidth measuring. Large number of reflections has to be considered in the algorithms. The lower voltage lines or cables have relatively large resistance which has obvious damping effect upon the transients [21].

The thesis is to explore the feasibility of applying the travelling wave based methods to the microgrid system at distribution voltage level, the special features of travelling waves in the distribution system should be summoned. Fundamentally, the use of the travelling wave based protection methods in distribution systems is more complicated than that in the transmission systems. However, the benefits of generally shorter distances and thus more readily available communication channels allow capturing the indicators on a broader scale, which may outweigh the disadvantages. Advantages of travelling wave based protection schemes, such as independence of the variability of load or fault conditions, are particular considering factors of the author's interest in developing the travelling wave based protection schemes suitable for inverter dominated microgrids.

3.6.3.1 Sampling and Instrument

The signal sampling rate is the main factor determining the ability of extraction of high frequency transients, and thus, is directly linked with the accuracy of the estimated fault location. For a travelling wave based method utilizing the reflections of the wavefronts, very high sampling frequency is required to obtain and discriminate the time intervals or polarity information of them. Furthermore, if applied to the distribution system, this requirement becomes even more rigid in that, the time intervals between wavefronts are very small due to the typically short length of lines/cables.

In either case, the bandwidth of a VT/CVT is much tighter than a CT. Hence, it is a well-accepted rule that the current measurements are more suitable for travelling wave based protection, and with existing instrument transformer technology it would be prohibitive to use both voltage and current measurements in the microgrid system.

Generally voltage sensors have poor response to get the high frequency transient travelling waves, except for low voltage level, where the high frequency voltage transients can be sensed using the coupling effect or optical sensor technology. Even with the long distance lines in transmission systems (up to several hundred kilometres), the broadly used CVT with a frequency bandwidth of tens of kHz it is still hard to measure the travelling waves up to 200 kHz. Therefore it is economically prohibitive to achieve high frequency sampling of both the voltage and current signals, especially for the voltage signals.

On the contrary, current transformer (CT) can normally achieve higher frequency bandwidth. It was stated in [69] that, the CTs that are used in the distribution systems are built in the same way as the ones used in the HV transmission system. They share the same principles with only minor differences in the size, isolation materials and installation positions. With the development of optical sensors and other special types of current sensors including Rogowski coils and Hall Effect instruments, the high frequency measurement of currents is expected to become much easier in the future. For the travelling wave protection based on current measurement only, these sensing technologies can potentially become the key enablers.

3.6.3.2 Line Type

Power lines in transmission systems are quite different from those in distribution systems and microgrids. The power lines at the lower voltage levels normally are highly resistive, which results in high damping of the travelling waves. In some urban or densely populated areas, underground cables are normally used. The cables differ from the overhead lines by their larger shunt capacitance and different insulation materials. The shunt capacitance enlarges the reflected current travelling waves, and different cable materials slow down the velocity of the travelling waves in different degrees [70]. Hence, the apparent features of travelling waves in cables

are: higher magnitude of the initial fault generated travelling waves, and larger intervals between the arriving pulses.

3.6.3.3 Topology

The transmission network differs significantly from the distribution network in terms of system topology. The transmission network is normally meshed and contains very long lines up to several hundreds of kilometres, whereas the distribution network is normally radial and the lines are considerably shorter. The distribution network further contains a large number of T-junctions leading to multiple reflections of travelling waves. These arriving wavefronts are hard to discriminate from each other if the sampling rate is not sufficiently high. Some microgrids can be deliberately designed as meshed networks (much like the transmission system), however, still subject to the short length of the lines.

In summary, there are several issues which should be considered before the design and implementation:

1) The line length in a microgrid is normally quite short, which implies much higher demand on sampling frequency.
2) The highly resistive lines in the MV/LV systems significantly damp the travelling waves. To minimise this effect the proposed protection scheme should be dependent on the initial travelling wavefronts rather than the series of wavefronts.
3) Faults with small fault inception angle (voltage close to zero) do not present easily detectable transient features for wavelet based protection. Therefore, supplemental protection schemes are always needed.
4) The cost and availability of high frequency transducers still are one of the major obstacles for the application of the wavelet-based protection. In distribution system, the cost of suitable voltage transducers is prohibitive, which implies that the wavelet based protection scheme should be merely relying on pure current measurements.

The magnitude of fault generated high frequency transients is greatly affected by the fault inception angle, fault resistance and distance to fault. Therefore, the magnitude is generally not a suitable indicator of the fault condition and its location. By contrast, the time and polarity information provides good fault indication, and has been widely used in travelling wave based methods [15,16].

3.6.4 Existing Protection Methods Based on the Travelling Wave Theory

Following the introduction of the basic theory of travelling waves, a review of the existing protection schemes based on this theory presented in the following subsections is aimed to build up a comprehensive understanding of the application and help to identify potential novel solutions.

3.6.4.1 Cross-correlation Function

The first method was developed using cross-correlation function (CCF) in the 80s of the last century [67]. This technique, using the Telegrapher's equation, derives the forward and backward travelling wave functions as (3-6):

$$\begin{aligned} S_1 &= 2f_2 = v(t) - Z_0 i(t) \\ S_2 &= 2f_1 = v(t) + Z_0 i(t) \end{aligned} \tag{3-6}$$

Where f_1 is the forward component and f_2 is the backward component; $v(t)$ and $i(t)$ are voltage and current measurements; and Z_0 is the characteristic impedance of the line. Extracting the incremental part of S_1 and S_2, the discrete CCF is performed between successive section $\hat{S}_1$ and the stored section $\hat{S}_2$ [68]:

$$CCF(\tau) = \frac{1}{N}\sum_{k=1}^{N} \hat{S}_2(k\Delta t - \tau) \cdot \hat{S}_1(k\Delta t) \tag{3-7}$$

The detector CCF measures the degree to which the incident and the corresponding reflected signals are correlated, that is, how similar they are [67]. It needs to be noted that initially, the valid stored section $\hat{S}_2$ was regarded as a collection of reflected signals from the fault. In fact, it might also be merged with travelling wavefronts from the behind of the relay, the other end of the line, or even remote lines. There is always a trade-off between the scheme's sensitivity of detecting close-up faults and stability against non-fault disturbances.

Modifications by using two window lengths made by [68, 71] only enhance the performance to some extent but do not fully resolve this issue. Two fixed windows are not able to provide accurate identification of the propagating waves with such large frequency range. Nevertheless, [71-72] prove that pure voltage signal alone contains all the features of the travelling waves. Different from [71], [72] uses a "stack-tuner" adjusted to certain frequency bandwidth to extract the high frequency fault transients. With the knowledge of the network data, the authors demonstrate that it is possible to define the frequency band of the travelling wave. The line traps are installed at each end of the line to confine the transients to the protected zone.

The paper [73] discovers another issue related to high impedance fault, which cannot provide larger reflected wavefront than that imposed by the remote-end solid fault. Based on this, the authors propose an adaptive strategy using two correlation functions, which is based on the time features of the wavefronts. However, all these techniques fail to solve the issue of the data window. It has been highlighted that a variable data window is necessary in travelling wave based analysis, which implies an inherent shortcoming of the CCF techniques. Furthermore, the features of corresponding reflected wavefronts are much more complex than stated in these references: they could cancel out each other with different polarities; their arrival sequence and polarities vary with line length, line materials, topologies and fault location.

3.6.4.2 Multi-channel Bandpass Filters

It is known that Bandpass filters can be tuned to extract the fault transients from the original voltage or current travelling waves [70, 72, 74-76]. The papers [74-76] use

multi-channel band-pass filters to extract the “operating” signal based on the a narrow band of frequencies centred around the tuned frequency, and the “restraint” signal based on another narrow band of frequencies centred around the lower than the tuned frequency. The ratio of these two signals determines whether a fault is internal or external. Unfortunately, this technology only takes account of the energy of the signals in frequency domain; any spurious noises within the electronic circuitry could affect the performance of the relays. Moreover, it is problematic to define the centre frequency for the fault generated noise, since the transients cover quite a broad frequency range.

Later on, [70] starts utilizing the features of the fault transients in time domain, proposing its application to fault location. Using the lattice diagram, reflection and refraction, travelling routes of the fault transients can be easily illustrated. Here the band-pass filtered signals can be directly used as the protective indicators. This idea is quite similar to that of the CCF method, which is based on the extraction and discrimination of the required reflected travelling waves from others. Of course, it can still be perceived as too complex, since the travelling wave routes vary according to different system topologies and fault locations.

Moreover, the noise interferences from the line and the monitoring equipment itself could also be an issue, although the impact should be theoretically reduced since only the polarity and arrival time of the signals are of interest. Nevertheless, the polarity and time information of the wavefronts cannot even be clearly seen in some cases according to the simulation results in [70]. The high oscillations around the arrival wavefronts make it hard to achieve correct discrimination. Due to these reasons, a better signal processing technology is needed to capture the wavefronts.

3.6.4.3 Wavelet Decomposition Filters

Main-stream technologies of signal processing are windowed Fourier Transform (WFT) and wavelet transform (WT). Fundamentally, these two technologies have a close relation regarding their principles: they both process the signals through a certain numerical window.

WFT was firstly proposed to give both the time and frequency information of the signals simultaneously. The WFT is defined by:

$$WFT(\tau,\omega)=\int_{-\infty}^{\infty}f(t)w(t-\tau)e^{-j\omega t}dt \tag{3-8}$$

The WFT specifies complex amplitude of the signal $f(t)$ versus time and frequency by the equal and fixed numerical windows $w(t-\tau)$ which is localized at time τ. Thus the processed signals can only be processed in one definite frequency, which assumes that the signal is stationary during an observation time period. Unfortunately, for non-stationary signals with large bandwidth of spectrum, this assumption is not true and the method's performance unsatisfactory.

Unlike WFT, with a suitable mother wavelet, WT can be applied as a flexible and effective high frequency bandpass filter [77-78], which uses short windows at high frequencies and long windows at low frequencies. WT is defined by (3-9):

$$WT(a,b)=\int_{-\infty}^{\infty}f(t)\cdot w_{a,b}(t)dt \tag{3-9}$$

$$w_{a,b}(t)=\frac{1}{\sqrt{a}}w(\frac{t-b}{a}) \tag{3-10}$$

Where $w_{a,b}(t)$ is the mother wavelet function, a is a positive real number which defines the scale, and b is a real number which defines a shift. Equation (3-9) defines continuous wavelet transform (CWT), which results in redundant wavelet coefficients. To avoid this redundancy, discrete wavelet transform (DWT) is a good solution, which is defined as:

$$DWT(m,n)=\sum_{k}f(k)\cdot w_{m,n}(k) \tag{3-11}$$

$$w_{m,n}(k) = \frac{1}{\sqrt{a_0^m}} \cdot w(\frac{k - a_0^m n}{a_0^m}) \tag{3-12}$$

Where the scale factor a is replaced by a_0^m, shift factor is replaced by n, and m is the decomposition level. Normally the dilating basis a_0 is set to 2, resulted in a down sampling along the dyadic sequence $2^j (j = 1{:}m)$. The construction of the dyadic bases can thus be related to the multiresolution analysis, and so that later Mallat et al. in [79] propose a pyramid algorithm of multiresolution to connect the wavelets with the filter banks. The detailed mathematical derivations and explanation can be seen in the existing text book [80]. In a simplified way, the pyramid decomposition can be presented in the form of a wavelet decomposition tree, as shown in Figure 3-7. At each level of decomposition, the approximation part ca_n is obtained by passing through a low-pass digital filter *LF* and down sampled by 2, while the detailed part cd_n is obtained by passing through hi-pass digital filter *HF* and also down sampled by 2.

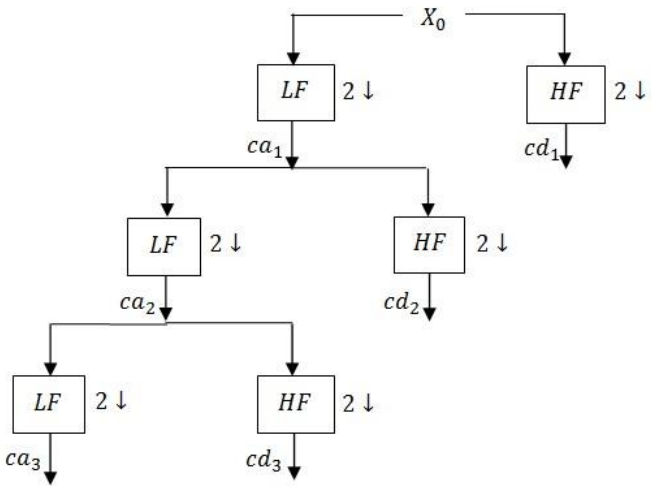

Figure 3-7: The DWT decomposition tree

At the n_{th} level of decomposition, the pseudo-frequency can be determined in (3-13) [81], where T_S is the sampling period of the input signal and f_s is the centre frequency of the mother wavelet function.

$$f_n = T_S f_S / a_0^n \tag{3-13}$$

By wavelet decomposition, certain frequency components can be clearly extracted, and this feature helps to achieve better performance for the travelling-wave-based protection techniques. Considering the characteristics of travelling waves in the power system, which cover a very wide range of frequency bandwidth, one scale of wavelet analysis is normally insuffcient.

Protection methods based on DWT analysis have drawn interest of many researchers [73, 82-88]. These protection schemes can be classified into following groups:

1) fault location alike protection based on the time information according to the modulus maxima after wavelet decomposition [73,87,82];
2) directional protection based on the polarity and amplitude of the initial travelling wavefronts [83-85];
3) directional protection based on the transient energy of certain frequency bandwidth [86,88];
4) hybrid methods combining the travelling wave theory with artificial neural network, PCA analysis or other similar methods [89-90].

Time intervals of the modulus maxima

These initially proposed DWT based protection schemes were actually more like fault location schemes, as they calculate the exact fault distance by using the time intervals of the modulus maxima after DWT decomposition [82, 86-87]. The paper [70] cited earlier in this chapter uses this principle, only utilizing a different signal processing tool: a hardware multi-band filter rather than the software DWT decomposition. Actually from the theory point of view, DWT decomposition can be also regarded as a multi-band filter, since it applies a series of hi-pass and lo-pass filters to disseminate the signal into separate frequency bands.

A modulus maximum is calculated by taking the maximum absolute value of the detailed coefficient along a certain numerical window of DWT. In this way, the method is much less contaminated by the oscillations around the wavefront's arrival.

As this method can be realized as a single-end method without any communication requirement, it avoids the costs and complexities associated with the remote-end synchronization.

However, similar to the statement in section 3.6.4.2, this algorithm is noted to be complex and erroneous for accurate fault location due to its difficulty in distinguishing between travelling waves reflected from the fault and from other ends of the system. Furthermore, the accuracy is subject to system noise and the method is insensitive to faults occurring at near zero voltage. Accurate detection of at least first two initial wavefronts by DWT itself could be a problem, and the consistency of the time location of the modulus maxima across multi-level DWT decompositions is still debatable. These issues will be further discussed in Chapter 4.

Methods based on the polarity or/and amplitude of both the initial voltage and current travelling wavefronts

Papers [77] and [83] proposed a DWT based directional protection scheme using the polarity of the initial voltage and current travelling waves. However, the authors of [83] have already raised an issue associated with the difficulty of sampling the voltage transients. The paper [84] develops an idea of "surge impedance relay" which also uses both the voltage and current travelling waves under multiple frequency bands. Unlike [83], this technique considers both amplitude and polarity of the initial travelling waves. Additional algorithm is also included to detect the near zero voltage fault. The work presented in [84-85] further developed the discrimination scheme to recognise the type of fault, which is demonstrated to work in the HV transmission system. However, because the indicator is highly affected by the fault inception angle, the reliability of this phase selection scheme is not well verified.

Methods based on transient wavelet energy

The transient wavelet energy is defined in two ways in technical literature: one is a sum of the square of the detailed/approximate coefficients after DWT decomposition [86], and the other is an absolute sum of the detailed/approximate coefficients [88]. Groups of methods based on both definitions were are good in sensitivity, reliability

and selectivity. They have the advantages of reducing the impact of random noise of the system by using summed coefficients, however, at the same time impose high computational burden. Results can be obtained only after a numerical window of one to three level DWT decomposition which is risky for the implementation of any time critical protection function.

Others

Jafarian et al in [89] described one example of the developed wavelet based protection, which is generally combined with other numerical analysis technologies, including neural networks, PCA, artificial intelligence, fuzzy logic, etc.

Aguilera et al [91] proposed a hybrid method based on a combination of transient wavelet energy and traditional distance protection principles.

Nonetheless, these techniques complicate protection schemes, and do not solve all the inherent issues of wavelet based protection. The main issues of the existing wavelet based methods can be summarised as follows:

1) The capabilities of wavelets are affected by the existence of system noise.
2) There is often an unresolved dispute in the identification of the most suitable wavelet family to achieve the most accurate extraction of the transient features.
3) Furthermore, most of the wavelet based protection schemes employ multi-level wavelet decomposition, and some of them use even complicated continuous wavelet transform or complex wavelet transform, which requires multi-level filtering followed by complex computations.

3.6.4.4 Mathematical Morphological Filters

An alternative method is proposed by Wu et al [92] using mathematical morphological filters (MMF). Mathematical Morphology (MM) theory was developed from set theory and integral geometry in 1964 by G. Matheron and J. Serra, and is concerned with the shape of a signal waveform in the time domain rather than the frequency domain [93]. The basic idea is to use a probe, which is

named as Structural Element (SE), to collect useful information of the signals. Depending on different usages, SE may be linear, square, disk beeline, inclined-line, curve, triangle, polygon, rotundity or ball-shaped [94]. Moving a SE probe along the signal wave, it can be decomposed into several parts that have different physical significances. This process is named as Morphological Transform (MT) and is a nonlinear approach inherently. In theory, with a proper SE, MT can help recognize the radical shape of a signal even mixed with large amount of noise [95]. It has been widely used in the areas of image processing, machine vision, and pattern recognition.

Dilation ($\oplus$) and erosion ($\ominus$) are two basic operations of MM to help extracting the needed features of the signal [92, 96-97]. If we name abrupt downward pulses of a signal as holes, erosion is like a shrinking transform, making the signal contract while enlarging the holes; and dilation is an expanding transform, expanding the signal while contracting the holes. To explain it explicitly, for example, if moving a flat SE with a moving window of 3 (i.e. SE = [0,0,0]) over a signal $f(n)$, the dilation process picks up the maximum value every three samples, and the erosion process takes the minimum one every three examples. Assuming an input signal $f(n)$ $(0 < \mathrm{n} < N)$ and $SE(m)$ $(0 < m < M)$ applied, mathematical functions of dilation (f_{dil}) and erosion (f_{ero}) processes are listed in (3-14) and (3-15).

$$f_{dil}(n) = f(n) \oplus SE(m) = max\begin{Bmatrix} f(n-m) + SE(m), \\ 0 < n-m < N, 0 < m < M \end{Bmatrix} \tag{3-14}$$

$$f_{ero}(n) = f(n) \ominus SE(m) = min\begin{Bmatrix} f(n+m) - SE(m), \\ 0 < n+m < N, 0 < m < M \end{Bmatrix} \tag{3-15}$$

In the above two equations, N represents the length of the moving window for the input signal and M stands for the length of the SE. Apart from dilation and erosion, two additional functions called opening ($\circ$) and closing ($\bullet$) [93, 98] are also popular operations of MM technology as defined in (3-16) and (3-17).

$$f_{op}(n) = f(n) \circ SE(m) = \big(f(n) \ominus SE(m)\big) \oplus SE(m) \tag{3-16}$$

$$f_{cl}(n) = f(n) \bullet SE(m) = \big(f(n) \oplus SE(m)\big) \ominus SE(m) \tag{3-17}$$

The opening process damps the sharp edges whereas closing process fills the narrow gaps in a contour. In one dimensional analysis, using one or a mixture of the basic operators (erosion, dilation, opening and closing), various types of MMFs are then established [96]. One typical MMF is a simple dilation-erosion difference filter (*DEDF*) and another is an opening-closing difference filter (*OCDF*). These MMFs have been recently used for event detection in the protection field [96]. *DEDF* and *OCDF* are defined in (3-18) and (3-19).

$$DEDF(n) = f_{dil}(n) - f_{ero}(n) \tag{3-18}$$

$$OCDF(n) = f_{op}(n) - f_{cl}(n) \tag{3-19}$$

The application of MM technique to power system protection area was firstly attempted for identification of transformer inrush current [99]. Wu et al. [92] introduces the technique to network protection area using two composite relaying signals correspond to forward and backward components of the travelling waves. This method has the similar principles with one of the DWT based schemes – using the time intervals of the modulus maxima as introduced in Section 3.4.3.3. Later on, more researchers provided detailed analysis of this application and extend the use of MM technique to the fault location field [100-102]. Generally, the discrimination of the arrival time of the first series of travelling wavefronts is the key point of these MM based protection methods, whereas apart from the Wu et al., the polarity information is not taken seriously in the algorithm. Owing to the advantages such as simple addition/subtraction operations of MM based nonlinear signal processing, the time intervals can be detected much more accurately and with much lighter computational burden.

3.7 Chapter Summary

This chapter focused on the review and discussion of the microgrid protection methods and schemes. The first part illustrated the DER impact on the protection of the distribution system and microgrid system. Following the description of the fault behaviour of different types of DERs, the issues and challenges associated with the integration of DER were summarized. The existing protection schemes for the protection of the microgrid are fully investigated and are classified according to their own advantages and addressed problems.

The second part of this chapter presented a detailed discussion of the travelling wave theory. The boundary characteristics were highlighted as one of the key factors affecting the effectiveness of the travelling wave based protection schemes. In order to avoid high complexity of the protection scheme, the travelling wave theory was recommended for the microgrid protection.

The existing travelling wave based protection schemes were classified into four groups by different signal processing technologies: CCF based methods, multi-channel based methods, wavelet based methods and MM based methods. It was demonstrated that among these signal processing tools, the most broadly studied and tested group were the methods based on wavelet analysis. Under this category, further classification was made according to four typical protective algorithms: the method based on time intervals of modulus maxima, the method based on the polarity and amplitude of initial travelling wavefronts, the method based on the transient wavelet energy, and hybrid methods combining the travelling wave theory with other protective principles.

As the most travelling wave based protection schemes are applied to the transmission system, a detailed discussion on the issues of their applications in distribution system and microgrid systems was presented at the final section of this chapter, in order to lay foundations for the introduction of the proposed protection scheme in the following chapter. The sampling instruments, line types and the typical system topology in distribution systems and microgrid systems put up a list of new requirements for the new proposed protection scheme.

3.8 References

[1] E. T. Association and I. of E. Engineers, Power System Protection 1: Principles and Components. IET, 1995.

[2] B. Ram and D. N. Vishwakarma, Power System Protection and Switchgear. Tata McGraw-Hill Education, 2001.

[3] Y. G. P., S. R. Bhide, Fundamentals of Power System Protection. PHI Learning Pvt. Ltd., 2010.

[4] IEC 61400-21 ed2.0, "Wind Turbines - Part 21: Measurement and Assessment of Power Quality Characteristics of Grid Connected Wind Turbines." DERlab, 13-Aug-2008.

[5] "IEEE Recommended Practice for Electric Power Distribution for Industrial Plants," IEEE Std. 141-1993, 1994.

[6] N. Jenkins, Embedded generation. IET, 2000.

[7] Working Group B5.34, "The Impact of Renewable Energy Sources and Distributed Generation on Substation Protection and Automation," CIGRE, Nov. 2009.

[8] J. Keller and B. Kroposki, "High Penetration Solar Portal: Understanding Fault Characteristics of Inverter-Based Distributed Energy Resources," National Renewable Energy Laboratory, Technical Report, US, Feb. 2011.

[9] W. Kramer, C. Pink, R. Deblasio, M. Simões, and P. K. Sen, "Advanced Power Electronic Interfaces for Distributed Energy Systems, Part I: Systems and Topoloties." NREL/TP561-42672. Golden, US: National Renewable Energy Laboratory, Mar-2008.

[10] B. Kroposki, C. Pink, R. DeBlasio, H. Thomas, M. Simões, and P. K. Sen, "Benefits of Power Electronic Interfaces for Distributed Energy Systems," IEEE Transactions on Energy Conversion, vol. 25, no. 3, pp. 901–908, Sep. 2010.

[11] A. Oudalov and A. Fidigatti, "Adaptive network protection in microgrids," International Journal of Distributed Energy Resources, vol. 5, no. 3, pp. 201–226, Sep. 2009.

[12] R. C. Dugan and T. E. McDermott, "Distributed generation," IEEE Industry Applications Magazine, vol. 8, no. 2, pp. 19–25, 2002.

[13] K. D and L. Kumpulainen, "Impact of Distributed Generation on the Protection of Distribution Networks," in Eighth IEE International Conference on Developments in Power System Protection, 2004, 2004, vol. 1, pp. 315–318 Vol.1.

[14] A. R. Haron, A. Mohamed, H. Shareef, and H. Zayandehroodi, “Analysis and Solutions of Overcurrent Protection Issues in a Microgrid,” in 2012 IEEE International Conference on Power and Energy (PECon), 2012, pp. 644–649.

[15] J. Driesen, P. Vermeyen, and R. Belmans, “Protection Issues in Microgrids with Multiple Distributed Generation Units,” in Power Conversion Conference - Nagoya, 2007. PCC ’07, 2007, pp. 646–653.

[16] Z. Jiang and R. A. Dougal, “Hierarchical Microgrid Paradigm for Integration of Distributed Energy Resources,” in 2008 IEEE Power and Energy Society General Meeting - Conversion and Delivery of Electrical Energy in the 21st Century, 2008, pp. 1–8.

[17] H. H. Zeineldin, E. F. El-Saadany, and M. M. A. Salama, “Distributed Generation Micro-Grid Operation: Control and Protection,” in Power Systems Conference: Advanced Metering, Protection, Control, Communication, and Distributed Resources, 2006. PS ’06, 2006, pp. 105–111.

[18] W. Bin, S. Ming, and D. Baole, “The Existed Problems and Possible Solutions of Distributed Generation Microgrid Operation,” in Power and Energy Engineering Conference (APPEEC), 2011 Asia-Pacific, 2011, pp. 1–4.

[19] R. C. Dugan and T. E. McDermott, “Operating conflicts for distributed generation on distribution systems,” in Rural Electric Power Conference, 2001, 2001, pp. A3/1–A3/6.

[20] A. R. Haron, A. Mohamed, and H. Shareef, “A Review on Protection Schemes and Coordination Techniques in Microgrid System,” Journal of Applied Sciences, vol. 12, no. 2, pp. 101–112, Feb. 2012.

[21] R. H. Lasseter, “MicroGrids,” in IEEE Power Engineering Society Winter Meeting, 2002, 2002, vol. 1, pp. 305–308 vol.1.

[22] M. N. Ambia, A. Al-Durra, C. Caruana, and S. M. Muyeen, “Stability enhancement of a hybrid micro-grid system in grid fault condition,” in 2012 15th International Conference on Electrical Machines and Systems (ICEMS), 2012, pp. 1–6.

[23] C. A. Plet, M. Brucoli, J. D. F. McDonald, and T. C. Green, “Fault models of inverter-interfaced distributed generators: Experimental verification and application to fault analysis,” in 2011 IEEE Power and Energy Society General Meeting, 2011, pp. 1–8.

[24] G. D. Rockefeller, C. L. Wagner, J. R. Linders, K. L. Hicks, and D. T. Rizy, “Adaptive Transmission Relaying Concepts for Improved Performance,” IEEE Transactions on Power Delivery, vol. 3, no. 4, pp. 1446–1458, 1988.

[25] K.-H. Zheng and M.-C. Xia, “Impacts of microgrid on protection of distribution networks and protection strategy of microgrid,” in 2011

International Conference on Advanced Power System Automation and Protection (APAP), 2011, vol. 1, pp. 356–359.

[26] S. M. Brahma and A. A. Girgis, “Development of Adaptive Protection Scheme for Distribution Systems with High Penetration of Distributed Generation,” IEEE Transactions on Power Delivery, vol. 19, no. 1, pp. 56–63, 2004.

[27] S. A. M. Javadian, M.-R. Haghifam, and P. Barazandeh, “An adaptive over-current protection scheme for MV distribution networks including DG,” in IEEE International Symposium on Industrial Electronics, 2008. ISIE 2008, 2008, pp. 2520–2525.

[28] N. Schaefer, T. Degner, A. Shustov, T. Keil, and J. Jaeger, “Adaptive Protection System for Distribution Networks with Distributed Energy Resources,” in Managing the Change, 10th IET International Conference on Developments in Power System Protection (DPSP 2010), 2010, pp. 1–5.

[29] P. Mahat, Z. Chen, B. Bak-Jensen, and C. L. Bak, “A Simple Adaptive Overcurrent Protection of Distribution Systems With Distributed Generation,” IEEE Transactions on Smart Grid, vol. 2, no. 3, pp. 428–437, 2011.

[30] R. M. Tumilty, M. Brucoli, G. M. Burt, and T. C. Green, “Approaches to network protection for inverter dominated electrical distribution systems,” in The 3rd IET International Conference on Power Electronics, Machines and Drives, 2006. PEMD 2006, 2006, pp. 622–626.

[31] Y. Han, X. Hu, and D. Zhang, “Study of Adaptive Fault Current Algorithm for Microgrid Dominated by Inverter Based Distributed Generators,” in 2010 2nd IEEE International Symposium on Power Electronics for Distributed Generation Systems (PEDG), 2010, pp. 852–854.

[32] K. Dang, X. He, D. Bi, and C. Feng, “An adaptive protection method for the inverter dominated microgrid,” in 2011 International Conference on Electrical Machines and Systems (ICEMS), 2011, pp. 1–5.

[33] T. S. Ustun, C. Ozansoy, and A. Zayegh, “Modeling of a Centralized Microgrid Protection System and Distributed Energy Resources According to IEC 61850-7-420,” IEEE Transactions on Power Systems, vol. 27, no. 3, pp. 1560–1567, 2012.

[34] M. Khederzadeh, “Adaptive Setting of Protective Relays in Microgrids in Grid-connected and Autonomous Operation,” 2012, pp. P14–P14.

[35] M. R. Islam and H. A. Gabbar, “Analysis of Microgrid Protection Strategies,” in 2012 IEEE International Conference on Smart Grid Engineering (SGE), 2012, pp. 1–6.

[36] J. Wei, H. Zheng-you, and B. Zhi-qian, “The Overview of Research on Microgrid Protection Development,” in 2010 International Conference on

Intelligent System Design and Engineering Application (ISDEA), 2010, vol. 2, pp. 692–697.

[37] X. Li, A. Dysko, and G. M. Burt, “Application of Communication Based Distribution Protection Schemes in Islanded Systems,” in Universities Power Engineering Conference (UPEC), 2010 45th International, 2010, pp. 1–6.

[38] M. Dewadasa, A. Ghosh, and G. Ledwich, “Protection of Microgrids Using Differential Relays,” in Universities Power Engineering Conference (AUPEC), 2011 21st Australasian, 2011, pp. 1–6.

[39] S. Conti, L. Raffa, and U. Vagliasindi, “Innovative Solutions for Protection Schemes in Autonomous MV Micro-grids,” in 2009 International Conference on Clean Electrical Power, 2009, pp. 647–654.

[40] E. Sortomme, S. S. Venkata, and J. Mitra, “Microgrid Protection Using Communication-Assisted Digital Relays,” IEEE Transactions on Power Delivery, vol. 25, no. 4, pp. 2789–2796, 2010.

[41] N. El Halabi, M. Garc ́a-Gracia, J. Borroy, and J. L. Villa, “Current phase comparison pilot scheme for distributed generation networks protection,” Applied Energy, vol. 88, no. 12, pp. 4563–4569, Dec. 2011.

[42] M. Dewadasa, A. Ghosh, and G. F. Ledwich, “Distance protection solution for a converter controlled microgrid,” Dec. 2008.

[43] M. Dewadasa, A. Ghosh, G. Ledwich, and M. Wishart, “Fault Isolation in Distributed Generation Connected Distribution Networks,” IET Generation, Transmission Distribution, vol. 5, no. 10, pp. 1053–1061, 2011.

[44] H. Nikkhajoei and R. H. Lasseter, “Microgrid Protection,” in IEEE Power Engineering Society General Meeting, 2007, 2007, pp. 1–6.

[45] H. Al-Nasseri, M. A. Redfern, and R. O’Gorman, “Protecting Micro-grid Systems Containing Solid-state Converter Generation,” in 2005 International Conference on Future Power Systems, 2005, p. 5 pp.–5.

[46] H. Al-Nasseri, M. A. Redfern, and F. Li, “A Voltage Based Protection for Micro-grids Containing Power Electronic Converters,” in IEEE Power Engineering Society General Meeting, 2006, 2006, p. 7 pp.–.

[47] M. A. Redfern and H. AL-Nasseri, “Protection of micro-grids dominated by distributed generation using solid state converters,” in IET 9th International Conference on Developments in Power System Protection, 2008. DPSP 2008, 2008, pp. 670–674.

[48] T. Loix, T. Wijnhoven, and G. Deconinck, “Protection of Microgrids with a High Penetration of Inverter-coupled Energy Sources,” in Integration of Wide-Scale Renewable Resources Into the Power Delivery System, 2009 CIGRE/IEEE PES Joint Symposium, 2009, pp. 1–6.

[49] Jiang Wei, He Zheng-you, and Bo Zhi-qian, “The Overview of Research on Microgrid Protection Development,” in 2010 International Conference on Intelligent System Design and Engineering Application (ISDEA), 2010, vol. 2, pp. 692–697.

[50] T. S. Ustun, C. Ozansoy, and A. Zayegh, “A Central Microgrid Protection System for Networks with Fault Current Limiters,” in 2011 10th International Conference on Environment and Electrical Engineering (EEEIC), 2011, pp. 1–4.

[51] U. A. Khan, J.-S. Hwang, J.-K. Seong, and B.-W. Lee, “Application and Positioning Analysis of a Resistive Type Superconducting Fault Current Limiter in AC and DC Microgrids Using Simulink and SimPowerSystem,” in 2011 1st International Conference on Electric Power Equipment - Switching Technology (ICEPE-ST), 2011, pp. 348–351.

[52] Y. Zhang and R. A. Dougal, “State of the Art of Fault Current Limiters and Their Applications in Smart Grid,” in 2012 IEEE Power and Energy Society General Meeting, 2012, pp. 1–6.

[53] D. M. Vilathgamuwa, P. C. Loh, and Y. Li, “Protection of Microgrids During Utility Voltage Sags,” IEEE Transactions on Industrial Electronics, vol. 53, no. 5, pp. 1427–1436, 2006.

[54] M. Khederzadeh, “Preservation of Overcurrent Relays Coordination in Microgrids by Application of Static Series Compensators,” in 11th International Conference on Developments in Power Systems Protection, 2012. DPSP 2012, 2012, pp. 1–5.

[55] N. Jayawarna, N. Jenkins, M. Barnes, M. Lorentzou, S. Papthanassiou, and N. Hatziagyriou, “Safety Analysis of a Microgrid,” in 2005 International Conference on Future Power Systems, 2005, p. 7 pp.–7.

[56] N. Jayawarna, M. Barnes, C. Jones, and N. Jenkins, “Operating MicroGrid Energy Storage Control during Network Faults,” in IEEE International Conference on System of Systems Engineering, 2007. SoSE ’07, 2007, pp. 1–7.

[57] N. Jayawarna and M. Barnes, “Central Storage Unit Response Requirement in ‘Good Citizen’ Microgrid,” in 13th European Conference on Power Electronics and Applications, 2009. EPE ’09, 2009, pp. 1–10.

[58] C. Jones, C. Fitzer, and M. Barnes, “Unified Control and Operation of a 20 kVA Laboratory Microgrid Incorporating Flywheel Energy Storage,” International Journal of Distributed Energy Resources, vol. 3, pp. 313–337, 2007.

[59] B. Hussain, S. M. Sharkh, S. Hussain, and M. A. Abusara, “Integration of Distributed Generation Into the Grid: Protection Challenges and Solutions,” in

Managing the Change, 10th IET International Conference on Developments in Power System Protection (DPSP 2010), 2010, pp. 1–5.

[60] F. van Overbeeke, “Fault current source to ensure the fault level in inverter-dominated networks,” in 20th International Conference and Exhibition on Electricity Distribution - Part 1, 2009. CIRED 2009, 2009, pp. 1–4.

[61] H. Al-Nasseri and M. A. Redfern, “Harmonics content based protection scheme for Micro-grids dominated by solid state converters,” in Power System Conference, 2008. MEPCON 2008. 12th International Middle-East, 2008, pp. 50–56.

[62] T. David, S. Mark, C. David, C. Ed, W. Xiaohui, and G. Rinze, “DC Power System Fault Protection - Test of Novel Techniques,” in Engine as a Weapon III, Portsmouth Historic Dockyard, UK, 2009.

[63] S. Shi, B. Jiang, X. Dong, and Z. Bo, “Protection of microgrid,” in Managing the Change, 10th IET International Conference on Developments in Power System Protection (DPSP 2010), 2010, pp. 1–4.

[64] A. T. Johns, “New ultra-high-speed directional comparison technique for the protection of e.h.v. transmission lines,” Generation, Transmission and Distribution, IEE Proceedings C, vol. 127, no. 4, pp. 228–239, Jul. 1980.

[65] G. W. Swift, “The Spectra of Fault-Induced Transients,” IEEE Transactions on Power Apparatus and Systems, vol. PAS-98, no. 3, pp. 940–947, May 1979.

[66] H. van der Merwe and F. S. van der Merwe, “Some features of travelling waves on cables,” IEEE Transactions on Power Delivery, vol. 8, no. 3, pp. 789–797, Jul. 1993.

[67] P. A. Crossley and P. G. Mclaren, “Distance Protection Based on Travelling Waves,” IEEE Transactions on Power Apparatus and Systems, vol. PAS-102, no. 9, pp. 2971–2983, Sep. 1983.

[68] E. H. Shehab-Eldin and P. G. McLaren, “Travelling wave distance protection-problem areas and solutions,” IEEE Transactions on Power Delivery, vol. 3, no. 3, pp. 894–902, Jul. 1988.

[69] M. Ohrstrom, M. Geidl, L. Soder, and G. Andersson, “Evaluation of travelling wave based protection schemes for implementation in medium voltage distribution systems,” in 18th International Conference and Exhibition on Electricity Distribution, 2005. CIRED 2005, 2005, pp. 1–5.

[70] Z. Q. Bo, G. Weller, and M. A. Redfern, “Accurate fault location technique for distribution system using fault-generated high-frequency transient voltage signals,” Generation, Transmission and Distribution, IEE Proceedings-, vol. 146, no. 1, pp. 73–79, Jan. 1999.

[71] C. Christopoulos, D. W. P. Thomas, and A. Wright, “Signal processing and discriminating techniques incorporated in a protective scheme based on travelling waves [power lines],” Generation, Transmission and Distribution, IEE Proceedings C, vol. 136, no. 5, pp. 279 –288, Sep. 1989.

[72] A. T. Johns and P. Agrawal, “New approach to power line protection based upon the detection of fault induced high frequency signals,” Generation, Transmission and Distribution, IEE Proceedings C, vol. 137, no. 4, pp. 307 – 313, Jul. 1990.

[73] L. Jie, S. Elangovan, and J. B. X. Devotta, “Adaptive travelling wave protection algorithm using two correlation functions,” Power Delivery, IEEE Transactions on, vol. 14, no. 1, pp. 126 –131, Jan. 1999.

[74] H. J. Laaksonen, “Protection Principles for Future Microgrids,” IEEE Transactions on Power Electronics, vol. 25, no. 12, pp. 2910–2918, 2010.

[75] J. A. S. . Jayasinghe, R. K. Aggarwal, A. T. Johns, and Z. Q. Bo, “A novel non-unit protection for series compensated EHV transmission lines based on fault generated high frequency voltage signals,” IEEE Transactions on Power Delivery, vol. 13, no. 2, pp. 405–413, Apr. 1998.

[76] Z. Q. Bo, “A new non-communication protection technique for transmission lines,” IEEE Transactions on Power Delivery, vol. 13, no. 4, pp. 1073–1078, Oct. 1998.

[77] C. Aguilera, E. Orduna, and G. Ratta, “Directional Traveling-Wave Protection Based on Slope Change Analysis,” IEEE Transactions on Power Delivery, vol. 22, no. 4, pp. 2025–2033, Oct. 2007.

[78] Chen XiaoNan, Xu Zhiyuan, and Suo Jidong, “Bandpass filter design based on wavelet packet,” in 2010 International Conference on Image Analysis and Signal Processing (IASP), 2010, pp. 75–78.

[79] S. G. Mallat, “A theory for multiresolution signal decomposition: the wavelet representation,” Pattern Analysis and Machine Intelligence, IEEE Transactions on, vol. 11, no. 7, pp. 674 –693, Jul. 1989.

[80] S. Mallat, A Wavelet Tour of Signal Processing, Third Edition: The Sparse Way, 3rd ed. Academic Press, 2008.

[81] D. Spoor and Jian Guo Zhu, “Improved single-ended traveling-wave fault-location algorithm based on experience with conventional substation transducers,” IEEE Transactions on Power Delivery, vol. 21, no. 3, pp. 1714–1720, Jul. 2006.

[82] S. Qianli, D. Xinzhou, Z. Q. Bo, and F. Jiang, “New approach of fault detection and fault phase selection based on initial current traveling waves,” in 2002 IEEE Power Engineering Society Summer Meeting, 2002, vol. 1, pp. 393 –397 vol.1.

[83] Wei Chen, O. P. Malik, Xianggen Yin, Deshu Chen, and Zhe Zhang, “Study of wavelet-based ultra high speed directional transmission line protection,” IEEE Transactions on Power Delivery, vol. 18, no. 4, pp. 1134– 1139, Oct. 2003.

[84] Xinzhou Dong, Yaozhong Ge, and Jiali He, “Surge impedance relay,” IEEE Transactions on Power Delivery, vol. 20, no. 2, pp. 1247– 1256, Apr. 2005.

[85] Xinzhou Dong, Wei Kong, and Tao Cui, “Fault Classification and Faulted-Phase Selection Based on the Initial Current Traveling Wave,” IEEE Transactions on Power Delivery, vol. 24, no. 2, pp. 552–559, Apr. 2009.

[86] C. Fan, K. K. Li, W. L. Chan, and W. Yu, “Study of protection scheme for transmission line based on wavelet transient energy,” International Journal of Electrical Power & Energy Systems, vol. 28, no. 7, pp. 459–470, Sep. 2006.

[87] A. H. Osman and O. P. Malik, “Wavelet transform approach to distance protection of transmission lines,” in Power Engineering Society Summer Meeting, 2001, 2001, vol. 1, pp. 115 –120 vol.1.

[88] Dong-Jiang Zhang, Q. H. Wu, Z. Q. Bo, and B. Caunce, “Transient positional protection of transmission lines using complex wavelets analysis,” IEEE Transactions on Power Delivery, vol. 18, no. 3, pp. 705– 710, Jul. 2003.

[89] P. Jafarian and M. Sanaye-Pasand, “A Traveling-Wave-Based Protection Technique Using Wavelet/PCA Analysis,” IEEE Transactions on Power Delivery, vol. 25, no. 2, pp. 588–599, Apr. 2010.

[90] M. M. Eissa, “Development and Investigation of a New High-Speed Directional Relay Using Field Data,” IEEE Transactions on Power Delivery, vol. 23, no. 3, pp. 1302–1309, Jul. 2008.

[91] C. Aguilera, E. Orduna, and G. Ratta, “Adaptive noncommunication protection based on traveling waves and impedance relay,” IEEE Transactions on Power Delivery, vol. 21, no. 3, pp. 1154–1162, Jul. 2006.

[92] Q. H. Wu, J. F. Zhang, and D. J. Zhang, “Ultra-high-speed directional protection of transmission lines using mathematical morphology,” IEEE Transactions on Power Delivery, vol. 18, no. 4, pp. 1127– 1133, Oct. 2003.

[93] J. Serra, Image Analysis and Mathematical Morphology. London: Academic Press, 1982.

[94] Y. Tingfang, L. Pei, Z. Xiangjun, and K. K. Li, “Application of Adaptive Generalized Morphological Filter in Disturbance Identification for Power System Signatures,” in International Conference on Power System Technology, 2006. PowerCon 2006, 2006, pp. 1–7.

[95] G. Li, M. Zhou, Y. Luo, and Y. Ni, “Power Quality Disturbance Detection Based on Mathematical Morphology and Fractal Technique,” in Transmission

and Distribution Conference and Exhibition: Asia and Pacific, 2005 IEEE/PES, 2005, pp. 1–6.

[96] S. Gautam and S. M. Brahma, "Overview of mathematical morphology in power systems — A tutorial approach," in IEEE Power & Energy Society General Meeting, 2009. PES '09, 2009, pp. 1–7.

[97] S. K. Buggaveeti and S. M. Brahma, "Improved Overcurrent Protection of Capacitor Banks Using Mathematical Morphology," IEEE Transactions on Power Delivery, vol. 26, no. 3, pp. 1972–1979, Jul. 2011.

[98] H. J. A. M. Heijmans, Morphological image operators. Academic Press, 1994.

[99] P. Sun, J. F. Zhang, D. J. Zhang, Q. H. Wu, and S. Potts, "Morphological identification of transformer magnetising inrush current," Electronics Letters, vol. 38, no. 9, pp. 437–438, 2002.

[100] D. J. Zhang, Q. H. Wu, J. F. Zhang, and K. I. Nuttall, "Accurate fault location based on transients extraction using mathematical morphology," Electronics Letters, vol. 38, no. 24, pp. 1583– 1585, Nov. 2002.

[101] L. Zou, P. Liu, and Q. Zhao, "Applications of multiresolution morphological analysis in ultra high speed protection of transmission line," Generation, Transmission and Distribution, IEE Proceedings-, vol. 153, no. 5, pp. 515– 523, Sep. 2006.

[102] Mingyu Yang and Shuping Tan, "Research on an Ultra-High-Speed Protection Based on Multiresolution Morphological Gradient," in International Conference on Power System Technology, 2006. PowerCon 2006, 2006, pp. 1–5.

4. An Enhanced Decentralized Control Scheme for the Multi-IIG Based Microgrid

4.1 Introduction

Connection of more than one IIG to a microgrid poses additional challenges to the control strategy, especially for large microgrids running under the islanded operation. In this case, the controllers are not only responsible for voltage and frequency regulation, but also for load sharing among the IIGs and minimization of the circulating power/current [1]. Schematic diagram of a multi-inverter system is presented in Figure 4-1, where $Z_{out}\angle\theta$ is the output impedance, $V_i\angle\varphi$ is the IIG internal voltage phasor and $V_g\angle 0°$ is the common bus voltage regarded as a reference. The circuit breaker controls the operational mode of this network to be islanded or grid-connected.

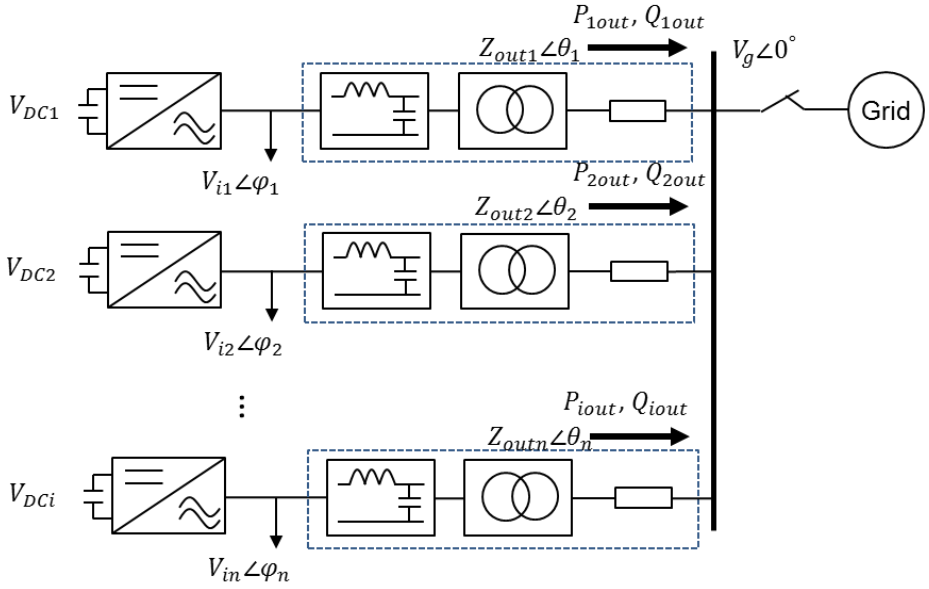

Figure 4-1: A brief diagram of the multi-IIG based system

In an ideal situation, when the IIGs with the same parameters and ratings are connected to a common bus through equal equivalent impedances ($Z_{out1}\angle\theta_1 =$

$Z_{out2}\angle\theta_2 = \cdots = Z_{outn}\angle\theta_{outn}$), a balanced power sharing of the loads connected to the common bus can be achieved. However, in reality, there is certain level of deviation in the IIG parameters which is likely to disrupt the balance of load sharing. Moreover, if IIGs are connected to each other with unequal and long lines, especially highly inductive lines, circulating currents will be generated between IIGs due to their output voltage angle and magnitude differences. These currents not only undermine the load sharing accuracy, but also reduce power transfer capacity of the network as well as degrade the transient response and operational stability of the overall system. Under the abovementioned scenario, fixed voltage and frequency control can no longer be employed in islanded multi-IIG system, since it does not allow any voltage magnitude or angle deviations.

In order to achieve the connection of multi-IIGs to the microgrid in islanded condition, much effort has been made as discussed in more detail in Chapter 2. These methods can be classified into communication assisted methods and non-communicating methods. Generally, communication assisted control strategies can achieve better voltage regulation and load sharing, in spite of reliability concerns and safety of the communication channels. Such designs are also likely to have a single mode failure because the performance of the whole controller relies on the control center decisions. The strategies without inter-unit communication for the primary control, on the other hand, are able to control the IIGs using local measurements only, and therefore, are more reliable and feasible for connection of multi-IIGs in rural areas with longer and weaker lines. They can be designed to have certain level of flexibility towards the changes of system topology and/or loading conditions. Due to these fundamental functional reasons, this chapter is dedicated to develop a new decentralized control scheme, independent of any communication media, or at least independent for its primary level of control.

The existing decentralized controllers are mostly based on drooped characteristics. These controllers are designed to emulate rotating machines, and have been proven to be effective in load sharing performance among the IIGs. However, the droop based methods have a number of inherent drawbacks, including bad operational stability under diverse output feeder connections, and a trade-off between balanced

load sharing and voltage magnitude/angle deviation [2-3]. Even with improvements made by implementing “virtual impedances”, the flexibility under system topology changes is rather restrained. In this thesis, this issue will be investigated both through theoretical analysis and simulation based verification.

In order to make the control scheme flexible under these changes, an innovative decentralized control regime, termed as “direct P/Q controller”, is proposed in this chapter. This controller is developed from the conventional grid-connected controller with an adaptive function for different modes of operation realized by introducing a wide-area based synchronization technique. It should be noted that this control scheme is designed to operate as a primary level of control, the tertiary control for power sharing management is not considered.

This chapter is organized as follows. In Section 4.2 the principles and inherent issues associated with the mainstream decentralized control of multi-IIG based systems are discussed. In Section 4.3a robust decentralized control scheme under islanded operation is proposed. Based on this, a mode flexible control scheme is further developed for both islanded and grid-connected operation. In order to validate the proposed new control strategy, simulation based comparison between the conventional drooped controller and the new direct P/Q controller is conducted using PSCAD/EMTDC. The tests start from the small steps using one or two IIG based simple network, and then goes to extensive set ups, unto a modified CIGRE prototype MV microgrid with four IIGs and multiple loads. Both the modes of operation and network topology are changed as different scenarios. It is however to be noted that the harmonics attenuation of the IIG control is out of the scope of this thesis.

4.2 Conventional Droop Based Control

From the literature review in Chapter 2, it is already known that the mainstream method for decentralized control of IIGs operating in parallel is the droop based methods. Featured by a decentralized control strategy without a communication network infrastructure, the droop based controller emulates the behaviour of rotating machines (i.e. synchronous generators) based on locally measured voltage and

current components. In this section, basic principles, the state-of-the-art enhancement and unsolved or inherent issues associated with this control scheme is investigated.

4.2.1 Droop Characteristics

The droop characteristics were firstly introduced for describing the features of power system with rotating machines. If the active power output is higher than the supplied mechanical power, the generator will slow down and the frequency will continue to decrease until the generation and load balance is restored. Additionally, if interconnecting lines present inductive characteristic, the larger the reactive power consumption, the lower the voltage magnitude. Hence, P-ω/Q-V droop characteristic is a common feature for the conventional rotating machine based power system. This is a self-regulating system where good load sharing between different generators can be automatically achieved.

In an IIG based system, the droop characteristic is analysed using basic electric equations based on a simplified diagram as shown in Figure 4-2.

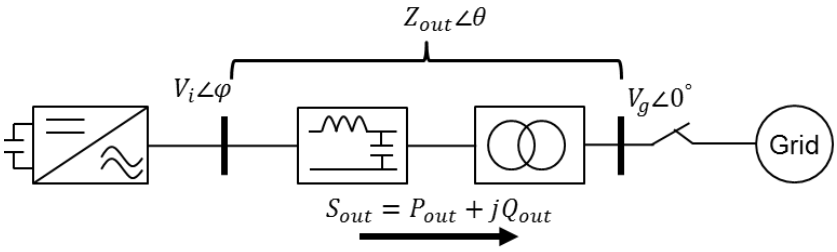

Figure 4-2: A brief diagram of a single IIG

A simple power flow function is presented in (4-1).

$$
\begin{aligned}
P_{out} + jQ_{out} &= \frac{V_i\angle\varphi - V_g\angle 0}{Z_{out}\angle\theta} \cdot V_g\angle 0 = \frac{V_i(cos\,\varphi + j\,sin\,\varphi) - V_g}{Z(cos\,\theta + j\,sin\,\theta)} \cdot V_g \\
&= \frac{V_g}{Z_{out}}\left[V_i(cos\,\varphi + j\,sin\,\varphi) - V_g\right] \cdot (cos\,\theta - j\,sin\,\theta) \\
&= \frac{V_g}{Z_{out}}\left[\left(V_i\,cos\,\varphi - V_g\right)cos\,\theta + V_i\,sin\,\varphi\,sin\,\theta\right] \\
&+ j\frac{V_g}{Z_{out}}\left[V_i\,sin\,\varphi\,cos\,\theta - \left(V_i\,cos\,\varphi - V_g\right)sin\,\theta\right]
\end{aligned}
\tag{4-1}
$$

Separating the real and imaginary part of the above equation, we can obtain the output real and reactive power of the IIG as presented in (4-2).

$$
\begin{aligned}
P_{out} &= \frac{V_g}{Z_{out}}\left[\left(V_i\,cos\,\varphi - V_g\right)cos\,\theta + V_i\,sin\,\varphi\,sin\,\theta\right] \\
Q_{out} &= \frac{V_g}{Z_{out}}\left[-\left(V_i\,cos\,\varphi - V_g\right)sin\,\theta + V_i\,sin\,\varphi\,cos\,\theta\right]
\end{aligned}
\tag{4-2}
$$

From the equation (4-2), it is found that the active power and reactive power are mutually coupled by the output impedance $Z_{out}\angle\theta$. In order to derive the equations which can describe clear relation between active power and frequency, as well as reactive power and voltage, a decoupling process should be conducted. One way to achieve this is to use an orthogonal frame transformation that transforms the actual real and reactive power (P_{out} and Q_{out}) into the virtual real and reactive power ($P_{out}{}'$ and $Q_{out}{}'$) [4]. With the knowledge of the output impedance phase angle θ, the decoupled virtual power can be obtained from (4-3).

$$
\begin{aligned}
P_{out}{}' &= P_{out} \cdot sin\,\theta + Q_{out} \cdot cos\,\theta \\
Q_{out}{}' &= P_{out} \cdot cos\,\theta - Q_{out} \cdot sin\,\theta
\end{aligned}
\tag{4-3}
$$

Replacing the actual power with the virtual power, the relationship of power and voltage phasor in (4-2) can be simplified as written in (4-4).

$$P_{out}{}' = \frac{V_g V_i}{Z_{out}} sin\,\varphi$$
$$Q_{out}{}' = \frac{V_g}{Z_{out}} (V_i\, cos\,\varphi - V) \tag{4-4}$$

As φ is normally very small and close to zero, the equation (4-4) can be reduced to (4-5), where$P_{out}{}'$ is more related to φ and Q′depends on $V_i - V_g$.

$$P_{out}{}' \approx \frac{V_g V_i}{Z_{out}} \varphi$$
$$Q_{out}{}' \approx \frac{V_g}{Z_{out}} \left(V_i - V_g\right) \tag{4-5}$$

Known that frequency is closely related to the phase angle, the real and reactive power can be controlled by adjusting the frequency ω and voltage magnitude $V_i - V_g$ respectively. In this way, the P-ω/Q-V droop characteristic can be used in the IIG based system, which is shown in Figure 4-3, given the radial frequency and voltage magnitude references ω^* and $V_o{}^*$ to the voltage loop. Apparently, in order to achieve good power decoupling, the output impedance of IIG needs to be estimated or obtained. Basically only output impedance angle is needed for the droop characteristic compensation.

The detailed droop characteristic equations with the droop coefficients are presented in (4-6) and (4-7). To be noticed, the radial frequency ω can be replaced by actual phase angle φ, and P- φ/Q-V droop characteristic is utilized.

$$\begin{aligned} \omega^* &= \omega_{max} - \frac{\omega_{max} - \omega_{min}}{P_{out,max} - P_{out,min}} \left(P_{out}{}' - P_{out,min}\right) \\ &= \omega_{max} - K_p \left(P_{out}{}' - P_{out,min}\right) \end{aligned} \tag{4-6}$$

$$V_o{}^* = V_{o,max} - \frac{V_{o,max} - V_{min}}{Q_{out,max} - Q_{out,min}}\left(Q_{out}{}' - Q_{out,min}\right) = V_{o,max} - K_q\left(Q_{out}{}' - Q_{out,min}\right) \quad (4\text{-}7)$$

where K_p and K_q are the droop gains of P-ω and Q-V characteristics. Their value depends on the rating and control bandwidth of each IIG.

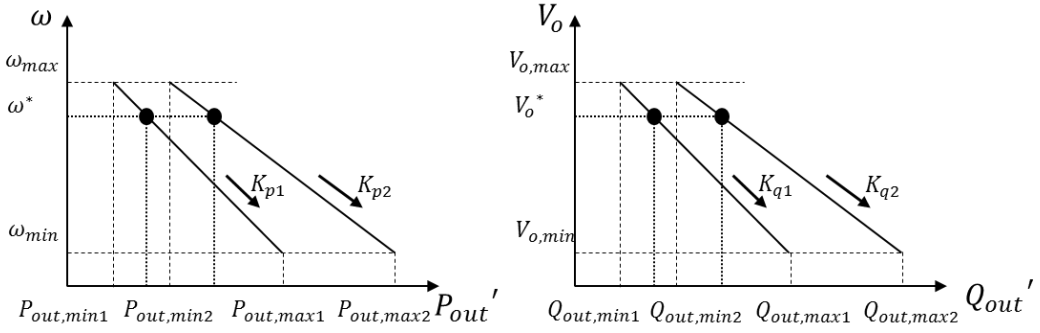

Figure 4-3: The P-ω/Q-V droop characteristics of the decoupled power

Normally the output impedance angle is estimated depending on different types of connecting feeders of the IIGs. Considering the inductive power filter, with very short connections, the IIG output impedance usually presents an inductive characteristic. In this case, θ is close to 90˚. On the other hand, if the IIGs are connected by long high resistive lines, output impedance may present a resistive characteristic. In this case, θ is much lower and can be close to 0° in extreme cases. Hence, for islanded mode of operation, two types of droop controllers were realized in the existing literature to cater for either inductive or resistive network [2,5]: P-ω/Q-V droop for the first case and P-V/Q-ω for the second case. The corresponding droop controllers are presented in Table 4-1. P_{local} and Q_{local} are the preset locally demanded power. ω_0 represents the nominal radial frequency, and V_0 is the nominal voltage of the IIG.

Table 4-1: Power droop with different output impedance

Inductive output impedance	Resistive output impedance
$\omega^* = \omega_0 - K_p(P_{out} - P_{local})$ $V_O{}^* = V_0 - K_q(Q_{out} - Q_{local})$	$\omega^* = \omega_0 + K_p(Q_{out} - Q_{local})$ $V_O{}^* = V_0 - K_q(P_{out} - P_{local})$

However in a microgrid, the equivalent output impedance of one IIG does not remain constant. Due to intermittent nature of the IIGs, the connections and disconnections of IIGs and their relevant branches and loads may occur, which indicates the intermittent changes of the system topology. Both the output impedance magnitude and phase angle may be changed. One particular consequence of this change is large circulating power/current between IIGs. The circulating power/current is one of the main challenges for operating the IIGs in parallel or in a multi-bus system. The circulating active and reactive power between the n_{th} and m_{th} IIGs connected in parallel can be derived from (4-8):

$$\begin{aligned} P_{nm} &= \frac{V_n}{Z_{nm}}[(V_m \cos\varphi_{nm} - V_n)\cos\theta_{nm} + V_m \sin\varphi_{nm}\sin\theta_{nm}] \\ Q_{nm} &= \frac{V_n}{Z_{nm}}[(V_m \cos\varphi_{nm} - V_n)\sin\theta_{nm} - V_m \sin\varphi_{nm}\cos\theta_{nm}] \end{aligned} \tag{4-8}$$

where $\theta_{nm} = \theta_n - \theta_m$, $V_{nm} = V_n - V_m$ and $\varphi_{nm} = \varphi_n - \varphi_m$. From this equation, it can be seen that if the phase angle difference φ_{nm} and voltage magnitude difference V_{nm} are controlled to be zero, the circulating power can be eliminated. However, in practice, there are natural voltage and angle deviations if the connection feeders are unequal under the conventional droop characteristic. Therefore, without controlling or compensating the output impedance differences, the circulating power/current is inevitable and may cause stability issues.

This decoupling strategy needs the awareness of the network topology and any change in the topology may have a negative impact on the load sharing performance.

Hence it becomes important to achieve real-time microgrid topology monitoring and to be able to manipulate the output impedance.

4.2.2 Virtual Impedance and Its Limitations

To enhance the solution described in the previous section, the virtual impedance was introduced to manipulate the output impedance [4]. As shown in Figure 4-4, by drooping the dq-transformed voltage references $V_{od}{}^{*}$ and $V_{oq}{}^{*}$ through a common virtual impedance in each IIG, the output impedance seen by each IIG is therefore compensated to be the same. The complex virtual impedance Z_d is depicted as $\mathrm{R}_d + j\omega_0\mathrm{L}_d$. Usually the virtual impedance is implemented in a $\alpha\beta$-frame, and the voltage reference can be easily transformed to the dq-frame. It is to be noted that virtual impedance can be set as purely resistive [6], inductive [5] or as complex impedance [7-8], according to different droop characteristics. In this thesis, in order to achieve the P-ω/Q-V type control, a virtual inductance is applied to the conventional controller. The overall block diagram of this control scheme is presented in Figure 4-5, where LF stands for a low pass filter, and the voltage controller and current controller have been introduced in Chapter 2.

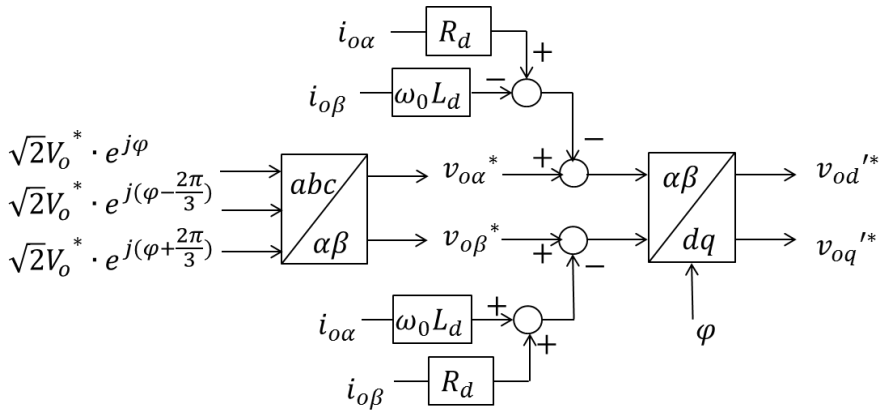

Figure 4-4: The implementation of the virtual impedance for conventional droop control [7-8]

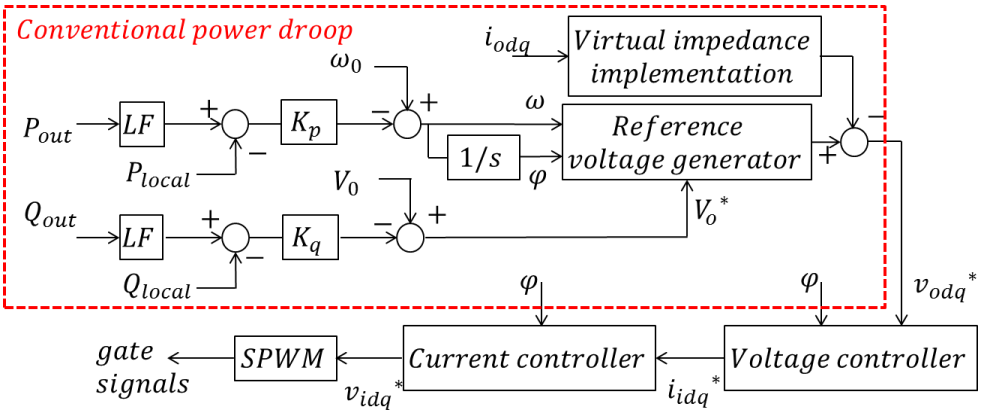

Figure 4-5: The block diagram of the conventional droop controller with virtual impedance

It needs to be highlighted that the virtual impedance needs careful design; otherwise it will adversely affect the system stability and dynamics. One design approach of the virtual impedance has been described by He et al in [9]. If necessary, the behavior under harmonics and unbalanced load conditions can be additionally improved by adding the frequency-layered and negative sequence virtual impedances [10-11]. Forcing the output impedance to be inductive is one of the particular solutions to meet the requirements of decoupling the real and reactive powers in P-ω/Q-V droop controller.

On one hand, the virtual impedance needs to be set sufficiently high to accommodate all potential network topologies, which means that the virtual inductance should be at least larger than the actual output reactance and feeder reactance of the IIG [12]. On the other hand, the virtual impedance cannot be too large, because it can cause problems with voltage regulation. From Figure 4-4 it can be seen that virtual impedance voltage drop is subtracted from the original voltage reference, which causes larger voltage sag in order to deliver the same output power. With the additional voltage sag, the maximum power output from the IIG is restricted.

4.3 Direct P/Q Controller to Achieve Good Operational Stability and Flexibility

4.3.1 Principle of Operation

A new direct P/Q controller is proposed in this section. The principle of this method takes the regular grid-connected controller as a basis. It has already been known that in grid-connected mode of operation, P_{out} is controlled by d-axis and Q_{out} is controlled by q-axis. When applying this principle to an islanded system, two additional considerations should be taken into account regarding the reference settings and inner loop structure:

1) The frequency regulation or phase angle references should be given.
2) The voltage control must be included in order to achieve a satisfactory voltage magnitude regulation.

Different from the conventional droop control, this controller adds the P and Q control directly to d and q axis of the widely used voltage and current control loops with fixed voltage references. The voltage references during the islanded operation are given by GPS time stamped ideal sine waves. As mentioned in the introduction section of this chapter, fixed voltage and frequency control normally cannot be employed in islanded multi-IIG system, since it does not allow any voltage magnitude or angle deviations. With the additional P/Q control, however, the IIGs will automatically minimize their voltage and angle deviations by properly arranging their own power output. The block diagram of this new controller is presented in Figure 4-6. where ω and V are measured output radial frequency and voltage, ω_0 and V_0 are inverter frequency and voltage references, K_p and K_q are the droop coefficients for active and reactive power, P_{local} and Q_{local} are the local condition (LC) settings, LF stands for the low-pass filter for power measurements, and V_{d0} and V_{q0} are the preset voltage settings. In the islanded mode of operation, ω_0 and V_0 represent the frequency and voltage references respectively. They are system nominal values during the islanded mode, while in the grid-connected mode of operation, they are measured from the IIG terminal.

The direct active and reactive power references are obtained according to (4-9).

$$P_{out}{}^{*} = K_p{}^{-1}(\omega_0 - \omega) + P_{local}$$
$$Q_{out}{}^{*} = K_q{}^{-1}(V_0 - V) + Q_{local} \quad (4\text{-}9)$$

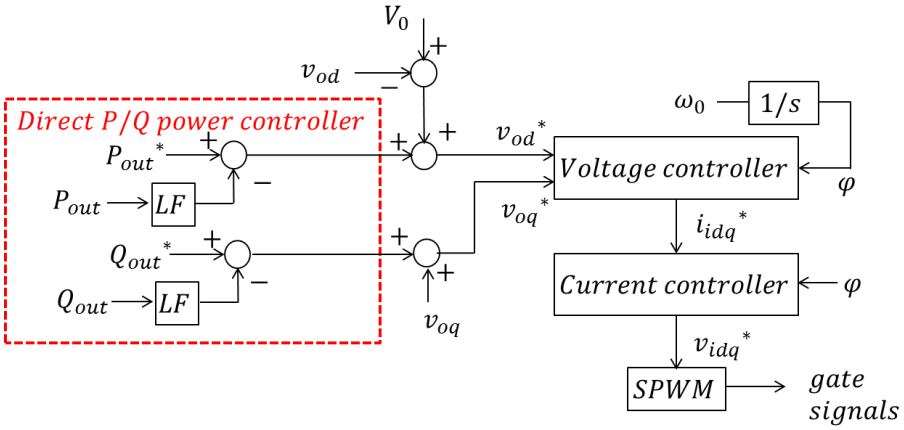

Figure 4-6: The block diagram of the proposed direct P/Q control

Significant feeder impedance can be regarded as part of the system load. The power sharing imbalance might be aggravated and necessary compensation is needed. Implementation of virtual impedance is a good solution to improve the load sharing performance, although it also imposes some negative impacts on the voltage regulation and power output capacity. It is recommended to activate the virtual impedance function only when the power deviation between generating units becomes larger than 10% of the rated power of the IIG.

In the proposed controller the reference voltage is directly presented in dq coordinates. In order to implement virtual impedance, the voltage should be transformed to the αβ axis. The control block diagram of the virtual impedance implementation is presented in Figure 4-7. As most microgrids are relatively compact, the power deviation of the IIGs (which is caused by the impedance variation of the interconnecting lines) is not likely to be large. Hence it is recommended to activate virtual impedance functionality by a central command

according to the real-time level of load sharing unbalance. This would ensure better voltage regulation under most operational conditions.

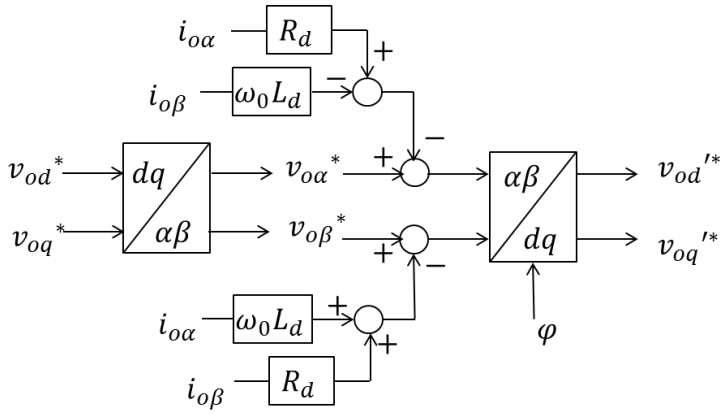

Figure 4-7: The implementation of the virtual impedance for direct P/Q control

4.3.2 Transition between Islanded and Grid-Connected Operation

An important element of the microgrid control is the ability to run in different modes of operation. Most of the existing methods include an external mode-transfer switch inside the controller which transfers the IIG from grid-connected operation to islanded operation, i.e. P/Q targeted control in the grid-connected operation and V/ω targeted control in the islanded operation. The mode-switched control strategy is regarded as the traditional one since it has been proposed quite early during the 80s of the last century [13]. With slight improvements only, this idea is still used widely at present [14]. A mode flexible control strategy for the IIGs is proposed by Kim et al. in [15]. The virtual impedance can be designed to adapt to reactive power consumption, and a low bandwidth communication channel is required to enhance the effectiveness of reactive power sharing and to achieve good virtual impedance set-up [16].

The proposed controller can be also achieved to run in both grid-connected and islanded modes with no switch on the hardware circuits, as the basic principle of the

proposed controller is very similar to the conventional grid-connected mode of operation: P and Q are both controlled by d and q axes independently without any application of virtual impedances.

When considering the transition from the grid-connected to islanded mode of operation, two types of islanding are possible: planned and unplanned. Both types generally do not bring problems to the microgrid. In grid-connected mode, the terminal voltage and frequency of the units are generally near their nominal values. The units will follow the reference power $P_{out}{}^{*}$ and $Q_{out}{}^{*}$.

Different from islanding transition, the transition from islanded to grid-connected mode needs to be planned. Before the transition, the phase angle and voltage magnitude at the PCC may be different. Moreover, the microgrid can operate at a different frequency from that of the grid. Therefore, reconnection of the microgrid without synchronization might lead to large transients, i.e. large voltage and phase angle changes. In order to realize a smooth mode transfer, a synchronization procedure is required. The synchronization procedure includes synchronization of the frequency, the RMS voltage and the phase angle before connecting the microgrid to the utility grid.

Figure 4-8 gives the block diagram of the angle and voltage synchronization procedure before the microgrid transferring from islanded operation to grid-connected operation. The RMS voltage synchronization block changes the output of the q-axis controller gradually, thus, by using a PI function, to force V_o to the utility voltage V_g. Phase angle synchronization is achieved by sending the referencing angle throughout the microgrid before connecting to the grid. Again a PI function is used to obtain a gradual synchronization. It is not recommended in this thesis to synchronize the closest IIG only, since in a system consisted of large number of IIGs, one IIG may not be strong enough to lead the whole angle network's synchronization. The integrator used in the angle reference generator in each IIG is clock synchronized and no wired communication is required.

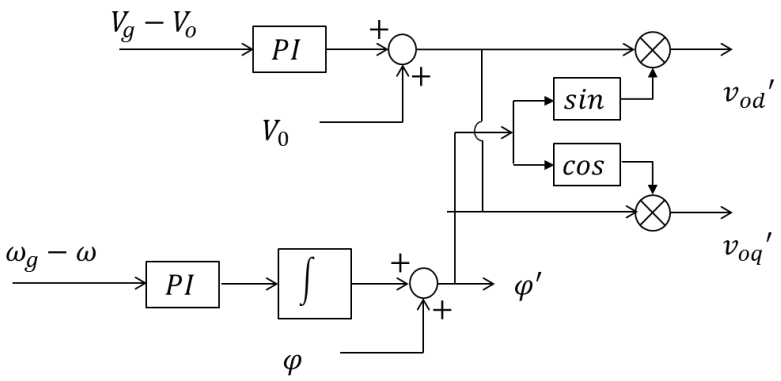

Figure 4-8: Control diagram of the voltage and phase angle synchronization

Figure 4-9 shows the overall block diagram of the proposed mode flexible control. This is implemented in all of the IIGs in the microgrid. During the modes transfer, the power references do not need to be configured instantly as the IIGs can be designed to initially meet the local power demand only.

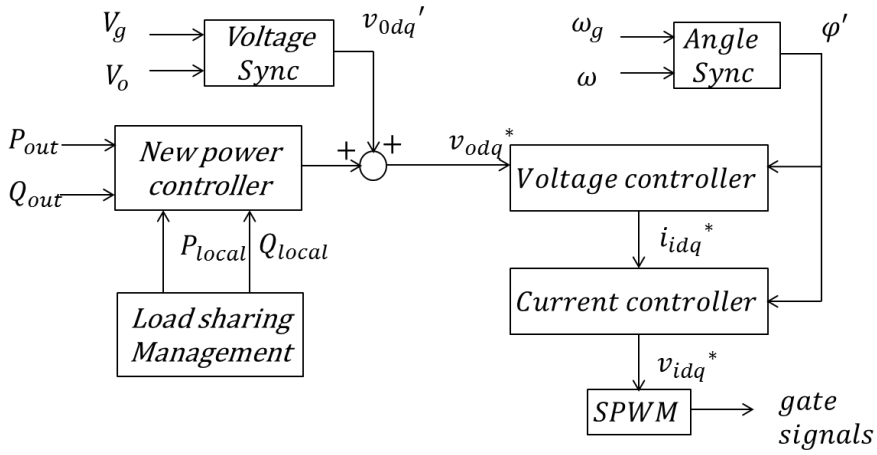

Figure 4-9: Overall block diagram of the proposed mode flexible control

4.4 Simulation Based Validation of the Controller's Performance in a Simple Network

As discussed in Section 4.2, the conventional controller has stability and power sharing imbalance issues when IIGs are connected through significantly different output impedances, or undergoing significant system topology changes. In order to provide detailed stability analysis of the proposed controller and the conventional controller, in the first stage, a simple network with two parallel IIGs is borrowed as presented in Figure 4-10 for dynamic transient simulation. The two IIGs are identical with the same specifications on control parameters and droop characteristics. The network and IIG parameters of this model are listed in Table 4-2. By step-load tests with different output feeder lengths and R/X ratios, the stability margin of the two controllers can be obtained.

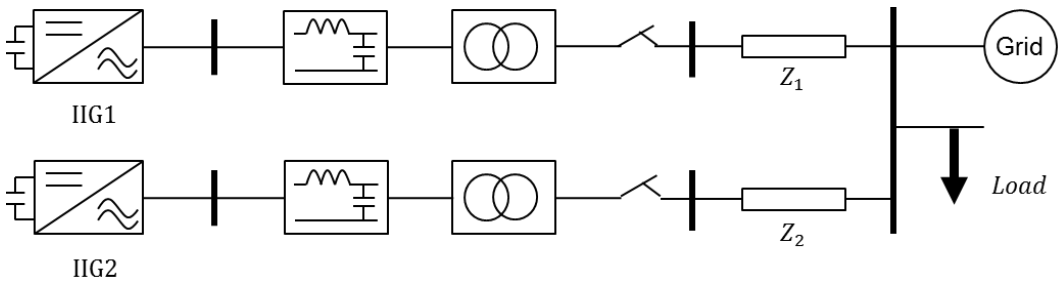

Figure 4-10: a simple two-IIG network for control study

Table 4-2: Parameters of the two-IIG based network model

	Parameters		**Value**
IIG1, IIG2	Inverter switching frequency		6750 Hz
	Inverter filter inductance		0.18 p.u.
	Inverter filter capacitance		95 μF
	Inverter nominated output voltage		400 V
	Inverter rated power		1.0 MVA
	Inverter nominated frequency		50 Hz
Controller parameters	P-ω droop k_P		0.1
	Q-V droop k_q		0.1
	Current PI controller (P,I)		10.5, 1000
	Voltage PI controller (P,I)		0.03, 10
	Angle synchronization PI controller		10,10
Cable $(\boldsymbol{Z_1 = 2Z_2 = 2km})$	Resistance	Positive sequence	0.6969 ohm/km
		Zero sequence	5.945 ohm/km
	Inductance	Positive sequence	1.566e-3 H/km
		Zero sequence	0.0246 H/km
	Capacitance	Positive sequence	6.78e-3 nF/km
		Zero sequence	6.78e-3 nF/km
Load	Fixed impedance		$R_{0\sim3s} = 400$ ohm, $L_{0\sim3s} = 2.546$ H $R_{3\sim8s} = 200$ ohm, $L_{3\sim8s} = 1.273$ H $R_{8\sim10s} = 400$ ohm, $L_{8\sim10s} = 2.546$ H
	Fixed power		$P_{0\sim3s} = 1MW \quad Q_{0\sim3s} = 0.5MVar$ $P_{3\sim8s} = 2MW \quad Q_{3\sim8s} = 1.0MVar$ $P_{8\sim10s} = 1MW \quad Q_{8\sim10s} = 0.5MVar$

4.4.1 Comparison of IIG's Transient Performance during Load Changes

In islanded operation, the switching of loads can cause significant voltage and current transients, which has a negative impact on the operational stability. Three types of loads are tested in this section: fixed impedance load (as shown in Figure 4-11), fixed power load (as shown in Figure 4-12) and dynamic motor load (as shown in Figure 4-13). In Figure 4-11 and Figure 4-12, the system load is stepped up to the IIG rating power output at 3s and back down to half of the IIG rating power at 8s. In Figure 4-13, a dynamic motor with a rated power of 0.1MVA is connected to the network by at 3s, and later on disconnected by open the CB at 8s.

From the three figures, it can be clearly seen that under all of the above scenarios, the two IIGs are able to share the load with good balance and good stability. However, the new controller appears to have better voltage regulation since it presents less voltage sag during fully loaded condition. Moreover, the new controller is able to deliver larger amount of power into the network when connected with the fixed impedance loads. This is mainly due to the impact of the implemented virtual impedance inside the conventionl droop based controller, which inherently reduces the actual power output capacity of individual IIG.

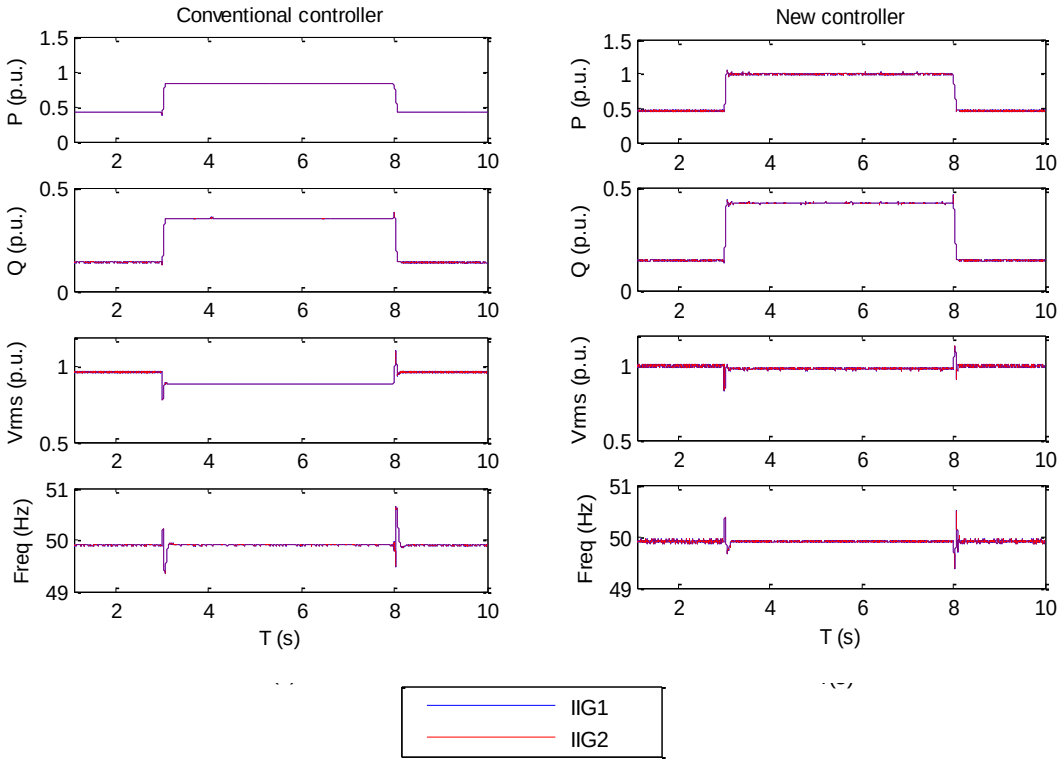

Figure 4-11: Comparison of IIG behaviour with fixed impedance load

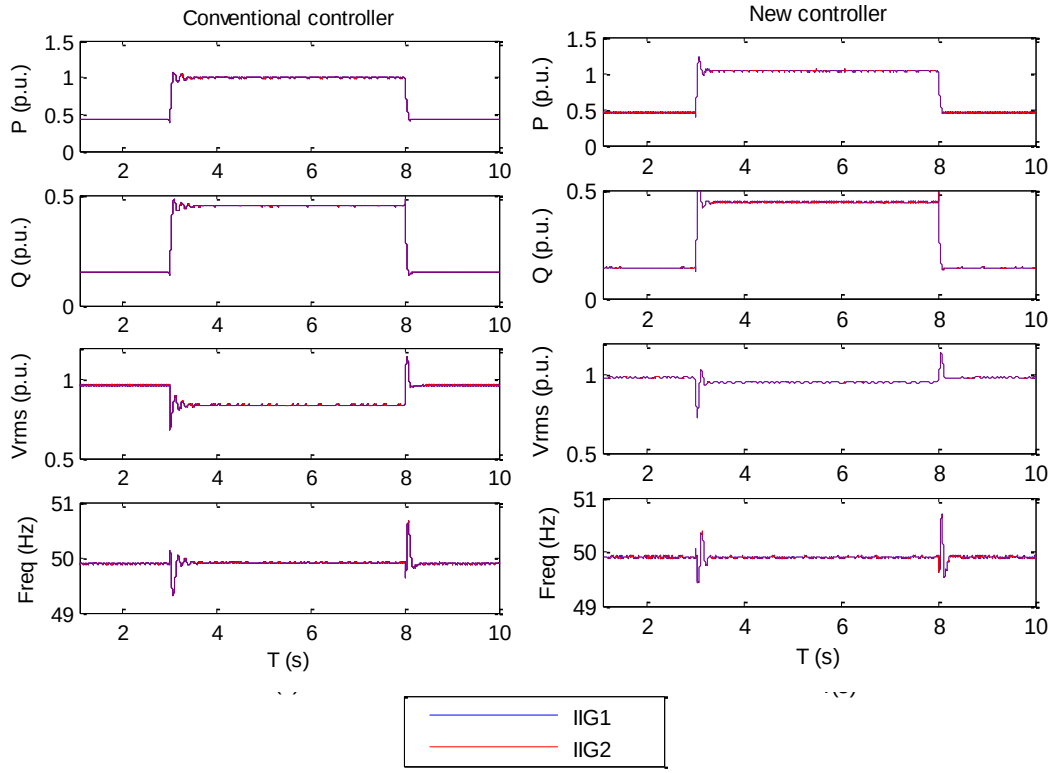

Figure 4-12: Comparison of IIG behaviour with fixed power load

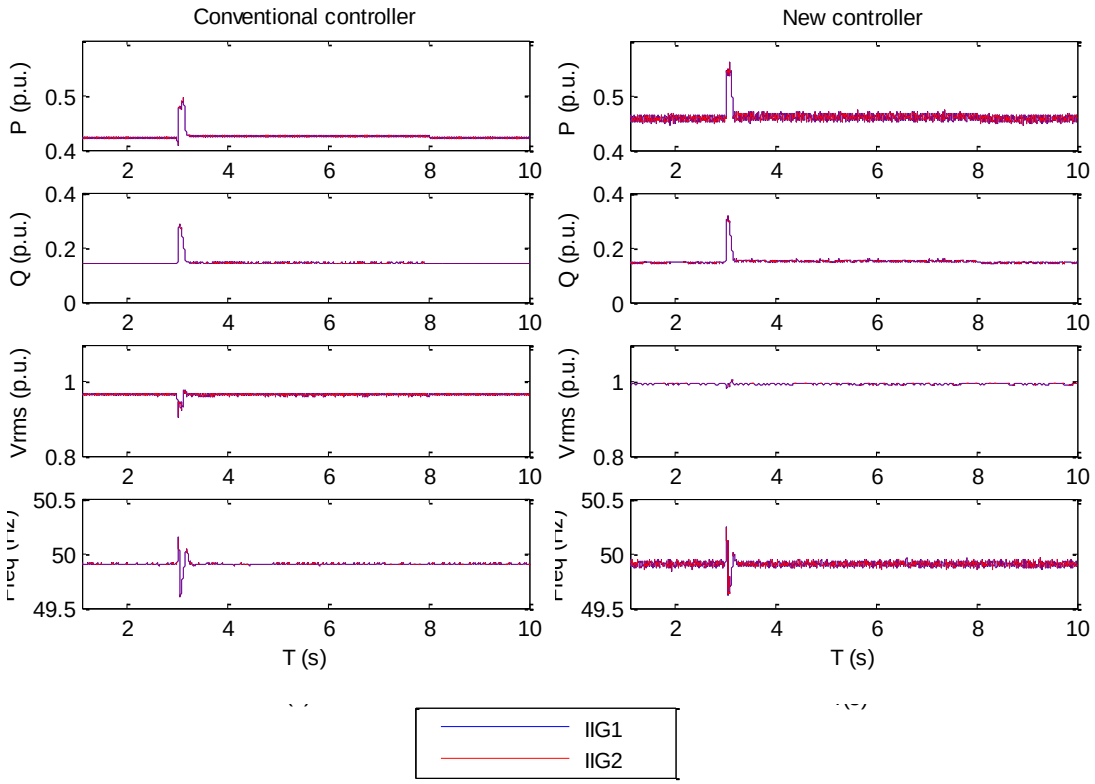

Figure 4-13: Comparison of IIG behaviour with motor starting

4.4.2 Comparison of IIG's Operational Stability with Unbalanced Output Impedances

It has been clearly stated in Section 2.4.2.2 that the output impedance imbalance has a considerable effect on the operational stability of multi-IIGs, since this imbalance might cause large circulating power inter between the IIGs. As discussed in Section 4.2.2, virtual impedances are applied to manipulate the output impedance of the IIGs to be proportional to their rating power in the conventional droop based controller. In order to investigate the impact of the virtual inductance in the conventional controller, the virtual inductances of the two IIGs are both reduced by 0.05p.u. every 1.5s ($Z_{d0-1.5s} = 0.4\text{p.u.}$). As shown in Figure 4-14, the IIGs appear increasingly significant oscillating transient performance and power sharing imbalance with the procedure of this graduate virtual inductance reduction. And they become unstable when the virtual inductance is reduced to be smaller than the filter inductance around 0.14 p.u.. Therefore it can be concluded that the virtual impedance should be set

larger than the IIG's output filter impedance. However, it should also be noticed that the virtual inductance cannot be set too large since from the voltage and power waveforms we can observe that the virtual inductance has a negative impact on the voltage regulation and output power capacity.

Figure 4-15 shows the transient response of the load step change using the conventional controller with different lengths of IIG2 output connecting feeder. In all these cases, the length of the IIG1 output connecting feeder is fixed to be 1km while the length of the IIG2 output connecting feeder varies ranging from 1km to 20km. The virtual inductance of both IIGs is chosen to be 0.18p.u, covering the filter inductance of the IIG. In this figure, dP and dQ represents the power difference between the expected average power output in balance and the actual individual IIG power output. It is clear that when the two feeders share the same parameters and length, the power is shared between two IIGs with perfect balance (dP and dQ are zero). However with increase of the length of the feeder, both the power sharing balance and transient response under the step load changes are significantly degraded. The duration of the transient oscillating behaviour can be as long as 2.5s.

In comparison with the conventional controller, the new proposed controller does not need any virtual impedance to guarantee its operational stability, as shown in Figure 4-16. It is also not affected by the varied output impedances, which provides smooth and sound transient response without oscillations occurred in the conventional controller.

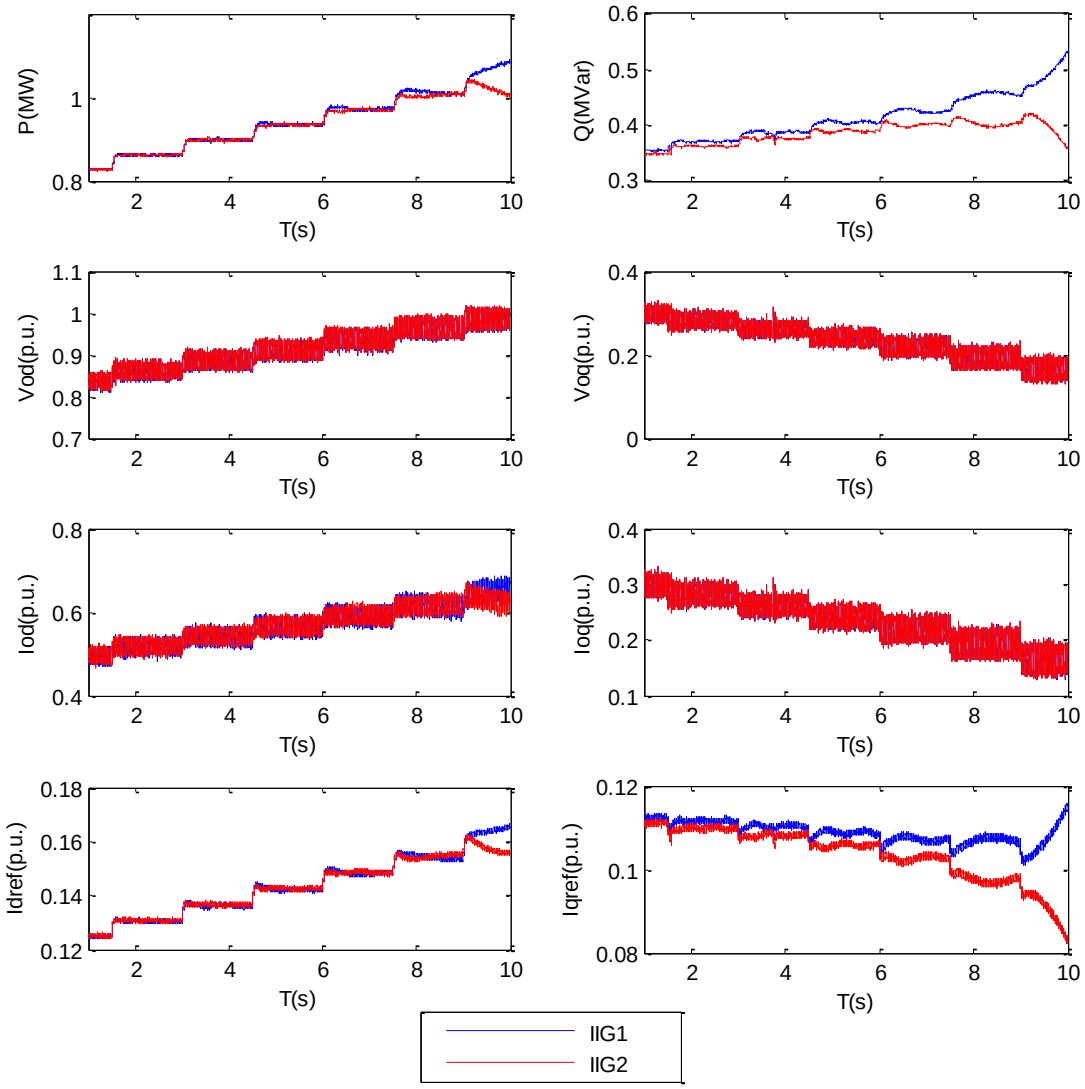

Figure 4-14: Transient performance under load step change using the conventional controller with different virtual inductance

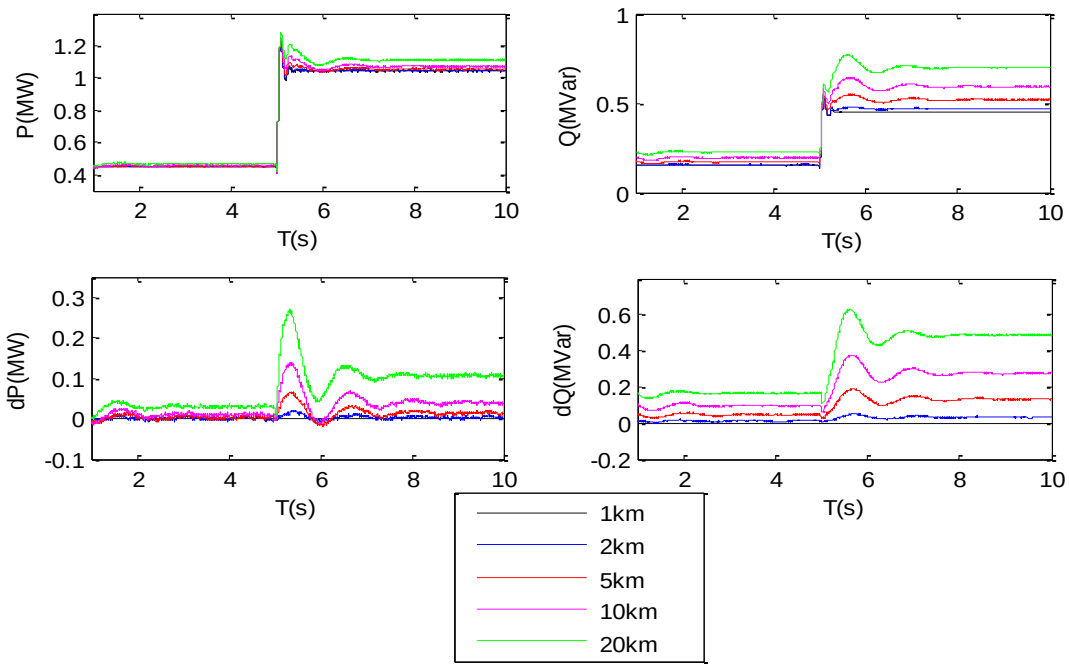

Figure 4-15: The response of the conventional controller to the change of length of output feeder

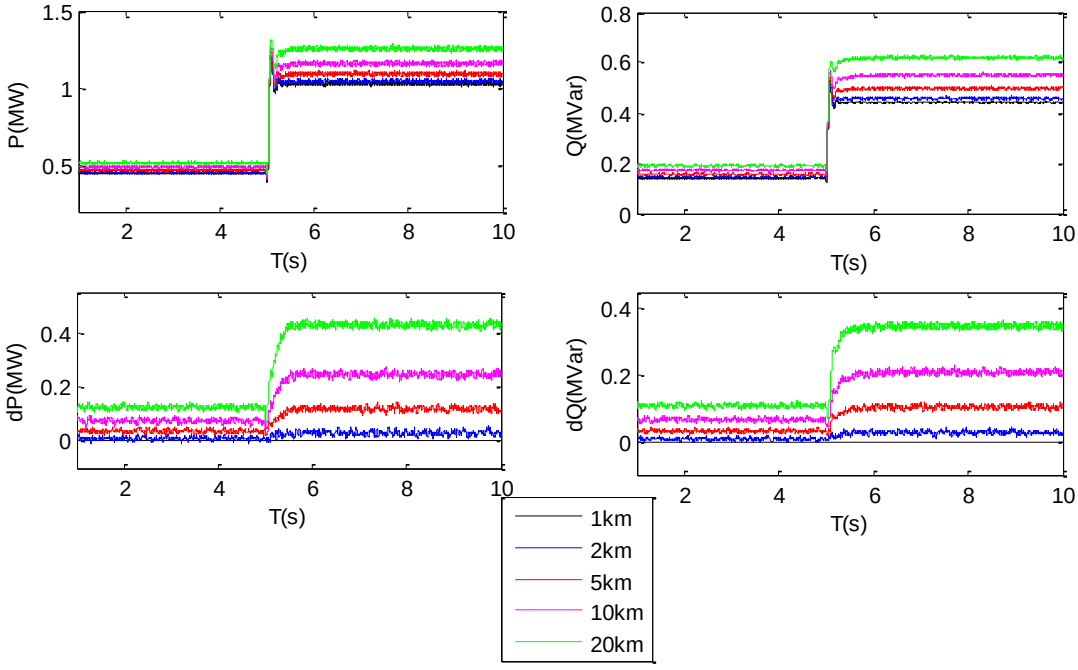

Figure 4-16: The response of the direct P/Q controller to the change of length of output feeder

4.5 Systematic Validation of the New Control Scheme

In order to evaluate the proposed technique in a systematic way, a 20kV MV microgrid model integrated with four IIGs is built in PSCAD/EMTDC as shown in Figure 4-17. The IIG model is a detailed switching model with an ideal source at the DC-link, which sufficiently emulates the present microturbines and fuel cell systems, or any other DC source [17]. The parameters of a single IIG are the same used in the above tests as presented in Table 4-2. Four such IIGs are connected to buses 2, 4, 6 and 8 respectively, each with a local load attached to the same connecting busbar between the IIG and the rest of the microgrid network. Additionally, two fixed power system loads are connected to buses 3 and 7. The system's topology can be changed from a radial network to a meshed network by closing CB3, and also can be divided into two separate microgrids by opening CB5.

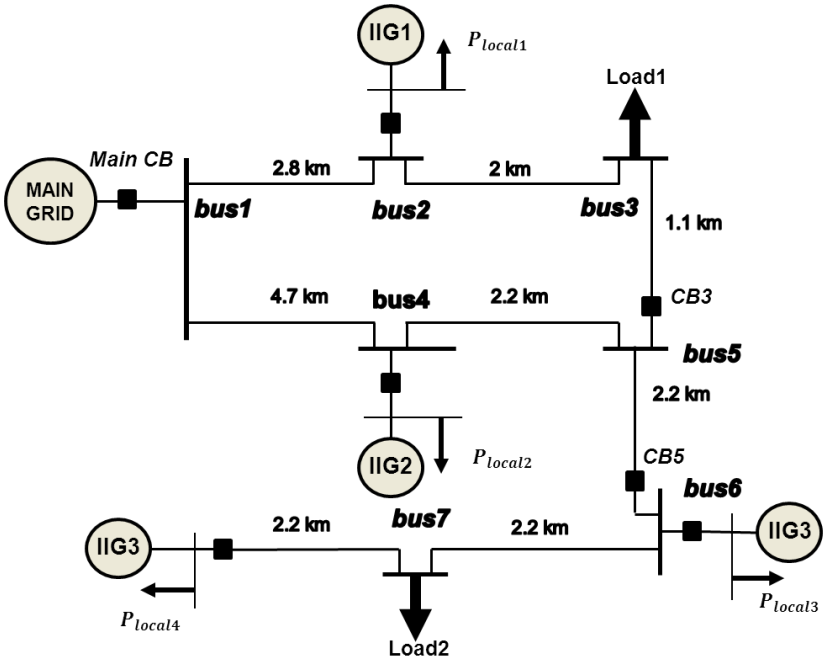

Figure 4-17: Benchmark mirogrid system model simulated to test the overall component controller

4.5.1.1 Transient Performance during Load Step Change

Load step change is one of the important tests to estimate the controller's dynamic stability. In a relatively large microgrid system as presented in Figure 4-17, a series of step-load tests can be established for islanded operation by changing the load position, amount of load and the ratio of the reactive to the active load. The load parameters for these step-load tests are listed in Table 4-3. In these tests, it is expected to observe balanced load sharing within different load conditions, and smooth and stable transition between different load conditions.

The corresponding active and reactive power sharing performance of the four IIGs is shown in Figure 4-18. In this figure, dP and dQ stand for the active and reactive power differences between the expected output power under accurately balanced power sharing condition and the actual power output from individual IIG. Under accurate power sharing balance, each identical IIG shall be loaded with the same amount of system demand (excluding the local demand). In the simulation, with differences in the load demand and significant output impedance imbalance (up to several kilometres), the power sharing of the IIGs have slight imbalance (lower than 0.1MW of active power and 0.05MVAr of reactive power). This is acceptable since the power sharing imbalance is less than 10% of the rated power of IIG.

Table 4-3: Load parameters of the 20kV MV microgrid model

Load Name	Parameters
Load1 (active power)	$P1_{0\sim3s} = 0.52MW$ $P1_{3\sim8s} = 1.74MW$ $P1_{8\sim10s} = 1.74MW$
Load 1 (reactive power)	$Q1_{0\sim3s} = 0.1MVAr$ $Q2_{3\sim8s} = 0.7MW$ $Q2_{8\sim10s} = 0.7MVAr$
Load 2 (active power)	$P2_{0\sim3s} = 1.4MW$ $P2_{3\sim8s} = 1.4MW$ $P2_{8\sim10s} = 0.2MW$
Load 2 (reactive power)	$Q2_{0\sim3s} = 0.7MVAr$ $Q2_{3\sim8s} = 0.7MVAr$ $Q2_{8\sim10s} = 0.1MVAr$
IIG1 local	$P_{Local-IIG1} = 0.3MW$
IIG2 local	$P_{Local-IIG2} = 0.15MW$
IIG3 local	$P_{Local-IIG3} = 0.1MW$
IIG4 local	$P_{Local-IIG4} = 0.2MW$

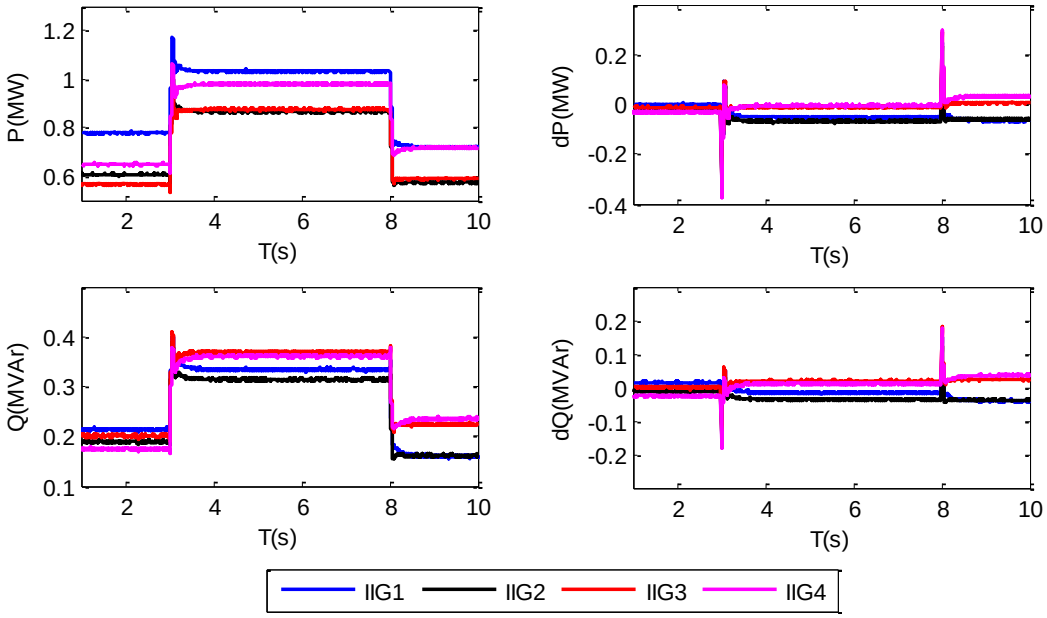

Figure 4-18: The active and reactive power sharing performance of four IIGs through the microgrid system under load step changes

4.5.1.2 Operational Stability under System Topology Change

In order to investigate the operational stability of the proposed controller under varied lengths of output connecting lines, a case study of its operational performance during system topology change was conducted. As shown in Figure 4-19, CB3 is opened at 3s to form a radial network. All of the four IIGs sustain the topology change and respond smoothly to this event without implementation of virtual impedance. However, it must be noted that after this topology change, the electrical distances from the IIGs to Load1 are significantly increased apart from IIG1, which leads to a maximum active power output deviation around 0.25 MW (after deducting the LC differences). This power deviation exceeds 10% of the rated power of a single IIG. In order to mitigate this issue, at 6s as shown in Figure 4-19, a virtual inductance of 0.3p.u. is applied to the new controller. The results validate the feasibility of power sharing enhancement using virtual inductance in the new controller.

Appling the same virtual inductance of 0.3 p.u. to both the new and the conventional droop-based controller, the power sharing performance of the two controllers is further compared. As shown in Figure 4-20, the system topology change causes the

obvious oscillation in the dynamic response of the conventional controller and poses concern over the operational stability. Therefore the new controller presents more stable and reliable dynamic power sharing performance. It needs to be noticed that in this figure, virtual impedance was not simulated which could provide optimal power sharing performance.

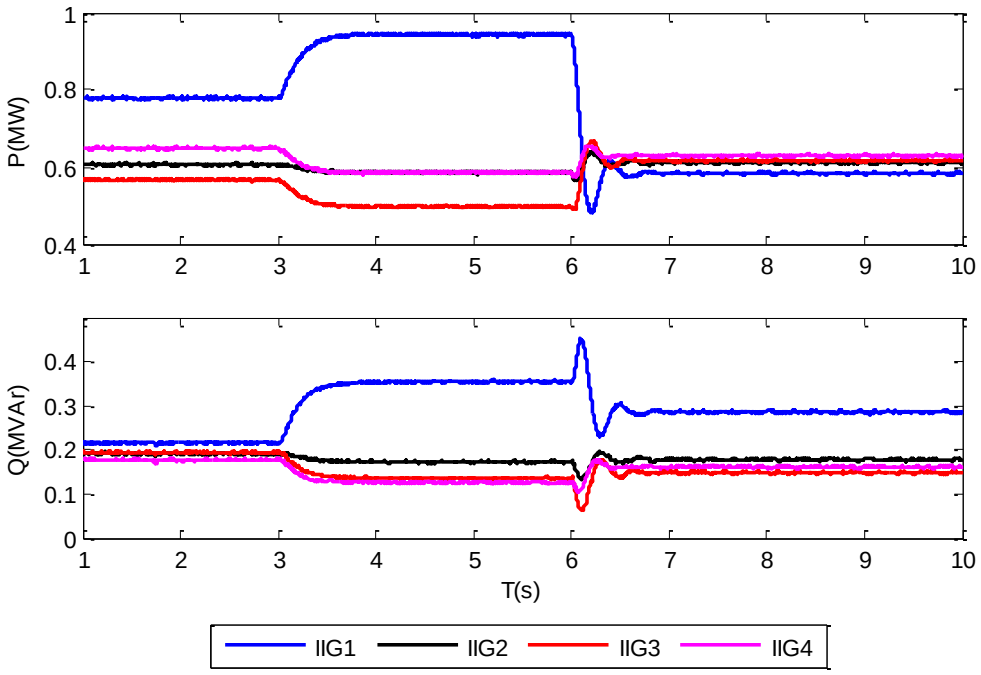

Figure 4-19: Active and reactive power sharing performance of the new controller during system topology change with (1~6s) and without (6s~10s) virtual impedance

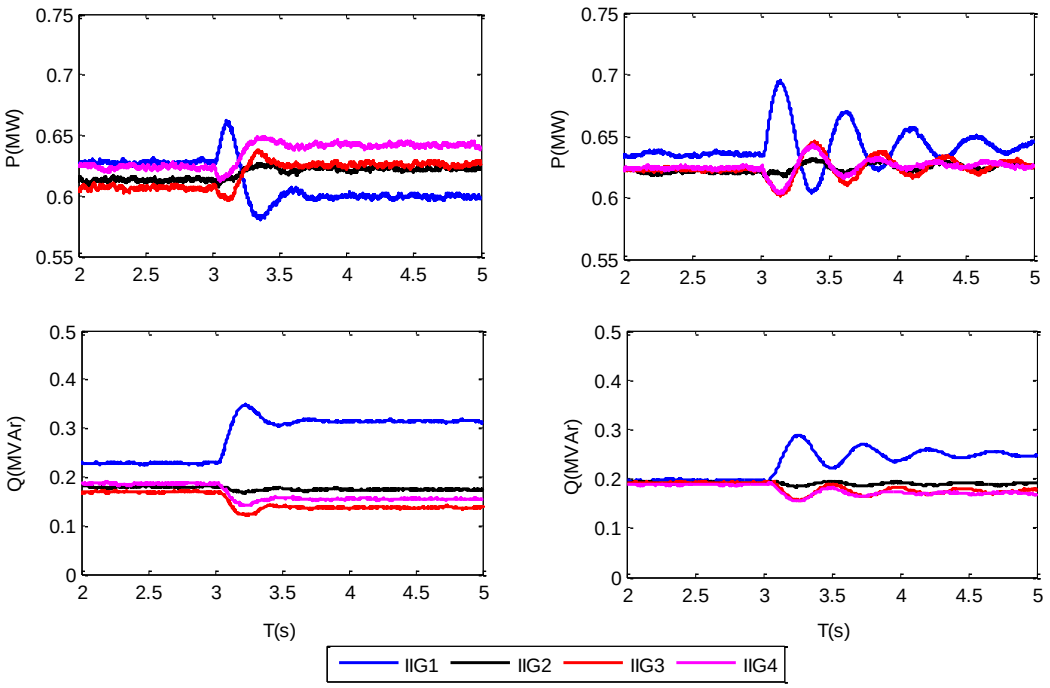

(a) Direct P/Q controller **(b) Conventional controller**

Figure 4-20: Comparison results of the active and reactive power sharing performance during system topology change from meshed network to radial network.

4.5.1.3 Transient Performance during Operational Mode Transfer

It is known that a microgrid can be running in either grid-connected or islanded condition. Therefore the control strategy of a multi-IIG based microgrid shall be able to work in both operational modes. The main challenge lies in the smooth mode transfer, especially for the process of the microgrid reconnecting to the main grid. It requires good voltage and angle synchronization with proper load sharing performance before and after the reconnection.

During islanded operation, individual IIGs generate their own voltage and angle references, even though preset LC settings are used. The IIGs actively respond to the system load in addition to the LC. In grid-connected mode, voltage magnitude and angle are synchronized with the common bus, and the LC settings are fixed by the demand side management asset in order to achieve the expected power flow from a system point of view. Therefore, there are two stages regarding the configuration of

LC settings: in stage 1, all IIGs feed the network based on the preset LC; in stage 2, the LC settings are updated by the local/central load management asset in order to satisfy a specific power management target. The LC settings and system load parameters are set as listed in Table 4-4.

Table 4-4: The load condition settings for transient performance assessment during mode transfer

	Parameters		**Value**
Load	**IIG1 LC settings**	Stage 1	0.3 MW, 0 MVar
		Stage 2	1.2 MW, 0 MVar
	IIG2 LC settings	Stage 1	0.15 MW, 0 MVar
		Stage 1	1.0 MW, 0.05 MVar
	IIG3 LC settings	Stage 1	0.1 MW, 0 MVar
		Stage 2	0.8 MW, 0.15 MVar
	IIG4 LC settings	Stage 1	0.2 MW, 0 MVar
		Stage 2	0.6 MW, 0.2 MVar
	System load 1		1.8MW, 0.7MVar
	System load 2		0.52MW, 0.1MVar
Cable	**Resistance**	R1	0.6969 ohm//km
		R0	5.945 ohm/km
	Inductance	L1	1.566e-3 H/km
		L2	0.0246 H/km
	Capacitance	C1	6.78e-3 nF/km
		C0	6.78e-3 nF/km

Figure 4-21 shows the power flows from four IIGs under transfer between seven operational modes:

- a – islanded mode for IIG1 and IIG2 with LC stage 1;
- b – islanded mode for IIG1, 2 and 3 with LC stage 1;
- c – islanded mode of four IIGs with LC stage 1;
- d – grid synchronization mode;
- e – grid connected mode with LC stage 1;
- f – grid connected mode with LC stage 2;
- g – islanded mode with LC stage 2.

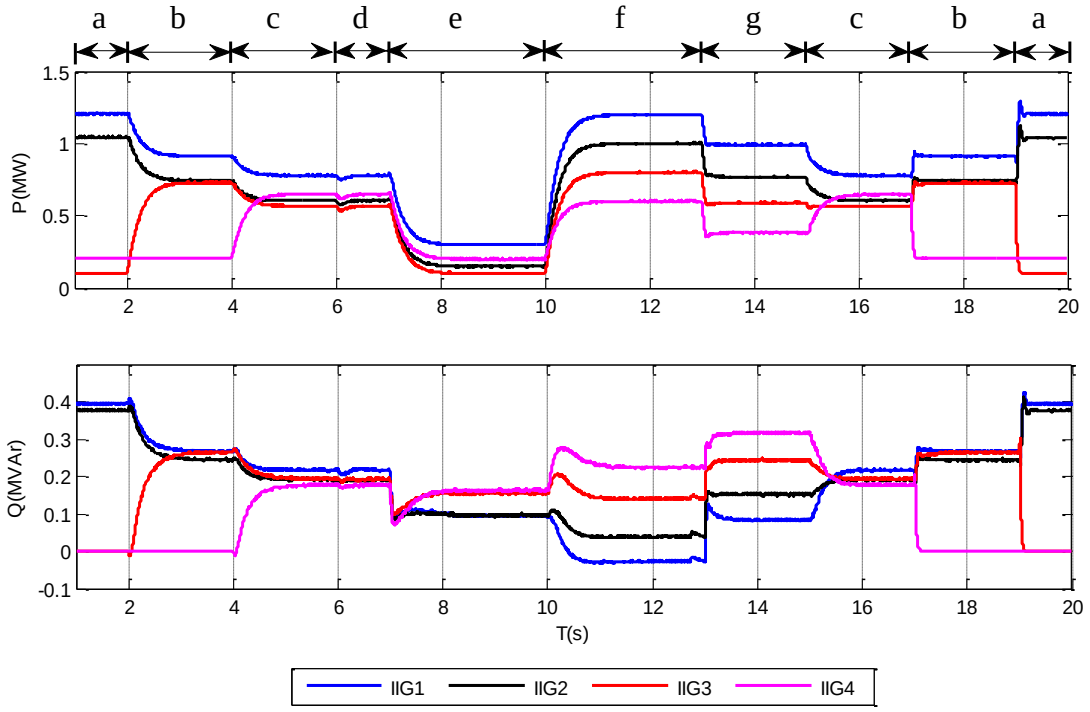

Figure 4-21: Active and reactive power sharing performance of four IIGs in a meshed 20KV microgrid system during mode transfer

From the four IIGs performance results under the operational mode transfer through a sequence of a→b→c→d→e→f→g→c→b→a as presented in Figure 4-21, we can see that the proposed controller enables black start of the IIGs in the islanded microgrid. Results of d→e and f→g show the controller's smooth transfer between

grid-connected state and islanded state. Good performance during e→f and g→c validates that the operational stability is independent of LC settings. Therefore it is not mandatory to update the LC settings instantly during mode transfer.

4.5.1.4 Wide-area Angle Synchronization

During grid reconnection, one of the critical processes involved is angle synchronization. As mentioned in Section III, the angle needs to be synchronized on the wide-area basis. The reference signal needs to be sent to each IIG, in order to guarantee the smooth resynchronization with the grid. However in practice, certain amount of communication delay is expected in the reference angle. In this case, there might be an out-of-step stability issue related to the transient response towards the angle synchronization. For example, as shown in Figure 4-22, IIG1 starts synchronizing at 1s, but IIG4 doesn't start until after a delay of 0.1s. This delay causes an obvious oscillation of the output power from all IIGs. Figure 4-23 shows the output response from IIG4 under different synchronization time delays (between 0.02s and 0.1s). From the figure, it can be seen that power output oscillations increase noticeably with the synchronization time delay of IIG4. Hence, it is clear that for the proposed microgrid control system, the angle synchronization instant for all IIGs should be as close as possible.

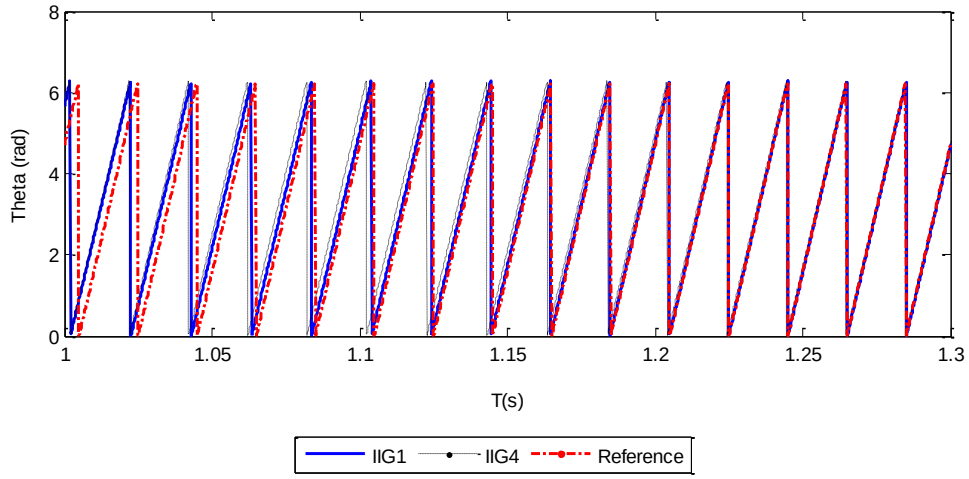

Figure 4-22: Angle synchronization of IIG1 and IIG4 at 1s and 1.1s respectively

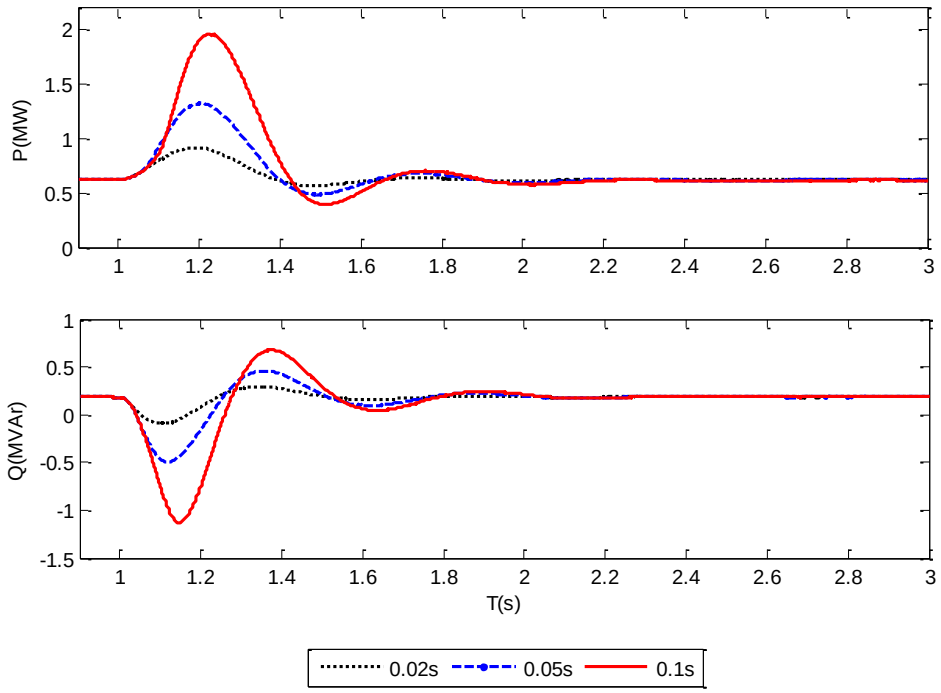

Figure 4-23: Output power response of IIG4 with different time deviation of the starting angle synchronization from other IIGs.

4.6 Chapter Summary

It was known from the review of Chapter 3 that the conventional decentralized control schemes are mostly based on the droop characteristics. However, the conventional droop based controller has the inherent issues such as poor stability under significantly deviated feeder connections. Even with the improvement by embedding the virtual impedance to compensate deviated equivalent output impedances, trade-off exists between voltage regulation and accurate power sharing. Based the detailed discussion on the application of the existing decentralized control schemes for the multi-IIG based system, this chapter developed a direct P/Q control scheme, which was based on the emulation of a regular grid-connected inverter with output power targeted control, permitting a mode-adaptive operation for both grid-connected and islanded state. In this control scheme, active power is independently controlled by the active current in d-axis and the reactive power is controlled by the reactive current in q-axis.

Comparison study between the new controller and the conventional method has been conducted in a simple two IIG based network. Simulation results have shown that the new method provided better operational stability regardless of the length of R/X ratio of the equivalent output impedance, better voltage regulation and smoother dynamic transient performance. Based on the new controller, a switch-free mode transition technique was achieved using communication assisted wide-area synchronization. The method was also enhanced by implementing the virtual impedance to have more balanced power sharing performance.

The study was then extended to a benchmark MV microgrid system integrated with four IIGs connected to different busbars. This system can be running in both radial and meshed network. From the transient simulation results in PSCAD/EMTDC, it can be clearly seen that the system topology has a significant impact on the IIG power sharing accuracy. The performance of virtual impedance applied a good compensation of load sharing unbalance and proved to be working well with the new proposed controller. In comparison with the conventional control scheme, the new controller was proven to have better voltage regulation and operational stability towards different system topologies and load conditions.

4.7 Chapter References

[1] M. Prodanovic, T. C. Green, and H. Mansir, "A Survey of Control Methods For Three-phase Inverters In Parallel Connection," in 8th International Conference on Power Electronics and Variable Speed Drives (IEE Conf. Publ. No. 475), 2000, pp. 472–477.

[2] J. M. Guerrero, L. G. de Vicuna, J. Matas, J. Miret, and M. Castilla, "A Wireless Load Sharing Controller to Improve Dynamic Performance of Parallel-connected UPS Inverters," in Power Electronics Specialist Conference, 2003. PESC '03. 2003 IEEE 34th Annual, 2003, vol. 3, pp. 1408–1413 vol.3.

[3] E. Rokrok and M. E. H. Golshan, "Adaptive voltage droop scheme for voltage source converters in an islanded multibus microgrid," IET Generation, Transmission Distribution, vol. 4, no. 5, pp. 562–578, 2010.

[4] K. De Brabandere, B. Bolsens, J. Van den Keybus, A. Woyte, J. Driesen, and R. Belmans, "A Voltage and Frequency Droop Control Method for Parallel

Inverters," IEEE Transactions on Power Electronics, vol. 22, no. 4, pp. 1107–1115, Jul. 2007.

[5] A. Engler, "Control of Parallel Operating Battery Inverters," presented at the PV Hybrid Power Systems, Germany, 2000.

[6] J. M. Guerrero, J. Matas, L. G. de Vicuna, M. Castilla, and J. Miret, "Decentralized Control for Parallel Operation of Distributed Generation Inverters Using Resistive Output Impedance," IEEE Transactions on Industrial Electronics, vol. 54, no. 2, pp. 994–1004, 2007.

[7] K. De Brabandere, B. Bolsens, J. Van Den Keybus, A. Woyte, J. Driesen, R. Belmans, and K. U. Leuven, "A Voltage and Frequency Droop Control Method for Parallel Inverters," in Power Electronics Specialists Conference, 2004. PESC 04. 2004 IEEE 35th Annual, 2004, vol. 4, pp. 2501–2507 Vol.4.

[8] W. Yao, M. Chen, J. Matas, J. M. Guerrero, and Z. Qian, "Design and Analysis of the Droop Control Method for Parallel Inverters Considering the Impact of the Complex Impedance on the Power Sharing," IEEE Transactions on Industrial Electronics, vol. 58, no. 2, pp. 576–588, 2011.

[9] J. He and Y. W. Li, "Analysis, Design, and Implementation of Virtual Impedance for Power Electronics Interfaced Distributed Generation," IEEE Transactions on Industry Applications, vol. 47, no. 6, pp. 2525–2538, 2011.

[10] D. De and V. Ramanarayanan, "Decentralized Parallel Operation of Inverters Sharing Unbalanced and Nonlinear Loads," IEEE Transactions on Power Electronics, vol. 25, no. 12, pp. 3015 –3025, Dec. 2010.

[11] J. M. Guerrero, J. C. Vasquez, J. Matas, M. Castilla, and L. G. de Vicuna, "Control Strategy for Flexible Microgrid Based on Parallel Line-Interactive UPS Systems," IEEE Transactions on Industrial Electronics, vol. 56, no. 3, pp. 726–736, Mar. 2009.

[12] J. M. Guerrero, L. G. de Vicuna, J. Matas, M. Castilla, and J. Miret, "A wireless controller to enhance dynamic performance of parallel inverters in distributed generation systems," IEEE Transactions on Power Electronics, vol. 19, no. 5, pp. 1205– 1213, Sep. 2004.

[13] T. Kawabata and S. Higashino, "Parallel operation of voltage source inverters," IEEE Transactions on Industry Applications, vol. 24, no. 2, pp. 281 –287, Apr. 1988.

[14] M. C. Chandorkar, D. M. Divan, and R. Adapa, "Control of parallel connected inverters in standalone AC supply systems," IEEE Transactions on Industry Applications, vol. 29, no. 1, pp. 136–143, Feb. 1993.

[15] Jaehong Kim, J. M. Guerrero, P. Rodriguez, R. Teodorescu, and Kwanghee Nam, "Mode Adaptive Droop Control With Virtual Output Impedances for an

Inverter-Based Flexible AC Microgrid," IEEE Transactions on Power Electronics, vol. 26, no. 3, pp. 689–701, Mar. 2011.

[16] J. C. Vasquez, J. M. Guerrero, A. Luna, P. Rodriguez, and R. Teodorescu, "Adaptive Droop Control Applied to Voltage-Source Inverters Operating in Grid-Connected and Islanded Modes," IEEE Transactions on Industrial Electronics, vol. 56, no. 10, pp. 4088–4096, 2009.

[17] P. Piagi and R. H. Lasseter, "Autonomous Control of Microgrids," in IEEE Power Engineering Society General Meeting, 2006.

5. Travelling Wave Based Protection Using Mathematical Morphology

5.1 Introduction

IIG based microgrids impose significant challenges on power system protection. The IIGs are mostly regarded as resources with low fault current contribution which can undermine the performance of traditional overcurrent relays typically used in distribution networks. In Chapter 3, it has been already pointed out that microgrid protection needs to be able to work under different modes of operation (islanded and grid-connected) and various system topologies (meshed and radial). It is also expected to be sufficiently fast to protect sensitive loads and power sources. Based on the comprehensive review of existing protection methods, the travelling wave based protection schemes were found with good potential to meet the key requirements, i.e. fault level independence and speed, since they are based on the transient feature of the fault and therefore totally independent on the fault current level. There are relatively few papers discussing the use of fault generated travelling waves as a guiding principle of the microgrid protection. It is difficult to apply travelling wave based protection to distribution systems mainly due to the special characteristics with MV/LV system, i.e. changeable operational mode, low fault contribution from IIG during islanded operation. Nevertheless, with full awareness of the existing obstacles and issues, this chapter explores a realistic possibility of utilising travelling wave based protection within the inverter dominated microgrid by considering certain modifications to the guiding principles of travelling wave based protection and by applying an innovative signal processing technique.

In the first section, the underlying principles of a new protection strategy are presented. Operation logic for the double-end protection scheme is developed, with special consideration given to the changeable microgrid topology. Based on the proposed principles, the minimum required information from the fault transients is defined: accurate time and waveform polarity information.

In order to accurately extract the time and polarity information from fault transients, the key point lies in the signal sampling rate and performance of signal processing tools. In following sections, firstly two potential signal processing tools – discrete wavelet transform (DWT) and mathematical morphology (MM) – will be investigated to assess their performance in polarity detection, time location and noise reduction. Based on the abovementioned studies, a new protection strategy is proposed using the verified best signal processing technique.

5.2 Underlying Principles of the New Protection Scheme

Based on the discussion in Chapter 3 which considered the key issues related to the application of travelling wave theory in a microgrid system, a new protection scheme has been developed. The travelling waves are usually illustrated in a Lattice diagram as shown in Figure 5-1. The routes of the two initial wavefronts towards both ends of the line RS are defined as: $PeakR_1$ for FR route; and $PeakS_1$ for FS route. In the diagram, + and – define the polarity of the signal. In this section the application of two types of travelling wave based protection schemes is discussed, namely: single end method and double end method.

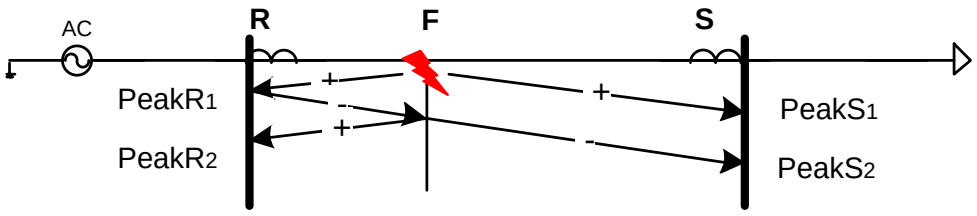

Figure 5-1: Lattice diagram for a fault at F

The magnitude of the fault generated high frequency transients is affected by the fault inception angle, fault resistance and distance to fault. Therefore, the waveform magnitude is generally not a suitable indicator of the fault condition. By contrast, the time and polarity information provide good fault indication, and have been widely

used in traveling wave based methods. Through systematic evaluation it can be concluded that the only feasible method is the double end method utilizing the initial current travelling waves' polarity and time information. The double end method needs to be designed to be the multi-end method for a meshed microgrid.

5.2.1 Single-end Method

For a single-end method, extraction of two consecutive wavefronts to obtain their polarity and timing information are mandatory. As shown in Figure 5-1, at end R, the first two peak arrivals are time stamped as $TpeakR_1$ and $TpeakR_2$. Their polarity information $PpeakR_1$ and $PpeakR_2$ are defined as: '1' represents positive polarity and '−1' represents negative polarity.

For simplicity, the wavefronts from the back of the instruments are removed. To discriminate the fault as 'in zone' or 'out of zone', fault location needs to be established. The calculation of fault location depends on whether the fault occurs in the first half of the line (Figure 5-1) or in the second half of the line. For the former case, the second wavefront has the same polarity as the first one. For the latter case, it has the opposite polarity. The equations of fault location calculation are presented in (5-1), (5-2) and (5-3).

$$\Delta Tpeak = TpeakR_2 - TpeakR_1 \tag{5-1}$$

$$PpeakR_1 \cdot PpeakR_2 = 1 \tag{5-2}$$
$$\Rightarrow Distance = \Delta Tpeak \cdot \mu$$

$$PpeakR_1 \cdot PpeakR_2 = -1 \tag{5-3}$$
$$\Rightarrow Distance = Length - \Delta Tpeak \cdot \mu$$

where μ is the velocity of the traveling wave along the line, *Length* is the length of the total cable/line, and *Tpeak* and *Ppeak* present the time and polarity information of the traveling wavefront. However, the single end method has the following inherent issues in microgrids:

1) The second wavefront is significantly damped by high resistive distribution lines.
2) The second wavefront can be cancelled out by the third wavefront or following wavefronts at specific fault locations, e.g. in the midpoint of the line.
3) To determine the fault position, the exact fault distance has to be calculated, which indicates that μ along the line and the total line length need to be known.
4) If the line behind the relay and source impedance are considered, the algorithm becomes even more complicated. Hence, it is highly recommended to add a line trap to isolate the signals from behind.
5) The requirement of sampling accuracy and frequency is very high when the line length is short, which is a typical situation for most microgrids.

5.2.2 Double and Multi-end Method

Originally, the indicator used in the double end method was similar to that of the single method, which is also based on the time intervals between the arrival times of the travelling waves. However, as concluded in the previous section, the performance of the algorithm based on mere time intervals has quite a few shortcomings when it comes to application in a microgrid system due to its relatively small scale. Hence, in this thesis, the polarity of the travelling waves detected at both ends as an alternative indicator for the double end method is used. When the fault occurs in the protected line, the polarities of the initial wavefronts are the same; otherwise, the polarities are opposite. Regardless of the scale of the system, the initial polarities of the travelling waves are always clear as demonstrated in [1]. Based on this, the proposed double-ended method can discriminate the faulty line correctly without establishing the exact fault location. Referring to Figure 5-1, the indicator is defined in the following equation:

$$PpeakR_1 \cdot PpeakS_1 = 1 \tag{5-4}$$

In a radial network with lines all equipped with double-end measurements, this method is sufficient as the travelling waves propagate in one direction only. Unlike single end method, this method has higher potential in practical microgrids since only the initial current wavefront is needed. Moreover, there is no "Non-Detection Zone" caused by specific fault locations; close-up forward and close-up backward faults can still be easily discriminated [2]. Nevertheless, in a meshed network or under some special scenarios, mere polarity information may not correctly indicate the faulty line. The propagation route becomes meshed and there will be a case when the current travelling wavefronts hit each other with the same polarity caused by an external fault. Furthermore, for some lines with only single end measurements available, the method based on the double end polarity comparison is not possible either. To solve these issues, two additional elements are included in the scheme logic: wide-area comparator of the wavefront arrival times, and local comparer of the polarity information for buses connected with more than two branches.

5.2.2.1 Wide-Area Comparison of the Time Information

In a meshed network, the route of the travelling wave is difficult to predict as the waveforms are travelling in both directions from the fault point and might meet at some place on a healthy line. Therefore, the indicator introduced in (5-4) is not sufficient to provide correct fault discrimination. Moreover, in some cases, the lines are only equipped with single-end measurement, mostly because they connect the remote power sources or loads. In order to provide correct fault detection in these cases, a wide-area comparison of the time information is added into the protection logic, which results in a multi-ended communication assisted method. Low bandwidth communication channels are, therefore, required to transport the time and polarity information from adjacent units. To cater for a meshed network, the following additional indicator (5-5) is also proposed:

$$T_{peak0} = min\left\{T_{peak0}, T_{peak1}, T_{peak2}, T_{peak3}, \dots T_{peakj}\right\} \tag{5-5}$$

where T_{peak0} is the time arrival of the first wavefront in the system, and $T_{peak1}, T_{peak2}, T_{peak3}, \dots T_{peakj}$ are the corresponding times obtained from the other

units. The communication technology used here can be internet, optical fibre, wireless or satellite. The busbar with the earliest detected waveform arrival time is used to define the potential faulty area, which prevents mal-operation in the case of a meshed network.

However, merely this indicator does not provide satisfactory performance in all meshed networks. Two specific situations are faults occurring in one of the parallel lines or on the lines with only single-end instrument. These two scenarios can be both illustrated in the model network presented in Figure 5-2. The network in this figure has a pair of parallel lines equipped with IT2, IT4 and IT3, IT5 accordingly, to be note that IT stands for instrument transformer for the measuring the current travelling waves. When a fault occurs in one of the parallel lines, the travelling wavefronts hit each other with the same polarity on the other parallel line; the instruments on both lines (IT2,IT4 and IT3,IT5) share the same information, which prevents proper discrimination of the fault location based on (5-4*)* and (5-5) only. Furthermore, for lines such as the one equipped with single-end instrument transformer IT6, since the busbar is connected to more than two branches, it is also a challenge to locate the fault.

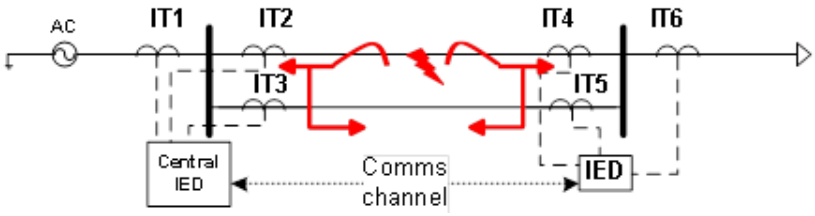

Figure 5-2: Meshed network with identical parallel

5.2.2.2 Comparison of Waveform Polarities at the Same Busbar

As discussed in the above section, in some cases, such as parallel lines, it is impossible to discriminate in which of the parallel branches the fault occurred. The time and polarity information are no longer useful as the instrument transformers

(ITs) installed on the parallel lines share exactly the same values. The IEDs will detect "faults" in both lines since the polarity information of both meet the indicator presented in (5-4*)* and (5-5). Moreover, for lines equipped with single-end instrument transformer, it is no longer feasible to use the indicator in (5-4*)*, which further highlights the need for improvement in the protection strategy.

In order to provide effective protection for these conditions, a comparer of polarities is built. It contains two elements which cater to different fault conditions. For buses with more than two lines connected, the faulty circuit is identified from the wavefront polarity information as the faulty branch will always have opposite polarity with respect to the remaining circuits. Assume one busbar is connected with total number of *j* branches, the indicator is presented in (5-6).

$$P_{peak0} = \prod_{i=1}^{j} P_{peak_i} = -1 \tag{5-6}$$

If P_{peak0} is -1, the fault occurs in one of the connected branches; otherwise, the fault is located at the busbar. The waveform with opposite polarity with respect to the others is the potential faulty branch. Combining logic with (5-4*)* and (5-5), the proposed protection scheme works for both parallel and single-ended lines.

5.2.2.3 Overall Strategy of the New Primary Protection Scheme

The entire updated protection strategy is developed to operate correctly in both radial and meshed network topologies. The indicators used in the protection are presented in (5-4*)*, (5-5) and (5-6). The logic can be described as follows:

1) Detect the initial arriving travelling wavefront of the fault transient in each IED. Select the reference phase with the highest amplitude of the travelling wave.
2) With comparison of the initial time stamp T_i, define the potential faulty area based on the earliest arrival time of the travelling wave among busbars all around the monitored network.

3) If more than two branches are in operation connected to the bus, apply (5-6) and discriminate the fault on the one with the opposite polarity with others.
4) If only two branches in operation, apply (5-4*)* to isolate or discriminate the healthy line.

The overall structure of the primary protection scheme is presented in Figure 5-3. For this proposed protection strategy, each bus is set up with a local IED which detects a wavefront above a certain threshold and sends the relevant data (IT and circuit number, the time of initial arriving wavefront and its polarity) to the central IED which subsequently evaluates which line is faulty and initiates the tripping signals to isolate the faulty zone. Hence, reliable but relatively low bandwidth communications are required as only the time and polarity information within the network during the fault need to be transported. It is to be noted that the detection of the initial current travelling wavefront is critical for this pilot protection scheme. A back-up protection scheme is therefore needed.

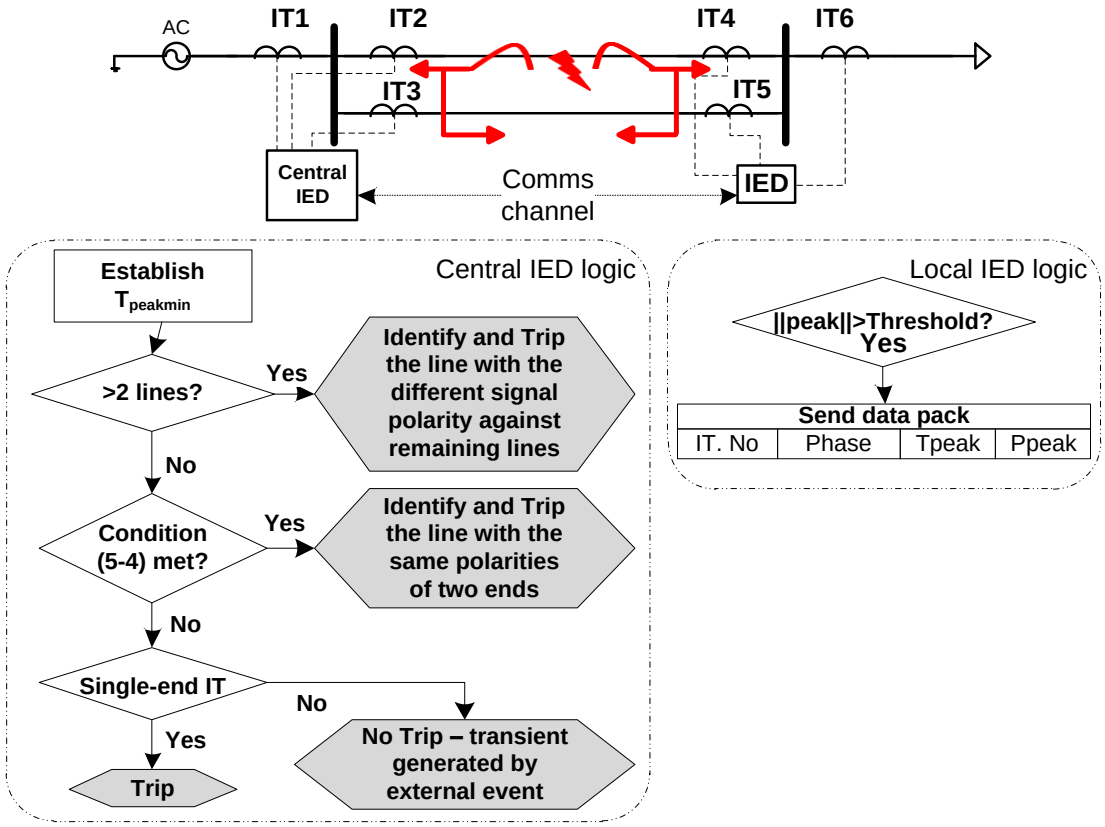

Figure 5-3: The overall protection logic diagram of the new protection scheme

In the central IED, the notation of the lines and busbars are stored. Moreover, it is to be noticed that the phase with highest amplitude of the earliest travelling wave is selected as the reference phase. The overall algorithm will be all based on this phase's measurement.

5.3 Comparison of the Signal Processing Techniques for the Travelling Wave Based Protection

As already explained in section 5.1, the choice of signal processing tools is critical for the performance of the travelling wave based protection scheme. For the proposed protection scheme as described in the previous section 5.2, three different processing tools found in protection related research and applications can be the candidates: WFT, DWT and MM. In this section in order to establish the best practical solution, the application of the three signal processing tools are discussed and compared.

Regarding WFT, the processed signals can only be analysed at one (or a series) definite frequency, which assumes that the signal is stationary during an observation time period. For the fault transients producing non-stationary signals with large frequency spectrum, this technique is unsatisfactory [18]. By contrast, with a suitable mother wavelet, DWT can be applied as a flexible and effective bandpass filter, which uses short windows at high frequencies and long windows at low frequencies. Therefore DWT has become one of the most popular signal analysis tools in the field of travelling wave based protection and fault location. According to the literature review in Section 3.6, many technical papers have been published on the application of DWT in the protection field. Besides, MM, an inherently a nonlinear approach, is an alternative signal processing tool for travelling wave based protection. Although MM has been proved to be light on memory requirements, efficient and accurate in extracting the high frequency transients, it has only been introduced to the protection

field very recently, which operation has not been fully studied. Hence this section is dedicated to present detailed discussion of these two techniques in order to select the optimal solution for the proposed travelling wave based microgrid protection..

To study the fundamental functions such as polarity detection and time location of the two techniques, a simple system consisted of one line with two end measurements is established, which is shown in Figure 5-4. It was assumed that the line between the two ends has a length of 5 km.

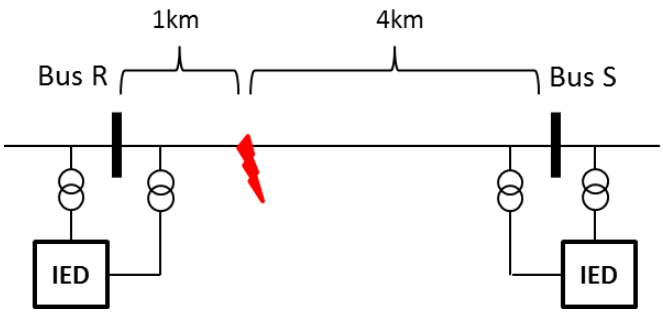

Figure 5-4: A simple two-end network with a fault in the middle

5.3.1 Critical Discussion on the Applicability of the DWT Technique to the Proposed Protection Scheme

Based on the discussion in Chapter 3, DWT based protection can be classified into one of the following three groups: 1) directional protection based on the transient energy of certain frequency bandwidth [3]; 2) directional protection based on the polarity and amplitude of the initial travelling wavefronts [4]; 3) fault location alike protection based on the time information according to the modulus maxima after wavelet decomposition [5].

DWT, indeed, has been applied to many phases of protection and fault location in the existing power system.

As the microgrid system has several features as in section 5.1, the methods utilizing the time information of series of arriving wavefronts become prohibitive. The wavelet energy requesting both high frequency voltage and current measurements are quite challenging. It seems like all three groups of existing methods are hard to achieve in an actual microgrid system. This section is supposed to test if DWT is a good signal processing tool to realize the proposed protection strategy in this chapter – in the other words, whether DWT is capable of detecting the waveform polarity and preserve timing information accurately.

5.3.1.1 Choice of Mother Wavelet

There are many mother wavelets used in DWT decomposition and reconstruction. Choosing or designing a suitable mother wavelet for DWT is crucial, but the answers are not very consistent in the literature [4-9]. Generally, the requirements of a good mother wavelet are:

1) The mother wavelet should be orthogonal or quasi-orthogonal, to achieve good reconstruction performance, so that to preserve the energy of the signal.
2) The time frame of the mother wavelet is tight, minimizing the overlap of the frequency bands between different levels of decomposition.
3) Smoothness and regularity of the wavelet are two characterisitics defined in [8]. They both work for getting better transient features and better denoising of the signals.

Normally to analyse the performance of a mother wavelet, one can conduct the wavelet transform to identify the one with maximum coefficient values, or pick up one with the minimum shape deviations before decomposition and after reconstruction. In this thesis, both of the methods will be used. The mother wavelet is adopted by compensation and integration of the results from both two tests. In the test, the same faulty signal will be analyzed by Daubechies wavelets, Coiflets, Symlets, and Biorthogonal wavelets, which are the mother wavelets broadly considered in fault diagnosis [4-9].

Based on a simple model presented in Figure 5-4, a fault is applied between bus R and bus S, 1 km away from bus R. The transients are recorded from the R side instrument and processed by the DWT. In Figure 5-5, the modulus maxima of the detailed coefficient after the first level decomposition are presented. This is followed by the analysis of the reconstruction performance where the error between the original signal and reconstructed signal is calculated and presented, in Figure 5-6.

The number at x-axis stands for different mother wavelets, as denoted in Table 5-1. Based on the simulation results in Figure 5-5 and Figure 5-6, it is clear that the best mother wavelets with good reconstruction performance are the Biorthogonal wavelets. The mother wavelet can therefore be selected from bior1.1~bior2.8.

Table 5-1: The number sequence of the corresponding mother wavelet

Number	Mother wavelets
1~12	bior 1.1, bior 1.3, bior 1.5, bior 2.2, bior 2.4, bior 2.6, bior 2.8, bior 3.1, bior 3.3, bior 3.5, bior 3.7, bior 3.9;
13~18	db1, db2, db3, db4, db6, db8;
19~23	coif1, coif2, coif3, coif4, coif5;
24~30	sym2, sym3, sym4, sym5, sym6, sym7, sym8;

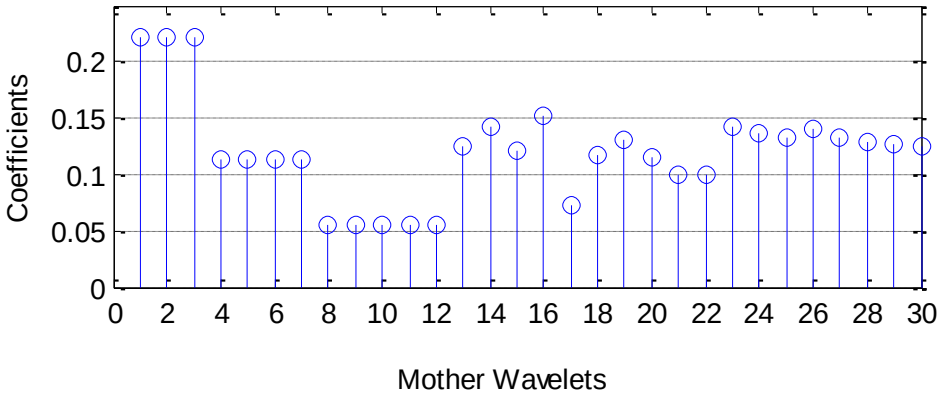

Figure 5-5: The modulus maxima with different mother wavelets

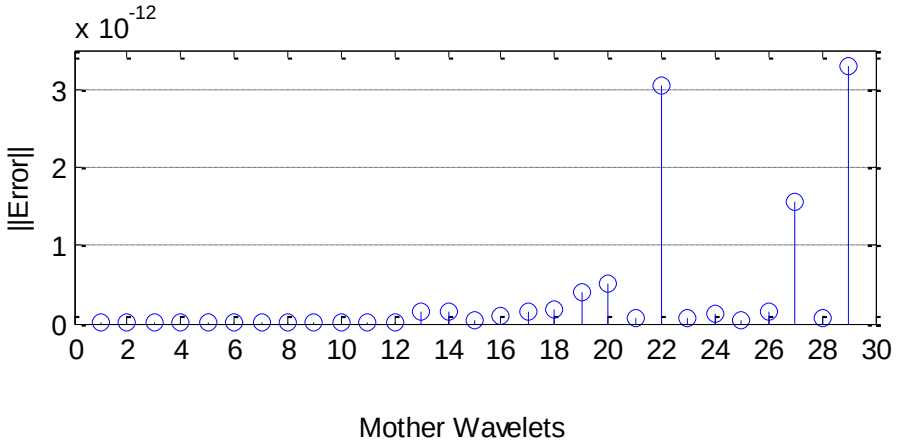

Figure 5-6: The error of the reconstruction with different mother wavelets

5.3.1.2 The Choice of the Level of DWT Decomposition

In theory, DWT decomposition decomposes a signal into different frequency bandwidths. The selection of decomposition level is also one of the challenges of DWT application. In this case, it mainly depends on the frequency bandwidth of the fault generated transients. However, the results from the study of the spectral analysis of the fault induced transients did not locate in a definite bandwidth according to the existing literature. For example, John et al. [10] declares that the main bandwidth of the fault-generated transients in the transmission system is centred on a frequency of 80 kHz, while Chen et al. [11] defines the main bandwidth

of the fault transients between 20kHz and 200kHz. Actually, the level of the DWT decomposition was chosen from practical tests and experience. In this thesis, we can roughly define the main frequency bandwidth of the fault transients under several scenarios by taking a multi-level DWT decomposition – to find out the level of decomposition with the largest absolute magnitude of the DWT decomposed detailed coefficients, in other words, the modulus maxima.

In order to apply multi-level DWT analysis, based on the analysis in Section 5.3.1.1, the Bior 2.2 mother wavelet is adopted. A phase-A-to-ground solid fault is applied to 1km away from the bus R in Figure 5-4. With five-level decomposition, the initial modulus maxima of each level are presented in the Figure 5-7(a), denoted as cd_1-cd_5. It can be seen that with different level of decomposition, the modulus maxima not necessary locate in the same point on the time axis of the signal. The high frequency decomposed component of above 500 kHz appears to have more abundant features than the second (250~500kHz) and the third (125~250kHz) level decomposed components. However, with a longer fault distance of 3 km, the frequency spectrum becomes different, as shown in Figure 5-7 (b). The dominant frequency band varies with the fault location.

The clearest features with tightest impulses are always presented at the first level of DWT decomposition, even though they are more affected by the system noises. When a careful look is taken at the Figure 5-7, it can been seen that the current travelling waves do not fall into a single frequency band, and multiple levels of decomposition bestow abundant features. This example verifies the previous research findings that the fault generated transients cover very broad frequency band. Although the detected singularities at different levels of decomposition are assumed to be the same in [11-12], as shown in Figure 5-7, the initial impulses are actually not located at exactly the same time.

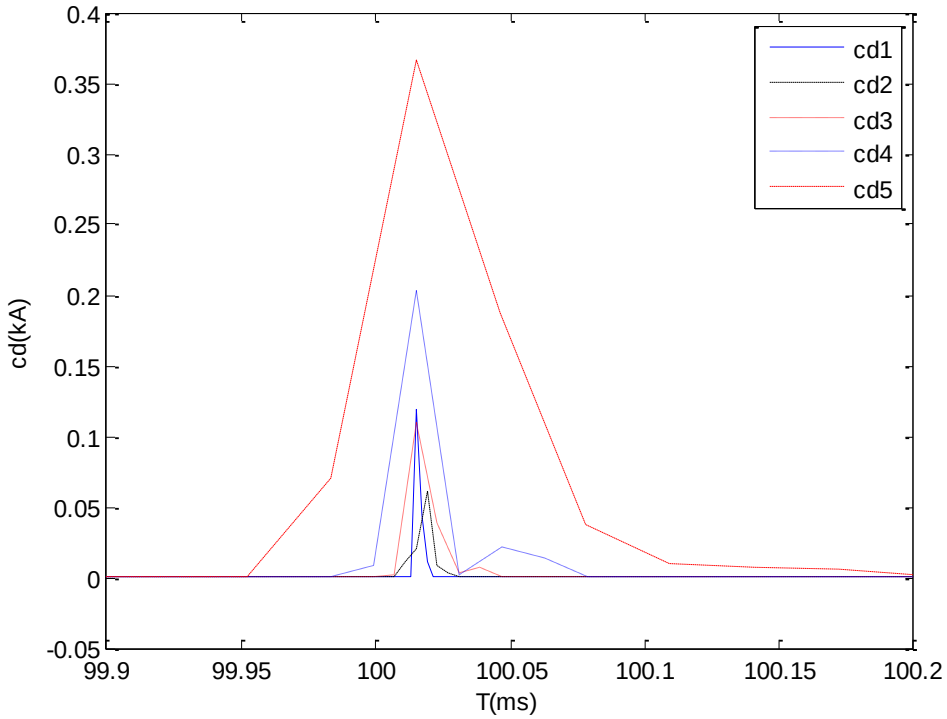

(a) 1km away from bus R

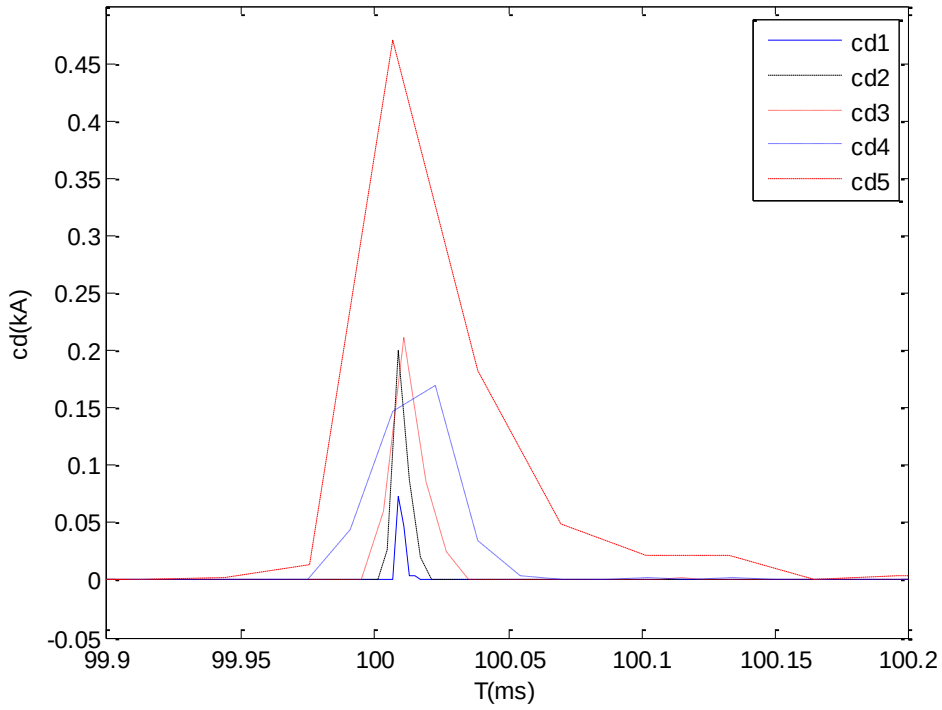

(b) 3 km away from bus R

Figure 5-7: The modulus maxima of the detailed coefficients with different levels of DWT decompostion

5.3.1.3 Polarity Detection Using DWT

The inherent features of the microgrid call for modification on the traditional travelling wave based protection schemes: only the initial wavefront can be clearly extracted due to the high damping along the resistive cables or lines. The polarity information of the travelling waves is one of the major features can be well used in the directional detection for the protection schemes. In most of the papers, the polarity is obtained using voltage and current signals [11-12]. If a forward fault occurs, the voltage and current share the same polarity; otherwise, they are of opposite polarity. A directional protection scheme using polarity information of mere current travelling waves is proposed by [13]. The principle is based on the fact that the polarity of the faulty line is different from other branches connected to the same busbar. However, the method is only feasible for the busbars with more than two circuits connected. In the distribution system, this is not always the case: the line may also be a dedicated line without side branches. In this thesis, the author proposes an alternative solution which is based on the comparison of the current wave polarity at the opposite ends of the line.

The capability of DWT to detect the polarity of the signals has been tested and is illustrated in Figure 5-8 and Figure 5-9. Figure 5-8 shows the consistency of polarity detection through different levels of DWT decomposition; Figure 5-9 presents the performance of DWT decomposition in the double-ended protection method under different fault distance.

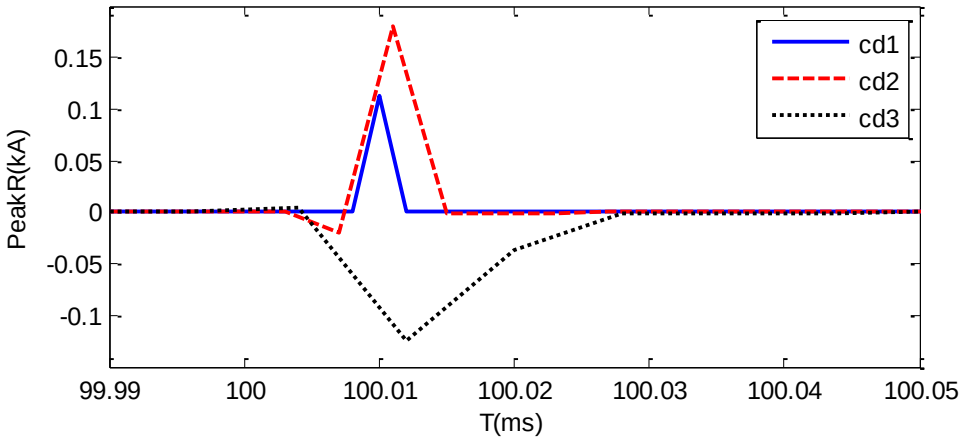

Figure 5-8: The polarity detection under different level of DWT decomposition

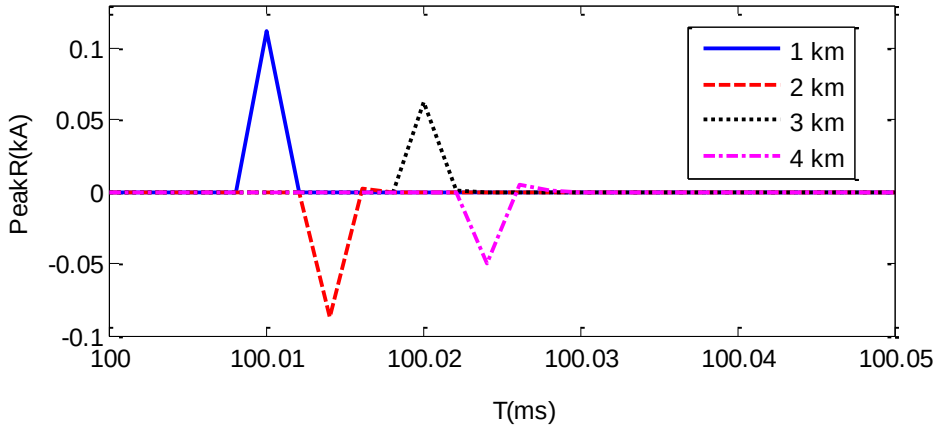

(a) IED at Bus R

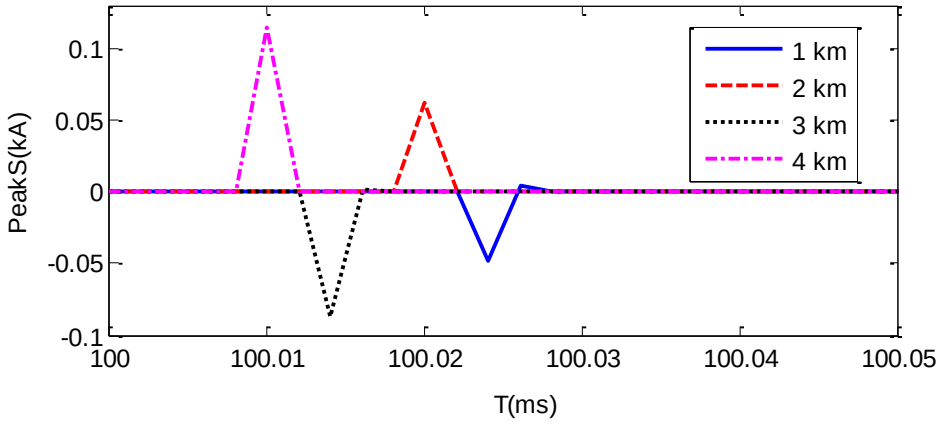

(b) IED at Bus S

Figure 5-9: The signs with different fault locations from both ends using DWT

From the fault detection point of view the polarity of the signal should ideally be the same regardless of the level of decomposition. However from Figure 5-8, it is quite clear that not only the shape, but also the polarity of the decomposed signal varies. After the second level of decomposition, the polarity of a single pulse fluctuates for a short time. This oscillating feature cannot be easily eliminated as it is also subject to the inherent features of DWT decomposition. This affects the sensitivity of accurate peak detection.

If the CTs at two ends of a line are connected in opposite directions, the decomposed signals are expected to have the same polarity under internal fault scenario, due to basic principles of double-ended method. A simulation study was performed using the system presented in Figure 5-4 where a fault was applied at four positions between Bus R and Bus S: 1km, 2km, 3km, and 4km from Bus R. The line was represented by a 20KV XPLE ABB underground cable. As shown in Figure 5-9, the result is opposite to the expectation. Hence, the DWT decomposition is unable to denote the real signal polarities.

Following from the discussion above, we can conclude that the standard DWT, suffers from four limitations: 1) shift sensitivity, 2) poor directionality, 3) absence of phase information, and 4) oscillations around singularities. Therefore, DWT is not an effective signal processing tool for double-end polarity comparison based protection.

5.3.1.4 Signal Denoising Using DWT

In addition to polarity detection, it is also necessary to investigate the denoising performance of DWT. The denoising process using DWT is generally consist of three steps:

1) Apply DWT decomposition up to the level at which the desired feature can be easily extracted.
2) Select proper threshold to eliminate the undesired noises.
3) Apply reconstruction based on the remaining coefficients (i.e. those above the selected threshold).

According to the Section 5.3.1.1. of this thesis, the good mother wavelets for signal reconstruction contain Biorgothonal wavelets, which are also suitable for signal denoising. Applying Bior 2.2 to a faulty signal with 20 dB white noise, the result for five level denoising is presented in Figure 5-10. The threshold is quite difficult to set, as the noise level is relatively high. As a consequence, the correct transient features cannot be discriminated from the noise during the process of reconstruction. Instead, a feasible way to denoise the signal is to replace the detailed coefficients with a sequence of zeros. The reconstructed signal is only built using the approximation part. From Figure 5-10, it can be seen that this process is very effective in the elimination of the noise after several levels of decomposition and reconstruction. Nevertheless, when extracting the feature from the denoised signals, one has to notify that the first level decomposed detailed coefficients are meaningless as they are always zero. The transient features can be extracted after the second level of DWT decomposition. The results in Figure 5-11 clearly show that the transient features can be successfully extracted based on the 4^{th} level reconstructed signal. However, the process leads to a linear increase in the computational burden, as several levels of reconstructions and decompositions need to be done before getting a clear polarity indication. The level of reconstruction and decompositions is all dependent on the noise level of the signal. It will be impossible to extract the transient feature when the noise is dominant in the signal.

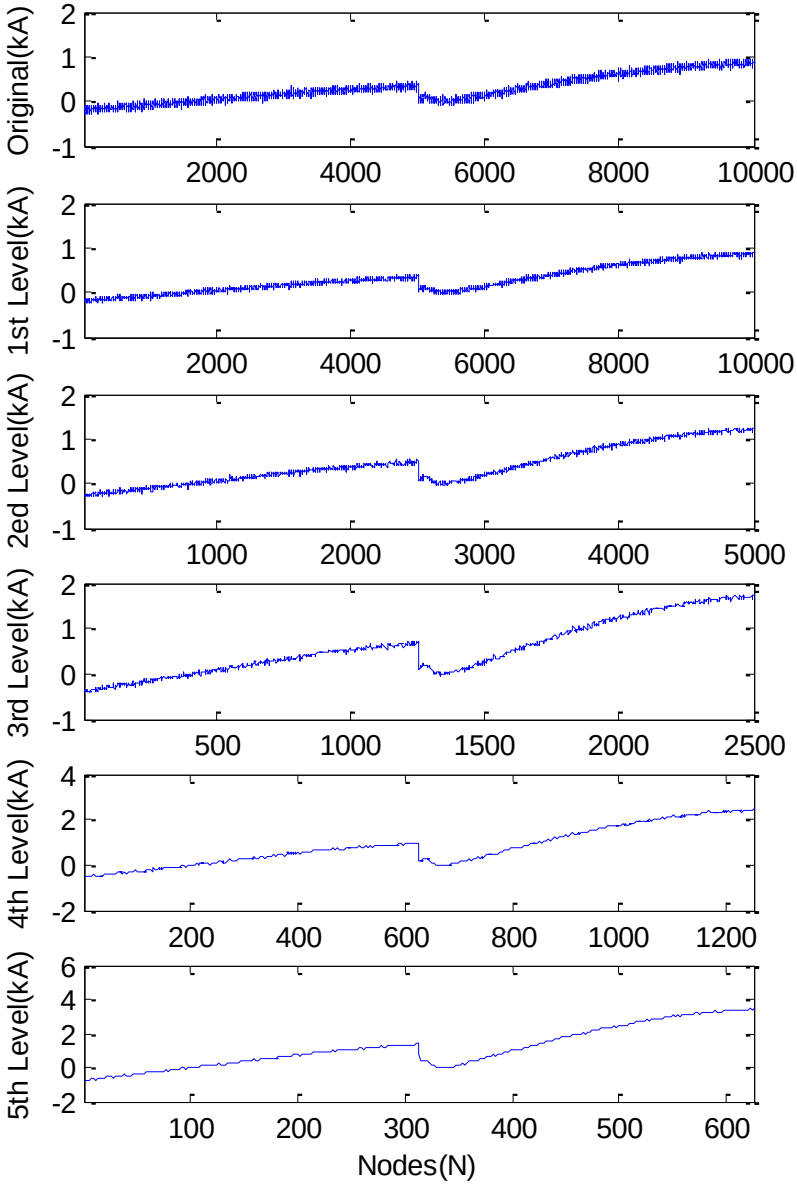

Figure 5-10: Signal denoising using five levels of DWT decomposition

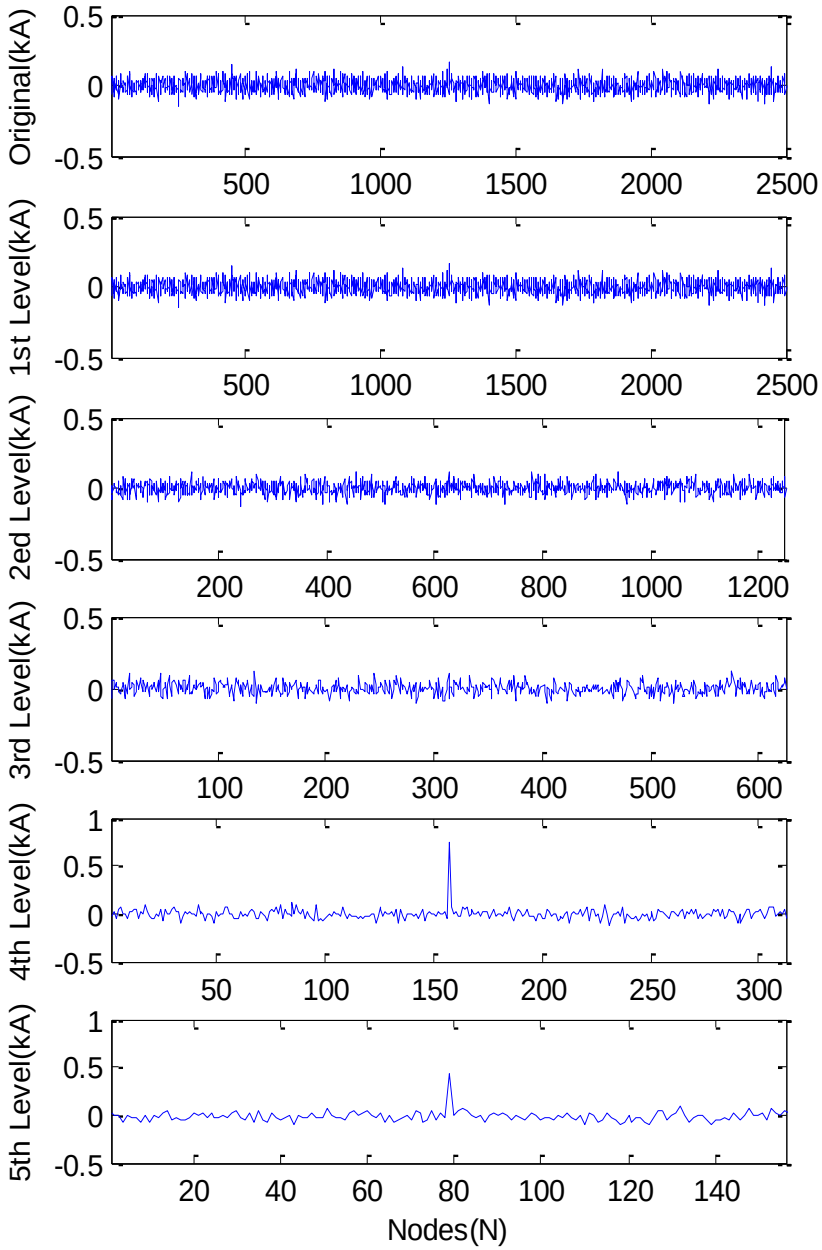

Figure 5-11: The corresponding transient feature extraction of denoised signals using DWT decomposition

5.3.2 Development and Analysis of a New MM Based Technique

As concluded in the previous sections, DWT is not an effective tool to meet the basic requirements for the proposed microgrid protection, which is based on accurate polarity information and accurate time location. Therefore, the author of this thesis considered MM as an alternative to DWT. Unlike DWT analysis, MM is a nonlinear analysis tool, which processes the signals in the time domain only. In section 3.4.3.4 of Chapter 3, the basic principle of MM has been introduced and it has been found out that the traditional MM filters (MMF) only uses simple mathematical operations (erosion and dilation) with relatively short numerical window, which only contains a series of plus and minus functions. This technology has been proven to have low memory requirements, high efficiency and accuracy in extracting high frequency travelling wave information [14].

5.3.2.1 Choice of Feature-Extraction MMFs and Corresponding SE

Some examples of MMFs used to extract the hidden signal features have been presented in Chapter 3. The choice of a suitable MMF is critical for the design of the efficient proposed MMF based protection scheme. . According to the discussion in session 3.4.3.4 of Chapter 3, the typical feature-extraction MMFs are dilation-erosion difference filter (DEDF) and opening-closing difference filter (OCDF). To achieve proper selection of detail-extraction aimed MMF, the tests are conducted on the same faulty signal as shown in Figure 5-12. Apparently, DEDF (red signal) is more sensitive to the fault and behaves as the better indicator of the detail-extraction filters compared to OCDF.

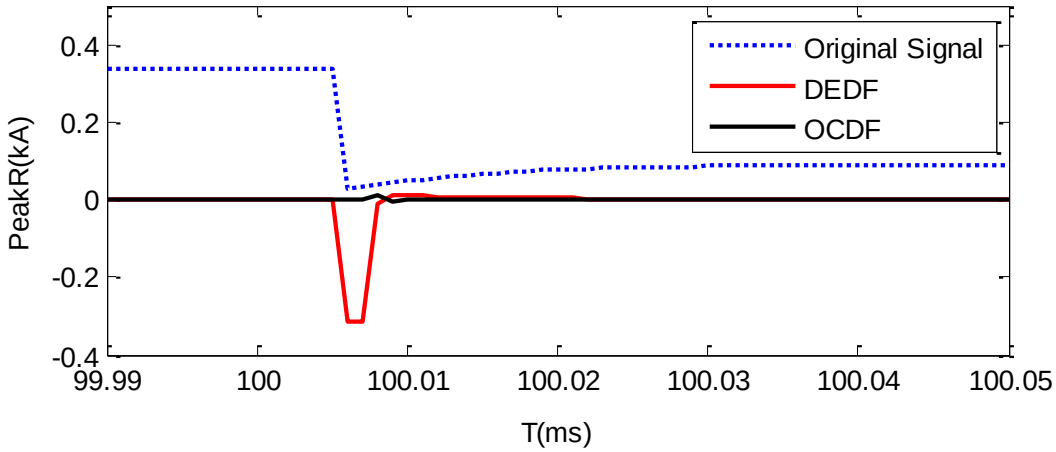

Figure 5-12: The comparison of MMFs (OCDF and DEDF) for extraction of fault transients

Regarding the choice of SE, no specific guidelines appear to provide a clear answer. The main concern about SE is its shape and length. One theory proposes that the shape of the SE should be similar to the basic waveform of the transient features of the signal [15]. In the power system, the travelling wave hits the singularities, causing a nearly quasi-step up/down feature on the electrical signals, shown in Figure 5-12. To extract this type of feature, the flat SE becomes the primary choice. In [15], the author suggested that the length of SE should be chosen by considering the corresponding sampling frequency and relay's response time; in this thesis, it is interesting to take one additional look at the choice of the length of the SE. Figure 5-13 shows the results extracted by DEDF using different lengths of SE.

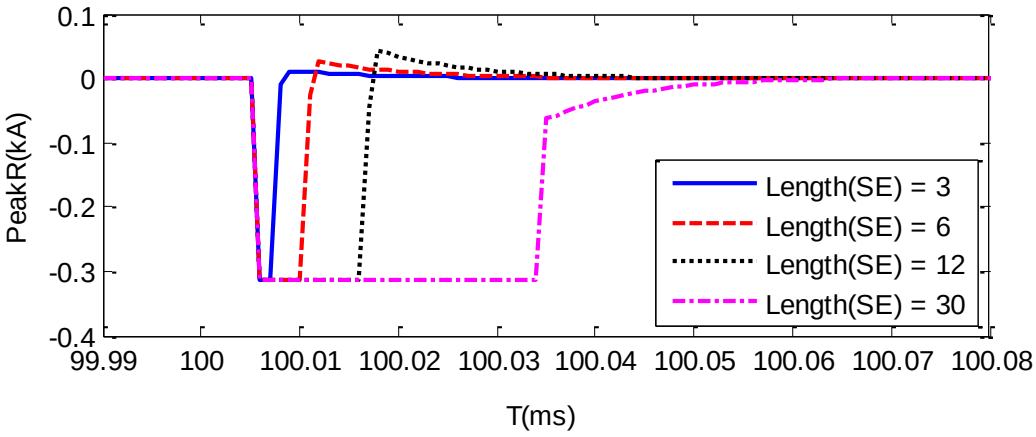

(a) Sampling frequency = 1 kHz

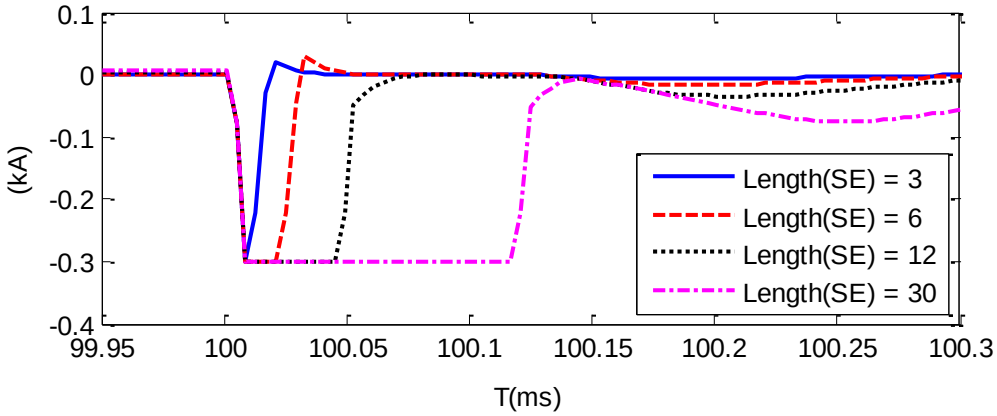

(b) Sampling frequency = 200 kHz

Figure 5-13: The transient features extracted by different length of SE at sampling rate of 1MHz (a) and 200kHz(b)

It can be seen that at either sampling frequency, with the increase of the SE length, the transient features can be detected with the only difference that the extracted pulse lasts longer and is wider. This has two effects on the protection logics: the first one is that the width of the pulse guarantees the relay has enough time to detect the feature; the second one is that the SE length defines the numerical window of the algorithm, which is critical for the speed of the relay operation. Ideally, an SE with length of 3 should be sufficient to achieve correct operation.

5.3.2.2 Polarity Detection Using MMF

Polarity detection is critical for the *MMF* based double-ended method. But conventional *DEDF* does not have function of polarity detection. First applied to the protection area, the authors in [14] have proposed a method to detect the polarity of the signals based on two quadratic flat *SE*s. In this thesis, the author observes that it is also possible to achieve the same goal with less computational burden by utilizing the apparent features of erosion and dilation waveforms. To explain this principle, a simple step signal tested.

As shown in Figure 5-14, an 80 node step signal $F(n)$ is processed by a flat SE ($SE(m) = [0,0,0]$, $M = \text{length}(SE(m))$). The resulting *DEDF(n)* using the traditional algorithm does not depict polarity characteristics. Nonetheless, it is to be noted that the dilation signal ($f_{ero}(n)$) lags erosion signal ($f_{dil}(n)$) *M*−1 nodes when there is an ascending edge, and leads erosion signal by M−1 nodes when there is a descending edge. This characteristic can be used to detect the signal polarity. This new modification to enable polarity detection is presented in (5-7) and (5-8), where ε is a small threshold close to zero for detecting the lag or lead feature ($\varepsilon = 0.0001$ was used).

$$\Delta f_{ero}(n) < \Delta f_{dil}(n) < -\varepsilon \qquad DEDF'(n) = f_{ero}(n) - f_{dil}(n) \tag{5-7}$$

$$\Delta f_{dil}(n) > \Delta f_{ero}(n) > +\varepsilon \qquad DEDF'(n) = f_{dil}(n) - f_{ero}(n) \tag{5-8}$$

The results of the modified method are presented together with those of a traditional MMF method and multi-level DWT method in Figure 5-14. It can be seen that the proposed method achieves the clearest and most accurate polarity detection. Moreover, the processing time for MM based method has been veriefied to be 25%-30% faster than that for DWT method (based on Matlab simulation).

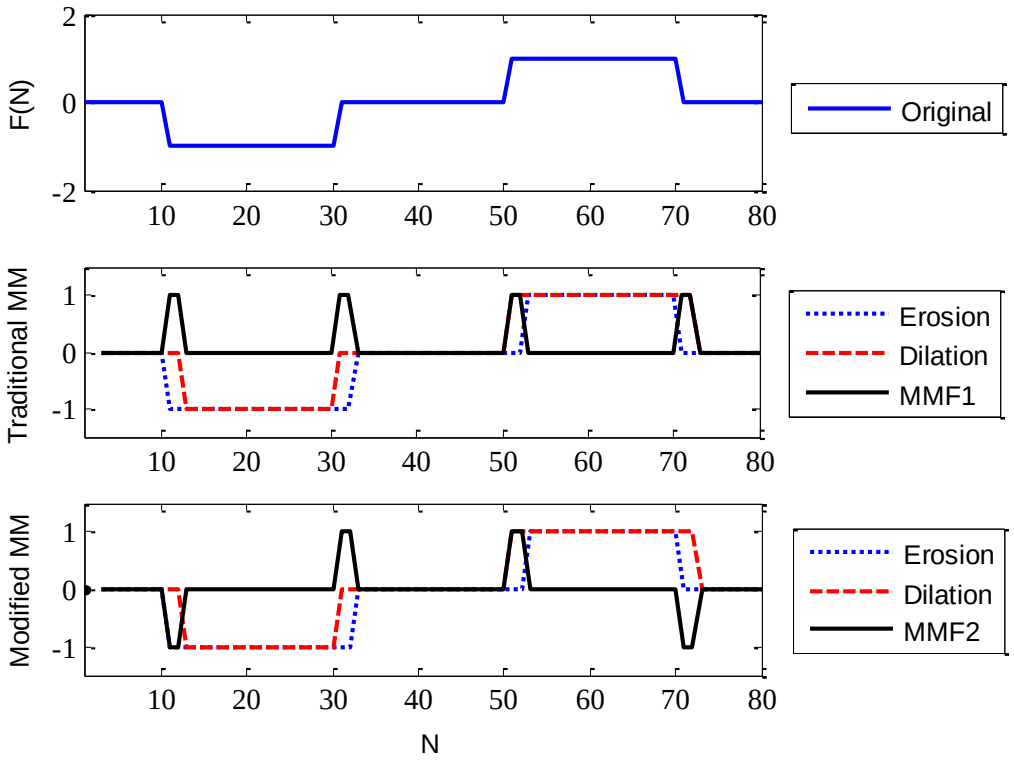

Figure 5-14: DEDF response comparison

To compare the performance with the DWT based method discussed earlier, under the same test scenario as presented in Figure 5-9, the proposed modified method is applied. As shown in Figure 5-15, the polarity of the signals with the same direction remains the same regardless of the distance. Moreover, apart from the magnitude, the shapes of the same transients do not change with the fault location or time of fault occurrence. The magnitude of the extracted transients varies with distances to fault due to the damping effect and boundary refraction index along the underground cable.

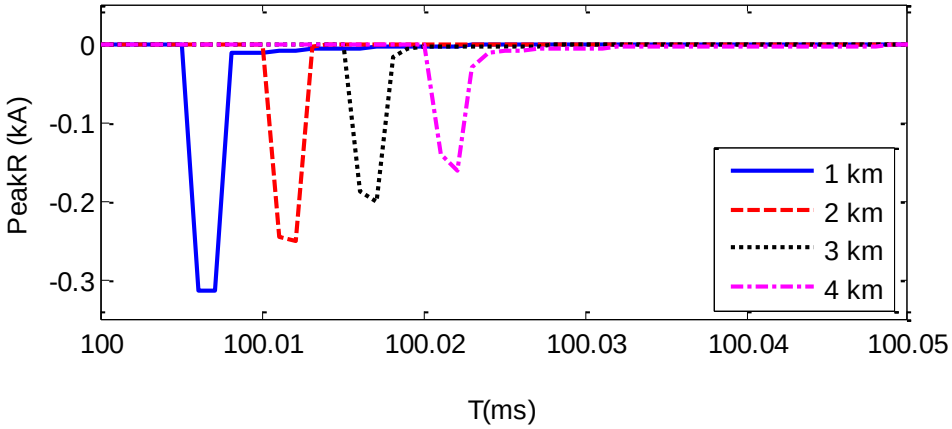

(a) IED at Bus R

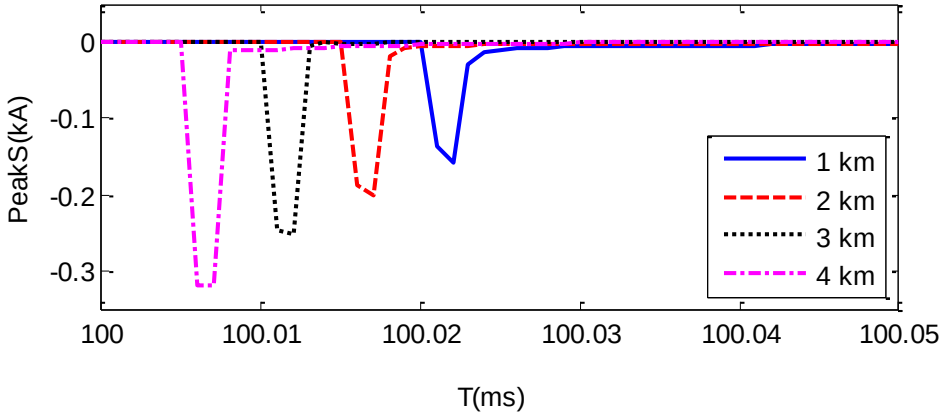

(a) IED at Bus S

Figure 5-15: Signal polarity at different fault locations using DEDF

5.3.2.3 Signal Denoising Using MM Technology

To deal with power system noise, several denoising *MMF*s can be also developed. Three major denoising *MMF*s, including Dilation and Erosion Median Filter (*DEMF*), Open and Close Median Filter (*OCMF*), Open-Close and Close-Open Median Filter (*OCCOMF*), are proposed as defined by (5-9), (5-10) and (5-11) respectively.

$$DEMF(n) = \frac{f_{dil}(n) + f_{ero}(n)}{2} \tag{5-9}$$

$$OCMF(n) = \frac{f_{cl}(n) + f_{op}(n)}{2} \tag{5-10}$$

$$OCCOMF(n) = \frac{f_{op}(f_{cl}(n)) + f_{cl}(f_{op}(n))}{2} \tag{5-11}$$

These three filters, based on the four basic operations (erosion, dilation, open and close), as well as much less repetitive deductions, all have very light computational burden. Assuming that the length of SE for the denoising is 40, and for the feature extraction is 3, the results of comparing the three denoising filters are presented in Figure 5-16. The corresponding transient features are extracted as shown in Figure 5-17. It can be clearly seen that the *OCCOMF* removes the most of the noise of the signals, and is also highly effective in transient feature extraction for the proposed protection.

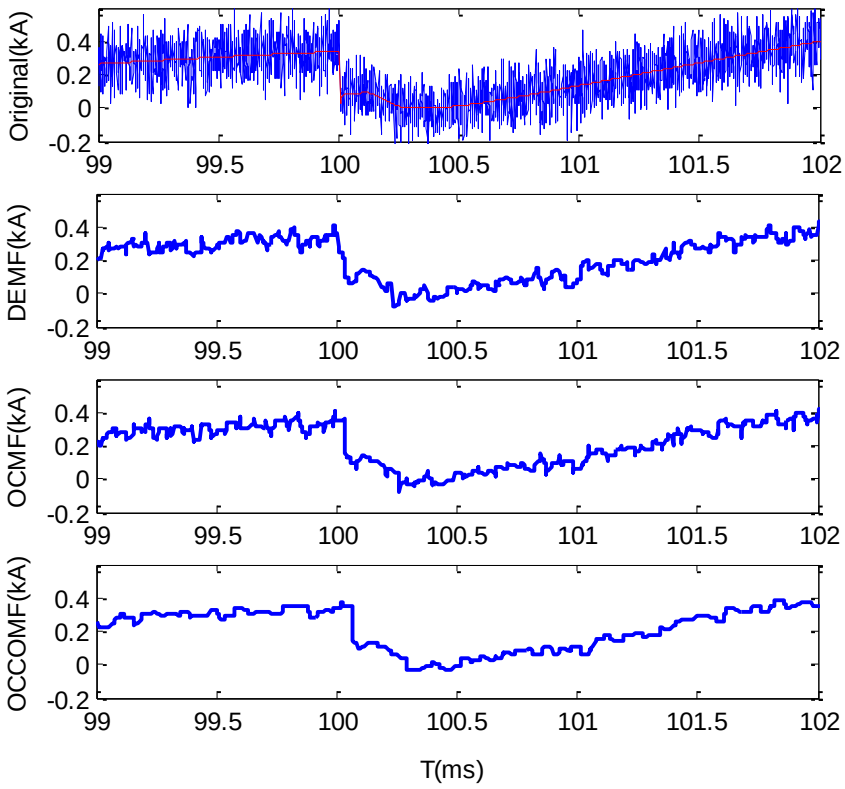

Figure 5-16: Signal denoising using three different MMFs (DEDF, OCMF, OCCOMF)

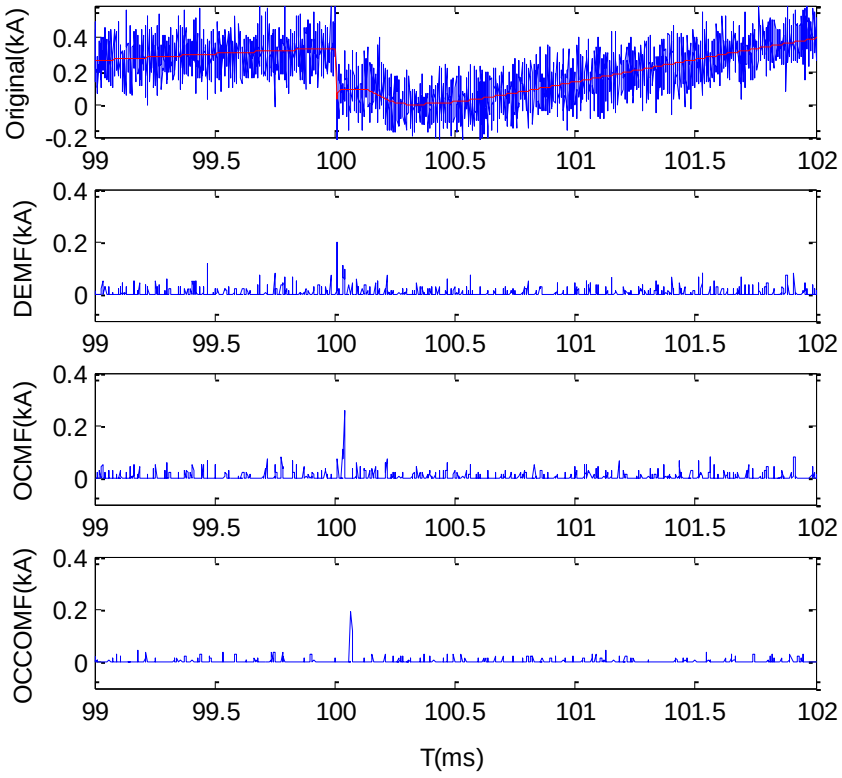

Figure 5-17: The corresponding transient feature extraction of denoised signals using different MMFs

Similar to the feature-extraction *MMF*s, there are no definite guidelines for defining the length of *SE* used for signal denoising. Basically, the length of *SE* has to be sufficient to smooth the signal, but should not be too long as it may cause excessive time delay which may prevent protection from detecting the transient step up/down features of the travelling waves. This has to be coordinated with the damping issue of the wavefront through the network – the length of SE should be considerably shorter than the transients decay time. To define the optimal length of SE, a test is conducted using *OCCOMF* with different *SE* lengths as shown in Figure 5-18. By extending the *SE* length, the noise of the signal is further damped, however, more delay occurs for the transient step down feature. The case of SE = 60 shows that the long length of *SE* will also distort the transient features. To achieve a good compromise, an *SE* with length around 30 is proposed since it appears to maintain the transient feature very well and also efficiently lower the noise level of the signal. However, it should be

noticed that after OCCOMF, there is still some noise in the indicator which might cause the relay to maloperate.

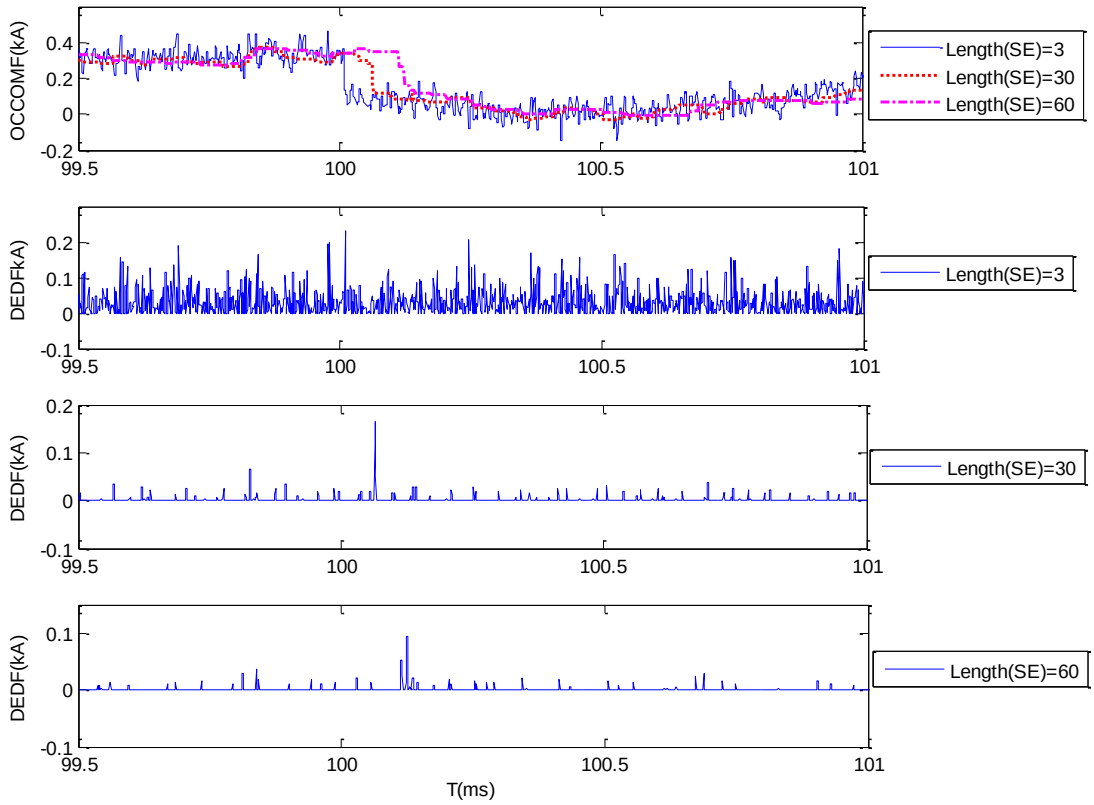

Figure 5-18: The denoised signal by different lengths of SE (3,30,60)

5.3.2.4 Analysis of the Application of Multi-Resolution MMFs

A multi-resolution MMF is a technology used in nonlinear pyramid analysis, which if properly applied, can be more suitable for the analysis of power system disturbances, since the power system signals under such events are intrinsically nonlinear. In the image processing area, the multi-resolution signal decomposition has been recognized as one of the most convenient ways to process information. In the signal processing area, a series multi-resolution dyadic DEDF (SDEDF) is proposed by [14-16], which is aimed to solve the issue that, under some scenarios, the components calculated from single level of detail-extractions MMFs might still

correspond to the low frequency band [17]. It was also argued in [18] that, multiresolution MMF provides an optimal analysis for transients with shapes resempling impulses. However, in this thesis, it is found that the fault transients are always dominant, showing very little low frequency component after single level MMF; and based on the transient simulation using PSCAD/EMTDC, most of the power system fault transients are actually quasi-step signals (except for arcing fault). Nevertheless, the idea of multiresolution decomposition might be used in arcing fault detection and signal denoising area.

5.3.2.5 Multi-resolution Feature-extraction MMF

It is now widely known that multi-resolution approaches, like pyramid decomposition, play a significant role in signal processing application. The underlying principle of the pyramid multi-resolution approach is conducted by applying a family of approximate analysis operators $\rho_n^{\uparrow}$ to decompose the signal from a lower level to a higher level ($X_n \rightarrow X_{n+1}$). The upward arrow represents an operator which maps the signal into an upper level. A basic multi-resolution morphological analysis can be presented in the pyramid as shown in Figure 5-19. It is to be noted that $\sigma_n^{\uparrow}$ is the detailed analysis operators used for perfect reconstruction of the signals. The Basic theory of multi-resolution MMFs can be learnt from [19-20]. The morphological Haar wavelet was developed in the two papers, where the major difference from the original linear Haar wavelet lies in the original linear analysis filter replaced by the basic morphological algorithms: erosion or dilation. According to [20], the analysis operators are defined in (5-12) and (5-13).

$$\rho_n^{\uparrow} \Rightarrow X_n \oplus SE_n(\downarrow 2) - X_n \ominus SE_n(\downarrow 2) \tag{5-12}$$

$$\sigma_n^{\uparrow} \Rightarrow X_n(\downarrow 2) - X_n \oplus SE_n(\downarrow 2) + X_n \ominus SE_n(\downarrow 2) \tag{5-13}$$

where $\oplus$ stands for the dilation operator and $\ominus$ stands for the erosion operator; n represents the decwmposition level, and the length of SE_n is scaled by 2^{-n}; $\downarrow 2$ represents the down sampling operator by 2. Based on these operators, the corresponding dyadic SDEDF_n can be obtained from (5-14).

$$SDEDF_n = \rho_n^{\uparrow} \tag{5-14}$$

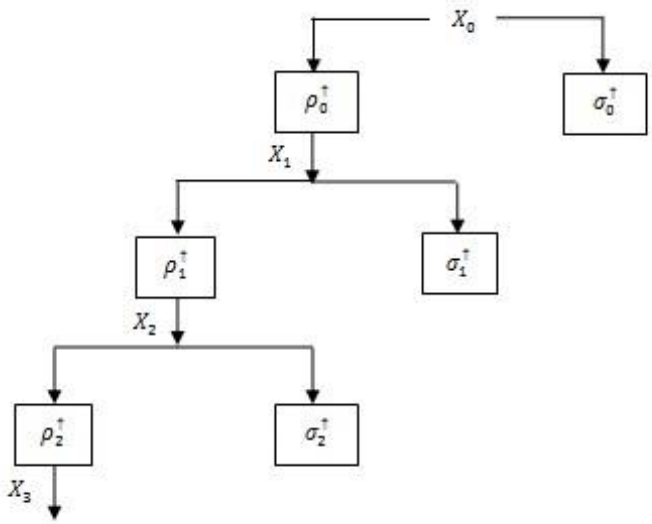

Figure 5-19: The pyramid of multi-resolution morphological analysis

For example, as shown in Figure 5-20, the signal *F(n)* is analysed by the multi-resolution mathematical morphological filters. The SEs for the this analysis are: $\mathrm{SE}_1 = [0,0,0,0,0,0]$ and $\mathrm{SE}_2 = [0,0,0]$. The horizontal axis is scaled to the same length, and it is found out that the detected transient feature of level 2 is expanded twice compared to that of Level 1. This is due to the down sampling operation in the decomposition.

Without arcing effect, the fault generated travelling waves are depicted as a series of step signals hitting at the singularities of the power system. Under this scenario, the multi-resolution analysis does not provide obviously optimal processing performance. A single level MMF analysis is sufficient for the feature extraction.

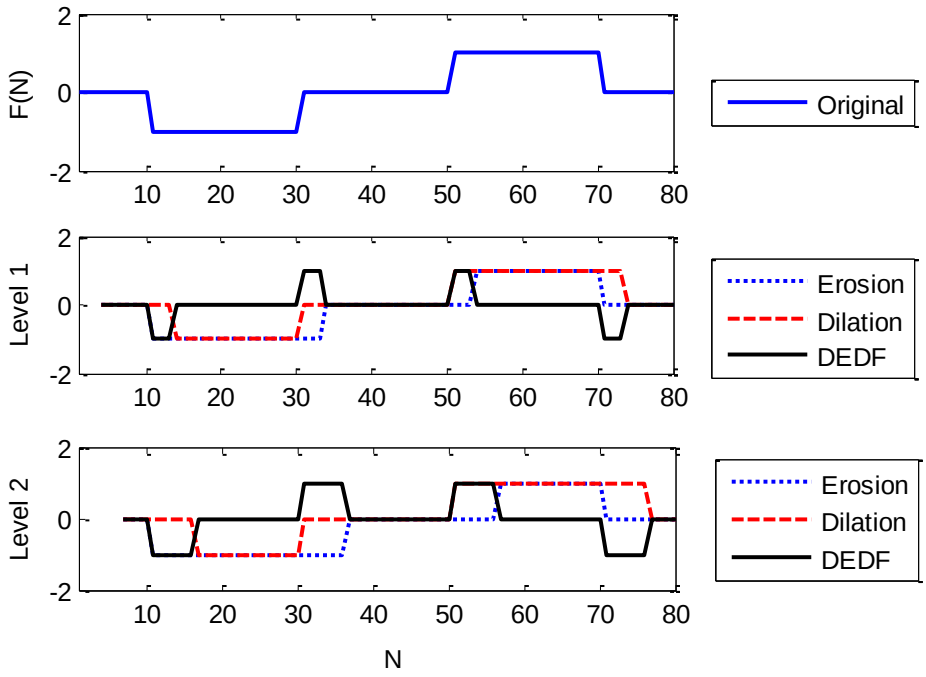

Figure 5-20: SDEDF analysis under two level of decomposition

5.3.2.6 Multi-resolution Signal-denoising MMF

The idea of multi-resolution decomposition can also be applied to signal denoising area. Based on the study in session 5.3.2.3., it is already known that the OCCOMF is the best MMF for signal denoising. Therefore a serial of OCCOMF (SOCCOMF) is established as shown in Figure 5-21.

Figure 5-21: The basic theory of SOCCOMF

This is investigated using the same noisy signal in Figure 5-16. The length of denoising SEs for three levels are $Length(SE_1) = 32$, $Length(SE_2) = 16$ and

$Length(SE_3) = 8$, where the subscript number denotes the level number. Results from Figure 5-22 indicate significant difference in terms of the denoising performance between each level of processing. Regarding the performance of indicator extraction based on denoised signals, referring to Figure 5-23, after two levels of progressing, we can see that the level of noise is clearly reduced, which proves that the multi-resolution denoising process can be used to lower the peak detection threshold. For this reason, in this thesis it is recommended to use the multi-resolution morphological analysis for noise reduction when the noise level is relatively high. It is to be noted that, under some fault conditions with high vibration characteristics (i.e. arching fault), the multi-resolution morphological analysis also presents optimal performance in both denoising and feature extraction operations [18].

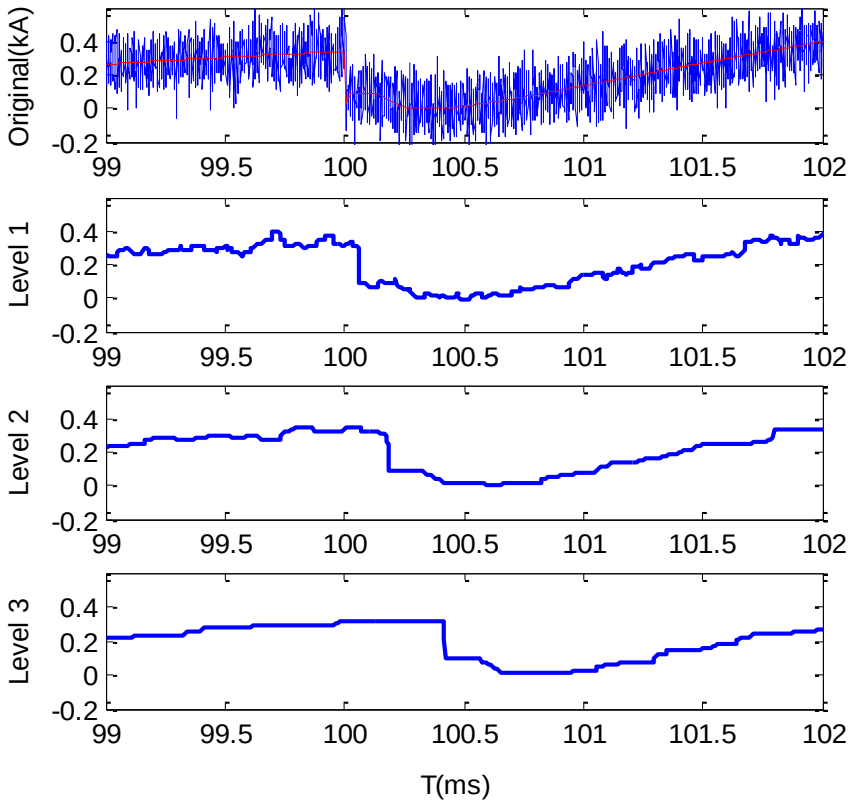

Figure 5-22: Signal denoising using SOCCOMF

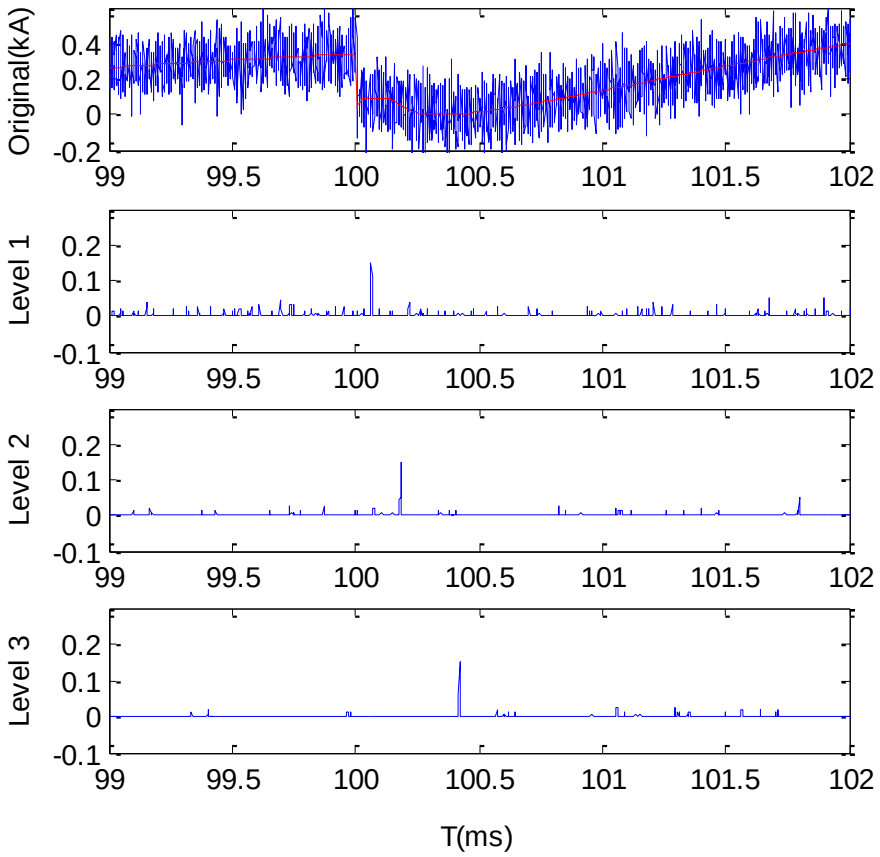

Figure 5-23: The corresponding transient feature extraction of denoised signals using SOCCOMF

5.4 Chapter Summary

A diagnosis of the application of travelling wave theory in microgrid protection using different signal processing tools was presented in the first part of the chapter. The minimum requirements for the choice of proper signal processing tools were given: they shall at least have good polarity detection and accurate time location. Considering these requirements, a new protection scheme based on the travelling wave theory has been proposed in this chapter. This scheme was based on time and polarity information of the traveling waves with only moderate communication requirements, delivering dependable and secure performance under different system topologies and modes of operation. For a radial microgrid with both end measurements available, a very simple algorithm of the protection can be applicable which is only based on the polarity comparison of the fault transients from both ends

of the line. For a meshed network, or a network consisting of some lines with only single-end measurement, additional logics named as wider-area time comparer and local bus polarity comparer included in the protection scheme can provide promising performance.

The signal processing tools applicable to the proposed protection schemes have been investigated in-depth. According to the literature review in Chapter 3, two existing popular processing tools for the signals covering large bandwidth of frequency, typically the power system fault imposed transients, are DWT and MM. Therefore in this chapter both of the tools were analysed in a network at distribution level. To the author's knowledge this is the first time MM analysis has been applied in distribution network protection. Based on the transient simulation in PSCAD/EMTDC, it was found out that the poor polarity detection and inconsistent time position of the fault through levels of decomposition are the critical drawbacks which intrinsically degrade the feasibility of the DWT based microgrid protection. Moreover, further investigation on the signal denoising performance confirmed high computational burden of the DWT method when conducting multi-level decomposition (in this thesis four-level decomposition was used).

MM introduced with the author's modifications in this chapter was found to be a better alternative. This technique was verified to be effective on both polarity detection and time location of the faults. Its polarity detection is achieved by modifying the traditional DEDF, by utilizing the apparent features of dilation and erosion signals. Moreover, the processing time used by MM was found to be 25%-30% shorter than the DWT method (based on Matlab analysis). In signal denoising area, OCCOMF is verified to be the best noise reduction MMF and therefore was chosen to be used in the proposed protection scheme. The multi-resolution MMF technique was applied to enhance the performance of the noise reduction. It has to be noted that the denoising performance is critically associated with the sensitivity of the protection scheme which will be systemically assessed in Chapter 6.

5.5 Chapter References

[1] Xinzhou Dong, Wei Kong, and Tao Cui, "Fault Classification and Faulted-Phase Selection Based on the Initial Current Traveling Wave," IEEE Transactions on Power Delivery, vol. 24, no. 2, pp. 552–559, Apr. 2009.

[2] X. Li, A. Dyśko, and G. Burt, "Enhanced protection for inverter dominated microgrid using transient fault information," in Managing the Change, 11th IET International Conference on Developments in Power System Protection (DPSP 2012), Birmingham, UK, 2012.

[3] C. Fan, K. K. Li, W. L. Chan, and W. Yu, "Study of protection scheme for transmission line based on wavelet transient energy," International Journal of Electrical Power & Energy Systems, vol. 28, no. 7, pp. 459–470, Sep. 2006.

[4] Xinzhou Dong, Yaozhong Ge, and Jiali He, "Surge impedance relay," IEEE Transactions on Power Delivery, vol. 20, no. 2, pp. 1247– 1256, Apr. 2005.

[5] L. Jie, S. Elangovan, and J. B. X. Devotta, "Adaptive travelling wave protection algorithm using two correlation functions," Power Delivery, IEEE Transactions on, vol. 14, no. 1, pp. 126 –131, Jan. 1999.

[6] S. Mallat and W. L. Hwang, "Singularity detection and processing with wavelets," Information Theory, IEEE Transactions on, vol. 38, no. 2, pp. 617 – 643, Mar. 1992.

[7] Feng Liang and B. Jeyasurya, "Transmission line distance protection using wavelet transform algorithm," IEEE Transactions on Power Delivery, vol. 19, no. 2, pp. 545– 553, Apr. 2004.

[8] B. N. Singh and A. K. Tiwari, "Optimal selection of wavelet basis function applied to ECG signal denoising," Digital Signal Processing, vol. 16, no. 3, pp. 275–287, 2006.

[9] C. Aguilera, E. Orduna, and G. Ratta, "Adaptive noncommunication protection based on traveling waves and impedance relay," IEEE Transactions on Power Delivery, vol. 21, no. 3, pp. 1154–1162, Jul. 2006.

[10] A. T. Johns, R. K. Aggarwal, and Z. Q. Bo, "Non-unit protection technique for EHV transmission systems based on fault-generated noise. Part 1: signal measurement," Generation, Transmission and Distribution, IEE Proceedings-, vol. 141, no. 2, pp. 133–140, Mar. 1994.

[11] Wei Chen, O. P. Malik, Xianggen Yin, Deshu Chen, and Zhe Zhang, "Study of wavelet-based ultra high speed directional transmission line protection," IEEE Transactions on Power Delivery, vol. 18, no. 4, pp. 1134– 1139, Oct. 2003.

[12] P. Jafarian and M. Sanaye-Pasand, “A Traveling-Wave-Based Protection Technique Using Wavelet/PCA Analysis,” IEEE Transactions on Power Delivery, vol. 25, no. 2, pp. 588–599, Apr. 2010.

[13] Z. Chen, Z. Q. Bo, Xiang-ning Lin, and B. R. . Caunce, “Integrated line and busbar protection scheme based on wavelet analysis of fault generated transient current signals,” in 2004 International Conference on Power System Technology, 2004. PowerCon 2004, 2004, vol. 1, pp. 396– 401 Vol.1.

[14] Q. H. Wu, J. F. Zhang, and D. J. Zhang, “Ultra-high-speed directional protection of transmission lines using mathematical morphology,” IEEE Transactions on Power Delivery, vol. 18, no. 4, pp. 1127– 1133, Oct. 2003.

[15] L. Zou, P. Liu, and Q. Zhao, “Applications of multiresolution morphological analysis in ultra high speed protection of transmission line,” Generation, Transmission and Distribution, IEE Proceedings-, vol. 153, no. 5, pp. 515– 523, Sep. 2006.

[16] Mingyu Yang and Shuping Tan, “Research on an Ultra-High-Speed Protection Based on Multiresolution Morphological Gradient,” in International Conference on Power System Technology, 2006. PowerCon 2006, 2006, pp. 1–5.

[17] L. Zou, P. Liu, and Q. Zhao, “Mathematical morphology based phase selection scheme in digital relaying,” Generation, Transmission and Distribution, IEE Proceedings-, vol. 152, no. 2, pp. 157– 163, Mar. 2005.

[18] L. Zhang, J. Xu, J. Yang, D. Yang, and D. Wang, “Multiscale morphology analysis and its application to fault diagnosis,” Mechanical Systems and Signal Processing, vol. 22, no. 3, pp. 597–610, Apr. 2008.

[19] J. Goutsias and H. J. A. M. Heijmans, “Nonlinear multiresolution signal decomposition schemes. I. Morphological pyramids,” IEEE Transactions on Image Processing, vol. 9, no. 11, pp. 1862 –1876, Nov. 2000.

[20] H. J. A. M. Heijmans and J. Goutsias, “Nonlinear multiresolution signal decomposition schemes. II. Morphological wavelets,” IEEE Transactions on Image Processing, vol. 9, no. 11, pp. 1897 –1913, Nov. 2000.

6. Modelling, Simulation and Analysis – Fault Behaviour and Systematic Verification of the New Protection Scheme

6.1 Introduction

Chapter 5 has developed a new protection scheme using travelling wave theory and mathematical morphology technique. It becomes necessary in this chapter to evaluate the proposed scheme in the simulated multi-IIG based microgrid system as presented in Section 4.5., particularly considering the actual fault behaviour from IIGs under the enhanced decentralized control. It has been pointed out in [1] that the IIG's fault behaviour is closely related to its control method, reference frame and design of current limiter . Therefore it is of significance of testing the fault behaviour under the new control before applying the systematic protection study.

A systematic study of the proposed protection scheme helps establishing a clear view of the collaboration between local and central IEDs. Firstly the protection scheme is tested at three different fault locations denoted as FLT1, FLT2 and FLT3 in Figure 6-1, representing the external grid fault, regular internal fault and remote-end fault. The sensitivity performance of the protection scheme is quantified and analysed by conducting a number of tests considering the impact of fault inception angle, fault impedance, noise level and sampling frequency. In order to investigate the stability of the protection scheme, tests are conducted to evaluate the dynamic response of the protection scheme under step load change, operational mode transfer and circuit breaker switching effects.

The codes of the protection schemes are all written in Matlab. Results can then be transformed from pure data to easily understandable figures and diagrams in Matlab, helping to construct a clear scope of the performance of the proposed protection scheme.

6.2 System Configuration for the New Protection Scheme

CIGRE Task Force C6.04.02 established some benchmark models for study of integration of small-scale distributed energy resources and loads, connected through local microgrids [2]. The model used in this thesis is a MV microgrid model as presented in Figure 6-1, which is formed by a ring circuit connected with a radial line [3]. By opening and closing the circuit breaker between bus3 and bus5, this MV microgrid is able to run in either radial or meshed topology. In connection with four IIGs at bus2, bus4, bus6 and bus8, a multi IIG based microgrid is established, where loads at bus3 and bus7 can be configured as fixed impedance, fixed power or motor loads accordingly. The current instrument transformers at each branch is named by "IT + line nodes".

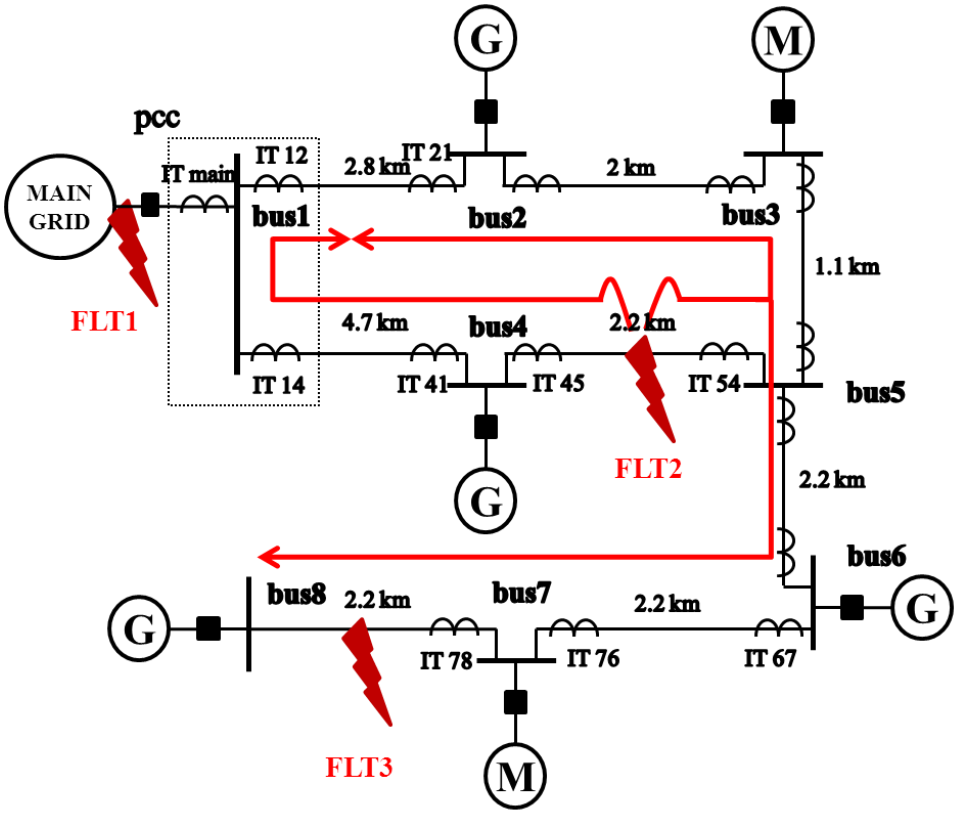

Figure 6-1: Single phase diagram of CIGRE 20kV benchmark microgrid system with three fault locations

The main grid source of the microgrid model is represented by a constant source with equivalent Thevenin impedance of 40.82 ohm. The operational voltage level is 20 kV.

The challenge is to find a close representation of a real cable that best depicts its response of high frequency transients. Since the simple π-model cannot represent accurate high frequency information, it is thus imperative to utilize the frequency dependent model making use of the geometric and material data. The most suitable model in PSCAD/EMTDC is the frequency dependent (Phase) model, which is able to represent well the frequency dependence of the distributed parameters over a wide range of frequencies [4]. Although this type of cable parameters in PSCAD/EMTDC is written based on the geometry and material property, there are still a few points missing in this model:

1) The real cable is consisted of many layers, including a semi-conducting layer screen, insulation screen, water seal, inner sheath, fillers, beddings, and outer cover. The PSCAD model, however, does not consider all these layers.
2) The dimensions of some of the layers are hard to obtain inherently, for example, the semi-conducting layer.
3) The core is always considered as a homogeneous solid conductor rather than the real one consisted of many strand conductors.

Therefore, in actual modelling of the underground cable, proper simplification of the original structure and dimensions of the cable is necessary. And in particular, the insulator and semiconducting layer are of significant influences upon velocity, surge impedance and the attenuation of the travelling waves [5]. Generally, there are two ways to achieve this in PSCAD/EMTDC: short-circuited method and add-to-insulation method [6-7]. Their principles are varied mainly due to the solution of the semi-conducting layer screen, which is normally wrapped around the conductor and insulation surface. The detailed calculation of the parameters of the cable model is presented in Appendix A.

6.3 Verification of the Low Fault Current Contribution from an IIG

It has been clearly stated in Section 3.3.1.3 that IIG has no inertia and can respond immediately to the faults by the associated voltage drop. Therefore, the fault current contribution from IIG is highly affected by the implemented control scheme which is built with current limiters. The current limiter at the input of the current controller of the IIG control system significantly restricts the fault current. As shown in Figure 6-2, based on the voltage and current controllers introduced in Chapter 4, a typical current limiting strategy in the rotating reference frame (RRF) is represented. The current limiting in dq coordinates is done by using two saturation blocks and limiting ${i_{id}}^*$ and ${i_{iq}}^*$ to two fixed values ${i_{satd}}^*$ and ${i_{satq}}^*$ as soon as the magnitude of the target inner current calculated from $\sqrt{({i_{id}}^*)^2 + ({i_{iq}}^*)^2}$ reaches the current limit I_{lim}.

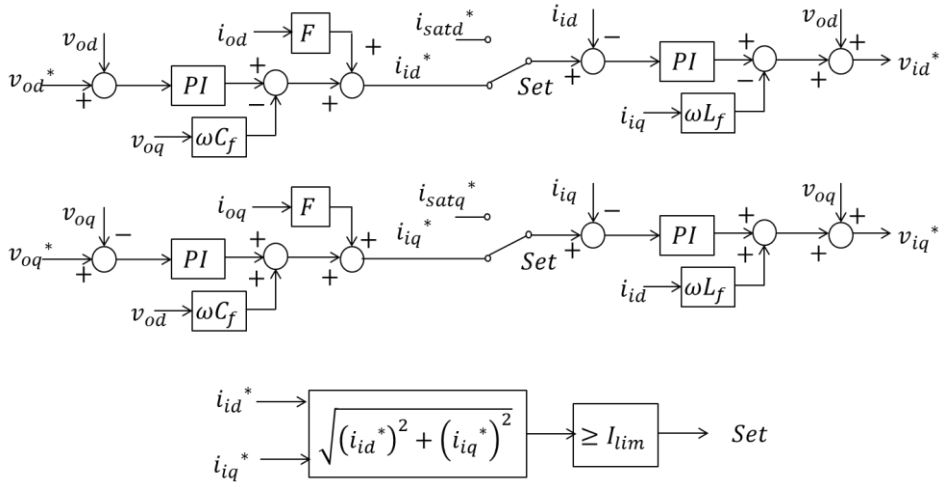

Figure 6-2: Fixed current limiter of the IIG

A case study of fault current behaviour under three main types of faults: three phase solid fault (ABC), inter-phase solid fault (AB) and single phase to ground solid fault (AG). A fault is applied to the FLT2 position, and the results from the nearest IIG2 are recorded in Figure 6-3. The fault resistance here is not considered in order to study the maximum fault current contribution from a single IIG. From Figure 6-3, the fault current level can be clearly observed to be comparable to the nominal current

during islanded operation. The single phase to ground fault cannot even reach the rated current level.

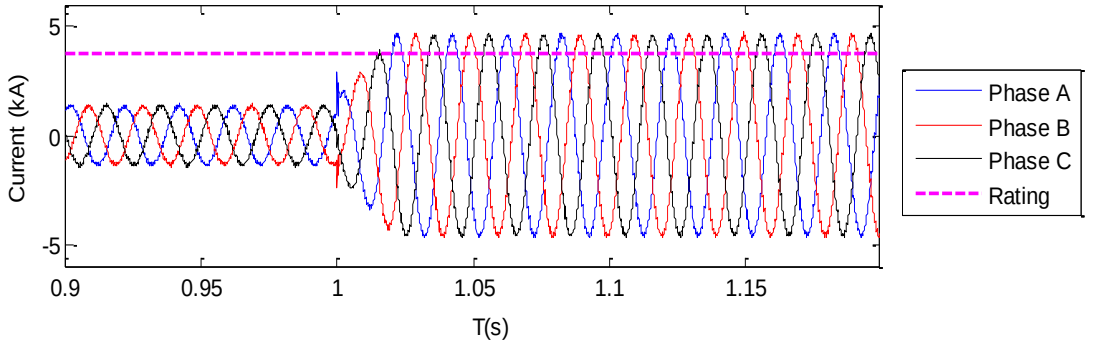

(a)

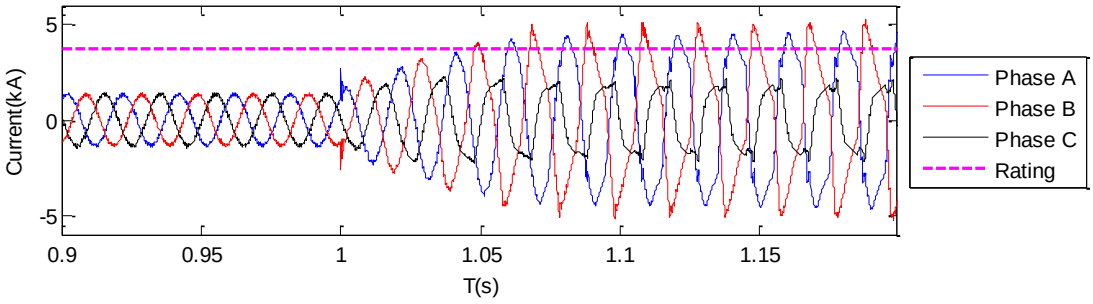

(b)

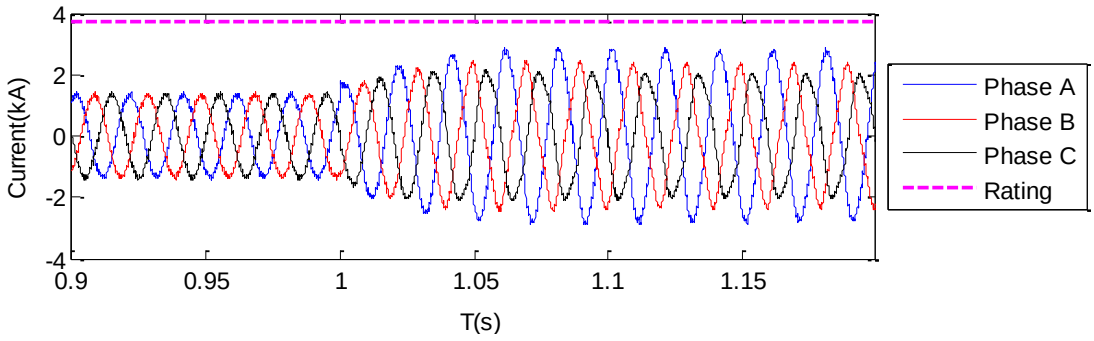

(c)

Figure 6-3: The fault behaviour of IIG under three different types of faults: (a) ABC fault; (b) AB fault; (c) AG fault.

6.4 Validation of the Performance of the Proposed Protection Scheme

As shown in Figure 6-1, three fault positions are studied to test the performance of the protection scheme: an external fault between the main grid and PCC of the microgrid (FLT1); an internal fault inside a ring circuit that may cause travelling wavefronts hitting each other in neighbouring lines (FLT2); and an internal fault at a radial downstream line with one end connection to the IIG (FLT3). Study under the second fault scenario is extended to provide more detailed studies of close-up faults, HIF and fault with low inception angle. The fault for all scenarios applied to the microgrid is single phase to ground fault, which is the dominant type of fault in distribution systems and microgrid systems. As there are normally no requirements for phase selection under this voltage level of system, this method is not a phase sensitive protection scheme. Other types of faults will provide similar results since the reflection and refraction of the travelling waves within the power system are the same regardless of the fault types. The algorithm will be conducted in each phase, and the phase with the indicator showing the highest amplitude is picked up as the objective phase in calculation. For example, if an AG fault occurs, the earliest indicators from phase A are observed to have the largest magnitude, and phase A is taken into concern for all the IEDs of the microgrid in practice.

6.4.1 CASE 1 – External Fault outside the Microgrid

In this section, an AG fault is applied to FLT1. FLT1 is a close-up external fault just at the output of the bus1. Throughout the microgrid, all the branches are equipped with IT. As shown in Figure 6-4, the disturbances and wavefronts can be easily detected at each IT. The polarities from all the IEDs are clear. For example, for IT12 or IT14, the polarity is detected to be negative, and the time stamp is 522.341ms. This time stamp from this bus can be recognized to be the earliest in the network, which implicates that the fault/disturbance should be located near bus 1. Based on the fact that ITmain detects the opposite polarity to IT12 and IT14, we can discriminate the fault from external main grid.

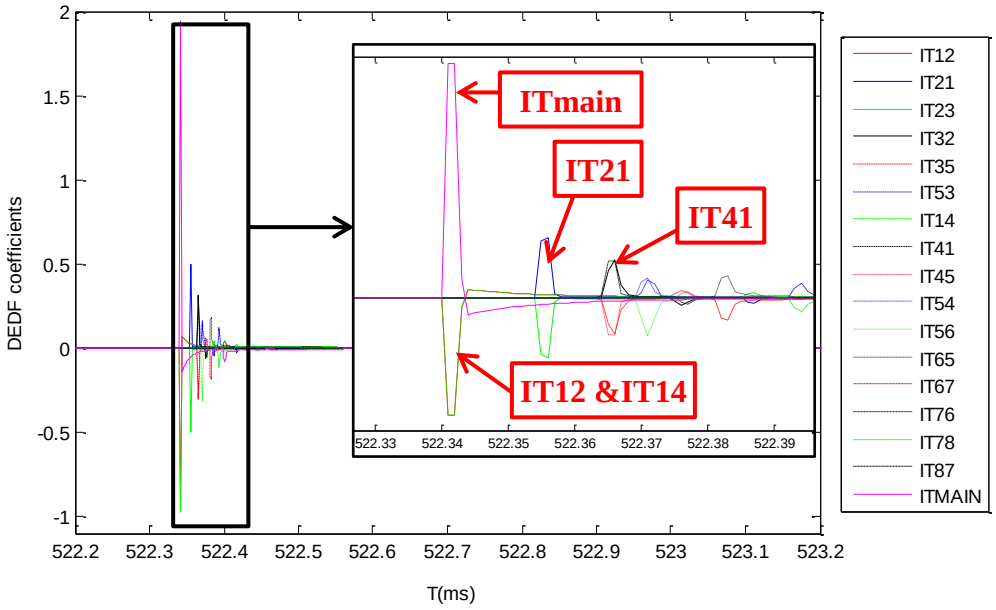

Figure 6-4: The detection of initial travelling wavefronts throughout the microgrid under CASE 1.

6.4.2 CASE 2 – Internal Fault in the Ring Network

In this section, the fault is applied to FLT2, the midpoint of the line 4-5. This fault location is within the ring part of the microgrid. The travelling waves flow via a route outlined as the red colour arrow in Figure 6-1. From the Figure 6-5, it can be clearly seen that the earliest travelling wavefronts are detected at Bus4 and Bus5 (t = 522.437ms). With the same polarity from IT45 and IT54, the fault can be easily discriminated at line45. It should be noticed that the algorithm merely based on detecting the double end polarity the same or not does not satisfy the protection in a ring network, since IT21 and IT12 also share the same polarity. In the later Section 6.5, more test scenarios will be conducted with the fault at FLT2, in order to investigate the sensitivity performance of the method with varied fault impedance, fault inception angle and modes of operation.

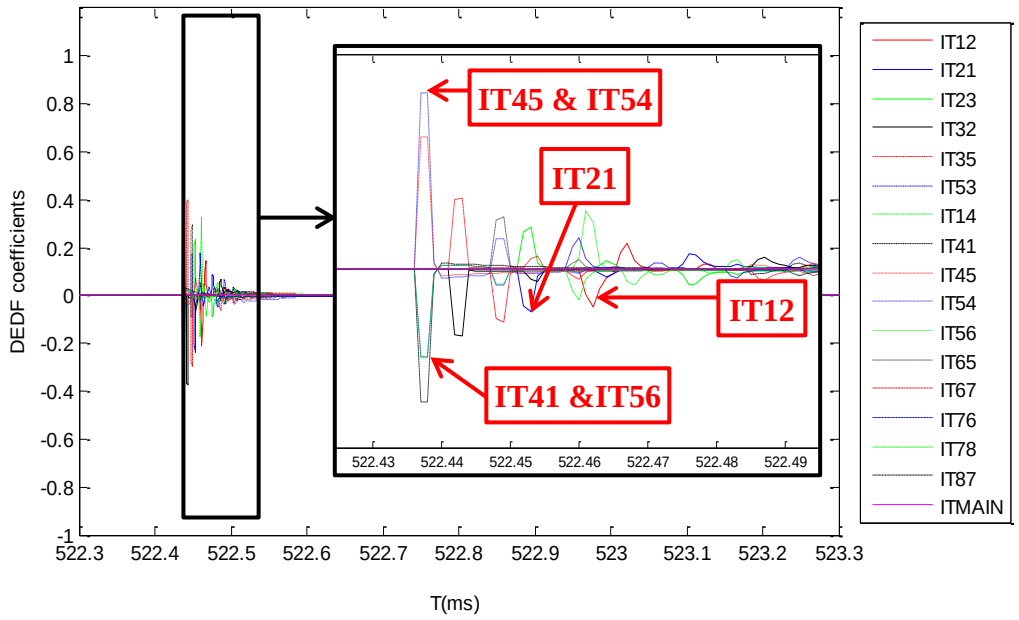

Figure 6-5: The detection of initial travelling wavefronts throughout the microgrid under CASE 2

6.4.3 CASE 3 – Internal Fault at a Line Equipped with Single-end Measurement

The third fault is applied to the line that is directly connected to an IIG at bus8. From the study of the boundary characteristics in Section 3.6.2, it is known that the IIG directly connected at bus 8 will smooth the current measurement which degrades the current travelling wave detection. As shown in Figure 6-6, IT87 does not detect any wavefronts. However, it can be easily recognized that the bus 7 is closest to the fault position since the wavefronts detected by IT78 and IT76 appear to be the earliest ones (t = 522.347ms). The obvious opposite polarities of IT67 and IT76 indicates that the fault is not at the line 6-7. Based on this, the fault can be distinguished to be at the line 7-8 or the IIG connected to bus 8.

In this case, the fault is not recognized by comparing the indicators from local bus, or by comparing the two-end polarities of the faulty line, since only one instrument is implemented at the faulty line. The faulty branch is actually discriminated by ruling out the chances of the fault occurring in the neighbouring lines.

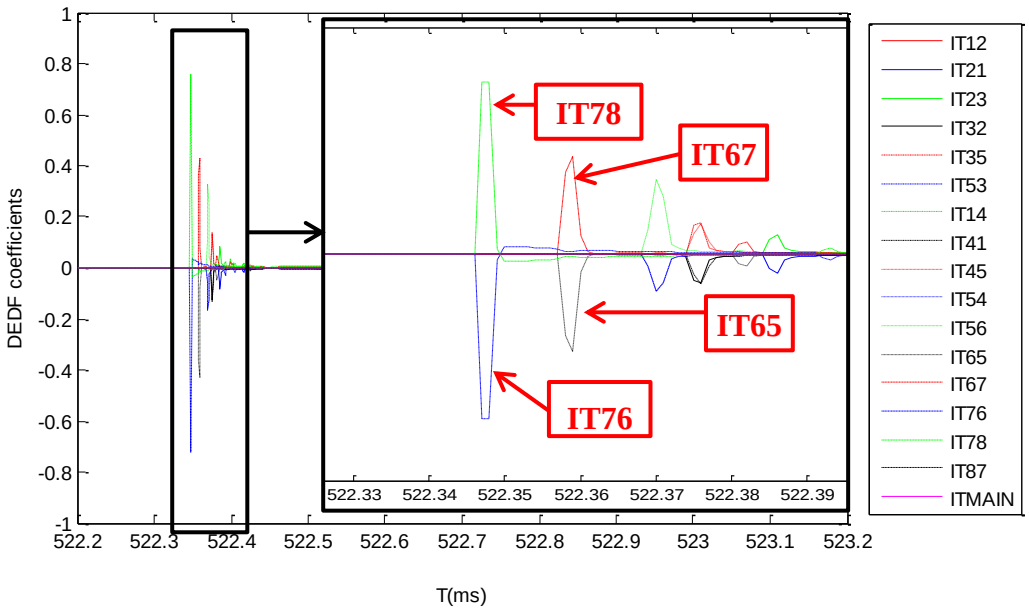

Figure 6-6: The detection of initial travelling wavefronts throughout the microgrid under CASE 3

All the time and polarity information recorded by the IEDs throughout the microgrid under the above three fault scenarios is listed in Table 6-1. The earliest detected wavefronts and their polarity information are highlighted in each case.

Table 6-1: Results Using MM Based Protection Scheme Under Different Fault Scenarios.

IT	FLT1			FLT2			FLT3		
	Polarity	**Time (ms)**	**Results**	**Polarity**	**Time (ms)**	**Results**	**Polarity**	**Time (ms)**	**Results**
Main	**+**	**522.341**	External System Fault	−	522.462	Internal fault at line 4-5	−	522.400	Internal fault at line 7-8
12	**−**	**522.341**		−	522.462		+	522.400	
21	+	522.356		−	522.453		−	522.386	
23	−	522.356		+	522.453		+	522.386	
32	+	522.366		−	522.443		−	522.376	
35	−	522.366		+	522.443		+	522.376	
53	−	522.371		−	522.437		−	522.371	
14	**−**	**522.341**		+	522.462		−	522.400	
41	+	522.366		−	**522.437**		−	522.382	
45	−	522.366		+	**522.437**		+	522.382	
54	+	522.371		+	**522.437**		−	522.371	
56	−	522.371		−	**522.437**		+	522.371	

65	+	522.383		+	522.449		−	522.359	
67	−	522.383		−	522.449		+	522.359	
76	+	522.394		+	522.460		−	**522.347**	
78	−	522.394		−	522.460		+	**522.347**	

6.5 Validation of the Sensitivity and Stability

To verify the proposed protection scheme, both sensitivity and stability were taken into account. The sensitivity case studies consider the impact of fault inception angle, fault impedance, fault location, noise level, earthing system and sampling frequency; stability case studies include the transient response of the protection scheme to load transients, operational mode transfer and switching effects.

6.5.1 Impact of Fault Inception Angle and Fault Resistance

Although the MM based primary protection only utilizes the time and polarity information of the initial traveling wavefronts, the magnitude of the travelling wavefront is compared against a fixed threshold to get an initiating trigger for this protection algorithm. Hence the magnitude of the travelling wavefront is also a significant factor for evaluating the protection sensitivity. Actually the magnitude of the wavefront may vary with the changes of the fault inception angle, line impedance and fault impedance. In order to test the dependence of the peak value of the wavefront detected on different fault inception angles and fault resistances, the CASE 2 fault scenario is applied to line 4-5. The results are shown in Figure 6-7 (islanded operation) and in Figure 6-8 (grid-connected operation). The threshold was set to 0.01kA ($\approx$ 20% of the rated current). In practice, this threshold can be adaptive to the actual signal magnitude level, which is actually a critical enhancement under noisy condition as discussed in Section 6.5.4. The fault is applied at the midpoint of line 4-5 (under the FLT2 scenario), with fault impedance varying between 0.01ohm and 50ohm and point on wave (POW) of the fault inception between $0°$ and $90°$. Although not possible to appreciate this from visual inspection it was established that the initial traveling wavefronts are all valid with the POW as low as $5°$ regardless of the fault resistance. To help illustrate this point a small section of the graph was magnified in Figure 6-7 and Figure 6-8.

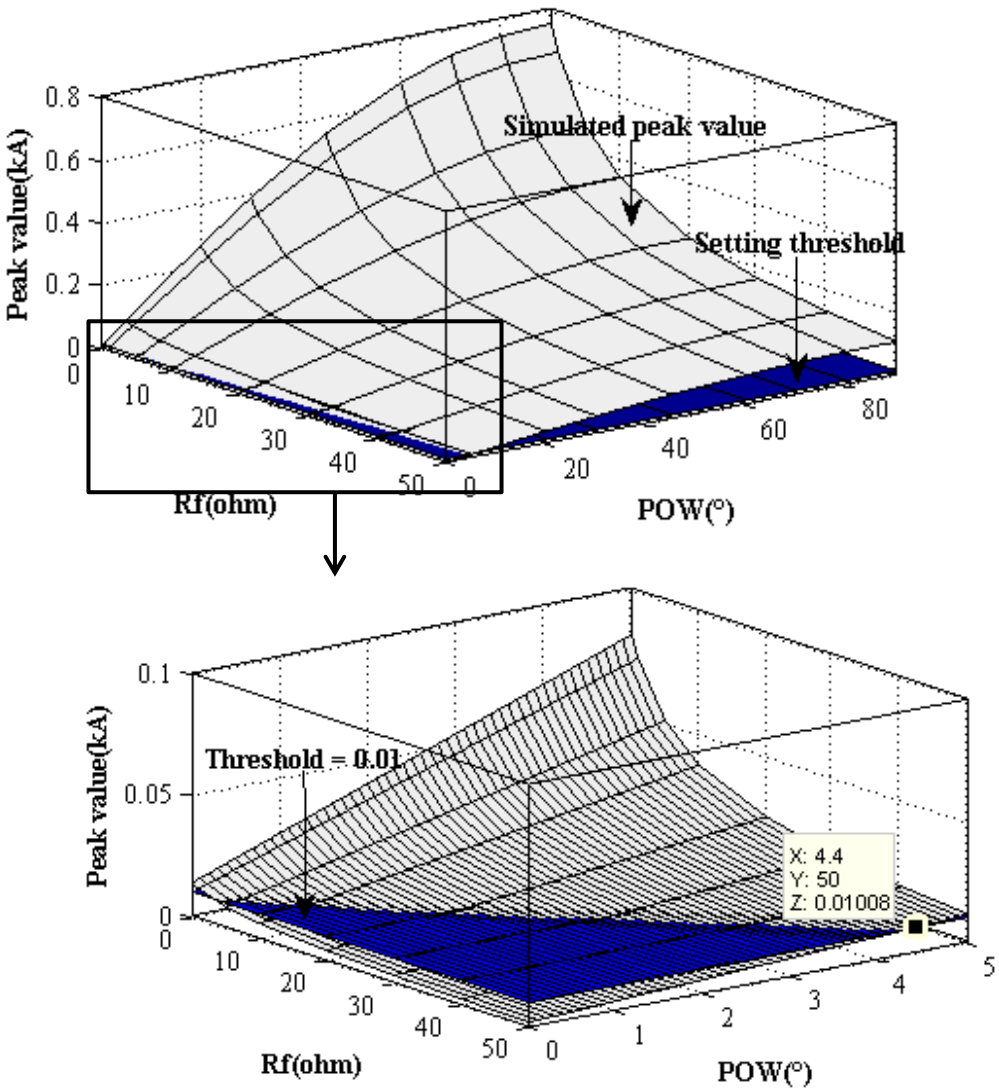

Figure 6-7: Peak value of the traveling wavefront according to different fault impedances and fault inception angles (islanded operation)

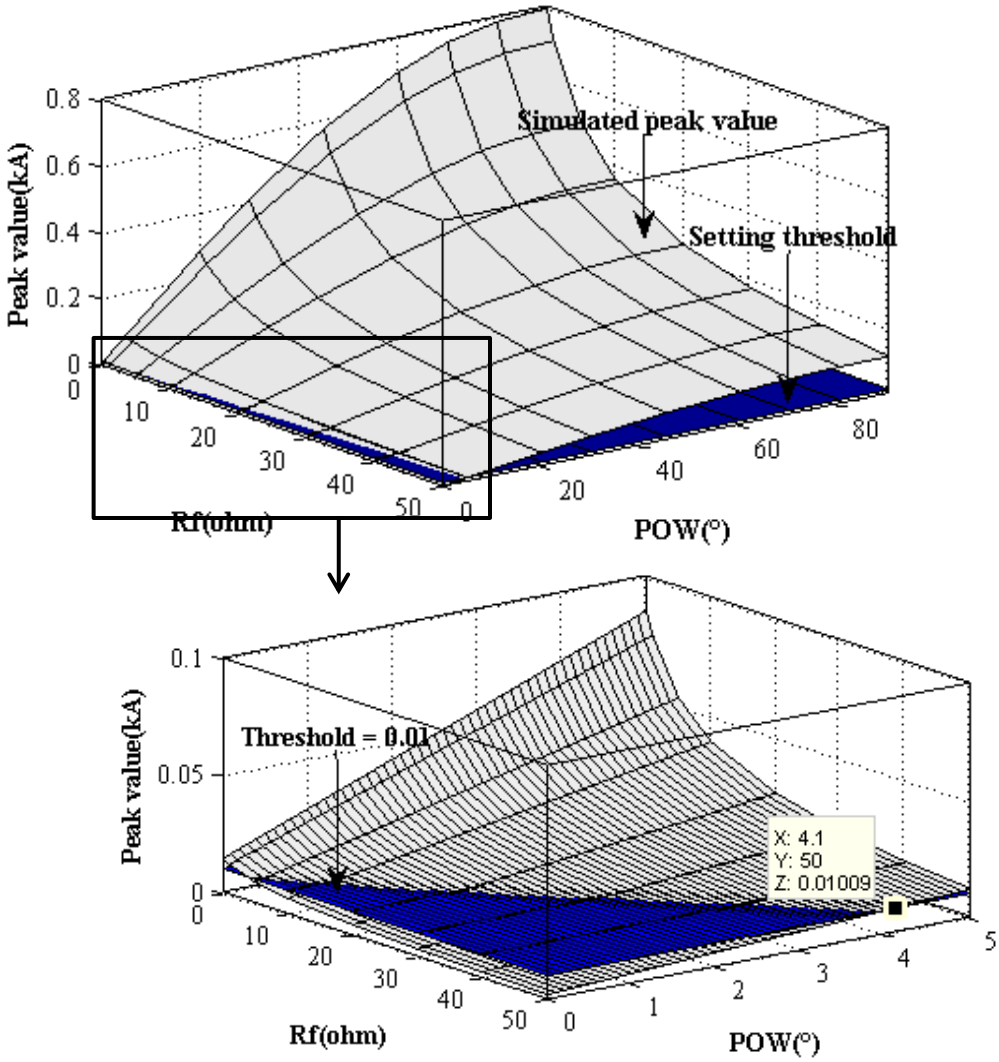

Figure 6-8: Peak value of the traveling wavefront according to different fault impedances and fault inception angles (grid connected operation).

6.5.2 Impact of Sampling Frequency

One key algorithm of the new protection scheme is the time discrimination between the wavefronts arriving at different units. This is closely related to the sampling frequency, the speed of traveling wave, and distance (cable length) between the units. After knowing the parameters of the cable, the speed of the traveling wave μ can be obtained. The requirement for the largest sampling time step T_s as a function of electrical distance $Distance$ between two units is presented in (6-1).

$$T_s = \frac{1}{f_s} < T_c = \frac{k_{safe} \cdot Distance}{\mu} \tag{6-1}$$

where f_s is the sampling frequency, T_c is the traveling time along the length of the cable, and k_{safe} is the safety factor ranging from 0.5~0.9 to ensure time discrimination of wavefront arrivals between two ends of a shortest line.

A case study is conducted by applying a solid fault with POW of 90 ° to the line 4-5 (under FLT 2 scenario). According to the basic principles of the proposed protections scheme, to isolate the healthy zone (i.e. bus 3), it is necessary to detect a time difference between bus 3 and bus 5. As the line 3-5 is the shortest neighbouring line with length of 1.1km, the capability of detecting a time difference between IT54 and IT35 is closely related with the sampling frequency of the current instrument. Figure 6-9 presents the extracted travelling waves measured from IT54 and IT35 under different sampling frequencies ranging from 100kHz to 1MHz. It can be seen from the figure that with increase of the sampling frequency, the time difference between IT54 and IT35 becomes clearer to be observed. When the sampling frequency is lower below 100kHz, the time deviation for a 1.1km cable is no longer sufficient for discrimination of fault location. It has to be noted that, the requirement of the sampling frequency is quite lower than the traditional travelling wave based methods, which utilize the time intervals to calculate the exact the fault location. This protection scheme is not dependent on the time intervals, but the time deviation between buses. It is only limited by the whole length of the cable/line, since the polarity is always able to be detected correctly regardless of the closeness of the fault.

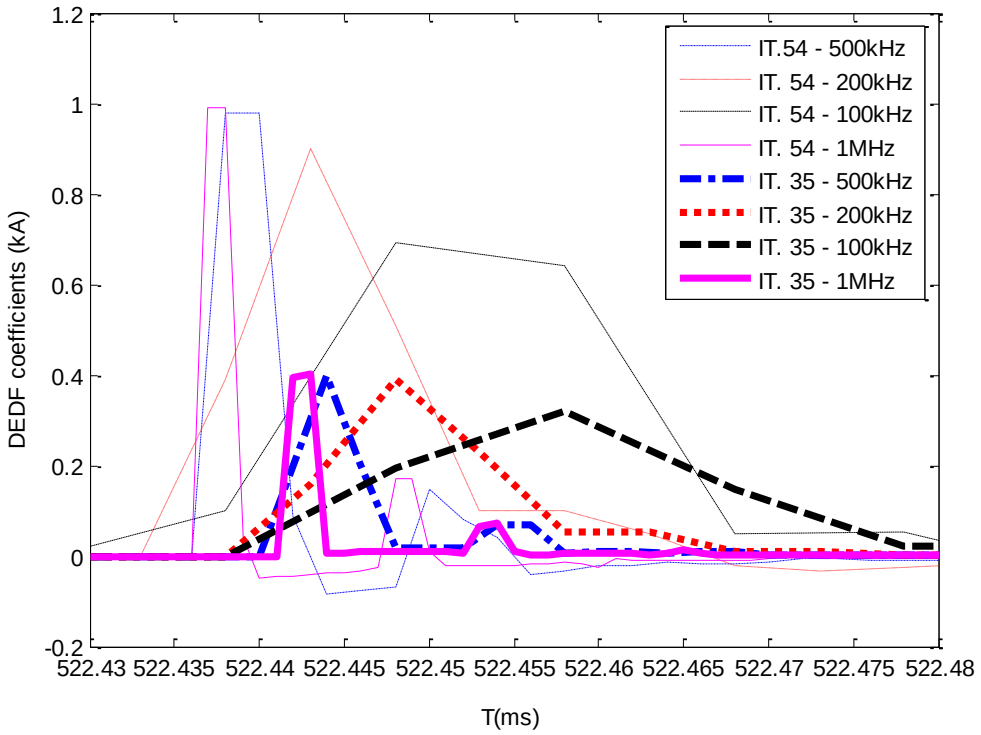

Figure 6-9: Time and polarity information of the extracted initial wavefronts from IT54 and IT35 with different sampling frequencies

6.5.3 Impact of Earthing Arrangement

Earthing point, either solid earthed or earthed through impedance, as discussed in Chapter 3, might bring great difference on the reflection factor of the current travelling waves. This section is dedicated to provide a systematic view of this issue and set the basic rule or restriction on the application of this method.

The earthing system plays an important role in defining the traveling wave routes. If the fault occurs close to a solid earthing point, the traveling wave generated by an earth fault cannot easily propagate through the earthing point to the adjacent circuits. To demonstrate this, the same fault at FLT1 is applied in the main grid, while a Y-ground-Y-ground transformer is installed between the main grid and the microgrid in this case. Figure 6-10 shows a diagram with this installation applied by a main-grid fault with POW of 90 ° close to the PCC. This external fault is expected to be

discriminated by the microgrid protection. However, results in Table 6-2, clearly demonstrate that the wavefronts are below the threshold of peak detection. The traveling wavefronts are significantly damped by the earthing point. Nevertheless, according to the typical earthing arrangements in Engineering Recommendation G59/2 [8], earthing of DER sources should not bring contradiction against the earthing system of main grid. In most existing MV microgrids, when running in the grid-connected mode, the earthing within the microgrid needs to be disabled. For this reason it seems that the arrangement of the earthing system will not affect the sensitivity of the protection scheme.

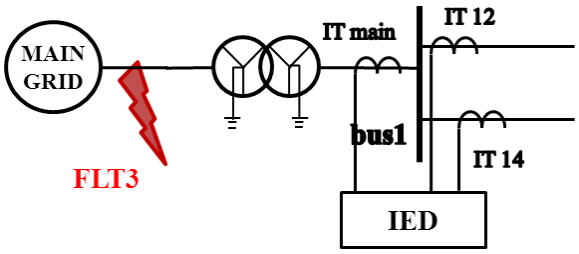

Figure 6-10: The PCC implemented with a Y-G-Y-G interface transformer.

Table 6-2: Results of a main-grid fault with POW = 90 °and a Yg-Yg interface transformer between microgrid and main grid.

Fault location	IT No.	Polarity (±1)	magnitude (kA)
FLT3	IT12	−1	0.013
	IT21	N/A	0.008
	IT14	−1	0.013
	IT41	N/A	0.006
	ITmain	1	0.026

6.5.4 Impact of Signal Noise

If the travelling waves contain noises, the sensitivity of the proposed protection scheme might be affected. In this section the current measurements from IT45 during fault at FLT2 are mingled with noises which have Signal-to-Noise Ratio (SNR) ranging from 40dB to 10dB. The corresponding performance of the protection scheme is presented in Figure 6-11. From this figure, it shows the noisy signal with up to SNR 10dB can still be processed with clear travelling wavefront sign and time location, however requiring slightly higher sensitivity threshold for peak detection. This could bring a sensitivity issue when the fault is happening with a very low fault inception angle, as shown in Figure 6-12 (d). A search through a short window for the maxima modulus can be one of the enhanced solutions. Normally as far as the feature of the initial wavefronts hasn't been overwhelmed by the noises, the transient feature can be extracted correctly.

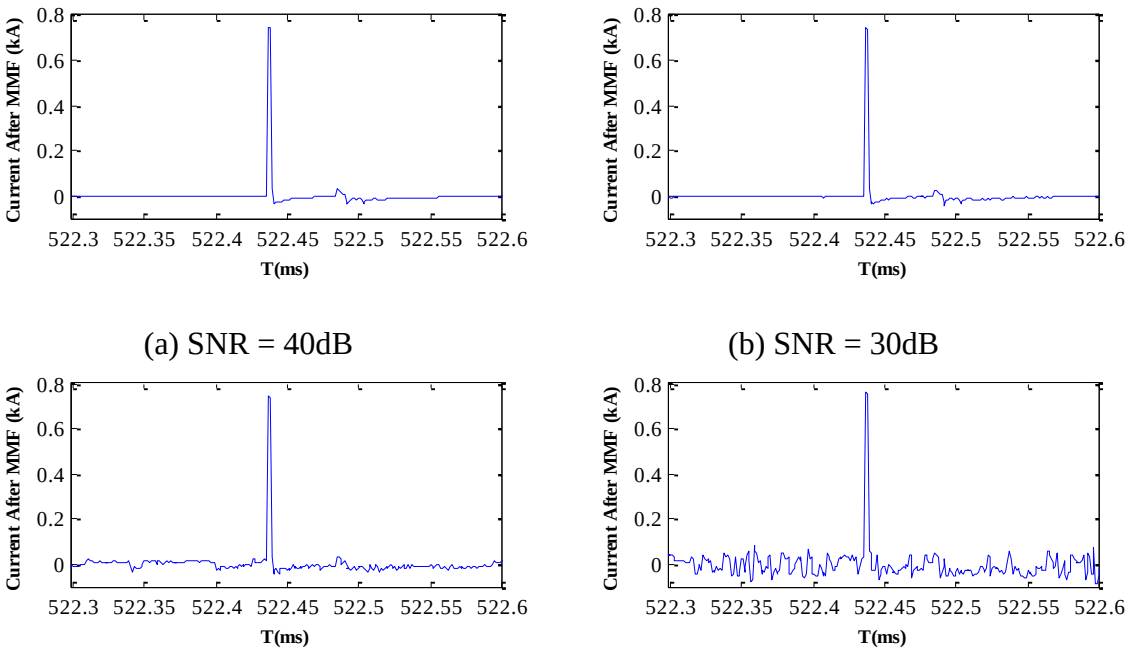

(a) SNR = 40dB

(b) SNR = 30dB

(c) SNR = 20dB

(d) SNR = 10dB

Figure 6-11: Detection of wavefronts after OCCOMF based noise-reduction (POW = 90˚)

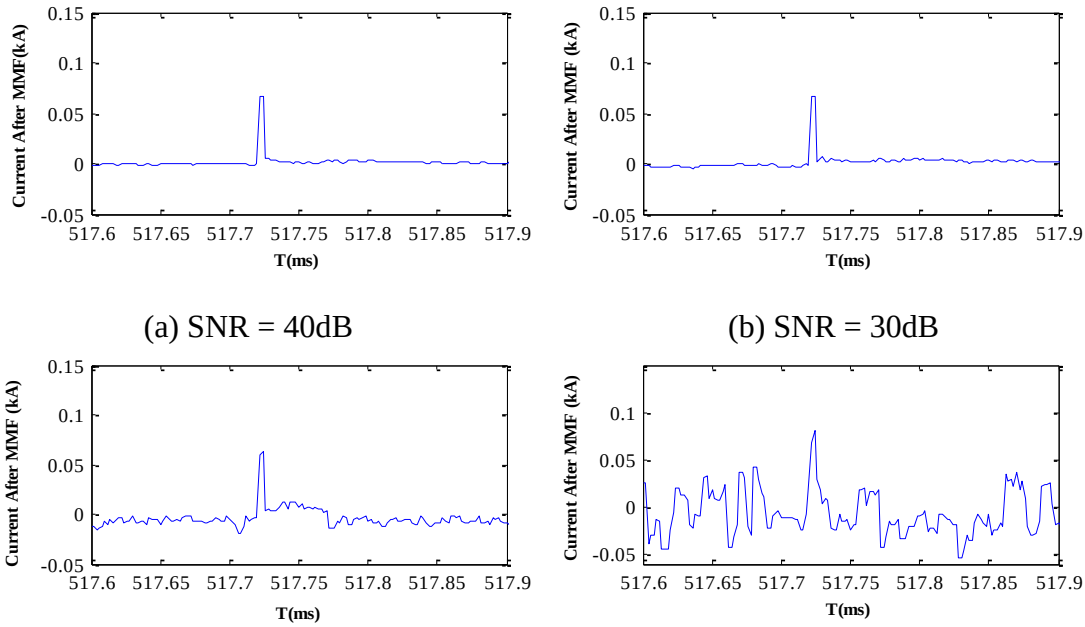

(a) SNR = 40dB

(b) SNR = 30dB

(c) SNR = 20dB

(d) SNR = 10dB

Figure 6-12: Detection of wavefronts after OCCOMF based noise-reduction (POW = 5°)

6.5.5 Stability under Non-fault Transient Disturbances

As stated above, the non-fault disturbances in the microgrid include load induced transients (i.e. motor-starting), transients during transition of the system operational modes (islanded ↔ grid connected), change of system topology, etc. The test results under these scenarios are presented in Figure 6-13. From the figure it can be clearly seen that due to the applied initial threshold of 0.01kA, the MM based main protection scheme presents no detectable response to these transients. Hence it can be concluded that the proposed scheme shows good stability in response to all simulated non-fault disturbances.

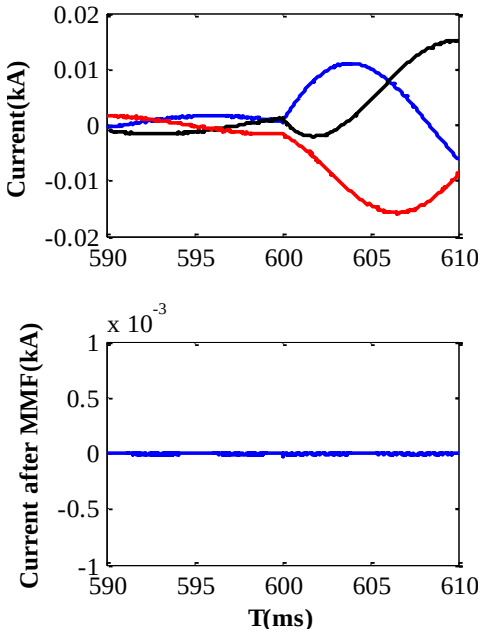

(a) Motor starting

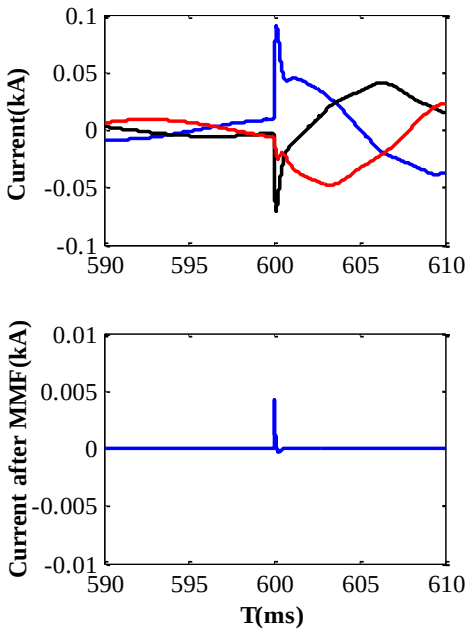

(b) Islanded to Grid-connected Transition

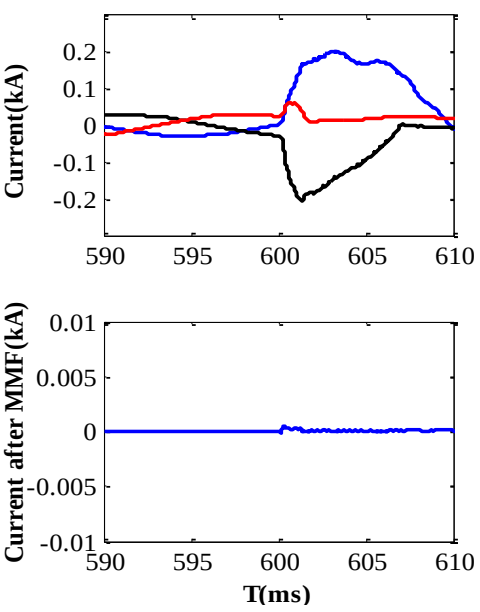

(c) Grid-connected to Islanded Transition

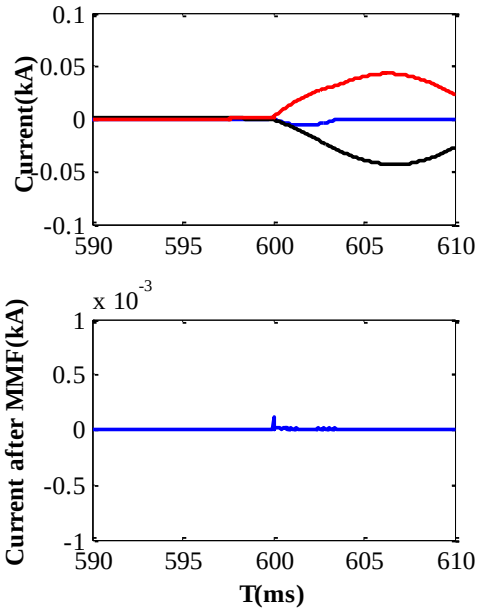

(d) Topology Change

Figure 6-13: The responses of MM based protection scheme to non-fault system disturbances

6.5.6 Performance under Connection with Synchronous Machine

The presented systematic performance assessment of the presented method demonstrates the practical application potential of this approach in microgrid applications regardless of the inverter characteristics. In fact, the method can actually be applied in microgrids integrating other types of distributed sources, since it is purely based on the fault generated transients. The following figure presents the results of a fault applied to the feeder fed by an IIG and a synchronous generator. As it can be seen, even though the fault response is drastically different, both the shape and magnitude of the indicator obtained from MM based algorithm are identical for both generators.

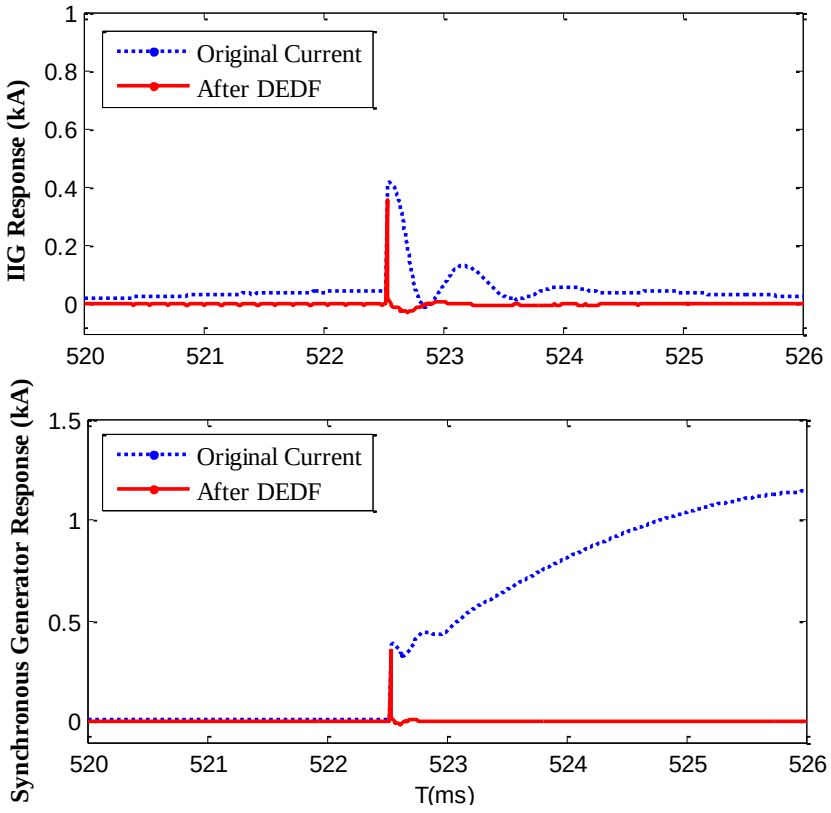

Figure 6-14: The responses of MM based protection scheme under Connection with Synchronous Machine

6.6 Potential Hardware Implementation

Although traveling wave based methods have been proposed for HV transmission system protection for more than twenty years, the practical implementation has been inhibited mainly by the limitations of signal processing hardware. A MM based signal processing algorithm, which only contains addition and subtraction operations within a numerical window of 3~12 samples, provides a promising approach for implementing the traveling wave based protection in modern power systems. Furthermore, communication channels are becoming increasingly more common in distribution grids, which can also satisfy the very moderate bandwidth requirements of the proposed protection scheme.

Despite many obvious advantages, high frequency sampling and accurate signal synchronization are still needed. As discussed in section IV.C, the sampling frequency for the MV benchmark microgrid needs to be in excess of 256kHz ($f_s = \frac{\mu}{k_s \cdot Distance} = \frac{2.25e5}{0.8 \times 1.1} \approx 256\text{kHz}$), which can be considered achievable by modern acquisition hardware. GPS based synchronization is taken into account in this paper, although a cheaper alternative such as the ping-pong algorithm may also be applied [9]. The errors in latency estimation can be compensated by scaling the safety factor k_s, which will be studied in the future.

Additionally, Rogowski coil or Hall Effect based current instruments should be considered as they are capable of covering wide frequency bandwidth, and are typically used in traveling wave applications. Hi-pass filters should be used to remove low frequency components and sample-and-hold elements to maintain synchronous sampling of all phases.

6.7 Chapter Summary

In this chapter, the IIG fault model has been developed based on the hard limiters at the input of the current control loop. The low fault current contribution from IIG was verified by applying AG, AB and ABC three types of solid faults at the terminal of the established IIG model.

This chapter conducted a systematic study of the proposed MM based protection scheme. The performance of this protection scheme was tested under three fault scenarios, including the external grid fault, the internal fault at the midpoint of the line within the microgrid and the fault at the line implemented with only one end measurement. Using transient simulation in PSCAD/EMTDC, the new protection scheme has been proven capable of accurately locating the fault with POW as low as 5 ° regardless of the fault resistance and system fault level. It was also confirmed that this protection scheme is effective under noisy conditions with SNR up to 10dB. Moreover, the stability of the proposed scheme has been verified under non-fault disturbances such as motor starting, operational mode transfer and topology changes. Through discussion of hardware requirements of the protection scheme, it has been considered as practically applicable and economically viable.

6.8 Chapter References

[1] M. Brucoli, T. C. Green, and J. D. F. McDonald, "Modelling and Analysis of Fault Behaviour of Inverter Microgrids to Aid Future Fault Detection," in IEEE International Conference on System of Systems Engineering, 2007. SoSE '07, 2007, pp. 1–6.

[2] K. Strunz, "Developing benchmark models for studying the integration of distributed energy resources," in IEEE Power Engineering Society General Meeting, 2006, 0-0 0.

[3] N. El Halabi, M. Garc á-Gracia, J. Borroy, and J. L. Villa, "Current phase comparison pilot scheme for distributed generation networks protection," Appl. Energy, vol. 88, no. 12, pp. 4563–4569, Dec. 2011.

[4] PSCAD, "PSCAD Users Guide v4.2.1," 2006.

[5] K. Steinbrich, "Influence of Semiconducting Layers on the Attenuation Behaviour of Single-core Power Cables," Gener. Transm. Distrib. IEE Proc.-, vol. 152, no. 2, pp. 271–276, Mar. 2005.

[6] A. Ametani, Y. Miyamoto, and N. Nagaoka, "Semiconducting Layer Impedance and Its Effect on Cable Wave-propagation and Transient Characteristics," IEEE Trans. Power Deliv., vol. 19, no. 4, pp. 1523–1531, Oct. 2004.

[7] B. Gustavsen, J. A. Martinez, and D. Durbak, “Parameter Determination for Modeling System Transients-Part II: Insulated Cables,” IEEE Trans. Power Deliv., vol. 20, no. 3, pp. 2045–2050, Jul. 2005.

[8] Energy Networks Association, “ER G59/2: Recommendations for the Connection of Generating Plant to the Distribution Systems of Licensed Distribution Network Operators,” 2010.

[9] D. Xie and J. Peng, “An Research of Ping-Pong Clock Synchronization Based on Quantum Optics,” in 2010 Symposium on Photonics and Optoelectronic (SOPO), 2010, pp. 1 –4.

7. Conclusions

7.1 Conclusions and Contributions

Microgrid, one of the existing well-known networks of integrating various distributed energy resources into an AC power system, is the objective network of the overall thesis. A widely accepted definition of a microgrid is a self-controlled entity integrating small scale distributed energy resources (DER) under distribution voltage level, which are designed to operate semi-independently: usually grid connected but can be islanded in case of emergency. As the number of inverter-interfaced generators (IIG) increases and the operation of an islanded microgrid is possible, it is of significance to develop advanced control and protection schemes – bearing in mind that traditional control and protection techniques do not support reliable islanded multi-inverter operation. It is also to be noted that the IIG's low fault current contribution undermines the feasibility of the traditional overcurrent protection at distribution level. One of the major objectives of this thesis is to establish a flexible microgrid which can present itself to utility grid as a self-controlled unit: both control and protection systems can satisfy different modes of operation, load and DER configurations.

Two major contributions have been established by this thesis. Firstly, an enhanced decentralized inverter control scheme predominantly dependent on local measurements only was developed for a MV microgrid system incorporating multi IIGs considering significant interconnection impedances, which include connecting line impedance and output impedance of each IIG. Moderate wireless communication is only required when the microgrid is trying to disconnect or reconnect with the utility for transmitting the grid-synchronization signal for each IIG, and for the tertiary control providing power demand settings in order to guarantee an accurate power sharing performance among the generators. A hierarchical control strategy is therefore established with focus on the primary control for IIGs. Secondly a new communication assisted travelling wave based

protection scheme was presented with the development of enhanced signal processing tool – modified Mathematical Morphology (MM) technology. A new technique of signal polarity detection using MM is achieved using the apparent features from dilation and erosion waveforms. Several different Mathematical Morphological Filters (MMFs) were employed and modified for both accurate extractions of the high frequency travelling waves and proper noise-reduction of power system measurements. Based on the transient simulation in PSCAD/EMTDC using a CIGRE benchmark microgrid model, this approach is proven to be fast, efficient and reliable.

7.1.1 Development of an Enhanced Control Scheme for Multi-IIG Based System

To accomplish the development of a proper control scheme for a microgrid integrated with a cluster of IIGs, a comprehensive system-level study of the requirements to be met and the potential scenarios has been carried out. The requirements to be met are driven by the concept of a flexible microgrid: good operational stability under change of system topologies and load conditions, consistent hardware control circuits for islanded and grid-connected modes of operation to prevent transient electrical spikes, and proper load sharing performance for energy consumption efficacy.

In order to meet these requirements, a major contribution of the thesis is the development and demonstration of a simple but effective decentralized control scheme for multi-IIG based system. Since this controller is developed based on one of the popular power targeted grid-connected controllers by directly delegating the d-axis component to control active power and q-axis component to control reactive power, the control switch for the operational mode transfer is thus avoided. A seamless mode transfer is achieved by updating the voltage and frequency references through low-bandwidth wireless communications. Since communication infrastructure is always needed for voltage resynchronization with the utility grid during mode transfer of a microgrid, this requirement of communication is not considered as an issue. In grid-connected operation, the controller operates as a repetitive controller with zero steady error at the power droop loop; and in islanded

operation, the controller operates as a nested controller responding to the droop loop. By simulation it was demonstrated that the mode-transfer transient takes less than 1s. And in comparison with the conventional droop control scheme, the oscillatory phenomenon during mode transfer and load step changes is avoided or significantly damped.

Another promising property of the new control scheme is its decentralized control characteristic: steady state operation of the multi-inverter based microgrid is maintained stable using only the local voltage and current measurements in both grid-connected mode and islanded mode. Power sharing accuracy in islanded mode of operation is guaranteed by not only implementing virtual impedance, but also using adaptive power references, which are automatically updated using a combined proportional and differential function of the IIG output voltage. In grid-connected mode, on the other hand, the energy manager as the secondary control can refresh the power references based on optimization calculation. This thesis recommends not activating virtual impedance function until 10% power sharing deviation between IIGs is detected. Although virtual impedance balances the load sharing performance of multi-IIGs, it is also found to have a negative impact on voltage regulation and the IIG's power exporting capacity to the extent dependent on the voltage droop coefficient.

As further highlighted in this thesis, the operational stability of the new control scheme is immune to varied output impedances of IIG and load dispatch, in contrast to the conventional droop based methods which are detrimentally affected by unequal IIG output impedances and unbalanced load dispatch. Circulating currents, the main reasons for operational instability in conventional droop controlled islanded microgrids, are minimized by implementing a clock-synchronized sine wave voltage reference generator in each IIG. Moreover, using this voltage reference generator, voltage regulation is significantly improved by reducing the voltage deviation among IIGs. A series of comparison case studies of the new control scheme and the conventional droop based control scheme, have validated the claims in this paragraph.

7.1.2 A Systematic Protection Scheme Based on Traveling Wave Theory Using Mathematical Morphology

The protection of the microgrid containing many IIGs is quite challenging due to its extremely limited fault current level (normally lower than twice of the rated current) during islanded mode. In order to develop such a protection scheme suitable for inverter based microgrid, detailed analysis of the state-of-the-art protection methods have been conducted to reveal the least requirements on protective principles: briefly, the proposed network protection scheme needs to be independent of the ratio of the fault current to the load current; and the protection scheme should be able to protect the network both in islanded and grid-connected mode. Considering the versatile configurations of application for academic interest, as well as aiming to avoid high bandwidth communication that is used in protection schemes at transmission system level, this thesis takes travelling wave based protection schemes. Advantages have been summarized throughout the review of the development in travelling wave based protection schemes, including fast and accurate fault discrimination, and feasibility for the microgrid regardless of the generation type, fault current level, the operational mode, the system topology or the load changes.

Following a deep analysis of the principles and application of travelling wave based protection scheme, application restrictions and challenges are found to be mainly due to its high sampling frequency requirements, computational burden and limited accuracy of signal processing tools.

To develop a protection algorithm with moderate sampling frequency requirements, careful search for the protection algorithms of utilizing the minimum amount of data has been completed in this thesis. As one of the major conclusions in this thesis, the double end method based on time and polarity information of initial travelling wavefronts is realized to be the best solution since it is only based on the initial wavefront detection, preventing the high demand of sampling rate for discriminating the corresponding reflected wavefronts that is required in the single end method based on the time intervals of a series of wavefronts. In the double end method, the faulty line is detected when the same polarity of the initial (earliest) travelling

wavefront from the both ends of the line is recorded. Thus, the basic required information for signal processing is the time and polarity of wavefronts from two ends. Moreover, based on the fact that voltage instrument transformers have much narrower frequency band than the current instrument transformers, protection scheme based on the current travelling waves is chosen. Hall-effect components or Rogowski coils are proposed for measuring the high frequency current signals.

A comprehensive study of the accuracy and computational requirements of different signal processing tools has been carried out, with the conclusion that discrete wavelet transform and mathematical morphology are two most potential options. Compared to these two, this thesis highlights the inherent deficiencies of inaccurate extraction of transient features of cross-correlation method and multi-channel bandpass filters. Continuous wavelet transform based method, on the other hand, is pointed out to be undesirable because of its complex continuous iterations in the algorithm.

Thorough investigation has been done on the widely-used and most popular signal processing tool of high frequency transients – DWT. With the demonstration using PSCAD/EMTDC simulation based on a simple two-end network in Chapter 5, this processing tool, also named as the wavelet filter is found to be ineffective on time location and polarity detection, due to its inherent deficiencies such as shift variant and lack of directionality.

In comparison, a comprehensive summarization of the advantageous features comparing MMF to the wavelet filters is completed in this thesis. Although traditional detail-extraction MMF doesn't appear to present polarity information, MMF's algorithm based on merely plus and minus functions is more attractive for practical protection implementation because of its light computational burden. DEDF, one of the major MMFs, is found to be effective in analysing nonlinear power system transient signals with better time location and shift invariance. Moreover, the nonlinear feature of this processing tool avoids the oscillating features induced by discrete wavelet transform.

In order to enable the DEDF to detect the polarity of the travelling wavefronts, this thesis creates a modified DEDF by utilizing the apparent features of the erosion and

dilation operations (two basic mathematical functions of mathematical morphology technique).

The SE, as defined as a probe to help extracting the shape feature of the processed signal, is an important component for design of a MMF based protection algorithm. In this thesis, the quantification of the length of the SE for the modified DEDF is achieved through exercises on a simulated ABB XPLE cable using frequency-dependent model in PSCAD/EMTDC library. It has been found out that the length of the flat SE as short as three nodes is able to minimize the calculation burden as well as maximize the sensitivity of initial wavefront detection. Besides, realizing that the power system fault transient is always in the wave shape of a quasi-step signal, the flat shape SE is used for best morphology performance.

Another promising feature of MMF has been found in noise-reduction performance. In order to find out the best noise-reduction MMF, three candidates have been compared in this thesis: DEMF, OCMF and OCCOMF. Through PSCAD/EMTDC simulation, the best solution is found to be OCCOMF, which supports the most accurate fault feature extraction. It has also been verified that the length of a flat SE with 30 nodes is sufficient for OCCOMF to eliminate the noise down to 20dB. In the thesis, a multi-resolution OCCOMF based on a series of OCCOMF processing is developed to improve the noise-reduction for analysing the noisy signal down to 10 dB.

Limitations of the fundamental protection algorithm are investigated under specific fault conditions. As an inherent issue of the travelling wave based method, the new protection algorithm lacks sensitivity in detecting faults with close-to-zero POW. The quantified limit of POW is 5° has been obtained based on PSCAD/EMTDC simulation with fault impedance up to 50ohms, fault distance up to 4.7km and 20kV XPLE cable resistance of 0.6969 ohm//km. It is established that the POW angle limit increases with fault impedance, distance to fault and the cable resistance. Although most of the faults occur at the POW near 90° (at the peak of the voltage), it is still mandatory to design a supplemental protection algorithm to eliminate the “non-detection zone”.

Hence, in addition to the creation and testing of the fundamental protection algorithm, a systematic protection strategy has been realized which involves additional protection algorithms for covering the fault "non-detection-zone" as well as effective fault discrimination in meshed networks with parallel lines and in networks containing feeders where only single-end measurement can be used. A supplemental protection algorithm based on combined Park-transformed voltage component and rate of change of the steady state current component, together with two additional protective elements belonging to the main protection algorithm, namely wide-area time stamp comparator and local-bus polarity comparator are introduced into the overall protection architecture.

The new protection strategy has been successfully implemented and tested in a CIGRE benchmark MV microgrid network containing multi IIG considering all potential scenarios. Through the simulations, it has been proven that 1) it is immune to different loading condition, operational modes and network topologies; 2) it has sufficient sensitivity and reliability to discriminate the internal faults, the external faults and non-fault disturbances. The protection scheme developed in this thesis primarily meets the specific needs of the protection of a multi-IIG based microgrid; nevertheless, it also works for a network containing other types of generators and loads, presenting good flexibility.

7.2 Future work

The microgrid model built in this thesis is based on IIG only, and can be expanded to include other types of generating technologies, such as synchronous machines. It can be predicted that some of the synchronous machines' controllers will interfere with the IIG controllers. Moreover, the DC side of the IIG models is simplified as a constant DC voltage source in this thesis, which only emulates the PV type of resources accompanied with storage. This model presents larger inertia and better dynamic stability compared to those who are not accompanied with storage support. The models considering the DC side dynamics are also in interest for better understanding of the behaviour both in control and protection mechanisms.

The protection scheme designed in this thesis is fit for a relatively large scale microgrid which contains cables/lines with length of at least hundreds of metres. Only the sampling frequency for this type of microgrid can be considered achievable by modern acquisition hardware. GPS based synchronization for time stamp was taken into account in this thesis, although a cheaper alternative such as the ping-pong algorithm may also be applied. The errors in latency estimation can be compensated by scaling the safety factor k_c (introduced in Chapter 5), which should be studied in the future.

In the benchmark microgrid the minimum sampling frequency requirement was assessed to be 265kHz, which can be considered achievable by modern acquisition hardware coupled with Rogowski coils or Hall-effect instruments. Therefore hardware requirements of the scheme have been considered as economically viable and future work will concentrate on the development of a laboratory prototype. However, the hardware requirement is still quite high since today's protection relays are based on sampling rate only around 10kHz, which implicates a need of hardware updates of the relay prototype. Besides, it is still desirable to develop a back-up solution which can operate in fully-decentralized mode without any communication assistance.

Appendix A: The parameters of the underground cable

Table 1: ABB 20kV XPLE cable data

Cross-section of conductor A_{cond}(mm2)	Diameter of conductor D_{cond}(mm)	Insulation thickness T_{insu}(mm)	Diameter over insulation D_{insu}(mm)	Cross-section of screen A_{screen} (mm2)	Outer diameter of cable D_{tot}(mm)
300	20.4	5.5	33.0	35	42.0

The geometry of the cable model is presented as below:

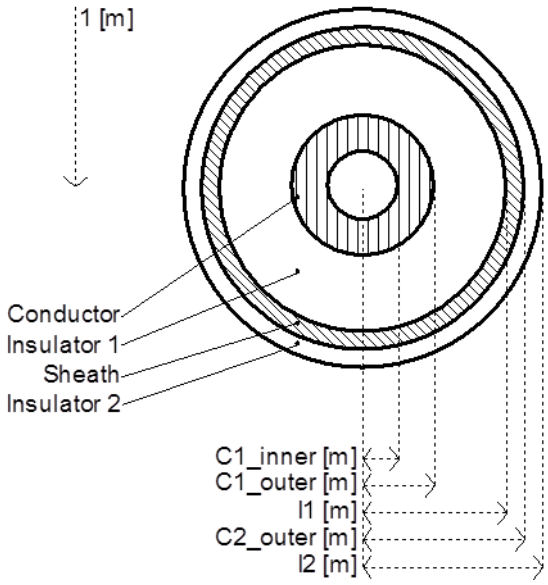

Figure 1: Geometry of the cable model in PSCAD/EMTDC

This used method treats the semi-conducting layer T_{semi} to be a part of the conductor. The calculation of the parameters is listed below.

$$C1_{outer} = \frac{D_{cond}}{2} + T_{semi} \quad (1)$$

$$T_{semi} = \frac{D_{insu}}{2} - T_{insu} \tag{2}$$

$$I_1 = C1_{outer} \cdot \exp\left(\frac{\varepsilon_r}{18 \cdot \mathrm{C}}\right) \tag{3}$$

$$\mathrm{C} = \frac{\varepsilon_r}{18 \cdot \ln(I_1 / C1_{outer})} \tag{4}$$

$$\mathrm{C1_{inner}} = \sqrt{{A_{cond}}^2 - {C1_{outer}}^2} \tag{5}$$

$$\mathrm{C2_{outer}} = \sqrt{\frac{A_{screen}}{\pi} + {I_1}^2} \tag{6}$$

$$I_1 = \frac{D_{tot}}{2} \tag{7}$$

Most of parameters used in the following equations can be referred to Table 1 and Figure 1, where ε_r is the relative permittivity of the XPLE insulation material ($\varepsilon_r = 2.3$).